Author:
Li, Yi-Yuan

Title:
Network-synthesis-based identification methodology for passive vibration suppression system design

Network-Synthesis-Based Identification Methodology for Passive Vibration Suppression System Design

Yi-Yuan Li

Department of Mechanical Engineering
University of Bristol

A dissertation submitted to the University of Bristol
in accordance with the requirements for award of the degree of
Doctor of Philosophy in the Faculty of Engineering

November 2021

Word count: 55000 (approx.)

Abstract

Network synthesis theory originally deals with the problem of realising optimal electrical networks based on the desired system performance. The introduction of a novel mechanical element, the inerter, has completed the electrical-mechanical analogy, allowing network synthesis to be directly applicable to mechanical systems. This method, however, can lead to complex realisations requiring many elements. Compared to electrical systems, the minimal realisation of mechanical networks is much more critical due to practical considerations around alignment, linkages and size. This has motivated our research on developing a network-synthesis-based approach to identify beneficial networks with pre-constrained network complexity. It leads to the design of compact and cost-effective multi-domain vibration suppression systems for a broad range of applications.

First, a series of generic networks, which contain the complete topological information of Immittance-Function-Blocks (IF-Blocks), are proposed to characterise connection possibilities of different types of networks. Desired networks will then be systematically enumerated by assigning a certain number of elements into these IF-Blocks. Since IF-Blocks are two-terminal sub-networks, their immittance functions can be represented as the structural immittances. Thus, combined with their mathematical expressions, the obtained networks can be used to identify optimal vibration suppression systems.

The proposed generic networks are termed as 1PT1NG, IFL, 2PT1NG, GIFN networks. Three of them include one reaction mass, which can be represented through the use of a notional ground as the mass element does not have a direct electrical equivalent. The 1PT1NG network has one physical terminal (PT) and one notional ground (NG) where the reaction mass is connected to; the Immittance-Function Layout (IFL) network represents networks with 2 IF-Blocks and one reaction mass in between; the 2PT1NG network has two PTs and one NG; the Generic-Immittance-Function-Network (GIFN) is the generic network of all possible three-terminal networks. All these networks contain an arbitrary number of transformerless elements connected in series and parallel.

This systematic approach, with its inherent advantages, can be directly used to identify optimal vibration absorbers for various engineering systems. The 1PT1NG network is subjected to offshore wind turbines to suppress their structural vibrations. The IFL and 2PT1NG networks are applied to a three-storey building to reduce its inter-storey drift. The GIFN network is used to design hydraulically interlinked suspensions for vehicles. Simulation results show that the proposed approach is effective in identifying beneficial vibration suppression systems with constrained network complexity compared to the conventional network synthesis methods.

To my family

Acknowledgements

First of all, I would like to give my deep and sincere gratitude to my supervisor, Prof. Jason Zheng Jiang, for his dedicated support, continuous guidance and encouragement throughout my entire PhD study in Bristol. I have benefited a lot from Prof. Jiang's great passion for research. I would also like to express my appreciation to my co-supervisor, Prof. Simon Neild, for his patience, motivation, immense knowledge and wisdom, which has inspired me a lot. It has been a great pleasure for me to learn from Prof. Jiang and Prof. Neild with their responsible attitude towards science.

I would like to extend my thanks to Prof. Matthew Lackner and Dr. Semyung Park from the University of Massachusetts Amherst, Prof. John MacDonald from the University of Bristol, Dr. Jason Jonkman from the National Renewable Energy Laboratory (NREL) and Ian Ward from Atkins, for their generous support and advice on my research. Without their help, I couldn't finish this study so smoothly. Special thanks to Dr. Djamel Rezgui, for guiding me through each of my annual review, and for all the valuable suggestions to my PhD topics and those in-depth discussions in terms of the philosophy of research.

Furthermore, I would also like to express my gratitude to my dissertation examiners, Prof. Fu-Cheng Wang and Prof. Kaoru Yamamoto, for their careful reading of my dissertation and for making insightful suggestions to improve the quality of this dissertation. I also really appreciate Dr. Branislav Tituru for his patience and encouragements to guide me through the PhD examination smoothly.

I would also like to acknowledge the University of Bristol and the Chinese Scholarship Council for their financial support during my PhD study.

It is my great pleasure to be able to work with all of my lovely and talented colleagues and friends at the ACTLab. I would like to thank my team members, Ying, Yuan, Jiannan, Xiaofu, Tim, Hui, Ming, Duanqi, Haonan, Cenxiao, Nick, and all other colleagues at the ACTLab, for bringing me lots of support and joy during and beyond the daily work. Special thanks to all my friends here in the UK and back in China, for their encouragements and company, which give me a lot of sweet memories and warmth.

Finally, I would like to express my deepest gratitude to my family, especially my parents, for their endless love and support, giving me strength to move forward with a grateful heart. I am who I am because of all the trips I went and all the kind souls I met. I really cherish this journey finishing my PhD at the University of Bristol. Thank everyone who has shown me kindness and love.

Author's declaration

I declare that the work in this dissertation was carried out in accordance with the requirements of the University's *Regulations and Code of Practice for Research Degree Programmes* and that it has not been submitted for any other academic award. Except where indicated by specific reference in the text, the work is the candidate's own work. Work done in collaboration with, or with the assistance of, others, is indicated as such. Any views expressed in the dissertation are those of the author.

SIGNED: Yi-Yuan Li

DATE: 7th November 2021

Contents

List of Figures

List of Tables

Nomenclature

General Notations

F	Applied force
v	Velocity
m	Reaction mass value
k	Stiffness
b	Inertance
c	Damping value
g	Gravitational constant
s	Laplace variable
ρ	Fluid density
$Y(s)$	System admittance
$Z(s)$	System impedance
J	Objective function
R	Hydraulic resistance
C	Hydraulic compliance
I	Hydraulic inertance

Chapter 2

i	Electrical current
U	Electrical voltage
Q	Flow rate
P	Flow pressure
g	Gravitational constant
R	Resistance
L	Inductance
C	Capacitance
$I(s)$	Electrical current in the Laplace domain
$V(s)$	Relative velocity in the Laplace domain

Chapter 3

$Y(s)$	Immittance function of a 2PT network
$H(s)$	Immittance function of a 1PT1NG network
m_t	Turbine total mass value
m_p	Platform mass value
I_t	Tower moment of inertia
I_p	Platform moment of inertia
R	Distance from the tower hinge to the tower top
R_t	Distance from the tower hinge to the turbine mass centre
R_p	Distance from the tower hinge to the platform mass centre
k_t	Rotary stiffness at the tower hinge
c_t	Rotary damping at the tower hinge
k_p	Rotary stiffness of the platform
c_p	Rotary damping of the platform
θ_t	rotational angle of the tower from vertical
θ_p	rotational angle of the platform from vertical
x_r	absorber's displacement relative to the nacelle
$M_{wind/wave}$	wind/wave input moment to the monopile turbine
M_{wind}	wind input moment to the tower of the spar-buoy type turbine
M_{wave}	wave input moment to the platform of the spar-buoy type turbine
$\boldsymbol{\omega}_f$	IBA's internal states
F_f	Force generated by the IBA.

Chapter 4

$M_{1,2,3}$	Mass value of the 3-DOF building's first, second and third floor, respectively
k_s	3-DOF building inter-storey stiffness
$X_{1,2,3}(s)$	Floor displacements in the Laplace domain
$X_{d_i}(s)$	Inter-storey drift between the ith and $i-1$th floors
$X_0(s)$	Reaction mass displacements in the Laplace domain
$R(s)$	Ground displacement in the Laplace domain
$F_l(s)$	Force exerted to the lower floor in the Laplace domain
$F_u(s)$	Force exerted to the upper floor in the Laplace domain
$YL_{u,i}(s)$	Structural immittance of the upper sub-network in the left IFL containing i non-mass elements

$YL_{l,(n_1-i)}(s)$	Structural immittance of the lower sub-network in the left IFL containing $n-i$ non-mass elements
$YR_{u,j}(s)$	Structural immittance of the upper sub-network in the right IFL containing j non-mass elements
$YR_{l,(n_2-j)}(s)$	Structural immittance of the lower sub-network in the right IFL containing $n-j$ non-mass elements

Chapter 5

$f_{1,2}$	Forces generated at the two physical terminals of the 2PT1NG network
R	number of IF-Blocks in a generic 2PT1NG network
$\mathbf{L}_R(s)$	Immittance-Function matrix of the 2PT1NG network with R IF-Blocks
$Y(s)$	Immittance function of a 2PT network
k_b	Brace stiffness
m_s	Mass value of the 3-DOF building's each floor
k_s	3-DOF building inter-storey stiffness
$F_l(s)$	Force exerted to the lower floor in the Laplace domain
$F_u(s)$	Force exerted to the upper floor in the Laplace domain
$X_{1,2,3}(s)$	Floor displacements in the Laplace domain
$X_{d_i}(s)$	Inter-storey drift between the ith and $i-1$th floors
$X_0(s)$	Ground displacement in the Laplace domain

Chapter 6

P_{ij}	Fluid pressure in the piston with $i=l$ or r stands for left or right, and $j=1$ or 2 stands for upper or lower piston chamber
q_{ij}	Fluid flow rate
A_{ij}	Piston cross-section area
v_{ij}	Velocity of each piston end
F_{id}	Dynamic force exerted to the interlinked suspension
Δv_i	Relative velocity exhibit at each end of the suspension strut
P_{A1} (P_{B1})	Fluid pressure at the bottle neck of each accumulator
P_{A0} (P_{B0})	Initial pressure inside the accumulator
P_{Aa} (P_{Ba})	Instant pressure inside the accumulator
q_{Aa} (q_{Ba})	Fluid flow rate going through each accumulator
$\mathbf{Z}_h$	Hydraulic impedance matrix of the interlinked system
$\mathbf{Z}_{hA}$	Hydraulic impedance matrix of the pipeline A

$\mathbf{Z}_{hB}$	Hydraulic impedance matrix of the pipeline B
$\mathbf{Y}_m$	Equivalent mechanical admittance matrix
$\mathbf{A}$	Piston cross-section area matrix
$\mathbf{D}$	Position matrix
Z	Impedance of an IF-Block
G	Graph representation
k_{sl} (k_{sr})	Conventional suspension stiffness
k_{tl} (k_{tr})	Tyre stiffness
c_{tl} (c_{tr})	Tyre damping
M	Sprung mass
I	Sprung mass moment of inertia
m_l (m_r)	Left and right unsprung mass
b_l (b_r)	Distance from the sprung mass centre to the suspension strut
ξ_l (ξ_r)	Road surface
$\mathbf{D}_y$	Suspension position matrix

Abbreviation

DEL	Damage Equivalent Loads
DLC	Design load cases
DOF	Degree of Freedom
FLS	Fatigue limit state
GIFN	Generic-Immittance-Function-Block
HIS	Hydraulic-interlinked system
IBA	Inerter-based absorber
IF	Immittance-Function
IFL	Immittance-Function-Layout
IF-Network	Immittance-Function-Network
IF-Block	Immittance-Function-Block
NG	notional ground
PPA	Platform pitch angle
PSD	Power Spectral Density
PT	Physical terminal
RID	Rotatonal Inertia Damper
SSP	Semi-submersible platform
SWL	Still water level
TVA	Tuned Vibration Absorber

TMD	Tuned Mass Damper
TVMD	Tuned Viscous Mass Damper
TID	Tuned Inerter Damper
TMDI	Tuned Mass Damper Inerter
TPIMS	Tuned Parallel Inerter Mass System
THPI	Tuned Heave Plate Inerter
$\mathrm{TTD}_{\mathrm{FA}}$	Tower top displacement in the fore-aft direction
$\mathrm{TTD}_{\mathrm{SS}}$	Tower Top Displacement in the side-to-side direction
ULS	Ultimate limit state
1PT1NG	1 physical-terminal 1 notional-ground
2PT1NG	2 physical-terminals 1 notional-ground

Chapter 1

Introduction

1.1 Research objectives

It has become more and more critical to suppress undesirable vibrations due to the increasing desire for sophisticated, high-performance dynamic systems. This has led to the demand for developing advanced vibration suppression techniques to satisfy various practical requirements.

The current vibration suppression techniques can be broadly divided into three categories: passive, active and semi-active. Although compared to the active and semi-active techniques, the passive one has its own limits such as depending on the precise tuning to the target frequency, it is still widely used for various engineering applications since it doesn't need any external energy input. This means the whole system is unconditionally stable, low-cost and highly durable. One of the simplest and most effective passive devices is the tuned mass damper (TMD) [9], which is to attach an additional reaction mass to the primary structure through a paralleled spring and damper, as shown in Fig. 1.1(a). The TMD is often tuned so that it oscillates at nearly the same frequency as the primary system. With the merits of simplicity, effectiveness and zero-energy input, the TMD has been widely used to suppress excessive vibrations of various dynamic systems. However, the TMD is sensitive to changes in the underlying structural frequencies [10]. Its performance improvement is also decided by the additional device mass, resulting in a compromise between the performance and the mass value, as too heavy an additional mass is undesirable for most engineering systems. Therefore, advanced passive vibration suppression techniques are still needed.

In 2002, Smith [11] introduced a novel passive mechanical element, the inerter, which has been proved to be effective in reducing vibrations of various engineering systems, such as the automotive [12–16], railway vehicles [17–20], building structures [21–24] and wind turbines [25–27]. The introduction of the inerter has revolutionised the discipline of vibration suppression by largely expanding the range of the realisable absorber configurations. Various types of inerter-integrated vibration absorbers, such as the tuned inerter damper (TID) [21] (Fig. 1.1(b)), the tuned viscous mass damper (TVMD) [22] (Fig. 1.1(c)), and the tuned mass damper inerter (TMDI) [23] (Fig. 1.1(d)), etc., are proposed. However, typically these was only one layout proposed and analysed each time in the previous studies, despite the fact that there are many other absorbers which haven't been investigated yet, and they could potentially provide better performance.

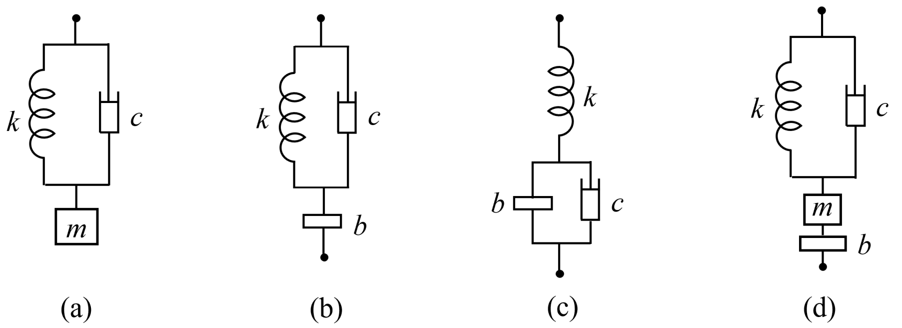

Fig. 1.1 Example vibration absorber layouts: (a) the TMD; (b) the TID; (c) the TVMD; (d) the TMDI.

One possible way to systematically analyses a full set of inerter-integrated vibration absorbers is to employ the network synthesis theory. This is because the inerter possesses the property that the force it generates is proportional to the relative acceleration across its two terminals. With such property, the mechanical elements - springs, dampers and inerters (instead of mass which always has one terminal notionally connected to the ground) are completely analogous to the electrical elements - inductors, resistors and capacitors. Thus, network synthesis theory originally developed in the electrical domain can be directly applied to realising passive mechanical networks that satisfy prescribed characteristics. Moreover, with the expanded analogy amongst electrical-mechanical-hydraulic-acoustic domains [28], network synthesis theory can be also extended to hydraulic and acoustic (pneumatic) domains.

A general electrical network realisability procedure established by Bott and Duffin [29] states that any positive-real function can be realised as the impedance of a one-port network consisting of inductors, capacitors and resistors. Through the Bott-Duffin theory, mechanical networks with any positive-real functions can also be realised using springs, inerters and dampers. However, the most noticeable drawback of the Bott-Duffin theory is that the network complexity and topology cannot be pre-constrained, which could potentially generate complex networks that require many elements while provide only modest improvements over simpler arrangements. As mentioned in [30], a positive-real biquadratic immittance realised using the Bott–Duffin synthesis requires 9 elements connected in series-parallel in the network. Thus, the realised network might be undesirable with excessive numbers of components. Unlike the electrical network, minimal realisations of networks in the mechanical domain is much more critical due to practical considerations around alignment, linkages and size. Although there are studies on the minimal realisation of networks, most of them focus on the restriction of immittance functions. For example, normally only biquadratic or bicubic functions are considered to realise the one-port networks, and it is still an open question in terms of the minimal realisation of immittance functions with higher order or of multi-port networks.

To address the aforementioned problems, a novel network-synthesis-based methodology is proposed in this study to identify beneficial vibration suppression systems with a specific focus on the network topology and complexity. This research focuses on the two- and three-terminal networks[1] – this is due to the fact that most independent- and interlinked-vibration suppression systems can be represented as two- or three-terminal networks. For example, the TMD (shown in Fig. 1.1(a)) is an auxiliary mass attached to the primary system through a paralleled spring and damper. This device is essentially a two-terminal network with one terminal notionally connected to the ground (details can be found in Fig. 3.1 of Chapter 3). And the aforementioned TMDI (shown in Fig. 1.1(d)) is equivalent to a three-terminal network with two physical terminals and one notional-ground terminal that the reaction mass is connected to (details can be found in Fig. 5.2 of Chapter 5). Another example is a hydraulically interlinked suspension applied to a vehicle system. Its network representation also has three terminals (details can be found in Fig. 6.3 of Chapter 6). Therefore, the primary motivation of this thesis is to develop a systematic identification methodology, which could cover a full set of specific two- and three-terminal network layouts with a predetermined number of passive elements and the explicit topological information.

Motivated by this, three objectives are proposed in this thesis:

[1]In the electrical domain, two-terminal network is termed as one-port network, and three-terminal network is a special case of the two-port network.

1. To derive generic networks with their corresponding mathematical expressions, which will contain the complete topology of the desired two- and three-terminal network types (i.e., to determine network topology).
2. To propose a systematic procedure to cover a full set of desired networks which contain a predetermined element numbers and types (i.e., to restrict network complexity). The obtained generic network will be used to facilitate the procedure.
3. To identify optimal vibration absorbers from the obtained full set of networks subjected to different engineering applications, e.g. for the structural control of offshore wind turbines and civil buildings, and for vehicle suspension design, etc.

1.2 Thesis outline

The remainder of this thesis is organised as six chapters with its structure and contents summarised below. The contribution of this thesis has been divided into four parts, demonstrated in Chapter 3, 4, 5 and 6, respectively. In each part a generic network will be derived with a corresponding identification procedure, and it will be subjected to a specific engineering application. These parts do not need to be read in order, although some conclusions in subsequent parts are obtained from the preceding ones:

Chapter 2 - Literature review

An extensive literature review is conducted in this chapter. It starts with the introduction of different types of vibration suppression techniques, including the passive, active and semi-active strategies. Emphasis will be on the advantages of the passive one and its applications to various systems. The inerter, as a novel passive two-terminal mechanical element, will be introduced in the following part. Physical realisations of the inerter and its applications to suppress vibrations of various engineering systems are introduced accordingly to demonstrate its performance advantages. Since the inerter is the mechanical coupling of the electrical capacitor, mechanical networks consisting of springs, dampers and inerters can be realised through the network synthesis approach which is originally developed in the electrical domain. Therefore, in Section 2.3, the classical network synthesis theory is reviewed, and its potential drawback of introducing redundancy is pointed out, followed by the review of those more recent approaches considering minimal elements realisations. Finally, the structure-immittance approach [30] is briefly introduced which integrates the pre-constrained network topology and complexity to the network synthesis approach.

Chapter 3 - Generic 1PT1NG network with application to offshore wind turbines

In Chapter 3, a systematic approach is proposed to characterise a full set of passive vibration absorbers which consist of one reaction mass and a pre-determined number of springs, dampers, inerters, and connect to the primary system with one attachment point. The mass element is treated as a special two-terminal element, with one terminal notionally connected to the ground, denoted as a notional-ground (NG). The attachment point is treated as a physical terminal (PT) in the corresponding network representation. The generic 1PT1NG network is derived by employing the graph theory. As an application example, the derived generic 1PT1NG network is used to identify beneficial inerter-based absorbers to reduce the structural vibrations of a fix-bottom monopile type and a floating spar-buoy type offshore wind turbine. Simplified linear wind turbine models are first established to identify the beneficial absorbers. To assess their performance under realistic load conditions, an offshore wind turbine simulation tool, the OpenFAST, is modified to include the transfer functions of all possible 1PT1NG networks. By employing the identified optimal absorbers, monopile and spar-buoy turbines are simulated under different wind and wave conditions, and the results are compared with the best performance that a conventional vibration absorber, the TMD, can be obtained.

Chapter 4 - Immittance-Function-Layouts with application to building structures

Although optimum 1PT1NG networks can be obtained through the approach provided in Chapter 3, there are still plenty of mass-included devices which have two physical terminals (2PTs) yet cannot be covered by the generic 1PT1NG network. One example is the tuned-mass-damper-inerter (TMDI). It has shown significant performance benefits of mitigating unwanted vibrations. To further investigate networks with two physical terminals and one notional-ground terminal (termed 2PT1NG network), inspired by the layout of the TMDI, an Immittance-Function-Layout (IFL) is introduced in Chapter 4. The IFL, as a subset of all 2PT1NT networks, is the generic layout of a reaction mass in between of two Immittance-Function-Blocks (IF-Blocks). To investigate the performance advantages of the IFL networks, single IFL-type and dual-IFL type devices are applied to an example 3-storey building system to reduce the maximum inter-storey drift subjected to base excitations. To further verify the results, real-life earthquake inputs are used on the 3-storey building model. Results show advantages of the identified absorbers on mitigating seismic vibrations compared to the optimum TMDI. A 10-storey building model subjected to the base excitation is also adopted to further verify the effectiveness of the identified absorbers.

Chapter 5 - Generic 2PT1NG networks with application to the building structure

In Chapter 5, generic 2PT1NG networks are derived where the graph theory is again employed to facilitate their topological connections. The series and parallel connections between a 2PT and a 2PT1NG network are firstly defined, after which a systematic procedure to formulate generic 2PT1NG networks is introduced. Based on the obtained generic 2PT1NG networks, the enumeration of all possible 2PT1NG network layouts is discussed, together with the Immittance-Function-Matrix (IF-Matrix) derived for systematic optimisation. Combining with the generic 1PT1NG network derived in Chapter 3, all possible networks with series–parallel connections of one reaction mass and a pre-determined number of springs, dampers and inerters can be covered. The derived generic 2PT1NG network is again applied to the three-storey building model to reduce its maximum inter-storey drift, where the number of inerters, dampers and springs included in the vibration suppression device is restricted to be one for each. Significant performance improvements are obtained with identified beneficial vibration absorbers.

Chapter 6 - Three-terminal networks with application to vehicle interlinked suspension design

For independent vibration absorbers which are normally used for uni-dimensional vibration suppression problems with no more than two attachment-points to the primary system, it is sufficient to use the generic networks developed in Chapters 3-5 to identify the optimum absorbers. However, for interlinked vibration suppression systems which are used for the multi-dimensional control of the primary system, a general network identification approach with constrained network complexity is needed. It is shown in Chapter 6 that, with a proper design, such interlinked absorbers can be represented as three-terminal networks. Therefore, an approach is proposed to realise a full set of series-parallel three-terminal networks with pre-determined number of transformerless elements. This is achieved by constructing the Generic-Impedance-Function-Network (GIFN) to represent all topological possibilities of three-terminal networks. A 4-DOF half-car model integrating a hydraulically-interlinked suspension (HIS) is adopted in Chapter 6 as an example to demonstrate the proposed approach. Signifiant vehicle ride comfort improvements are obtained with no compromise for the vehicle roll performance. Moreover, more than one network configurations with the same performance improvements are obtained, this could potentially provide more design possibilities for the next-step physical realisation of such HIS system to fit into specific manufacturing requirements.

Chapter 7 - Conclusions and outlook

Conclusions are given in Chapter 7, where the network-synthesis-based identification methodology introduced in this study is summarised, together with the results obtained from various vibration suppression case studies. Advantages of this methodology is also summarised based on these results. Discussion is then extended to the potential avenues of the future work.

Chapter 2

Literature review

A detailed literature review is undertaken in this chapter to provide a broader context for the subsequent analysis, where the vibration suppression techniques, the inerter concept, and the network synthesis theory with applications to the inerter-integrated network realisation are introduced.

2.1 Vibration suppression systems

It has become more and more critical to suppress undesirable vibrations due to the increasing desire for sophisticated, high-performance dynamic systems. Hence, a substantial amount of vibration suppression techniques are developed to satisfy various engineering requirements. Noted that the literature on these techniques is vast so this review should not be taken as an exhaustive discussion on all the references. Rather, different vibration suppression strategies are introduced, together with an emphasis on some notable applications of passive vibration suppressions due to their merits of simplicity, effectiveness and reliability.

2.1.1 Different vibration suppression techniques

Vibration suppression techniques can be broadly divided into three categories: passive, active and semi-active. Each technique has their merits and limits with a certain range of applications.

Passive vibration suppression

Passive vibration suppression is to reduce vibrations of different systems without any external energy input, thus the system stability [31] (i.e., the system tends towards a point of equilibrium on its own accord) is always satisfied as it does not increase the output beyond the input. Passive vibration systems are normally achieved through two mechanisms: vibration damping and vibration isolation. Vibration damping is the process of dissipating kinetic energy induced by movements to reduce the amount of energy in the primary system. This is normally achieved by a damping system, such as a viscous damper. While vibration isolation prevents energy from entering the primary system. One example is the tuned vibration absorber (TVA) proposed by Frahm [32]. It consists of an additional mass-spring device attached to the primary system. If the absorber's natural frequency is tuned to be the same as the frequency of the external force, the amplitude of the primary system's steady state response will become zero. In fact, the TVA is always tuned to the natural frequency of the primary system where resonance occurs to prevent vibrations of the primary system. Normally, vibration damping and isolation mechanisms are combined together to maximise the dissipated energy by adjusting the relative motion and phase shift between the primary and vibration absorbing systems.

Active vibration suppression

Unlike the passive vibration suppression technique, external energy is required in the active ones to control or modify the motion of a primary system. The control forces generated by active control devices are typically based on the feedback information from the measured response of the primary system and/or feedforward information from the external excitation [33], which are normally measured by sensors. The generated control forces will vary depending on the primary system's instant responses, therefore, they can be used for a wide range of excitation and operation conditions. Compared to the passive suppression strategies, the active one has the following advantages: (a) enhanced performance improvements of the primary system; (b) less sensitivity to site conditions and the model accuracy of primary systems; (c) applicability to multi-hazard mitigation situations [10]. However, to provide accurate actuator forces, sufficient signals measured by sensors must be provided, along with an appropriate control law and ideal hardware, which inevitably increase the costs, complexity and energy consumption. In addition, with insufficient signal dataset or inadequate control law, deleterious actuator forces could be applied, causing system instability and even worse vibration problems.

Semi-active vibration suppression

Compared to passive and active vibration suppression techniques, the semi-active is an attractive alternative, as it takes advantages of the adjustable parameter characteristics of an active device while maintain the stability of the passive device [34]. Similar to the active control technique, a pre-determined control algorithm is also required for the semi-active device to monitor the feedback measurements and to generate appropriate command signal to adjust mass, stiffness and/or damping properties of the semi-active device. But it will not inject external energy into the primary system. Therefore, the semi-active control devices will not destabilize (in the bounded input/bounded output sense) primary systems [35]. Semi-active devices can be achieved in various ways, such as controllable friction devices [36], variable-orifice fluid dampers [37], variable-stiffness devices [38], and controllable fluid dampers (such as the electrorheological (ER) fluid damper [39] and the magnetorheological (MR) fluid damper [40]). There are quite a lot researches have been done to employ the semi-active vibration suppression for various engineering applications, such as the civil structures [41], railway vehicles [42] and automotive systems [43]. Whereas, similar to the active one, semi-active could also lead to expensive and complex systems due to the requirement of a large amount of measurements and an accurate control algorithm.

Although compared to the active and semi-active vibration suppression, the passive one has its own limits, it is still widely used for various engineering applications since it doesn't need any external energy input. This means the whole system is unconditionally stable, low-cost and highly durable. With these merits, passive vibration suppression techniques have been widely used to reduce excessive vibrations of various dynamic systems. In this thesis, our focus will be on the development of novel and effective passive suppression systems.

2.1.2 Traditional passive vibration suppression applications

Design of passive vibration suppression systems has a long history. One of the most effective passive devices is the tuned mass damper (TMD), which attaches an additional mass to the primary system through a paralleled spring and damper [44, 45]. To maximize energy dissipation, Den Hartog [9] proposed the tuning method of choosing appropriate stiffness and damping ratio of the TMD. He assumed no damping presented in the primary system to facilitate the derivations. While only viscous damping is considered by Den Hartog in [9], Snowdown [46] extended it to different types of absorber dampings. Falcon *et al.* [47] derived a procedure to optimise an absorber incorporating a restricted amount of damping for a damped primary system. Ioi and Ikeda [48] used correction factors to represent the absorbers' parameters as a function of the primary system's damping ratio. Warburton [49, 50] derived the closed form expressions for optimum absorber parameters subjected to various exciation combinations, and he extended the method to multi degree-of-freedom (DOF) systems. In terms of the practical application of the TMD, although its performance will be improved as the mass of the TMD increasing, the amount of mass that is acceptable to be added to the original system in most applications is no more than 10% of the targeted vibration mode [21] due to space and weight limitations. Moreover, the TMD will provide best performance if positioned at locations where the target mode has the largest movements [21]. This results in, for example, the need to place the mass at the top of a building to suppress its fundamental mode, see example analysis in [51, 52]. In additional to the single TMD, vibration suppression effectiveness using multiple TMDs was also investigated by many researchers. In 1984, Iwanami and Seto [53] proposed dual tuned mass dampers (2TMDs) to suppress the vibration of a single DOF structure with harmonically forced oscillation. It was shown that 2TMDs with the same total mass value are more effective than a single TMD. Later, an alternative connection arrangement was proposed by Ren [54], termed the non-traditional TMD. Unlike the traditional TMD which has one point attached to the primary structure, this device has two attachment points, which holds the layout of having one reaction mass in between of a spring and a damper. Effective seismic-vibration mitigation performance was also demonstrated by Xiang, *et al.*, using this type of device [55].

Generally speaking, conventional passive device types are limited. Its performance will degrade with the reduction of the reaction mass value, while too heavy of a reaction mass is undesirable for most engineering systems. Therefore, there is still a demand to develop advanced passive vibration suppression techniques. Recently, with the introduction of a novel passive mechanical element, the inerter, together with the network-synthesis approach, this problem can potentially be addressed, as discussed in the following sections.

2.2 Inerter-based vibration suppression

2.2.1 Multi-physical domain analogy and inerter concept

The first analogy used between the electrical and mechanical systems was the force–voltage analogy [11], which is introduced by Maxwell in the 19th century [56]. Later, Firestone proposed an alternative, the force-current analogy [57], which possesses the topological connections (i.e. parallel, series, etc.) of the mechanical and electrical networks. In his work, the idea of *through* and *across* variables was introduced. As described in [11], a *through* variable (such as force and current) involves a single measurement point, which requires the system to be severed at that point to actually make the measurement. An *across* variable (such as velocity and voltage) can be measured without breaking into the system, where the relevant quantity for network analysis is the difference of that variable between two points. With this analogy, the traditional mechanical elements – the spring, damper and mass, can partially be mapped to the electrical elements – the inductor, resistor and capacitor, respectively. While the resistor and inductor can be fully analogous to the damper and spring, a capacitor is not completely equivalent to a mass. This is because, following Newton's Second Law, one terminal of the mass is its centre and the other terminal is always considered as nominally grounded, while a capacitor can be connected across two physical terminals and not necessarily have a grounded terminal.

In 2002, Smith [11] introduced a novel two-terminal passive mechanical element, the inerter, which completed the force-current analogy with the inerter fully analogous to the capacitor. The ideal inerter has the property that the equal and opposite force applied to its two terminals is proportional to the relative acceleration between them [11]. This can be represented mathematically as:

$$F = b(\dot{v}_1 - \dot{v}_2) \tag{2.1}$$

v_1 and v_2 denote velocities of the inerter's two terminals; b is termed inertance and has the unit of kilograms. In this sense, the ideal inerter is the true mechanical dual of the ideal spring regardless of any analogy principles employed [11]. Similar to the spring and damper elements, There are four conditions proposed by Smith [11] for an inerter device to be practically useful: (1) it should have a small mass value compared to the required inertance; (2) there is no need to have a grounded terminal; (3) it should have a designable but limited size; (4) the device is able to work in any spatial orientation and motion.

The across and through concepts introduced by Firestone provide a unifying framework to extend these analogies to other physical domains, such as the pneumatic, hydraulic and thermal systems. Thus, in addition to mechanical, electrical or combined devices, hydraulic and/or pneumatic devices like the hydraulic/pneumatic vehicle suspensions [58, 6, 59] can also be explored in a similar way. Table 2.1 summarises the mechanical-electrical-hydraulic-pneumatic analogy together with the mathematical expressions of their respective elements. With this analogy, a linear vibration suppression system can be represented as a corresponding network where the network analysis and synthesis theory originally developed in the electrical domain can be directly applied to these systems to investigate their dynamics. Furthermore, it provides a solution to model and analyse multi-physical domain systems, such as a mechatronic device [15] (combining mechanical and electrical domains) or a hydro-pneumatic device [60] (combining hydraulic and pneumatic domains).

Table 2.1 Multi-physical domain analogy [8]

Mechanical	Electrical	Hydraulic/Pneumatic
Stiffness $F = k\int (v_1 - v_2)dt$ $Y(s) = \frac{k}{s}$	Inductance $i = \frac{1}{L}\int (U_1 - U_2)dt$ $Y(s) = \frac{1}{Ls}$	Compliance $P_1 - P_2 = \frac{1}{C}\int Qdt$ $Y(s) = \frac{1}{Cs}$
Damping $F = c(v_1 - v_2)$ $Y(s) = c$	Resistance $i = \frac{1}{R}(U_1 - U_2)$ $Y(s) = \frac{1}{R}$	Resistance $P_1 - P_2 = RQ$ $Y(s) = \frac{1}{R}$
Inertance $F = b\frac{d(v_1 - v_2)}{dt}$ $Y(s) = bs$	Capacitance $i = C\frac{d(U_1 - U_2)}{dt}$ $Y(s) = Cs$	Inertance $P_1 - P_2 = I\frac{dQ}{dt}$ $Y(s) = Is$

2.2.2 Physical realisations

There are different types of physical realisation of the inerter. These realisations can all be viewed as an approximation of its mathematical ideal in the same way that real springs, dampers, etc., approximate their mathematical ideals [1]. Two typical realisation approaches are widely investigated, i.e., the flywheel-based mechanical one and the fluid-based hydraulic one.

Flywheel-based inerter

Flywheel-based inerter takes the advantage of inherently significant inertia of a rotating flywheel to provide acceleration resistance effects. In Smith's paper [11], he proposed a simple approach to realise the inerter by driving a flywheel through a rack, pinion, and gears, termed as rack-and-pinion inerter – schematic plot is shown in Fig. 2.1(a). One terminal of the device is the piston rod and the other one is the cylinder, none of which is needed to be fixed to the ground and the mass of the device is very small compared to the inertance of the device. With such mechanism, by assuming the mass of all other components as negligible except for the flywheel, the induced inertance b can be expressed as:

$$b = m\alpha_1^2\alpha_2^2 \tag{2.2}$$

where m is the mass of the flywheel, $\alpha_1 = \gamma/r_3$ is the ratio of the flywheel radius to the flywheel pinion radius, and $\alpha_2 = r_2/r_1$ is the ratio of the gearwheel radius to the rack pinion radius. Later, a ball-screw inerter was proposed in [13]. The inertance of such device is determined by the pitch of the screw thread and the moment of inertia of the flywheel. A schematic plot of this ball-screw inerter can be found in Fig. 2.1(b). Again, assuming the mass of all other components is negligible except for the flywheel, the induced inertance b can be derived as [61]:

$$b = I(\frac{2\pi}{p})^2 \tag{2.3}$$

where I is the the mass moment of inertia of the flywheel, and p is the pitch of the ball-screw. Certainly the direct inertial effect of the flywheel mass comes into play, but this will only slightly affect the induced force providing $\alpha_1^2\alpha_2^2$ and $(\frac{2\pi}{p})^2$ are large enough. For example, it is shown in [12] that a rack-and-pinion inerter device with 0.225 kg flywheel mass can provide an inertance of 726 kg. Generally the effect of the device mass can be neglected, as is commonly done for springs and dampers.

However, rack-and-pinion inerters and ball-screw inerters are more easily suffering from detrimental breaks due to friction, backlash and elastic effects, producing potentially unquantifiable system nonlinearities [62, 1]. The performance benefits of the inerter are degraded due to the existence of nonlinearities. Papageorgiou, *et al.* [1] showed that both the rack-and-pinion and ball-screw inerters can cause instability problems using a hydraulic damper test rig in displacement control model, which will induce a nonlinear spiking characteristic. This is due to the backlash in these devices and its interaction with a closed-loop system instability in the presence of inertial loads. Although it has been shown that the backlash of a ball-screw inerter can be eliminated through different preloading methods in the manufacturing process [62], these inerters still possess nonlinearity due to the friction and elastic effects. Therefore, there is limited usage of the flywheel-based inerter on the industrial application.

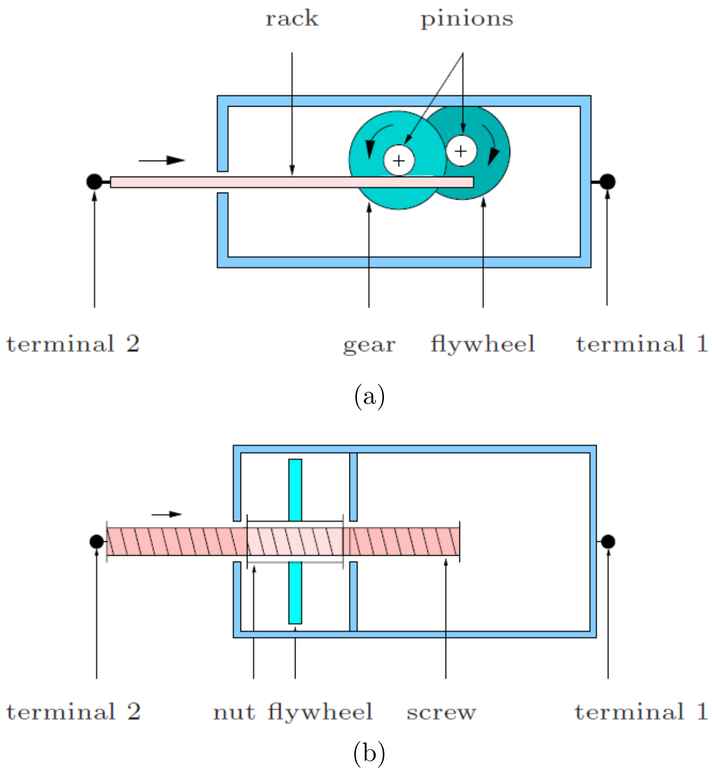

Fig. 2.1 Two flywheel-based inerter realisations (a) rack-and-pinion inerter; (b) ball-screw inerter, reproduced from [1]

Fluid-based inerter

With above mentioned drawbacks of the flywheel-based inerter, the fluid-based inerter becomes an attractive alternative with the advantages of durability and simplicity. Moreover, series or parallel damping effects can be directly integrated to the device to simplify the system design. The idea of a hydraulic inerter was first proposed in [63], which suggested the use of a gear pump to convert linear motions into rotational motions. Wang, *et al.*, [2] used a gear motor to realize this hydraulic inerter, as shown in Fig. 2.2. There is a hydraulic cylinder, a gear motor and a piston in the schematic plot with a shaft moving in the cylinder. It can be seen that the piston separates the cylinder into two parts, with each connected to the inlet or outlet of the hydraulic motor. Two terminals of the hydraulic inerter are the hydraulic cylinder (terminal 1) and the piston (terminal 2). When the shaft is moving through the cylinder, the fluid inside the cylinder and the pipeline will be pushed through the hydraulic motor where the inertance will be generated. The derived ideal inertance of this device can be represented as:

$$b = I(\frac{A}{D})^2 \tag{2.4}$$

I is the moment of inertia of the hydraulic motor; A is the area of the piston; D represents the volume of fluid required to turn the motor output shaft through one revolution [2].

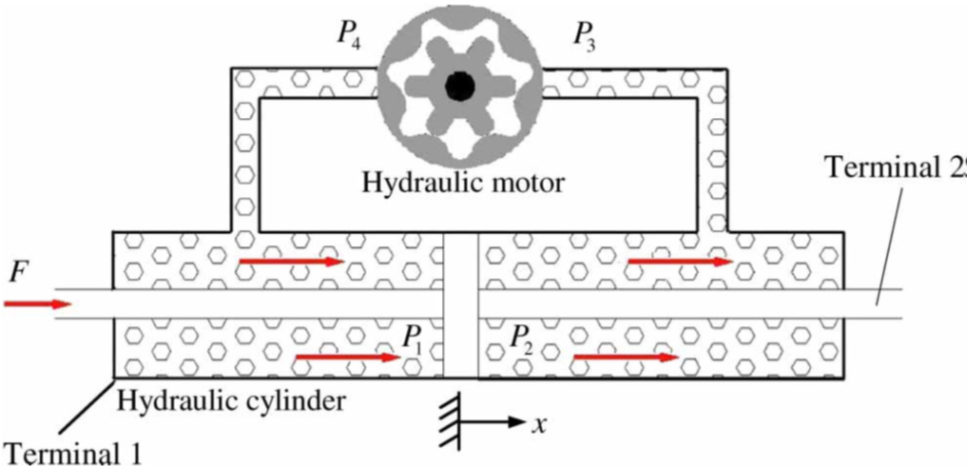

Fig. 2.2 Hydraulic inerter realisation using hydraulic motor, reproduced from [2]

In addition to this hydraulic inerter device making use of the motor inertia, an alternative is the helical-tube inerter introduced in [3, 64]. A schematic plot is shown in Fig. 2.3. Again, two terminals of the inerter are the hydraulic cylinder and the piston, respectively. The inertance of this device is mainly from the moving of the piston rod to push the fluid flowing through the channel which generates an inertia force. It can be derived as:

$$b = \rho l \frac{A_1^2}{A_2} \tag{2.5}$$

where l is the channel length, ρ is the fluid density, A_1 and A_2 are the piston area and

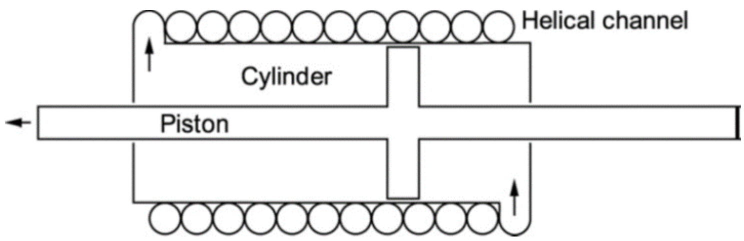

Fig. 2.3 Helical-tube hydraulic inerter realisation, reproduced from [3]

the channel cross-section area, respectively. In particular, a lumped parameter hydraulic model with its equivalent mechanical model are proposed in [64], by considering the resistance (resp. damping), inertance (resp. inertance) and compliance (resp. stiffness) effects. The inherent nonlinear properties in the device is also investigated in [64].

2.2.3 Applications to engineering systems

Several inerter application possibilities have been proposed in Smith's ground-breaking paper [11], such as for vibration absorber design to replace the traditional tuned spring–mass system, or integrating the inerter with the traditional vehicle suspension strut, etc. Since then, the inerter has been employed in a wide range of engineering applications, with significant performance improvements obtained.

Vehicle suspension

The first physical application of the inerter was as a 'J-damper' on Formula One racing cars suspension design for McLaren in 2005, where a paralleled spring-damper-inerter layout is used. The term 'J-Damper' itself was merely a codename to keep the technology secret from potential competitors [65]. Although advantages of the 'J-damper' were kept secret for Formula One racing cars, there were still plenty of open-source academic studies on the inertance-integrated suspension for other road vehicles.

In [12], vehicle performances, including the ride comfort, dynamic load carrying and tyre grip, were investigated and optimised incorporating eight candidate inerter-integrated suspension layouts with no more than one inerter and one damper in each layout. Compared to the conventional suspension strut, considerable improvements were obtained for both quarter- and full-car models. Moreover, the phase-advance that an inerter induces was demonstrated experimentally using a rack-and-pinion inerter prototype. Contrary to proposing fixed-layout candidate suspensions as in [12], Papageorgiou and Smith [13] made the first attempt to identify beneficial mechanical networks by considering positive-real admittances with a predetermined order in the optimisation procedure, which was to employ the matrix inequalities. This enabled a more systematic way to identify beneficial inerter-integrated suspension layouts using the network synthesis approach. Later, in [14], analytical solutions of ride comfort and tyre grip were derived for a quarter-car model incorporating six suspension layouts, with global optima obtained. In 2011, Wang and Chan [15] proposed a mechatronic strut and demonstrated its performance benefits for vehicle suspension control both theoretically and experimentally. Shen *et al.* [16] investigated a hydraulic-electric inerter to achieve its optimal performance for vehicle suspension design. In additional to passive inerter-integrated suspensions, semi-active studies were also carried out in [66, 67].

With substantial performance benefits obtained for automotive suspension design, the inerter-integrated suspension is also investigated for railway vehicle systems. Significant contributions towards this topic was made by Wang *et al.* [17, 18, 68]. In [17], two fixed-layout candidate suspensions were investigated, and a linear matrix inequality approach was also used to further improve the passenger comfort and system damping ratio. The nonlinear properties of inerters were also investigated and experimentally verified. It showed an improved overall system performance by using the inerter, even though its nonlinearity slightly degraded the performance benefits. In [18], three candidate suspension layouts were employed to improve the railway lateral stability where a 16 degrees-of-freedom (DOF) train model was used. Later, a 28-DOF full train model was established in [68]. It was incorporated firstly with a parallel inerter layout, and then followed by an inertance-integrated mechatronic network, to verify the performance advantages in terms of the critical speed, settling time, and passenger comfort of the trains. A detailed investigation on the secondary lateral and vertical suspension systems was first made by Jiang *et al.* [19]. It was demonstrated in this study that, the inerter-integrated suspension system can improve the lateral and vertical ride comfort, as well as lateral body movement when curving, compared with the conventional suspension layout. Track irregularities were further investigated in [20]. Moreover, inerter-based mechatronic solutions for the vertical secondary suspension of the railway vehicle were proposed in [69] incorporating an active strategy. Results showed substantial improvements of the inerter-based mechatronic technology in railway vehicle vertical ride quality with the reduced actuator force.

Infrastructure vibration absorber

Another possible application of the inerter is to design suitable vibration absorbers, which can be used in various infrastructure systems, such as buildings, bridges, wind turbines, etc. The first inerter-based vibration absorption was proposed by Wang *et al.*, [70] where three fixed-layout candidate absorbers were introduced for numerical optimisations of the building structure. Results showed that inerter-based absorbers are effective in reducing vibrations from earthquakes and traffic. Built on this, a higher-order transfer function with more complicated network layouts was employed to seek further performance improvements in [71]. In Japan, studies on the inertance-property-included elements named 'inertial dampers' and 'dynamic masses' were conducted, as stated in

[72] and [73] respectively, to improve the building vibration performance. Moreover, Ikago [22] proposed a tuned viscous mass damper (TVMD), which also provides mass amplification through the ball-screw mechanism, to reduce the seismic excitation of a single-DOF system. The TVMD concept was later extended to multi-degree-of-freedom system through modal analysis in order to better capture the building responses [74]. Lazar *et al.* [21] proposed a tuned-inerter-damper (TID) as an attractive alternative to the conventional TMD. Numerical results showed two significant benefits of the TID compared to the TMD: (1) the most desirable location for the TID is between the first and ground floors, which provides potential installation benefits as part of the device can be held by the ground; (2) the seismic response is improved with an increased inertance vs storey mass ratio. This can be achieved easily by the TID through gearing the inertance, while the increase of the TMD mass value could be problematic for practical application. Another notable inerter-based absorber is the tuned mass-damper-inerter (TMDI) [23]. A series studies [23, 75, 76, 24] were conducted on the vibration suppression performance of the TMDI under various inputs, such as the seismic or wind-induced excitations. It was concluded in [23] that, the incorporation of the inerter in the proposed TMDI configuration can either replace part of the TMD vibrating mass to achieve lightweight passive vibration control solutions, or improve the performance of the building structure with a given mass value compared to the TMD. Yamamoto and Smith [77] also studied the passive control of a chain system of interconnected masses with a single point subjected to an external disturbance. A graphical method for selecting impedance functions of the interconnected parts was developed, where the inerter was also included. This approach can be directly applied to the multi-storey building vibration attenuation subjected to earthquake inputs.

In additional to applications on building structures, there are several investigations of the inerter-integrated vibration absorbers on wind turbines. The first study was made by Hu and Chen [78]. Beneficial absorbers, within the range of first- and second-order admittances, were identified to reduce wind-included structural loads. This work was extended to a barge-type floating wind turbine [25, 79]. Performance improvements were verified in a wind turbine simulation tool, FAST, under combined wind and wave loads. Later, Zhang *et al.* [26] investigated the seismic load mitigation of the wind turbine tower by employing the Tuned Parallel Inerter Mass System (TPIMS). Optimal TPIMS parameters were obtained in this study and robustness for tower seismic vibration control was also investigated. The above introduced studies on wind turbine vibration suppression only included absorbers with one terminal attached to the wind turbine nacelle. In [27], Sarkar and Fitzgerald proposed to use the TMDI for spar-type floating wind turbine tower vibration control where one terminal of the TMDI is attached to the nacelle, and the other terminal is to the tower. Remarkable performance improvements were obtained in this study under normal operational and extreme wind-wave interacted load conditions. In addition to wind turbine tower vibration suppression, the inerter was also used to suppress platform vibrations. Ma *et al.* [80] proposed a tuned heave plate inerter (THPI) to control the heave vibration of a semi-submersible platform (SSP). The THPI replaced one damper of the traditional tuned heave plate (THP) by a predetermined inerter-based layout. Simulation results showed that the THPI system can reduce the heave motion of the platform by 19% compared to the traditional THP system. Then, a novel hydraulic Rotational Inertia Damper (RID) was proposed in [81] to reduce the heave motion of the semi-submersible platform. By replacing the entire THP system, the physical mass of the absorbing device can be significantly reduced (less than 0.8% of the physical mass of the traditional heave plate). This provides an attractive alternative to effectively and economically suppress the heave motions of SSP in the shallow sea.

Other infrastructural vibration control applications, such as for cables [82–84] and bridges [85, 86], adopting the inerter are also developed.

2.3 Synthesis of a network

The introduction of the inerter element has fundamentally enlarged the vibration suppression ability which can be realised passively. Even though plenty of candidate layouts, such as the TID, TVMD, and TMDI as mentioned in Section 2.2, are simple and relatively easy to manufacture, considering the fact that there are countless possible network layouts, this inevitably limits the achievable performance of mechanical systems. Therefore, it is desirable to have a systematic approach which can be used to identify the optimum configuration subjected to various engineering applications. This is where the network-synthesis approach comes into play.

2.3.1 Classical network-synthesis theory

Preliminaries

Network synthesis originally deals with the problem of realising electrical systems or "black boxes" that provide desired excitation response characteristics. In general, electrical systems that the network synthesis theory focuses on are assumed to be passive, linear, time-invariant, and include ideal lumped elements [87]. Networks that comprise finite interconnections of resistors, inductors and capacitors satisfying Kirchoff's laws can be referred to as RLC networks. Standard symbols of these electrical elements with their corresponding mathematical expressions can be found in Table 2.1. The inductor and capacitor having impedance sL and $1/(Cs)$ represent the inductance and capacitance, respectively, with $L > 0$ and $C > 0$. They are termed *reactive elements*. The resistor has impedance R, which represents the resistance with $R > 0$.

For any network, there must be at least two terminals. The current entering the network through one terminal will leave it through the other terminal. A two-terminal network can be described with a current going through the network, and a voltage measured between its two terminals, as shown in Fig. 2.4(a). These two terminals can be paired to form a *port* whenever it is characterised by one current and one voltage. Similarly, an n-port network is the one with n pairs of terminals that connect to external circuits, where a voltage is across each terminal pair, and a current leaving one terminal of a port equals the current entering the other terminal of that port [87, 88]. Alternatively, given a network with a list of terminals rather than ports, if one properly constructs ports by selecting terminal pairs and appropriately constraining the excitations, it is permissible to have a *common-terminal* in several port pairs [87, 89]. An example can be seen in

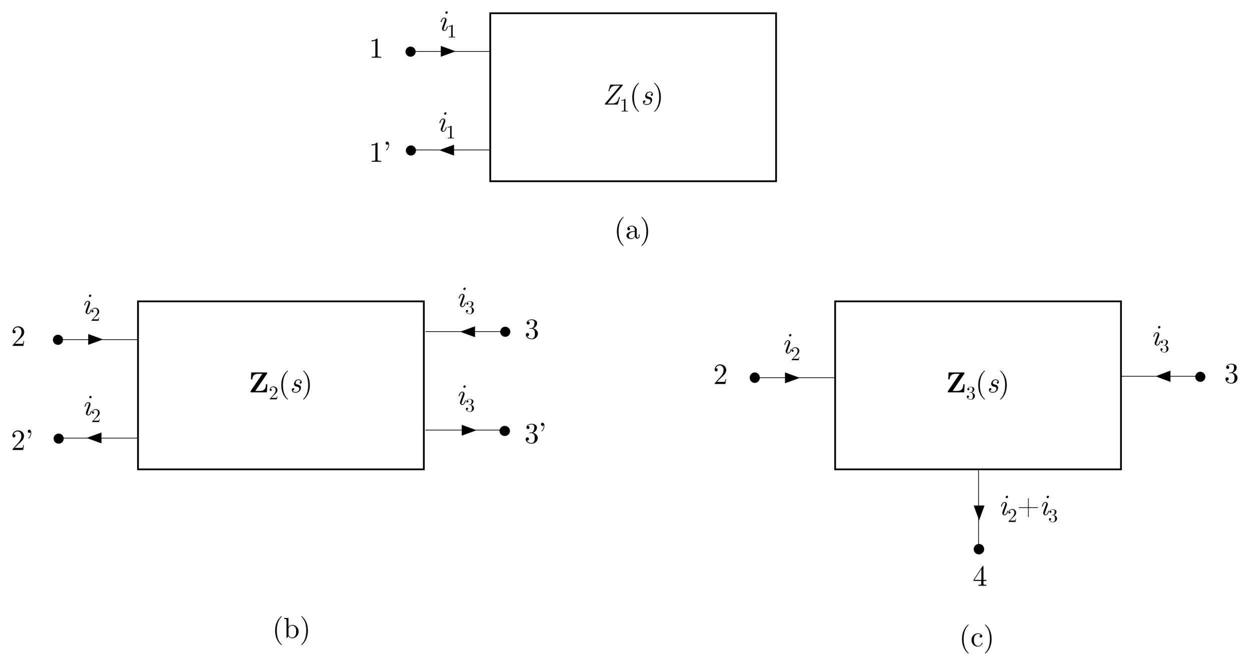

Fig. 2.4 Electrical networks: (a) One-port network with two external terminals 1 and 1'; (b) Two-port network with four external terminals 2 and 2', 3 and 3'; (c) Three-terminal network with external terminals 2, 3, and 4.

Fig. 2.4(b) for a two-port network $\mathbf{Z}_2(s)$ with terminals 2, 2', 3, 3'. Current i_2 flows between terminal pair 2 and 2', and current i_3 flows between terminal pair 3 and 3'. It is equivalent to a three-terminal network as in Fig. 2.4(c) with lower terminals 2' and 3' of each port are joined together to form terminal 4. Fig. 2.4 shows the general representation of one-port, two-port, and three-terminal networks, where $Z_1(s)$, $\mathbf{Z}_2(s)$ and $\mathbf{Z}_3(s)$ are their impedance functions. $Y_1(s) = 1/Z_1(s)$, $\mathbf{Y}_2(s) = \mathbf{Z}_2^{-1}(s)$ and $\mathbf{Y}_3(s) = \mathbf{Z}_3^{-1}(s)$ are the corresponding admittance functions.

Significant contributions in network synthesis

Foster's Reactance Theorem[90] is often regarded as the first contribution to passive network synthesis in its modern sense. The following fifty years was the 'golden era' for passive network synthesis developments where plenty of significant contributions were made. In Foster's theorem, it provided the necessary and sufficient conditions for a real-rational function to be realisable as the driving point impedance of a series-parallel LC one-port network by a partial fraction expansion. Shortly after that, Cauer [91] extended Foster's work to RC and RL networks. With Cauer's and Foster's theorems, the synthesis problem for a certain type of one-port network containing only two types of elements in series-parallel can be realised.

A significant further step was made by Brune in his PhD thesis [92] where the *positive-real function* was first defined. Positive-real function is a rational function $Z(s)$ satisfying the condition that its real part is positive when the real part of s is positive, and $Z(s)$ is real when s is real. With this definition, Brune showed that the impedance (and also the admittance) of a network which contains only resistors, inductors, capacitors and transformers is necessarily positive-real. Conversely, a procedure is always available to realise a network which contains these passive elements given any positive-real function. However, the requirement of realising a network with transformers introduces practical issues as the properties of physical transformers differ considerably from their ideal ones. Hence, there is a real need for network realisations which avoid the use of transformers [93].

In 1949, Bott and Duffin [29] provides an alternative procedure to replace the stage where transformers were used in Brune's approach. Thus, the transformer is not needed any more to realise such networks, which means any positive-real function can be realised as the driving-point impedance (resp. admittance) of a one-port series-parallel passive network consisting of only resistors, inductors, and capacitors. However, the most noticeable drawback of the Bott-Duffin theory is that the network complexity and topology cannot be pre-restricted. This could potentially generate complex networks that require many elements while provide only modest improvements over simpler arrangements. As mentioned in [30], a positive-real biquadratic impedance realised using Bott–Duffin synthesis requires nine elements connected in series-parallel in the network. Although a slight improvement on the Bott-Duffin procedure was provided by several researchers [94, 95] to reduce six elements to five through bridged networks, the minimal realisation is far from solved.

Another significant contribution was made by Darlington [96] who provided a completely different procedure to synthesis driving-point impedances. It was shown that any positive-real function is realizable as the input impedance to a lossless two-port network containing inductors, capacitors and transformers only, and terminated in a pure resistance at one port, at shown in Fig. 2.5 (a). This method was also called 'resistance extraction'. Later, another approach, known as the 'reactance extraction', was proposed by Youla and Tissi [97], which can be considered as complementary to Darlington's method. Using this approach, any positive-real function can always be realised as the driving-point impedance (admittance) of an n-port network comprising only resistors and ideal transformers with $n-1$ of the ports terminated by reactive elements, as shown in Fig. 2.5 (b). This approach is based on a state space formulation where the impedances is given as a symmetric bounded-real scattering matrix.

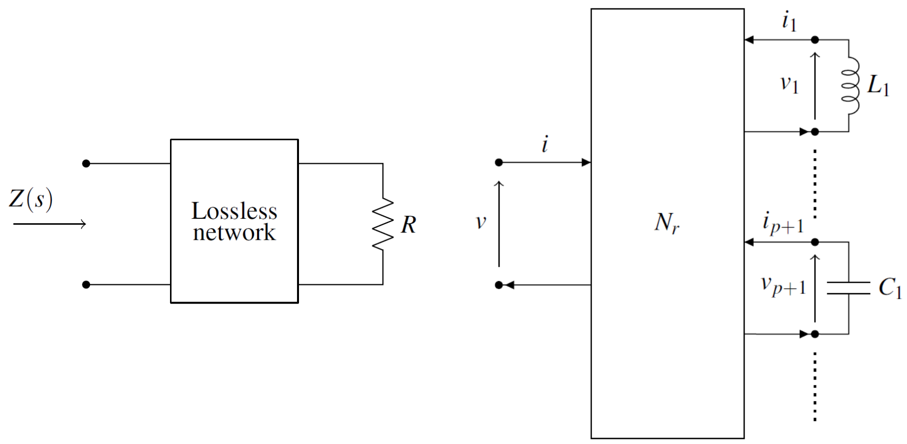

Fig. 2.5 (a) Resistance extraction; (b) Reactance extraction, reproduced from [4].

During this period, many contributions were also made on multi-port network realisations. In [98], Gewertz defined the positive-real matrix by adopting Brune's definition on positive-real function, and proposed a general method to realise four-terminal network which contains resistors, inductors, capacitors and transformers given the prescribed driving-point and transfer functions. The zero-shifting technique was applied by Guillemin [99] to realise passive RC networks as a group of paralleled ladders. Fialkow and Gerst [100] derived the necessary and sufficient conditions for transfer functions to be realisable as two-port RC networks. Furthermore, Fialkow [95] proposed a realisability condition for RC series-parallel grounded two-port networks. By means of simple transformations, the results in the RC-case can be made applicable to networks containing any two kinds of elements only. Building on this, more works were done to realise the RC ladder two-port networks [101–105]. However, a systematic procedure which considers all possible realisations within a certain space is less well developed for the multi-port network, although many studies have used ideas from the classical network synthesis theory.

2.3.2 Passive network synthesis involving minimal realisation

More recently, with the completion of the force-current analogy, all passive network synthesis theory derived for the electrical system can be directly applied to the mechanical system. The field of passive network synthesis has had a resurgence. Kalman made an independent call for a renewed attempt in this field [106], with an emphasis on Ladenheim's minimal enumeration approach [107] (this approach will be introduced later in this section). This is because the minimal realisation of networks in the mechanical domain is much more critical than in the electrical domain due to practical considerations around alignment, linkages and size. Researches to realise passive networks with a focus on the minimal realisation problem will be reviewed in the following part.

Auth [108, 109] provided conditions to realise a biquadratic impedance function as a three-port resistive network terminated by one inductor and one capacitor (minimum reactive elements). Unlike the reaction extraction approach proposed by Youla and Tissi [97], no transformer is needed to synthesis three-port resistive network in Auth's work. Moreover, built on the work done by Tellegen [110], Auth stated that at most six resistors are needed to realise the three-ports containing only resistors. Later, in [111], Chen and Smith reduced the maximum resistor number to be four with necessary and sufficient conditions provided. The authors also extended this work to mechanical one-port networks with at most one damper, one inerter and an arbitrary number of springs [112]. This work uses element extraction of the damper and inerter, followed by the derivation of a necessary and sufficient condition to realise the spring-only three-port network, similar to realising the resistive three-port network. In [113], Chen *et al.* further constrained the number of springs to be no more than three. The minimal realisation of a three-port four-terminal resistive network is also studied by Wang and Chen [114].

However, all these works involve deriving the necessary and sufficient condition of a third-order non-negative definite matrix to be reducible to a paramount matrix. The definition of paramountcy [115, 116] is a necessary condition to realise an n-port resistive network without ideal transformer, which means only one element type can be included in the three-port networks.

An alternative strategy to solve a network realisation problem in terms of minimal realisation is to enumerate and analyse all RLC networks within a given class. In Ladenheim's Master's thesis [107], 108 transformerless networks in total (referred to as the Ladenheim catalogue) are listed, representing the whole possible one-port network layouts with at most two reactive elements and no more than five elements in total. This appears to be the first exhaustive enumeration approach when considering network realisations. In 1969, Reichert [117] proved in German that any biquadratic function which can be realised using two reactive elements and an arbitrary number of resistors can be realised with two reactive elements and three resistors. With Reichert's theorem, it is concluded that any positive real function that can be realised with two reactive elements and an arbitrary number of resistors can also be realised by a network in the Ladenheim catalogue. This result was later reworked by Jiang and Smith [118] with some expanded new lemmas on the main topological argument. More recently, an alternative proof of Reichert theorem was provided by Zhang *et al.* [119].

Later, the *regular* positive function was proposed by Jiang and Smith [120] to investigate a complete class of biquadratic functions containing five elements. The concept of regularity has greatly facilitated the classification of impedances. It was shown that a biquadratic can be realised by a series-parallel network with two reactive elements if and only if it is regular. It also showed that 106 out of 108 Ladenheim catalogue are regular, where two network quartets are introduced to realise these regular biquadratics. Moreover, the nonregular biquadratics can be arranged into three network quadratics. Necessary and sufficient realisability conditions are derived for each of these networks. The regularity is also employed in [121] to investigate the nonregular biquadratics that can be realised by series-parallel six-element networks, which are those with three or four reactive elements. Realisability conditions for the networks are also given in terms of a canonical form for biquadratics. Later on, in Morelli's PhD thesis [4], he introduced a formal classification tool with a focus on the Ladenheim catalogue, which can be partitioned into 24 subfamilies, each comprising a certain number of equivalence classes and orbits [4]. This enables the simplification of analysing networks in different catalogue and helps make the procedure as systematic as possible. This work is also formulated in a book by Morelli and Smith [122].

The aforementioned realisation approaches focus on the biquadratic functions. For a positive-real function with higher McMillan degree, e.g. a bicubic function, studies involving minimal realisation are limited. In the 1920s, Tirtoprodjo [123, 124] investigated the general bicubic impedances by starting from the bicubic functions with multiple real poles and zeros. However, the realisation procedure is highly redundant considering the number of reactive elements it used. Not much further progress has been made until very recently. Hughes [125] proposed a continuity-based approach to solve the minimal network realisation problem using at most three reactive elements for impedances realised by series-parallel bicubic networks. Wang and Chen [126] also made an investigation on realisations of bicubic impedances with no more than five elements, where 22 series-parallel and 11 non-series-parallel configurations are presented to cover the conditions.

2.3.3 The structure-immittance approach

Although many approaches have been proposed, it is still an open question in the synthesis of passive networks that contains the least possible number of elements to realise an arbitrary given impedance function. Recently, an attractive alternative, the structure-immittance approach, was proposed by Zhang *et al.* [30]. It tackles the minimal realisation problem in a different way where generic networks, together with their structural-immittance functions, are obtained to cover a full set of one-port network layouts with explicit information of the network topology and complexity. This approach has greatly facilitated the systemic identification of beneficial mechanical networks. In this part, two mechanical network examples will be given to demonstrate the main steps of the structure-immittance approach. These two examples are denoted as 1k1c1b case (including one spring, one damper and one inerter) and 2k1c1b case (including two springs, one damper and one inerter).

Networks of the one spring, one damper and one inerter case

The admittance of a one-port electrical network is expressed as:

$$Y_e(s) = \frac{I(s)}{U(s)} \tag{2.6}$$

where s is the complex frequency parameter of the Laplace transform, $I(s)$ and $U(s)$ are the current and voltage across the two terminals of the network in the Laplace Domain.

By employing the force-current analogy [57], the admittance of the mechanical network is defined as:

$$Y_m(s) = \frac{F(s)}{V(s)} \tag{2.7}$$

$F(s)$ and $V(s)$ are the force and relative velocity across the mechanical network's two terminals in the Laplace domain.

For networks with one spring, one damper and one inerter (i.e. 1k1c1b case), there are totally 8 absorber layouts. By using the structure-immittance method, two networks termed as Q_{11} and Q_{12}, which contain the possibilities of all the 8 layouts arrangements, can be obtained, where 4 steps are needed [30] to find Q_{11} and Q_{12}. It should be noticed that the networks obtained in each step must satisfy the condition that at most one spring is present.

- **Step 1**: Two generic sub-networks M_{11} and M_{12} are constructed as shown in Step 1 of Fig. 2.6. Here we assume the inerter and damper are taken as the base elements and spring is the added element (total added element number will be $r+1$ if there are r added elements). Sub-network is constructed by adding a spring element to the base element in parallel, then adding a second spring element in series to the resulting network, and then a third one in parallel and so on until all spring elements are added (in this case the total number of the added spring elements is 2). Note that using the adding sequence of series, parallel and then series will generate different generic sub-networks, but the resultant networks will still be the same.

- **Step 2**: Two sub-networks M_{11} and M_{12} are connected to each other in parallel and in series to form two new networks N_{11} and N_{12}, as shown in Step 2 of Fig. 2.6.

- **Step 3**: Since in networks N_{11} and N_{12}, some of the springs are redundant and can produce the same effect on the network, redundancy of the springs in networks N_{11} and N_{12} need to be checked and removed. For example, in network N_{11}, considering $0 < 1/k_1 < \infty$, $k_2 = 0$, $1/k_3 = 0$ and $k_4 = 0$, one layout with inerter, damper and spring in series connection can be obtained; considering $0 < 1/k_3 < \infty$, $k_2 = 0$, $1/k_1 = 0$ and $k_4 = 0$, same layout can be obtained. Hence, k_1 is redundant and can be removed. All of the springs in N_{11} and N_{12} should be checked one by one to guarantee that there is no redundancy left in the networks. As a result, two simplified networks P_{11} and P_{12} can be obtained, as shown in Step 3 of Fig. 2.6.

- **Step 4**: Springs will be added to the network in parallel and in series again to form the final networks. The adding rule is: a spring will be first added in series and the redundancy will be checked for this added spring. Then, another spring will be added in parallel and the redundancy will also be checked. Repeat the same procedure until no new spring is needed (Note: it is the same when a spring is added in parallel first). Thus, the final networks can be constructed. Following this, the final generic networks for the 1k1c1b case can be obtained as Q_{11} and Q_{12} as shown in Step 4 of Fig. 2.6.

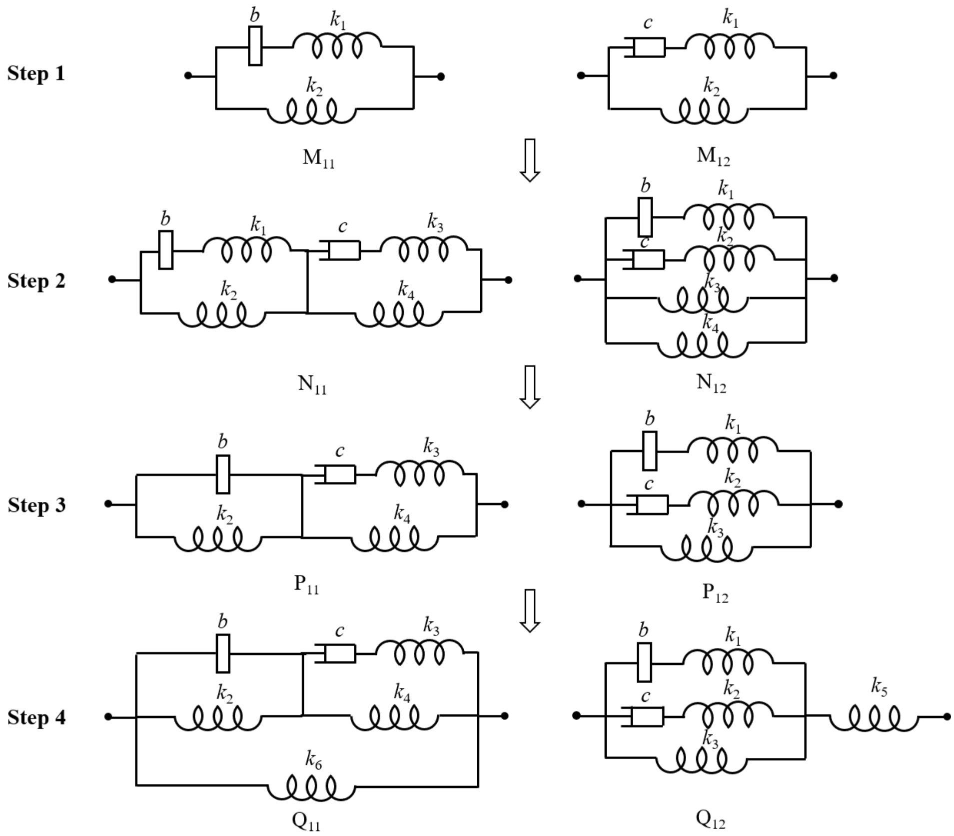

Fig. 2.6 Construction of the two-terminal generic networks for the 1k1c1b case

The structural admittances of the networks Q_{11} and Q_{12} are:

$$
\begin{aligned}
Y_{11}(s) &= \frac{bcs^2 + b(k_4 + k_6)s + c(k_2 + k_6)}{bc(1/k_3)s^3 + bs^2 + cs + k_2 + k_4} \\
Y_{12}(s) &= \frac{bc(1/k_1 + 1/k_2)s^3 + bs^2 + cs + k_3}{b(1/k_1 + 1/k_5)s^3 + c(1/k_2 + 1/k_5)s^2 + s}
\end{aligned}
\tag{2.8}
$$

For $Y_{11}(s)$, only one of k_2, $1/k_3$, k_4 and k_6 is positive and all the others should be equal to zero. Similarly, for $Y_{12}(s)$, only one of $1/k_1$, $1/k_2$, k_3 and $1/k_5$ is positive and all the others are equal to zero. In this way, $Y_{11}(s)$ and $Y_{12}(s)$ include the complete transfer function expressions of the one inerter, one damper and one spring combinations. These transfer functions can be used, along with the constraints listed here to find the optimal one spring, one inerter, one damper configuration subjected to a given application and objective function.

Networks of the two springs, one damper and one inerter case

For networks with two springs, one damper and one inerter (i.e. 2k1c1b case), there are, in total, 18 absorber layouts. By using the structure-immittance method, two networks termed as Q_{21} and Q_{22}, which contain the complete topological information of all 18 layouts, can be obtained. Similarly, 4 steps are needed to obtain the final networks Q_{21} and Q_{22}, as shown in Fig. 2.7. It should also be noted that at most two springs are present for the networks obtained in each step. Steps used to obtain Q_{21} and Q_{22} are similar to those used to obtain Q_{11} and Q_{12}, so they are not listed here.

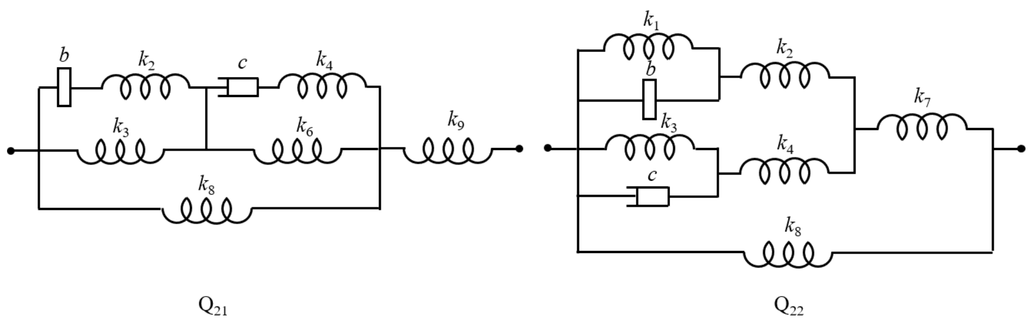

Fig. 2.7 Generic networks Q_{21} and Q_{22} for the 2k1c1b case

The structural admittances of networks Q_{21} and Q_{22} are:

$$Y_{2i}(s) = \frac{n_i(s)}{m_i(s)} \quad (i = 1, 2), \tag{2.9}$$

where

$$\begin{aligned}
n_1(s) =& bc(k_3/k_2 + k_8/k_2 + k_6/k_4 + k_8/k_4 + 1)s^3 + b(k_6 + k_8)s^2 + \\
& c(k_3 + k_8)s + k_3k_6 + k_3k_8 + k_6k_8, \\
m_1(s) =& s\Big[bc(1/k_2 + 1/k_4 + 1/k_9)s^3 + b(k_3/k_2 + k_6/k_2 + k_6/k_9 + k_8/k_9 + 1)s^2 + \\
& c(k_3/k_4 + k_3/k_9 + k_6/k_4 + k_8/k_9 + 1)s + k_3 + k_6\Big], \\
n_2(s) =& bc(1/k_2 + 1/k_4)s^3 + b(k_3/k_2 + k_3/k_4 + k_8/k_2 + k_8/k_7 + 1)s^2 + \\
& c(k_1/k_2 + k_8/k_4 + k_1/k_4 + k_8/k_7 + 1)s + k_1 + k_3 + k_8, \\
m_2(s) =& s\Big[bc(1/(k_2k_4) + 1/(k_2k_7) + 1/(k_4k_7))s^3 + b(1/k_2 + 1/k_7)s^2 + \\
& c(1/k_4 + 1/k_7)s + k_1/k_2 + k_1/k_7 + k_3/k_4 + k_3/k_7 + 1\Big].
\end{aligned}$$

$Y_{21}(s)$ and $Y_{22}(s)$ include the complete transfer functions of two springs, one damper and one inerter networks. For $Y_{21}(s)$, only two of $1/k_2$, k_3, $1/k_4$, k_6, k_8 and $1/k_9$ are positive and all the others are equal to zero. For $Y_{22}(s)$, only two of k_1, $1/k_2$, k_3, $1/k_4$, $1/k_7$ and k_8 are positive and all the others are equal to zero. These transfer functions can be used, along with the constraints listed here to find the optimal two springs, one damper and one inerter configuration subjected to a given application and objective function.

2.4 Summary of the chapter

A survey on conventional vibration suppression, inerter-based vibration suppression and network syntheis theory is presented in this chapter. Different vibration suppression techniques are reviewed and compared in Section 2.1, with an emphasis on the passive strategy due to its unique merits of simplicity, reliability and low costs. The newly introduced passive mechanical element, the inerter, has revolutionised the discipline of vibration suppression by vastly expanding the range of realisable absorber's layouts. A detailed review is provided in Section 2.2 on the origin of the inerter and its applications to various dynamic systems, including the automotive and railway vehicle suspension design, and the vibration mitigation of infrastructures such as buildings and wind turbines. With the completion of the electrical-mechanical analogy, network synthesis theory originally developed to realise electrical circuits can be directly applicable to mechanical systems to facilitate obtaining beneficial networks. A survey on the classical network synthesis, which was developed for electrical systems between twenties and seventies of last century, is given in Section 2.3.1. Studies during this period mainly focus on how to realise desired electrical networks with prescribed immittance function characteristics, where plenty of impressive theories were developed such as the Foster and Cauer canonical forms, Brune cycle, Bott-Duffin theorem, etc. However, since element number for mechanical networks is more critical than electrical ones, and none of the above theories addresses this problem, a more specific review on the network synthesis with the focus on minimal realisation is provided in Section 2.3.2, most of which was developed more recently with the consideration of inerter-based networks. Finally, a novel network realisation approach, named the structure-immittance approach, was introduce. This approach tackles the problem of how to realise a network using the least number of elements. This is achieved by proposing a generic network to cover a full set of one-port networks with a pre-determined element number. This approach significantly expanded the applicability of the inerter-based absorbers to practical engineering problems. A brief review of this approach is given in Section 2.3.3. All works reviewed in this chapter has facilitated our study on developing a systemic methodology to identify beneficial inerter-integrated vibration suppression systems with explicit network topology and complexity information.

Chapter 3

Generic 1PT1NG network with the application to offshore wind turbines

The concept of attaching an additional reaction mass to a dynamically excited system for the suppression of its oscillatory motion was amongst the first suggested passive vibration control strategies in the area of structural dynamics, and it remains popular today. In this context, the tuned mass damper (TMD) was introduced, which is a linear spring-mass-damper device to suppress excessive vibrations of a variety of engineering systems [9, 44, 10, 45]. Den-Hartog proposed an effective tuning approach [9] to determine the parameter values of the TMD to maximise its vibration suppression effects. Generally speaking, performance of the TMD will be improved as the mass of the TMD increasing. However, in most applications, the amount of mass that is acceptable to add to the original system is no more than 10% mass of the targeted vibration mode [21].

With the introduction of a novel passive mechanical element – the inerter [11], it is used to replace the mass element to fully achieve the force-current analogy [57]. Thus, for any two-terminal mechanical networks consisting of passive non-mass elements, the network synthesis theory (e.g. the Bott-Duffin theory [29]), developed in the electrical domain, can be used to facilitate a systematic mechanical network synthesis. However, compared to the electrical realisations, minimal realisation of a mechanical network is critical due to practical considerations around alignment, linkages and size. This has led to the structure-immittance approach [30] being proposed for devices consisting of the least possible number of non-mass elements (i.e., springs, dampers and inerters).

While the mass element still has its unique merit in terms of the vibration absorber design even with the presence of the inerter, as attaching absorbers' terminals physically to the ground might be unrealistic for many applications. When a reaction mass is included into the networks, a systematic approach becomes challenging, as the ideal lumped reaction mass has only one physical terminal (which is the centre of the mass, as shown in Fig. 3.1(a1)). Although many mass-included-inerter-based absorbers have been proposed, such as the viscous mass damper (VMD), the tuned viscous mass damper (TVMD) [22], and the tuned mass damper inerter (TMDI), they are all proposed in an *ad hoc* manner, which is termed the structure-based approach. There are still countless other connection possibilities, some of which might potentially provide much more advantageous performance.

In this study, a systematic approach is first proposed to characterise a full set of independent passive vibration absorbers. Such devices consist of one reaction mass and a pre-determined number of non-mass elements, and connect to the primary system with one attachment point. The mass element in the device can be treated as a special two-terminal element, with one terminal notionally connected to the ground, denoted as a notional-ground (NG), as shown in Fig. 3.1(a2). Mathematically, it is equivalent to an inerter with one of the two terminals physically connected to ground, as shown in Fig. 3.1(a3). The attachment point is treated as a physical terminal (PT) in the corresponding network representation.

In this chapter, we start with networks containing one PT and one NG (1PT1NG). Considering the fact that most independent vibration absorbers are used for uni-dimensional vibration suppression of the primary system, they normally have no more than two attachment points to the primary system. Therefore, in Chapter 4, we extend this approach to a certain type of 2PT1NG networks which possess a similar layout as the widely used TMDI. Later, based on the work developed in Chapter 4, a full set of 2PT1NG network representations will be introduced in Chapter 5. Thus, grouping Chapters 3, 4 and 5, a complete set of passive mechanical networks consisting of one reaction mass and a pre-determined number of springs, dampers and inerters connected in series-parallel with at most two PTs will be able to be systematically investigated.

Graph theory [127, 128] is employed here to facilitate the enumeration of topological connection possibilities. Using the proposed approach, optimum inerter-based absorbers can be obtained for given vibration suppression problems. Two 5MW offshore wind turbines are used to demonstrate the effectiveness of the proposed approach. The 1PT1NG network is implemented in an offshore wind turbine simulation tool, OpenFAST [129], to assess the performance of the identified beneficial inerter-based absorbers. A fixed-bottom monopile turbine and a floating spar-buoy turbine are investigated to show the performance improvements of the optimum IBAs under both normal operation and extreme loading conditions.

This chapter begins with the network representation of the reaction mass and the mass-included networks. Then the problem of identifying optimum mass-included vibration absorbers with one physical terminal is formulated. In Section 3.2, a generic 1PT1NG network is constructed, with all possible series-parallel 1PT1NG networks enumerated. Optimal absorber configurations are identified in Section 3.3 by using simplified linear monopile and spar-buoy models. In Section 3.4, the identified absorbers are assessed in OpenFAST under both normal operational and extreme loading conditions. In order to achieve such simulations, the implementation of the IBAs' transfer functions to OpenFAST is also introduced in Section 3.4. Finally, conclusions are drawn in Section 3.5.

The models and methods introduced in this chapter formed the basis for the following publications:

- Y.-Y. Li, S. Park, J. Z. Jiang, M. Lackner, S. Neild, I. Ward (2020). Vibration suppression for monopile and spar-buoy offshore wind turbines using the structure-immittance approach. Wind Energy, 23(10), 1966-1985.
- S.Y. Zhang, Y.-Y. Li, J. Z. Jiang, S. Neild, J. H. MacDonald (2019). A methodology for identifying optimum vibration absorbers with a reaction mass. Proceedings of the Royal Society A, 475(2228), 20190232.
- Y.-Y. Li, S.Y. Zhang, J. Z. Jiang, S. Neild, I. Ward (2018 September). Passive vibration control of offshore wind turbines using structure-immittance approach. *In Proceedings of the International Conference on Noise and Vibration Engineering.*
- Y.-Y. Li, S.Y. Zhang, J. Z. Jiang, S. Neild (2018 June). Vibration Suppression Using a Passive Reaction Mass Incorporating Inerters in a Multi-storey Building. *In 16th European Conference on Earthquake Engineering.*

The systematic approach is developed together by Yi-Yuan Li and Dr. Sara Ying Zhang. The implementation of the 1PT1NG network to OpenFAST is finished by Yi-Yuan Li with supports from Dr. Semyung Park and Dr. Matthew Lackner. Dr Jason Zheng Jiang, Prof. Simon Neild, Prof. John MacDonald and Ian Ward have provided valuable suggestions on this research.

3.1 Problem formulation

Following Newton's Second Law, an ideal lumped reaction mass has only one physical terminal (which is the centre of the mass, as shown in Fig. 3.1(a1)). In order for network synthesis to be directly applicable to the systematic enumeration of vibration absorbers with a reaction mass, it is necessary to treat the mass as a special two-terminal element, with one terminal notionally connected to the ground, denoted as a notional-ground (NG). Note it is not actually connected to ground, in contrast to an electrically grounded capacitor which is equivalent in the force-current analogy [11]. The network representation of the mass is shown in Fig. 3.1(a2), with the property that $F(s) = m(sV_m - 0)$, where V_m is the velocity of the mass with its value defined as positive to the right. Accordingly, in this work, terminals connected to physical attachments are denoted as physical-terminals (PTs) when considering their network representations. Mathematically a mass element is equivalent to an inerter with one of the two terminals physically connected to ground, see Fig. 3.1(a3). However, the mass element has its unique merit since attaching absorbers' terminals physically to the ground is unrealistic for a lot of applications.

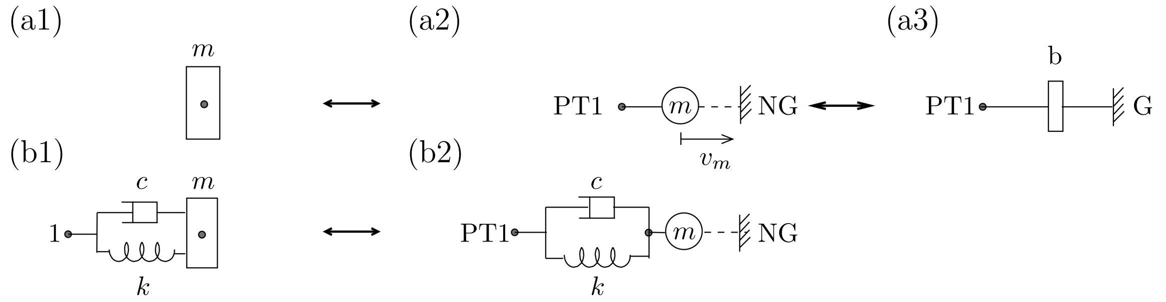

Fig. 3.1 Absorber schematic plots and their network representations: (a1) a reaction mass with (a2) its network representation, and (a3) an inerter with one terminal connected to ground (G); (b1) The TMD with its network representation (b2).

With the proposed network representation of a mass element (Fig. 3.1(a2)), the vibration absorber TMD (Fig. 3.1(b1)) can be depicted as a network, as shown in Fig. 3.1(b2). By denoting the absorber attachment point 1 as PT1 in the network representation, the TMD with one attachment point becomes a two-terminal network with one PT and one NG, termed a '1PT1NG network'. Similarly, the non-mass absorbers with two attachment points are termed '2PT networks'. Note that the spring, damper and inerter elements can be regarded as special cases of 2PT networks, and are termed '2PT elements'. The 1PT1NG network, represented by its force-velocity transfer function $H(s) = F_1(s)/V_1(s)$

is shown in Fig. 3.2(a), where at the PT1, the force f_1 ($F_1(s)$ in the Laplace domain) is applied and results in a velocity v_1 ($V_1(s)$).

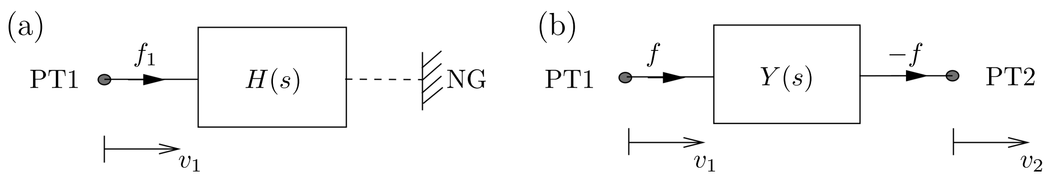

Fig. 3.2 (a) 1PT1NG network; (b) 2PT network.

In order to enumerate all possible series-parallel 1PT1NG network layouts given one reation mass and an arbitrary number of inerters, dampers and springs, procedures to construct 1PT1NG Immittance-Function-Networks (IF-Networks) need to be introduced. Here, an IF-Network refers to a network layout with its 2PT sub-networks represented by Immittance-Function-Blocks (IF-Block, e.g. Fig. 3.2(b)). Generic IF-Networks which capture all IF-Network possibilities for given conditions will be identified. Different distribution cases of the pre-determined numbers of inerters, dampers and springs in the IF-Blocks of the generic IF-Network will then be discussed, to obtain all possible series-parallel 1PT1NG network layouts.

3.2 1PT1NG network layout enumeration

This section considers the 1PT1NG network layouts with a reaction mass. The series and parallel connections between a 2PT network (represented by an IF-Block) and a 1PT1NG network are first described using concepts defined in graph theory [128]. A generic IF-network is then formulated, from which all possible 1PT1NG networks with a pre-determined number of 2PT elements can be enumerated.

3.2.1 Connection between 2PT and 1PT1NG networks

In the electrical domain [130], a graph is used as a general representation of topological connections, consisting of a finite number of vertices and branches. Here the correspondence between graphs and mechanical networks are introduced.

A graph $G = (V, E)$ is a pair consisting of a finite set V whose elements are vertices, and a finite set E, which are paired vertices with elements called branches (or edges) [127]. For a two-terminal mechanical network with specific connection topology, it can be represented as a graph, by depicting each element of the network as a branch, and the two terminals and internal connection points as vertices, with a set of branches interconnected at their vertices. For example, consider a network with only one mechanical element, such as the spring shown in Fig. 3.3(a1), this can be represented as a graph with one branch - Fig. 3.3(b1), where two vertices shown as solid circles correspond to the two PTs, termed the terminal-vertices. The graph representation of an example 2PT network, the TID in Fig. 3.3(a2), is provided in Fig. 3.3(b2). In this example, an intersection vertex exists, shown as a hollow circle, representing the inter-connected node of the TID. Considering the TMD (Fig. 3.3(a3)) as a 1PT1NG network example, its graph is shown in Fig. 3.3(b3) with one terminal-vertex corresponding to a NG in the mechanical domain. In this way, all 2PT and 1PT1NG networks can be represented as a graph with two terminal-vertices.

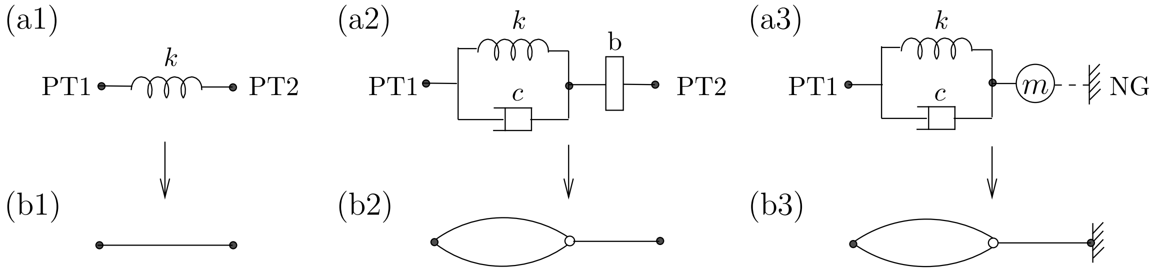

Fig. 3.3 Example two-terminal mechanical networks and their corresponding graphs: (a1) a spring, (a2) the TID, (a3) the TMD, and (b1), (b2), (b3) the corresponding graphs.

In [128], the series and parallel connections between graphs with two terminal-vertices are defined. It states that the series connection is to coalesce one terminal-vertex of each graph into an intersection-vertex of the resulting two-terminal graph, of which the two terminal-vertices are the remaining ones of the two connected graphs. On the other hand, a parallel connection is where two terminal-vertices of each graph are connected together to formulate the two terminal-vertices of the resulting two-terminal graph. Note that both these connection types can only be applied to terminal-vertices. Based on this definition, we consider joining a 2PT network with a 1PT1NG network. Taking the graphs of Fig. 3.4(a1) and (a2) as an example, we can note that only the series-connection is possible, as a parallel connection would necessitate a NG being connected with a PT. The series connection between these two graphs results in the graph shown in Fig. 3.4(a3). The three graphs, Fig. 3.4(a1-a3), can correspond to the three general network representations shown in Fig. 3.4(b1-b3), where $Y(s)$ is an IF-Block representing any possible series-parallel 2PT network and $H(s)$ is a 1PT1NG network. As an example, by depicting the IF-Block $Y(s)$ as a spring (Fig. 3.4(c1)) and the 1PT1NG network $H(s)$

as a TMD of Fig. 3.4(c2), the series connection between them formulates the network shown in Fig. 3.4(c3).

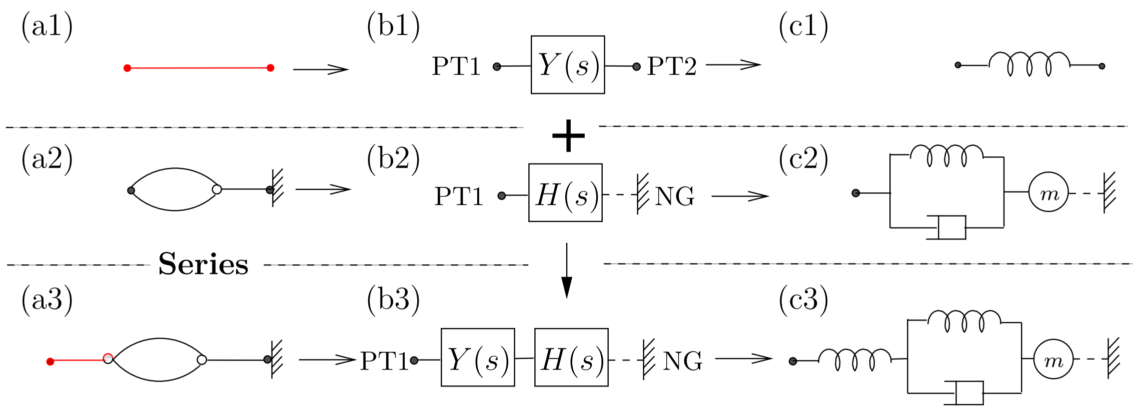

Fig. 3.4 Example series connection between a 2PT network and a 1PT1NG network, represented as connections between (a) graphs, (b) IF-Networks, (c) example network layouts.

3.2.2 Network layout enumeration using the generic 1PT1NG IF-Network

In order to formulate series-parallel 1PT1NG IF-Networks, a collection of one reaction mass and a finite number of IF-Blocks is now considered. A non-unique connection sequence is proposed, with which all possible 1PT1NG IF-Networks can be obtained. In the procedure, after each step, any obvious network simplification will be carried out. For example, if two IF-Blocks are connected in series or in parallel, they will be *reduced* to a single IF-Block. The terminology *reduced* is used here to indicate that the IF-Network can be simplified by combining adjacent IF-Blocks as a single IF-Block based on the series-parallel connection principle. Start with a single IF-Block, it can be connected in series or in parallel with other IF-Blocks, however, these always reduce to a single IF-Block. At a certain step, the resulting IF-Block is connected to the mass, based on Fig. 3.4, where only a series connection is possible, resulting in a new 1PT1NG network. Further addition of IF-Blocks can only be connected in series with this 1PT1NG network, which can be *reduced* to a single IF-Block. Hence, all IF-Networks can be represented by the generic IF-Network shown in Fig. 3.5 with a single IF-Block $Y(s)$.

Consider the 1PT1NG network layouts with one reaction mass and a pre-determined number, N, of 2PT elements. All network possibilities can be obtained using the generic IF-Network in Fig. 3.5, by enumerating the full class of 2PT network possibilities

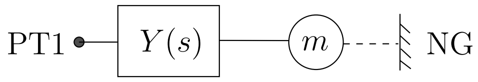

Fig. 3.5 The generic 1PT1NG IF-Network.

consisting of N elements in the IF-Block $Y(s)$. To this end, the structure-immittance approach [30], developed to systematically express all possible series-parallel networks with pre-determined number of 2PT elements, can be directly applied. The obtained structural admittance $Y(s)$ is then used to express the transfer function of the generic IF-Network (see Fig. 3.5) as:

$$H(s) = \frac{Y(s)ms}{ms + Y(s)} \tag{3.1}$$

With this transfer function, the optimum 1PT1NG inerter-based absorber (IBA) with one reaction mass can be identified for a given vibration suppression problem. In this chapter, offshore wind turbine (OWT) systems are employed to demonstrate the advantages of the proposed generic 1PT1NG network. First, simplified linear OWT models are established to identify beneficial 1PT1NG absorber configurations. The performance advantages will then be verified by using OpenFAST – a nonlinear aero-hydro-servo-elastic coupled simulation tool developed by the National Renewable Energy Laboratory (NREL) [129].

3.3 Identification of beneficial 1PT1NG absorbers for offshore wind turbines

In OpenFAST, the NREL 5-MW wind turbine [131] is adopted as the default turbine model, which is a conventional three-bladed, upwind, variable-speed, blade-pitch-to-feather-controlled turbine. This 5-MW turbine model is a representative utility-scale multi-megawatt turbine and has been used as the reference model in a variety of wind turbine studies [5, 132–134, 25]. It can be modelled with different support structures, including the monopile, jacket, tripod, barge, spar-buoy, or tension-leg-platform. Throughout this study, the dynamics of a monopile and a spar-buoy turbine are investigated and the performance of the IBAs are assessed. This assessment will be across a family of 1PT1NG network layouts given certain network complexity in terms of component numbers and types. It should be noted that the optimum network configurations can also be identified by carrying out the optimisation within OpenFAST, but this is not computationally feasible. For example, a simulation with 10 minutes time length requires around 5 minutes of the calculation time using a desktop computer with processor of 3.40 GHz and 16.0 GB

RAM was used to conduct the computational procedure. Moreover, to find the optimum values, thousands of function calls might be needed, with numerous candidate absorber layouts considered as well. Therefore, simplified linear models are needed in order to identify the optimum 1PT1NG networks.

3.3.1 Linear offshore wind turbine models

Fig. 3.6(a) and (b), respectively, show linear monopile and spar-buoy wind turbine model, where the absorbers are represented by the 1PT1NG networks with a connection point to the nacelle of the turbines.

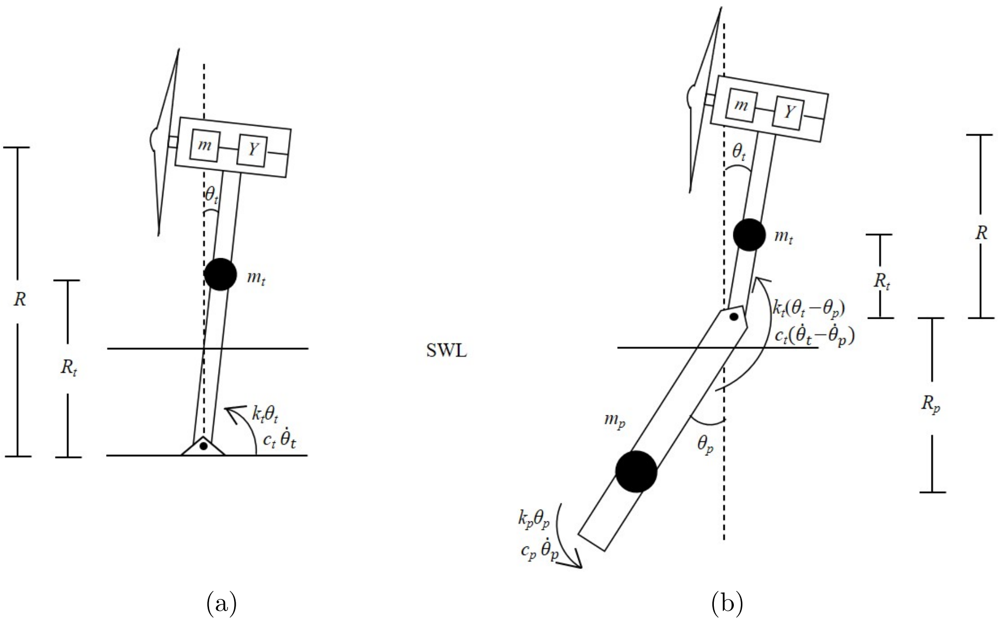

Fig. 3.6 Simplified linear offshore wind turbine models following [5]: (a) the monopile turbine; (b) the spar-buoy turbine.

Monopile Wind Turbine Model

The 5-MW wind turbine is first connected to a monopile platform which has a constant diameter of 6 m and a constant thickness of 0.060 m. The tower base begins at an elevation of 10 m above the still-water level (SWL) and the monopile extends from the tower base down to the mudline, which is 20 m below the SWL [135].

Following the previous work [5], a simplified linear monopile turbine model is established based on the above stated OpenFAST monopile turbine model. The tower fore-aft bending mode is responsible for the most of the fatigue loads, hence two degrees-of-freedom (DOFs) are considered here: the tower fore-aft bending DOF and the absorber's reaction mass DOF. Due to the gravity effects of the reaction mass under rotational movements, instead of using a single equation to represent the monopile system by employing $H(s)$ as an expression shown in Eq. 3.1, it is more straightforward to represent the system with two equations of motion by considering the reaction mass as an additional DOF and including $Y(s)$ in the equations of motion. Section 3.2 serves the purpose to prove that the absorber layouts shown in Fig. 3.6 cover all possible 1PT1NG networks. Applying the small angle approximation and considering the absorber in the non-inertial reference frame, equations of motion of the monopile turbine system are given in the Laplace domain:

$$\begin{cases} m\tilde{x}_r(s)s^2 = & mg\tilde{\theta}_t(s) - Y(s)\tilde{x}_r(s)s - mR\tilde{\theta}_t(s)s^2 \\ I_t\tilde{\theta}_t(s)s^2 = & m_t g R_t \tilde{\theta}_t(s) + RY(s)\tilde{x}_r(s)s - (k_t + c_t s)\tilde{\theta}_t(s) + mg\tilde{x}_r(s) + M_{wind/wave} \end{cases} \tag{3.2}$$

where m_t is the turbine's total mass and m is the absorber's mass. $M_{wind/wave}$ is the input wind/wave moment to the monopile turbine. The angle that the tower has deflected from vertical is denoted by θ_t. The nacelle of the OWT is considered as a reference frame and the displacement of the absorber x_r is relative to the nacelle. So the term $mR\tilde{\theta}_t(s)s^2$ exists due to the non-inertial reference frame. Note that $\tilde{\theta}_t(s)$ and $\tilde{x}_r(s)$ are the Laplace domain expression of $\theta_t(t)$ and $x_r(t)$. R and R_t are the distances from the tower hinge to the absorber's mass and the centre of the turbine total mass, respectively. k_t and c_t are the rotary stiffness and rotary damping constants at the tower base. $Y(s)$ is the representation of the transfer function of an absorber consisting of inerters, dampers and springs. The absorber's mass m is taken to be equal to 10000 kg, which is approximately 1% of the turbine's total mass m_t.

First, model parameters must be determined. I_t, m_t, R_t and R can be obtained from [135, 136] and the OpenFAST input files, which are summarised in Table 3.1. The rotary stiffness k_t and the rotary damping c_t need to be determined by matching the linear model response to the OpenFAST output under the same input conditions. Here an initial condition of the tower top displacement (TTD) equal to 1 m is used in OpenFAST, which is the amount of tower bending in meters measured at the top of tower. The response of the linear model is fit to the OpenFAST output in MATLAB® by minimising the root-mean-square of the discrepancy between the OpenFAST output and the linear model response. *patternsearch* and *fminsearch* command in MATLAB® are used to identify the optimum parameter values with *fminsearch* refining the results obtained via *patternsearch*. Results of the TTD for the monopile turbine model in the time and frequency domains are shown in Fig. 3.7(a) and (b), respectively. The frequency domain response is obtained by applying the Fast Fourier Transform (FFT) to the time domain response. The resulting rotary stiffness and damping values are identified as $k_t = 1.32 \times 10^{10}$ N·m/rad and $c_t = 2.65 \times 10^7$ N·m·s/rad, respectively. It should be noted that all the DOFs are activated in OpenFAST to make sure the modal frequencies of the OWT system are captured accurately. It can be seen from Fig. 3.7(a) that there are certain discrepancies in the first 30 s. This is mainly caused by the presence of a flexible foundation in the full model (i.e. use *CompSub* in OpenFAST). In this case, the first 30 s response is omitted when fitting the simplified linear model with the OpenFAST response in order to neglect the foundation dynamics. Moreover, non-zero mean responses causes the non-zero value at 0 Hz of the frequency domain response as shown in Fig. 3.7(b). This is mainly because the nacelle mass centre is not aligned with the tower mass centreline in OpenFAST, which results in a constant moment applied to the tower base. Furthermore, it can be noted from Fig. 3.7(b) that the monopile turbine oscillates at a frequency of approximately 0.28 Hz.

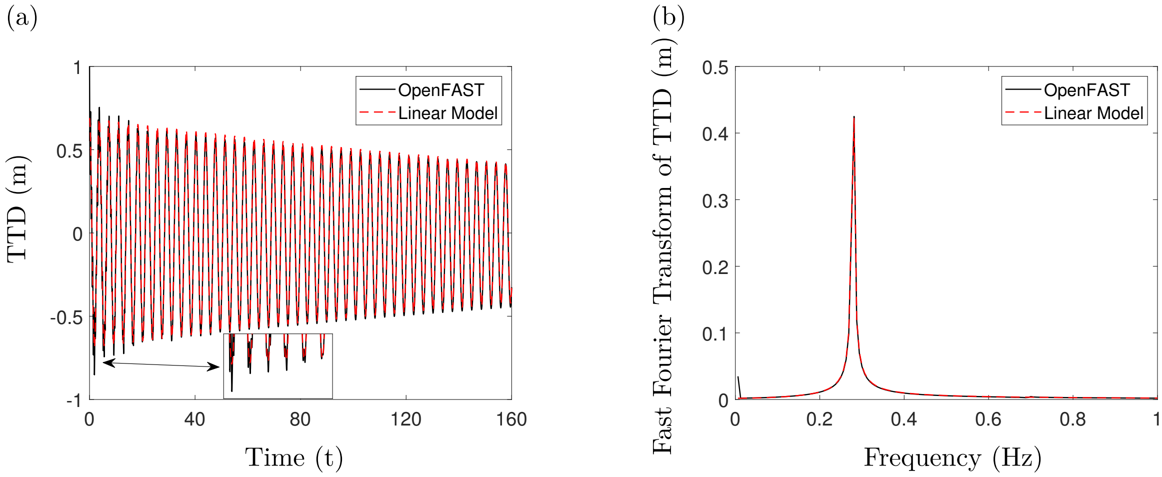

Fig. 3.7 Comparison of the tower top displacement (TTD) responses of the monopile turbine by employing the linear model and OpenFAST in (a) the time domain; (b) the frequency domain.

Spar-buoy Wind Turbine Model

In OpenFAST, the NREL 5-MW turbine can be coupled with a spar-buoy floating platform called 'Hywind'. This platform was originally developed by the company – Statoil. The turbine tower is cantilevered at an elevation of 10 m above the still-water level to the top of the floating platform. The length of the platform is 120 m and its mass is centred at 89.92 m along the platform centreline below the still-water level [137].

Table 3.1 Parameter values of the linear monopile and spar-buoy turbine models

Properties	**monopile turbine**	**spar-buoy turbine**
Total turbine mass m_t	929,397 kg	656,498 kg
Absorber's mass m	10,000 kg	10,000 kg
Tower inertia I_t	4.30×10^9 kg·m^2	2.73×10^9 kg·m^2
Platform mass m_p	/	7,466,330 kg
platform inertia I_p	/	1.54×10^{11} kg·m^2
Turbine's height to tower hinge R	107.6 m	77.6 m
Turbine mass centre to tower hinge R_t	67.997 m	64.5 m
Platform mass centre to tower hinge R_p	/	-99.9155 m
Rotary stiffness of the tower k_t	1.32×10^{10} N·m/rad	2.43×10^{10} N·m/rad
Rotary damping of the tower c_t	2.65×10^7 N·m·s/rad	1.02×10^8 N·m·s/rad
Rotary stiffness of the platform k_p	/	0 N·m/rad
Rotary damping of the platform c_p	/	3.55×10^9 N·m·s/rad
Dominant mode frequencies	0.28 Hz	0.035 Hz, 0.48 Hz

The simplified linear spar-buoy turbine model is established accordingly. Here the tower fore-aft bending and platform pitch modes are responsible for the most of the fatigue loading. Therefore, three DOFs are of concern: the tower fore-aft bending DOF, the platform pitch DOF and the absorber's mass DOF. Similarly, after applying the small angle approximation and considering the absorber in the non-inertial reference frame, equations of motion of the spar-buoy system in the Laplace domain are:

$$\begin{cases} m\tilde{x}_r(s)s^2 = mg\tilde{\theta}_t(s) - Y(s)\tilde{x}_r(s)s - mR\tilde{\theta}_t(s)s^2 \\ I_t\tilde{\theta}_t(s)s^2 = m_tgR_t\tilde{\theta}_t(s) + RY(s)\tilde{x}_r(s)s - (k_t + c_ts)(\tilde{\theta}_t(s) - \tilde{\theta}_p(s)) + mg\tilde{x}_r(s) + M_{wind} \\ I_p\tilde{\theta}_p(s)s^2 = -m_pgR_p\tilde{\theta}_p(s) + (k_t + c_ts)(\tilde{\theta}_t(s) - \tilde{\theta}_p(s)) - (k_p + c_ps)\tilde{\theta}_p(s) + M_{wave} \end{cases} \tag{3.3}$$

where m_p is the mass of the platform and I_p is the inertia of the platform; $\theta_p(t)$ is the angle that the platform has rotated from vertical and $\tilde{\theta}_p(s)$ is the corresponding Laplace expression; R_p is the distance from the tower hinge to the centre of the platform mass; k_p and c_p are the rotary stiffness and damping constants of the spar-buoy platform, which are the summation of hydrostatic and mooring line effects. All the other parameters have the same definitions as those used for the linear monopile turbine model. Note that according to the definition in OpenFAST, tower top displacement is relative to the platform coordinate system. This means that if the platform is pitched while there is no bending of the tower, then the tower top displacement is zero.

Again, the model parameters must be determined first. m_t, I_t, m_p, R, R_t and R_p can be obtained from the definition of 5-MW spar-buoy wind turbine [137] and the OpenFAST input files. Detailed information is also summarised in Table 3.1. The tower and platform rotary stiffness and damping constants, k_t, c_t, k_p and c_p, are identified by fitting the response from the linear model to that from OpenFAST. In addition, the platform inertia I_p needs to be identified. This is because the inertial effect of the water must be included in I_p. The platform inertia shown in the OpenFAST input file is the true platform inertia, whereas movement of the platform through the water will cause substantial added inertial effect, which should be considered in the simplified model. Since the added inertial effect varies little across oscillation frequency [137], it is regarded as constant here. For the spar-buoy turbine, an initial condition of the platform pitch angle (PPA) equal to 5° is used to obtain the FAST output. Fig. 3.8(a) and (c)

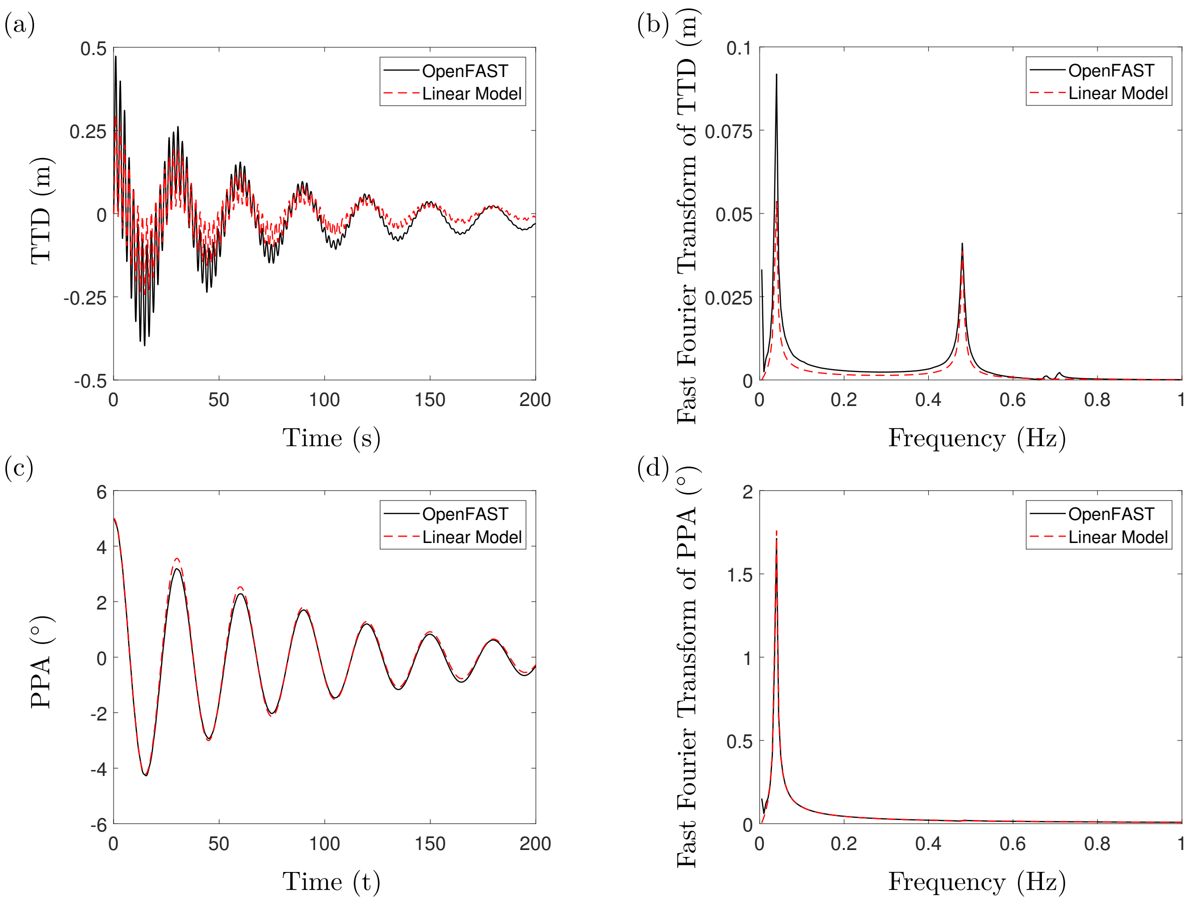

Fig. 3.8 Comparison of the spar-buoy turbine responses employing the linear model and OpenFAST with tower top displacement (TTD) in (a) the time domain; (b) the frequency domain; and with platform pitch angle (PPA) in (c) the time domain; (d) the frequency domain.

show the fitted plot for the tower top displacement and the platform pitch angle of the spar-buoy turbine. The same identification approach as the one used in the monopile turbine linear model is employed here to obtain the spar-buoy turbine parameters. Their corresponding frequency responses are shown in panels (b) and (d). Again, since the nacelle mass centre is not along the tower and platform mass centreline in OpenFAST, non-zero mean responses are obtained, which cause the non-zero value at 0 Hz of the frequency domain responses as shown in Fig. 3.8(b) and (d). Note that the fit between the simplified model and OpenFAST is not perfect. This is mainly caused by: (1) the surge and heave DOFs are important for the dynamics of the spar-buoy turbine [132]. Frequency of the heave mode is around 0.035 Hz, which is close to the platform pitch mode frequency, and hence will affect the responses; (2) the platform rotary damping constant c_p includes hydrodynamic damping, wave radiation and viscous damping. These terms are nonlinear, so the approximated linear damping constants used in the linear model leads to discrepancies. A more accurate 5-DOF model has been developed by Si *et al.* [132]. However, this model is not adopted here. As the passive absorbers used in this study are tuned to the system natural frequencies, optimisation results will be representative as long as the frequency of each mode of the main system is accurate. It can be seen from Fig. 3.8(b) and (d) that the frequencies for both the platform pitch (0.035 Hz) and the tower fore-aft bending (0.48 Hz) modes are accurately captured, hence the linear spar-buoy turbine model is maintained as 2 DOFs for simplicity. The resulting rotary stiffness and damping constants of the tower and platform are $k_t = 2.43 \times 10^{10}$ N·m/rad, $c_t = 1.02 \times 10^8$ N·m·s/rad, $k_p \approx 0$ N·m/rad and $c_p = 3.55 \times 10^9$ N·m·s/rad, respectively. Identification results indicate that the platform pitch stiffness is not provided by the external rotary stiffness k_p. Instead, it is mainly provided by the gravity of the platform.

3.3.2 Cost functions and constraints for the optimisation

For the monopile turbine, the tower top displacement is taken as the performance index as it is deleterious to the tower fatigue life. The objective function is defined as the H_2 norm of the transfer function from the wind/wave load input $M_{wind/wave}$ to the tower rotational angle output $\tilde{\theta}_t(s)$, denoted as $T_{M_{Wind/Wave} \to \tilde{\theta}_t(s)}$ (T stands for 'Transfer Function'), which can be obtained from Eq.3.2. The static stiffness of IBAs is limited to be no less than the static stiffness of the TMD to constrain the maximum displacement of IBAs due to the space limitation within the turbine nacelle:

$$\begin{aligned} &J = ||T_{M_{Wind/Wave} \to \tilde{\theta}_t(s)}||_2 \\ &\text{where} \\ &(Y_{IBA}(s) \times s)_{s \to 0} \geqslant (Y_{TMD}(s) \times s)_{s \to 0} \end{aligned} \tag{3.4}$$

The H_2 norm of the transfer function represents the root-mean-square of the impulse response of a linear dynamic system. $Y_{TMD}(s)$ and $Y_{IBA}(s)$ represent the transfer functions of the TMD and the IBA, respectively, from the relative terminal velocity to the force across the devices. Therefore, $(Y_{TMD}(s) \times s)_{s \to 0}$ and $(Y_{IBA}(s) \times s)_{s \to 0}$ represent the static stiffness of the TMD and the IBA, respectively. In the previous study [5], the maximum strokes for the TMD have been pointed out: ± 8 m in the fore-aft direction, and ± 2.5 m in the side-side direction, which are also checked for the IBAs in this study.

For the spar-buoy turbine, since there are two independent outputs for the main system (i.e. $\tilde{\theta}_t(s)$ and $\tilde{\theta}_p(s)$), and two inputs to the main system (i.e. M_{Wind} and M_{Wave}), it is a multi-input-multi-output (MIMO) system. Moreover, depending on the definition in OpenFAST, the tower top displacement is the tower top movement relative to the platform movement (i.e. $(\tilde{\theta}_t(s) - \tilde{\theta}_p(s))$). Hence six transfer functions, $T_{M_{Wind} \to \tilde{\theta}_t(s)}$, $T_{M_{Wave} \to \tilde{\theta}_t(s)}$, $T_{M_{Wind} \to \tilde{\theta}_p(s)}$, $T_{M_{Wave} \to \tilde{\theta}_p(s)}$, $T_{M_{Wind} \to (\tilde{\theta}_t(s) - \tilde{\theta}_p(s))}$, $T_{M_{Wave} \to (\tilde{\theta}_t(s) - \tilde{\theta}_p(s))}$, are derived as shown in Fig. 3.9, where no device is deployed. Since the tower base bending moment is crucial to the tower fatigue life, the tower top displacement is taken as the performance index, and the objective function is defined as:

$$\begin{aligned} &J = ||T_{M_{Wind} \to (\tilde{\theta}_t(s) - \tilde{\theta}_p(s))}||_2 + ||T_{M_{Wave} \to (\tilde{\theta}_t(s) - \tilde{\theta}_p(s))}||_2 \\ &\text{where} \\ &(Y_{IBA}(s) \times s)_{s \to 0} \geqslant (Y_{TMD}(s) \times s)_{s \to 0} \end{aligned} \tag{3.5}$$

which is the sum of H_2 norm of transfer functions from wind and wave load inputs to the tower relative rotational angle with the same static stiffness constraints as the one used for the monopile turbine. In this study, objective functions are optimised using a combination of *patternsearch* and *fminsearch* in MATLAB® with *fminsearch* refining the results obtained via *patternsearch*. Same approach is used for all other optimisations conducted in this dissertation. Although *patternsearch* and *fminsearch* are both local optimisation algorithms and they could possibly lead to local minima for the non-convex optimisation problems stated in each chapter, it could potentially be avoided with a proper setting of the optimisation parameters (such as the maximum mesh size of the *patternsearch* and the maximum iteration steps of both algorithms). Moreover, there is always a trade-off between the optimisation accuracy and the consumed time. We choose to use these algorithms because they are proved to be effective optimisation tools to find the optimum results, and have been widely used, see for example [17, 138, 78]. Other software with effective optimisation algorithms, such as the particle swarm optimisation [139], can also be used for the optimisation procedure.

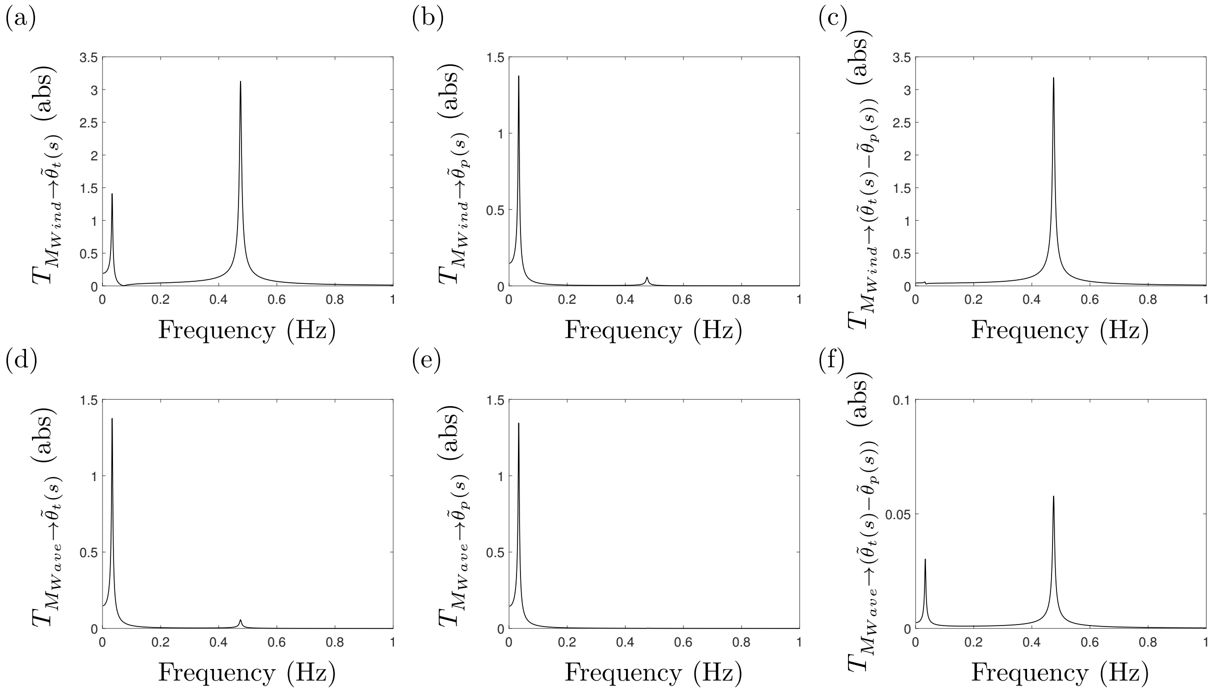

Fig. 3.9 Transfer functions of the spar-buoy turbine tower absolute rotate angle ($\tilde{\theta}_t(s)$), platform absolute rotate angle ($\tilde{\theta}_p(s)$) and tower relative rotate angle ($\tilde{\theta}_t(s) - \tilde{\theta}_p(s)$) with respect to the wind input (i.e.(a), (b) and (c)) and the wave input (i.e. (d), (e) and (f)).

3.3.3 Beneficial inerter-based absorber configurations

In this section, optimisations are conducted in the frequency domain with the conventional vibration absorber, the TMD, considered as the benchmark for comparison. The absorber's reaction mass is taken as 10000 kg for both TMD and IBA. By employing the structure-immittance approach [30], IBAs with no more than 6 elements are considered for both the monopile and spar-buoy turbines. For 3-element IBAs, all 1 spring, 1 damper and 1 inerter combinations (totally 2 generic networks covering 8 layouts) are considered; 4-element IBAs with all 2 springs, 1 damper and 1 inerter (totally 2 generic networks covering 18 layouts) are considered; IBAs with 2 springs, 2 dampers and 1 inerter are considered as the 5-element case (totally 8 generic networks covering 79 layouts); finally

6-element IBAs consider a certain range of 3 springs, 1 damper and 2 inerters (regarded as one spring paralleled to all 2 springs, 1 damper and 2 inerters case (totally 8 generic networks covering 79 layouts). Using the objective functions defined in Eqs.3.4 and 3.5 for the monopile and spar-buoy turbine models, respectively, the IBAs with no more than 6 elements are investigated.

Beneficial absorber configurations with no more than 4 elements

For IBAs containing 3 elements or less, optimisation results show that there is no further improvements can be obtained compared to the TMD. For IBAs containing 4 elements (2 springs, 1 damper, 1 inerter), IBA_{4E1} is obtained for both the monopile and spar-buoy turbines, with its layouts shown in Fig. 3.10. Optimisation results and its parameter values are shown in Table 3.2 and Table 3.3 correspondingly, with the TMD as a benchmark. Here, as the full range of 4-element layouts are considered, we found that IBA_{4E2}, IBA_{4E3} and IBA_{4E4} can provide the same performance improvement (i.e. 6.5% and 5.8% for the monopile and spar-buoy turbines, respectively) as the IBA_{4E1}. This indicates that, with more beneficial IBA layouts identified by using the structure-immittance approach, wider design choices to realise the IBA can be obtained for its practical applications. We also notice that the IBA_{4E2} is the layout proposed in the previous study [26] on wind turbine vibration suppression, which serves as an evidence for the fact that the IBA layouts obtained by the structure-based approach can be regarded as a subset of the ones obtained through the structure-immittance approach. For simplicity, parameter values of the IBA_{4E2}, IBA_{4E3} and IBA_{4E4} are not displayed here. It is worth mentioning that the IBA_{4E1} and IBA_{4E2} are topologically equivalent to the two piezoelectric proof-mass absorbers studied by Høgsberg [140], where similar level of improvements compared with TMD have been reported.

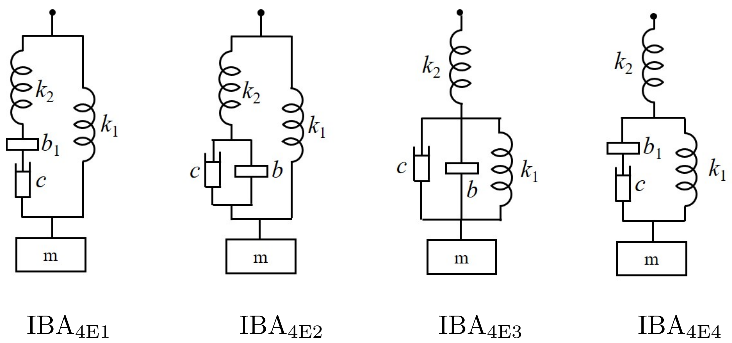

Fig. 3.10 The identified beneficial 4-element IBA layouts with same performance improvements (i.e. 6.5% for the monopile turbine and 5.8% for the spar-buoy turbine) by employing the generic 1PT1NG network.

Table 3.2 Optimisation results for the linear monopile turbine model

Absorber	TMD	$\text{IBA}_{4\text{E}1}$	$\text{IBA}_{6\text{E}1}$
J	0.248	0.232	0.230
Mass value (kg)	10000	10000	10000
Improvement	/	6.5%	7.3%
k_1 **(kN/m)**	28.1	28.3	28.3
k_2 **(kN/m)**	/	1.64	1.05
k_3 **(kN/m)**	/	/	0.081
c**(kN·s/m)**	2.81	3.26	0.126
b_1 **(kg)**	/	563.4	27.8
b_2 **(kg)**	/	/	345.2

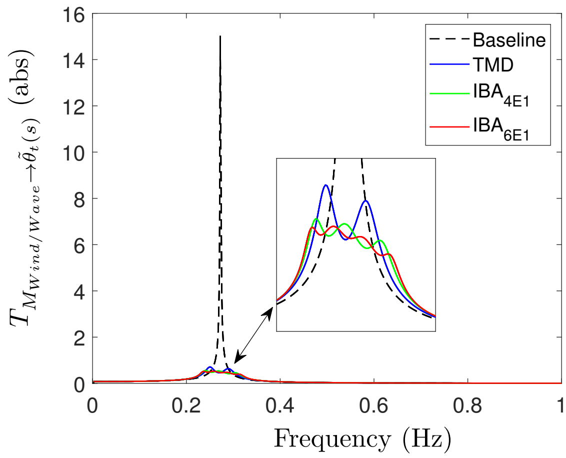

Fig. 3.11 Transfer function plots of the monopile turbine tower rotational angle $\tilde{\theta}_t(s)$ with respect to the wind/wave input considering the baseline, TMD, $\text{IBA}_{4\text{E}1}$ and $\text{IBA}_{6\text{E}1}$.

Frequency response plots of the tower top motion with the TMD and the beneficial IBAs employed for the monopile and spar-buoy turbines are shown in Fig. 3.11 and 3.12, respectively. Tower top responses without an absorber included are also shown as the baseline (black dashed line) in Fig. 3.11 and 3.12. The response without an absorber highlights the effectiveness of employing passive vibration absorbers. Note that the aim of this study is to improve the performance of the traditional passive vibration absorber TMD, therefore, all improvements obtained in this chapter are compared to the TMD rather than the case without an absorber. It can be observed that the frequency of the tower fore-aft mode is split into two peaks by the TMD, where its natural frequency is 0.265 Hz. $\text{IBA}_{4\text{E}1}$ have further split the tower fore-aft mode into three peaks. Natural frequencies of it are 0.245 Hz and 0.296 Hz. Similarly for the spar-buoy turbine, the TMD and the IBA_{4E1} have split the tower fore-aft mode into two and three peaks, respectively, with natural frequency of the TMD as 0.467 Hz, of the IBA_{4E1} as 0.433 Hz and 0.512 Hz. It should be noted that, unlike the results provided by Den Hartog [9] and Krenk [45], the tuned two peaks by employing the TMD are not entirely flat. This is because, for the classical Den Hartog tuning approach and the relatively new equal modal damping concept proposed by Krenk, the objective is to minimise the H_∞ norm of the system responses in the frequency domain. This is achieved by setting the dynamic amplification at two specific frequencies equal. In contrast, this study adopts the H_2 norm of the system responses as the objective function, as the H_2 norm is more relevant to the damage equivalent fatigue load. Therefore the dynamic amplifications at these two specific frequencies do not have to be equal anymore.

Table 3.3 Optimisation results for the linear spar-buoy turbine model

Absorber	TMD	IBA_{4E1}	IBA_{6E3}
Mass value (kg)	10000	10000	10000
J	0.173	0.163	0.162
Improvement	/	5.8%	6.4%
k_1 **(kN/m)**	86.1	86.6	85.7
k_2 **(kN/m)**	/	3.96	3.43
k_3 **(kN/m)**	/	/	1.91
c**(kN·s/m)**	4.35	5.09	4.53
b_1 **(kg)**	/	447.5	145
b_2 **(kg)**	/	/	421.7

Beneficial absorber configurations with 5 and 6 elements

For IBAs with 5 elements (2 springs, 2 dampers, 1 inerter), it shows that the 5-element IBAs always reduce to 4-element IBAs with one damper not functioning for no matter the monopile or the spar-buoy offshore wind turbines. Therefore, performance improvements provided by the 5-element IBAs as shown in [25] all can be replaced by 4-element IBAs. According to Den Hartog's tuning method [9], for a TMD, the ratio of the stiffness over mass results in the additional resonant points (introducing an additional peak), and the damping value adjusts the amplitude of these peaks. With more spring-inerter pair introduced, more resonant points (either target one modal frequency or multiple modal frequencies) could be introduced. With more modes targeted, more dampers can be

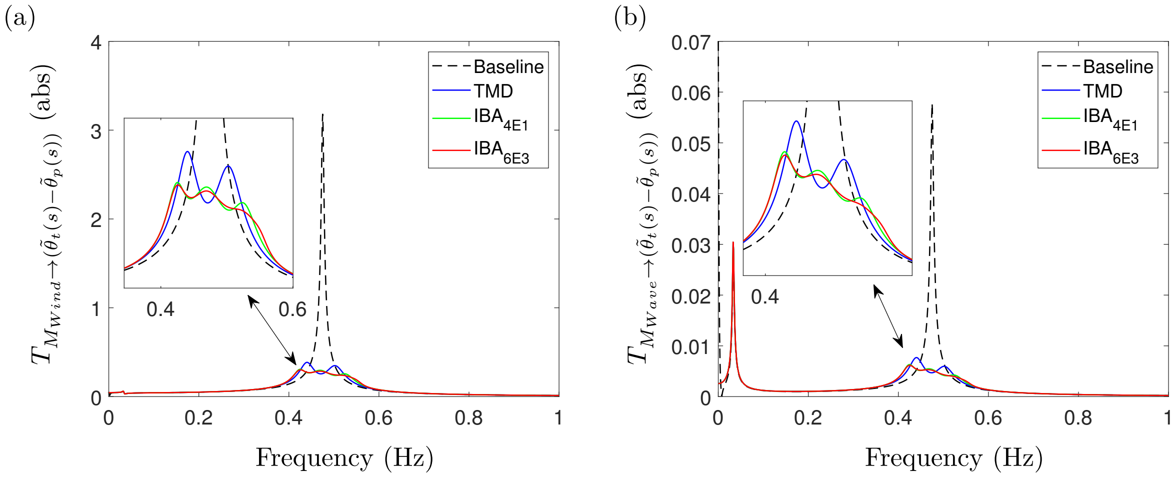

Fig. 3.12 Transfer function plots of the spar-buoy turbine tower relative rotational angle $(\tilde{\theta}_t(s) - \tilde{\theta}_p(s))$ considering the baseline, TMD, $\mathrm{IBA_{4E1}}$ and $\mathrm{IBA_{6E3}}$ with respect to (a) the wind input; (b) the wave input.

expected to adjust the peaks at each mode. While for this specific wind turbine system, the identified absorbers are all tuned to one modal frequency. That's why we suspect only one damper would be sufficient to adjust these peaks at this modal frequency. If the identified networks target more frequencies, more dampers might be needed. For 6-element IBA layouts, a certain range of 3 springs, 1 damper and 2 inerters combinations is considered (considered as one spring paralleled to all 2 springs, 1 damper and 2 inerters case). Employing the structure-immittance approach, beneficial IBAs with the same performance improvements (i.e. 7.3% and 6.5% for the monopile and spar-buoy turbines, respectively) are obtained. Their layouts are shown in Fig. 3.13, with $\mathrm{IBA_{6E1}}$ and $\mathrm{IBA_{6E2}}$ for the monopile turbine and $\mathrm{IBA_{6E3}}$ and $\mathrm{IBA_{6E4}}$ for the spar-buoy turbine. Optimisation results are also shown in Table 3.2 and Table 3.3 for the monopile and spar-buoy, respectively, where only the $\mathrm{IBA_{6E1}}$ and $\mathrm{IBA_{6E3}}$ are displayed for simplicity.

Again, frequency response plots of the monopile and spar-buoy turbines tower top motion with the $\mathrm{IBA_{6E1}}$ and $\mathrm{IBA_{6E3}}$ are shown in Fig. 3.11 and Fig. 3.12, respectively. It can be seen that the tower fore-aft mode of the monopile turbine is further split into four peaks by the $\mathrm{IBA_{6E1}}$ with its natural frequencies at 0.238 Hz, 0.272 Hz and 0.311 Hz. Similarly, the tower fore-aft mode of the spar-buoy turbine is also split by $\mathrm{IBA_{6E3}}$ to four peaks with natural frequencies at 0.432 Hz, 0.510 Hz and 0.556 Hz. Therefore, we can conclude that with extra introduced DOFs within the absorber, the IBAs have the ability of further tuning a specific mode of the main system. However, it should also be noted that with more elements introduced, the combined nonlinearity of the complete network might be more significant, which could degrade the system performance. For example, as stated in [1, 62], the rack-and-pinion inerters and ball-screw inerters are more easily suffering from detrimental breaks due to friction, backlash and elastic effects, producing potentially unquantifiable system nonlinearities and degrade the absorber's performance. Moreover, Dall'Asta, *et al.* [141] showed that the viscous damper nonlinearity level strongly affects the example building performance, and different system dynamic trends are observed for the demand parameters of interest. Therefore, nonlinearities of each element and their combined effects might have great impact on the overall system dynamics and could potentially degrade system performance. Such nonlinear effect should be fully investigated before they are used for practical engineering applications, which can be considered as the future work.

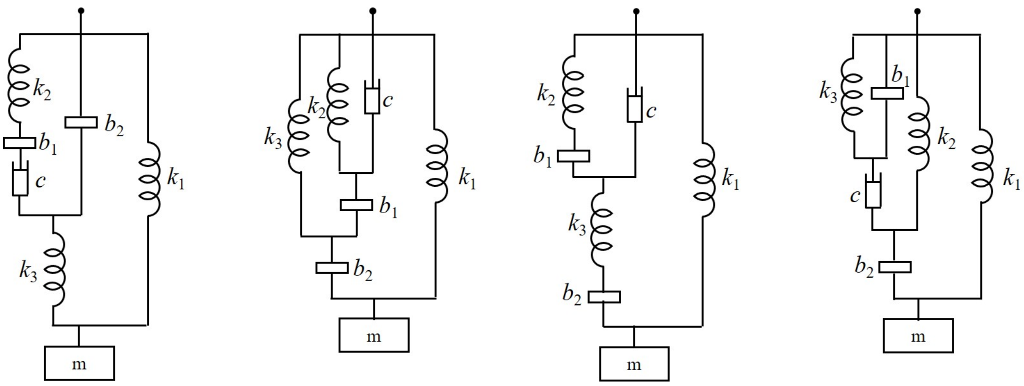

IBA_{6E1} IBA_{6E2} IBA_{6E3} IBA_{6E4}

Fig. 3.13 The identified beneficial 6-element IBA layouts with the same performance improvements (i.e. 7.3% for the monopile turbine and 6.4% for the spar-buoy turbine) by employing the generic 1PT1NG network.

To view the significance of these improvements, the mass value reductions of the identified IBAs to achieve the same performance as the TMD are now considered. In general, the performance improvements will increase as the IBAs' mass increases. However, diminishing returns can be seen in this trend, as shown in Fig. 3.14. Fig. 3.14(a) and (b) show the relationships between the performance index J and the optimum IBAs mass values for the monopile and spar-buoy turbines, respectively. The absorber's mass value varies from 0 kg to 20000 kg. Results show that the mass value of the IBA_{6E1} for the monopile turbine can be reduced by 25.1% (i.e., 7486 kg) to achieve the same performance as the TMD - this requires an optimum stiffness of $k_1 = 21.3\,\mathrm{kN/m}$, $k_2 = 0.123\,\mathrm{kN/m}$, $k_3 = 0.795\,\mathrm{kN/m}$, damping of $c = 0.101\,\mathrm{kNm/s}$ and inertance of $b_1 = 40.3\,\mathrm{kg}$, $b_2 = 257.7\,\mathrm{kg}$. The mass value of the the IBA_{6E3} required for the spar-buoy turbine in order to achieve the same performance as the TMD is 23.2% (i.e. 7680 kg) lower. The resulting optimum parameter values are $k_1 = 66.3$ kN/m, $k_2 = 6.00$ kN/m, $k_3 = 2.62$ kN/m, $c = 3.49$ kNm/s and inertance $b_1 = 157.2$ kg, $b_2 = 312.0$ kg.

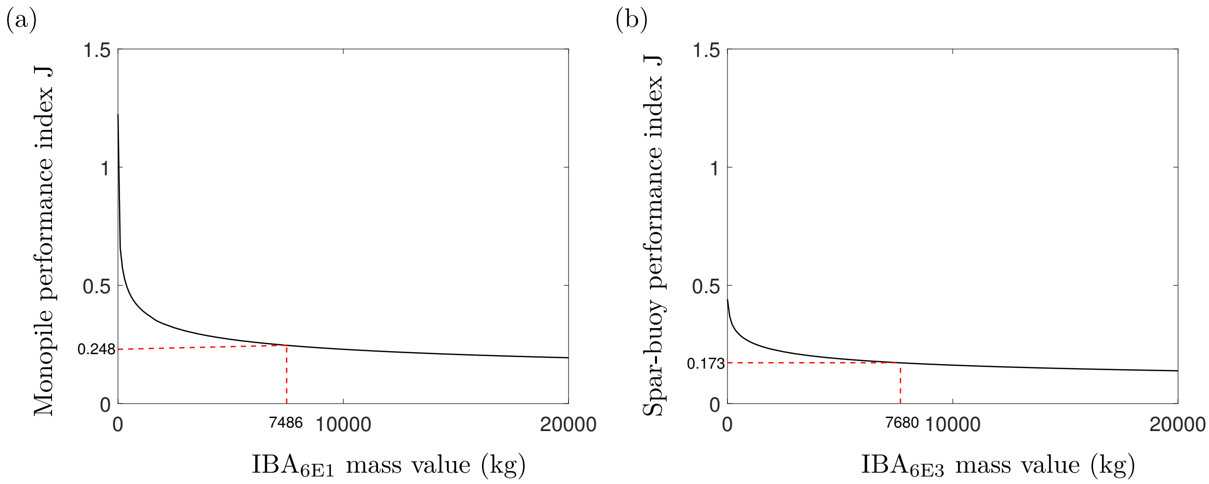

Fig. 3.14 Relationships of the optimum IBAs' mass values and the turbine performance index J for (a) the monopile turbine; (b) the spar-buoy turbine, where the reduced mass values are 7486 kg and 7680 kg for the $\text{IBA}_{6\text{E}1}$ and $\text{IBA}_{6\text{E}3}$, respectively, to achieve the same performance as the TMD with 10000 kg mass value.

3.4 Performance assessment in realistic metocean external conditions

The above mentioned optimisations are all based on the simplified linear turbine models. To show the performance improvements of the IBAs for the vibration mitigation of offshore wind turbines, it is necessary to verify the obtained optimisation results in OpenFAST, where more realistic models can be used with representative wind and wave loading considered. First, the source code of OpenFAST is modified to allow the fully exploration of the performance of a whole range of IBAs, which is described by the transfer functions representing its two-terminal properties. Then, simulations are conducted in OpenFAST under normal operation and extreme conditions for offshore wind turbines supported by the monopile and the spar-buoy platform. For the normal operation and extreme conditions, fatigue limit state (FLS) and ultimate limit state (ULS) are considered, respectively.

3.4.1 Implementation of inerter-based absorbers in OpenFAST

In order to implement structural control techniques in offshore wind turbines, two independent, single-DOF TMD systems are incorporated in FASTv7 by Lackner and Rotea [142], named "FAST-SC". The new version source code, OpenFAST, allows for a modular approach to model the turbine dynamics, and thus an additional TMD module has been coupled to the original code. Unlike the previous version of FAST-SC (one dimension motion), the new TMD module in OpenFAST is capable of modelling either two independent, single-DOF TMDs that can oscillate in their respective direction or a single pendulum TMD that can oscillate in two dimensions. The pendulum TMD modelled in the TMD module can be utilised as a passive device with constant parameters or semi-actively in which the damping force can be controlled [143]. In this study, the TMD module in OpenFAST is modified in order to include all potential IBAs, where the modified module is named as the IBA module. Note that only the two independent, single-DOF IBA systems are modified to include the IBAs so far.

Based on the property of an IBA, $Y'(s)$ is defined as the transfer function from force to acceleration:

$$Y'(s) \quad = \quad \frac{Y(s)}{s} = \frac{F(s)}{\Delta a(s)} \tag{3.6}$$

For a passive absorber, $Y'(s)$ is always positive-real [144], hence it can be written as one of the non-unique canonical state-space form:

$$Y'(s) \quad = \quad \mathbf{c}_1(s\mathbf{I} - \mathbf{A}_1)^{-1}\mathbf{b}_1 + d_1 \tag{3.7}$$

where $\mathbf{A}_1 \in \mathbb{R}^{N\times N}$, $\mathbf{b}_1 \in \mathbb{R}^{N\times 1}$, $\mathbf{c}_1 \in \mathbb{R}^{1\times N}$ and d_1 are the state matrix, input vector, output vector and feed-forward, respectively. N is the dimension of the internal states $\boldsymbol{\omega}_f$ (i.e. internal DOFs) of IBAs. These internal states $\boldsymbol{\omega}_f \in \mathbb{R}^{N\times 1}$ and output force F_f of $Y'(s)$ can be represented as follows,

$$\dot{\boldsymbol{\omega}}_f \quad = \quad \mathbf{A}_1\boldsymbol{\omega}_f + \mathbf{b}_1\ddot{x} \tag{3.8}$$

$$F_f \quad = \quad \mathbf{c}_1\boldsymbol{\omega}_f + d_1\ddot{x} \tag{3.9}$$

x is the displacement of the absorber's mass m, therefore $\ddot{x}$ is the corresponding acceleration, which is also the relative acceleration across the network's two terminals considering the other terminal is not moving within the reference frame of this subsystem, hence the IBA system input in the time domain (i.e., $\mathcal{L}(\ddot{x} - 0) = s^2x(s) - 0 = \Delta a(s)$). A derivative of the force can be obtained by substituting Eq.(3.8) into Eq.(3.9):

$$\begin{aligned} \dot{F}_f &= \mathbf{c}_1 \dot{\boldsymbol{\omega}}_f + d_1 \dddot{x} \\ &= \mathbf{c}_1(\mathbf{A}_1 \boldsymbol{\omega}_f + \mathbf{b}_1 \ddot{x}) + d_1 \dddot{x} \end{aligned} \tag{3.10}$$

Combining the IBA's mass states with its ficitious states $\boldsymbol{\omega}_f$, the entire IBA system can be rewritten in state-space form in the time domain. Transfer functions of different IBAs can then be included in OpenFAST. A detailed procedure is shown in Appendix A. Then, results of the absorber's mass movements simulated by the IBA module are compared to the responses from MATLAB with a constant force applied. Here only the displacement and velocity of the $\text{IBA}_{6\text{E}1}$ are shown in Fig. 3.15 for simplicity. It can be obtained that the responses simulated by the IBA module are the same as the ones from MATLAB, which justifies the implementation procedure. Note that the simulation is valid only when the absorber has all zero initial conditions as stated in Appendix A, which is most of the case where the absorber starts to move from the rest.

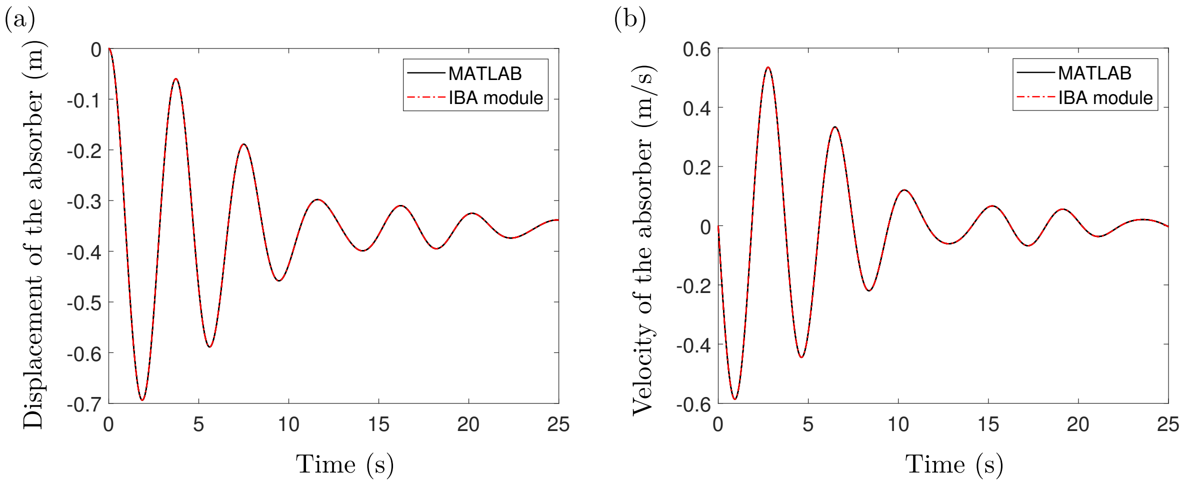

Fig. 3.15 (a) The displacement and (b) the velocity responses of the $\text{IBA}_{6\text{E}1}$ under a constant force input.

3.4.2 Assessment of the monopile turbine response in realistic metocean conditions

An investigation of the impact of the TMD and IBAs for the monopile turbine is conducted by considering a set of FLS and ULS design load cases (DLCs). The DLCs are chosen based on the data gathered from the Dutch North Sea [145] where the relevant design parameters and methods within the design basis are taken from the IEC-61400-3 standard [146]. Conditions for the FLS and ULS analysis are defined by DLC 1.2 and 6.1a, respectively. Detailed information can be found in Table 3.4. The FLS analysis models normal power production conditions of the offshore wind turbines with mean wind speed varies from 4 m/s to 24 m/s with bins of 4 m/s. Each simulation lasts 660 s with the first 60 s omitted [147] to guarantee the generator torque and the blade pitch motion are in their normal operational states. The ULS cases model extreme conditions such as storms that occur rarely, but may cause failure of the structure. Under extreme conditions, the wind turbine rotor is shutdown, and the blades are pitched to feather. The simulation time is 1 hour for extreme load conditions. For the monopile turbine, the water depth is considered as 20 m.

Table 3.4 External conditions of DLC 1.2 (FLS) and DLC 6.1a (ULS).

DLC	Wind Speed (m/s)	Turb. Int. (%)	blade pitch angle (°)	Wave Height (m)	Peak Period (s)	Percentage time per year (%)
1.2 (FLS)	4	20.4	0	1.10	5.88	11.90
	8	16.0	0	1.31	5.67	16.48
	12	14.6	3.83	1.70	5.88	12.29
	16	13.9	12.06	2.19	6.37	5.86
	20	13.4	17.47	2.76	6.99	1.88
	24	13.1	22.35	3.42	7.80	0.41
6.1a (ULS)	41.5	11.7	90	4.9	9.43	0.003

Monopile turbine FLS analysis

By applying the external condition of DLC 1.2 listed in Table 3.4, FLS analysis results of the monopile turbine are obtained and shown in Table 3.5. Mlife [148] is employed to calculate the Damage Equivalent Loads (DELs). Since the wind turbine does not experience an equal amount of time for each wind speed in practice, performance indices in this section are weighted according to the Weibull distribution based on the UpWind Project [145]. An example result for the monopile turbine responses at a 16 m/s wind speed are illustrated in Fig. 3.16. Here the Power Spectral Density (PSD) of the tower top responses in the fore-aft and side-to-side directions are shown in Fig. 3.16(a) and (d), which are calculated by the *pwelch* function in MATLAB with the window number chosen as 8. Corresponding time domain responses are shown in Fig. 3.16(b) and (e). Narrowed time domain responses are also shown in Fig. 3.16(c) and (f). Since the performance difference between the $\mathrm{IBA}_{4\mathrm{E}1}$ and $\mathrm{IBA}_{6\mathrm{E}1}$ are not significant, only the responses with the TMD and $\mathrm{IBA}_{6\mathrm{E}1}$ are shown. It can be seen that the $\mathrm{IBA}_{6\mathrm{E}1}$ has the ability to further suppress the mode of the monopile turbine at around 0.3 Hz, which is the natural frequency of the tower fore-aft and side-to-side bending modes. $\mathrm{IBA}_{4\mathrm{E}1}$ can reduce the DELs by 0.9% and 5.4% in the fore-aft and side-to-side direction, respectively, compared to the TMD. $\mathrm{IBA}_{6\mathrm{E}1}$ can further reduce the DELs by 1.0% and 5.8%.

Results show that IBAs are more effective in the side-to-side direction, which is thought to be because there is less aerodynamic damping in this direction. The absorber stroke is also assessed under the FLS analysis. For the TMD, the maximum stroke for wind speeds under 24m/s is 2.38 m in the fore-aft direction and 0.55 m in the side-to-side direction. While for the $\mathrm{IBA}_{4\mathrm{E}1}$ and $\mathrm{IBA}_{6\mathrm{E}1}$, the maximum stroke is 2.82 m and 2.94 m in the fore-aft direction, 0.68 m and 0.68 m in the side-to-side direction, respectively. It can be seen that by limiting the static stiffness of the IBAs, even though strokes of the IBAs are slightly larger than the TMD, they are still within the space limits of the turbine nacelle. Moreover, the mass optimisation obtained from Section 3.3 is also verified in OpenFAST. Results show that, with a reduced mass value of 7486 kg, the $\mathrm{IBA}_{6\mathrm{E}1}$ can provide similar performance as the optimum TMD with a 10000 kg mass in both the fore-aft and the side-to-side direction. Therefore, the identified IBA is potentially beneficial for the offshore wind turbine applications in practice.

Monopile turbine ULS analysis

Simulations subjected to the DLC 6.1a are also performed for the optimised TMD and IBAs, where performance metrics are defined as the absolute maximum tower top displacement and tower base bending moment of each simulation averaged over six different random simulations.

The amplitude of the tower top displacement and tower base bending moment in the frequency domain (around 0.2 Hz-0.4 Hz) are included in Fig. 3.17 for comparison. Results are shown in Table 3.6. It can be observed that the IBAs can reduce the maximum tower bending moment by up to 2.4% and 1.4% in the fore-aft and side-to-side directions,

Table 3.5 Monopile turbine FLS analysis results

Wind Speed	**Fore-aft tower base fatigue load (kNm)**			**Side-to-side tower base fatigue load (kNm)**		
	TMD	**IBA_{4E1}**	**IBA_{6E1}**	**TMD**	**IBA_{4E1}**	**IBA_{6E1}**
4	2575	2525	2523	106.0	102.0	101.8
8	7790	7714	7713	718.0	681.9	679.4
12	12896	12809	12810	754.6	713.6	710.8
16	13833	13671	13660	1447	1359	1350
20	26170	26013	26018	1754	1656	1646
24	19008	18686	18664	4122	3914	3894
Aggregated	455475	451173	451090	35834	33904	33748
Improvements	-	0.9%	1.0%	-	5.4%	5.8%

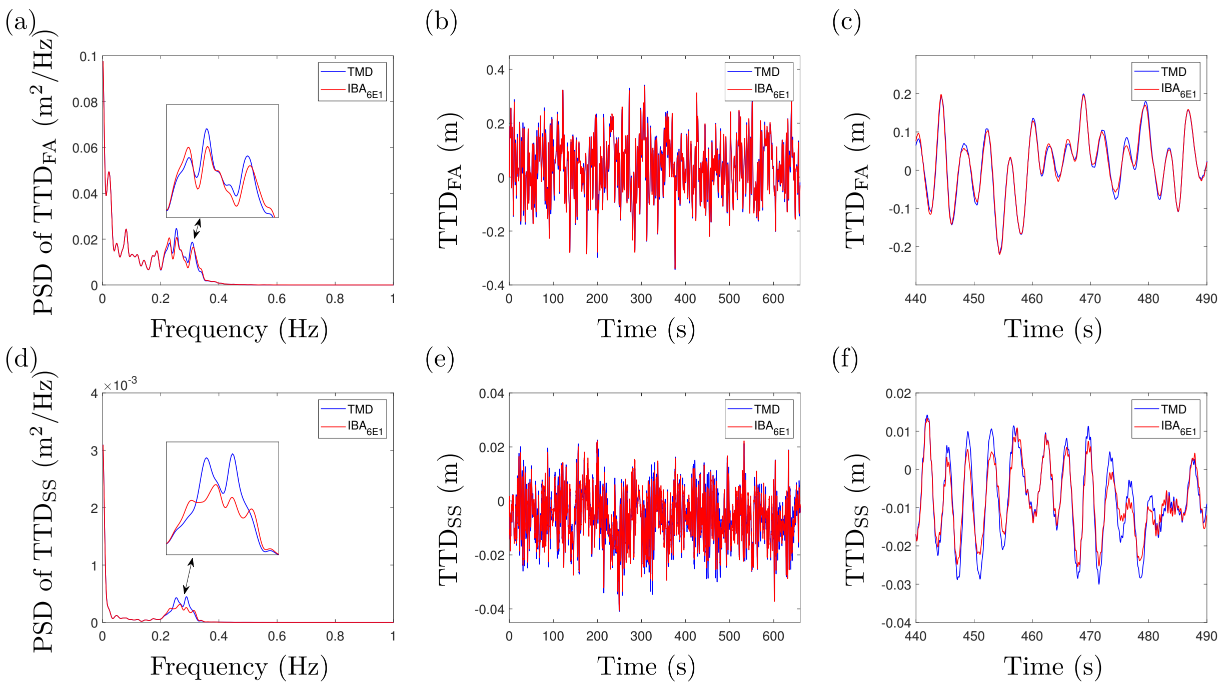

Fig. 3.16 Frequency domain responses (left), time domain responses (middle) and narrowed time windows responses (right) of the monopile turbine tower top displacement (TTD) under the DLC 1.2 (16 m/s wind speed) in the fore-aft (FA) direction ((a), (b), (c)) and in the side-to-side (SS) direction ((d), (e), (f)).

respectively. Moreover, the amplitude reduction of the tower bending mode in the frequency domain is more significant, which can be up to 37.0% and 27.4% in the fore-aft and side-to-side directions, respectively. The Power Spectral Density of one of the ULS simulation results is shown in Fig. 3.17(a) and (b) via *pwelch* with 36 windows. It can be observed that both IBAs are effective in suppressing the tower bending mode, around 0.28 Hz, under the extreme load case. As the blades are all feathered, drag forces and aerodynamic damping become larger in the side-to-side direction. This explains why the performance is better in the fore-aft direction while the absolute values are larger in the side-to-side direction, which is contrast to the situation under normal operational conditions.

Table 3.6 Monopile turbine ULS analysis results

Evaluation type	**Evaluation index**	**TMD**	**IBA$_{4E1}$ (Imp.)**	**IBA$_{6E1}$ (Imp.)**
Time domain responses	Max TTD fore-aft (m)	0.284	0.275 (3.0%)	0.274 (3.4%)
	Max TTD side-side (m)	0.551	0.546 (0.9%)	0.543 (1.4%)
	Max tower bending moment fore-aft (kN·m)	50323	49122 (2.4%)	49159 (2.3%)
	Max tower bending moment side-side (kN·m)	86084	85262 (1.0%)	84880 (1.4%)
PSD of the responses (between 0.2-0.4 Hz)	Amplitude TTD fore-aft (m^2/Hz)	0.0144	0.0092 (36.3%)	0.0090 (37.2%)
	Amplitude TTD side-side (m^2/Hz)	0.0878	0.0673 (23.4%)	0.0638 (27.4%)
	Amplitude tower bending moment fore-aft ((kN·m)^2/Hz)	3.52×10^8	2.25×10^8 (36.1%)	2.22×10^8 (37.0%)
	Amplitude tower bending moment side-side ((kN·m)^2/Hz)	2.15×10^9	1.64×10^9 (23.5%)	1.56×10^9 (27.4%)

3.4.3 Assessment of the spar-buoy turbine response in realistic metocean conditions

The impact of the optimised TMD and IBAs under FLS and ULS analysis is assessed for the spar-buoy turbine by considering the same DLCs as for the monopile turbine (listed in Table 3.4). Only a different water depth (320 m) is considered for the spar-buoy turbine.

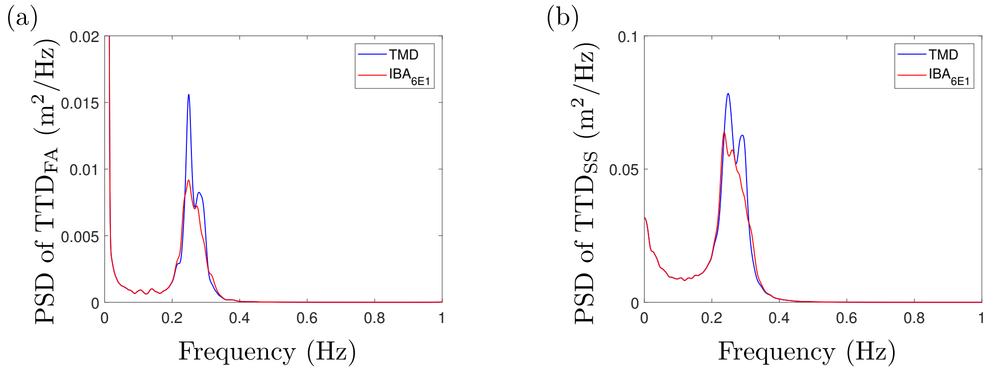

Fig. 3.17 Frequency domain responses of the monopile turbine tower top displacements (TTD) under DLC 6.1a in the (a) fore-aft (FA) direction, and (b) side-to-side (SS) direction.

Spar-buoy turbine FLS analysis

Following the same procedure as outlined in Section 3.4.2, FLS analysis results of the spar-buoy turbine are obtained and listed in Table 3.7. The aggregated DELs with the same Weibull distribution are also calculated. Simulation results of the wind turbine responses when subjected to an average wind speed of 16 m/s are illustrated in Fig. 3.18.

Table 3.7 Spar-buoy turbine FLS analysis results

Wind Speed	**Fore-aft tower base fatigue load (kNm)**			**Side-to-side tower base fatigue load (kNm)**		
	TMD	**IBA$_{4E1}$**	**IBA$_{6E3}$**	**TMD**	**IBA$_{4E1}$**	**IBA$_{6E3}$**
4	4569	4555	4525	186.3	178.8	175.8
8	8597	8568	8559	659.3	644.0	642.9
12	12861	12761	12808	838.3	821.5	821.1
16	14006	13836	13927	1457	1405	1404
20	23563	23373	23440	2526	2362	2366
24	18636	18558	18493	3848	3720	3717
Aggregated	488022	484764	485458	38249	37037	36979
Improvements	-	0.7%	0.5%	-	3.2%	3.3%

The Power Spectral Density (PSD) of the tower top displacement in the fore-aft, side-to-side directions and platform pitch movement are shown in Fig. 3.18(a), (d) and (g), with a same window number as the one used in the monopile turbine FLS analysis. Their corresponding time domain responses are shown in Fig. 3.18(b), (e) and (h). Narrowed time window responses are also shown in Fig. 3.18(c), (f), (i). Again, only responses with the TMD and IBA_{6E3} are illustrated in the figures due to the moderate performance improvements of the IBA_{6E3} compared to IBA_{4E1}.

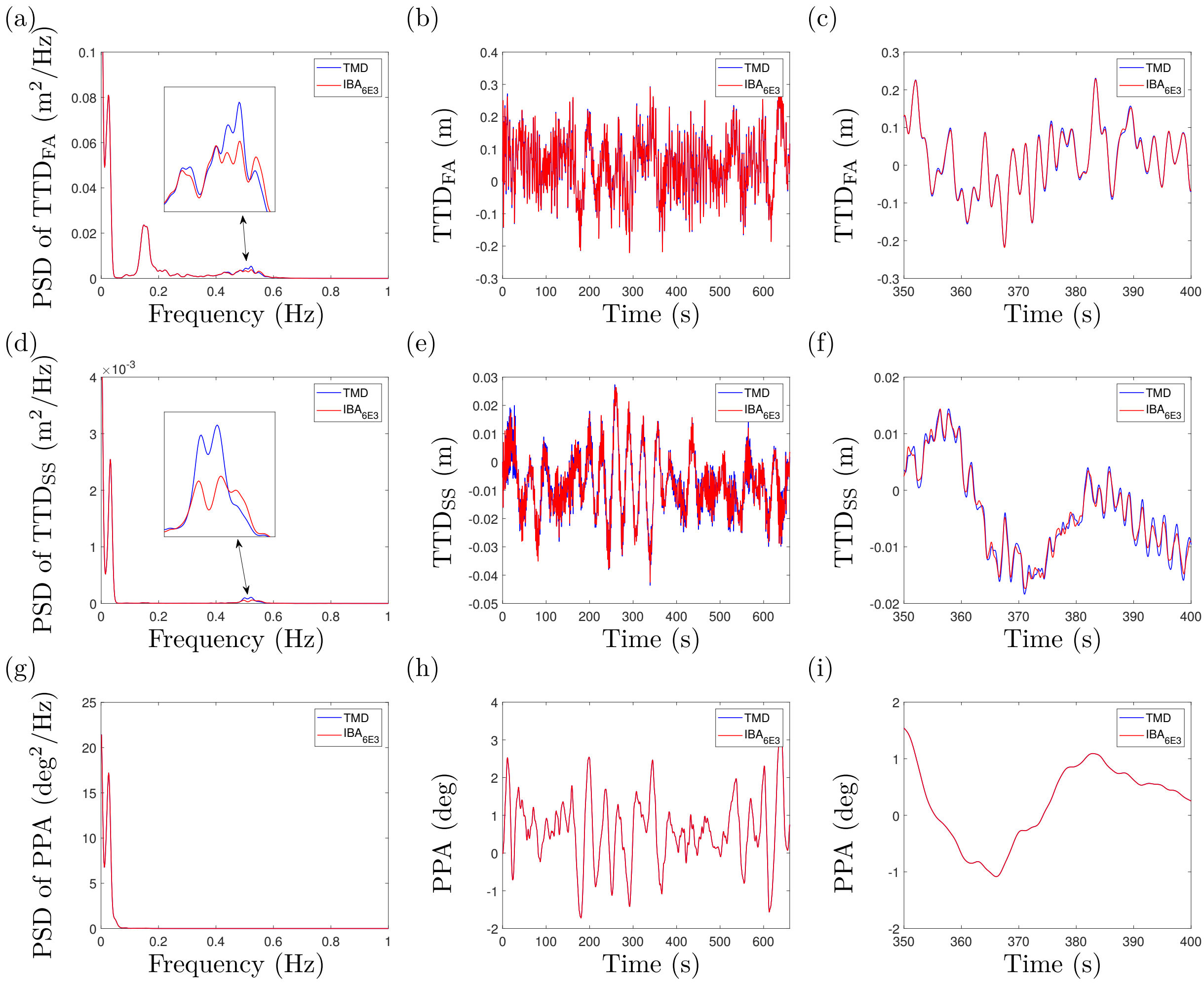

Fig. 3.18 Frequency domain responses (left), time domain responses (middle) and narrowed time windows responses (right) of the spar-buoy turbine under DLC 1.2 (16 m/s wind speed) with the tower top displacement (TTD) in the fore-aft (FA) direction ((a), (b), (c)), in the side-to-side (SS) direction ((d), (e), (f)) and with the platform pitch angle (PPA) ((g), (h), (i)).

It can be seen that IBAs have the ability to further suppress the tower bending mode of the spar-buoy turbine at around 0.5 Hz. Similarly, IBAs are more effective in the side-to-side direction where the improvement can be up to 3.3%, as there is less aerodynamic damping in this direction. However, the platform pitch mode (around 0.035 Hz) is not effectively suppressed regardless of either a TMD or an IBA is employed. Therefore, the platform pitch angle is unaltered. The peak in Fig. 3.18(a), at around 0.15 Hz, is the spectrum of the wave load. This is not observed in the side-to-side direction as the wind and wave loads are always considered aligned. The stroke is also investigated under the FLS analysis. For the TMD, the maximum stroke under 24 m/s wind speed is 0.62 m in the fore-aft direction and 0.13 m in the side-to-side direction. While for the $\mathrm{IBA}_{\mathrm{4E1}}$ and $\mathrm{IBA}_{\mathrm{6E3}}$, the maximum stroke is 0.71 m and 0.74 m in the fore-aft direction, 0.13 m and 0.13 m in the side-to-side direction, respectively. It can be seen that the stroke of the IBAs are slightly larger than the TMD, but it is still within the space limit of the turbine nacelle. Again, in order to achieve a similar performance as the optimum TMD, the $\mathrm{IBA}_{\mathrm{6E3}}$ with a reduced mass values of 7680 kg is also verified with slightly better performance than the TMD in both the fore-aft and side-to-side directions. This demonstrates the identified IBA has practical advantages for the offshore wind turbine applications compared to the TMD.

Spar-buoy turbine ULS analysis

Simulations with DLC 6.1a are performed for the spar-buoy turbine, where the performance indices are defined as the absolute maximum tower top displacement and tower base bending moment of each simulation averaged over six different random simulations. The amplitude of the tower top displacement and tower base bending moment in the frequency domain around the tower bending mode (between 0.4 Hz and 0.6 Hz) are also included for comparison. Results are shown in Table 3.8, where improvements in the time domain with up to 1.4% are obtained. Moreover, improvements in the frequency domain can be up to 6.9% and 39.7% in the fore-aft and side-to-side direction, respectively. The Power Spectral Density calculated by *pwelch* with 36 windows for one of the ULS simulation results is shown in Fig. 3.19(a), (b) and (c), which are the tower fore-aft, side-to-side responses and the platform pitch movement, respectively. It can be observed that the $\mathrm{IBA}_{\mathrm{6E3}}$ is effective for the tower bending mode around 0.5 Hz under extreme load case. However, the platform pitch mode is dominant in both the fore-aft and side-to-side directions at around 0.035 Hz. This phenomenon perhaps explains why the improvement of the maximum tower fore-aft and side-to-side displacements under ULS is less significant. Moreover, the load spectrum is dominant in the fore-aft direction at around 0.1 Hz and is not effectively suppressed (as shown in Fig. 3.19(a)), hence the performance is less significant in this direction even though the blades are all feathered.

Table 3.8 Spar-buoy turbine ULS analysis results

Evaluation type	Evaluation index	TMD	IBA_{4E1} (Imp.)	IBA_{6E3} (Imp.)
Time domain responses	Max TTD fore-aft (m)	0.576	0.576 (0%)	0.576 (0%)
	Max TTD side-side (m)	0.401	0.398 (0.9%)	0.411 (-2.4%)
	Max tower bending moment fore-aft (kN·m)	119205	119115 (0%)	119117 (0%)
	Max tower bending moment side-side (kN·m)	78113	77034 (1.4%)	78395 (-0.3%)
PSD of the responses (between 0.4-0.6 Hz)	Amplitude TTD fore-aft (m^2/Hz)	0.00129	0.00126 (2.5%)	0.00122 (6.1%)
	Amplitude TTD side-side (m^2/Hz)	0.0203	0.0129 (18.7%)	0.0123 (20.1%)
	Amplitude tower bending moment fore-aft ($(kN{\cdot}m)^2$/Hz)	4.04×10^7	3.90×10^7 (3.4%)	3.76×10^7 (6.9%)
	Amplitude tower bending moment side-side ($(kN{\cdot}m)^2$/Hz)	6.66×10^8	4.22×10^8 (36.6%)	4.01×10^8 (39.7%)

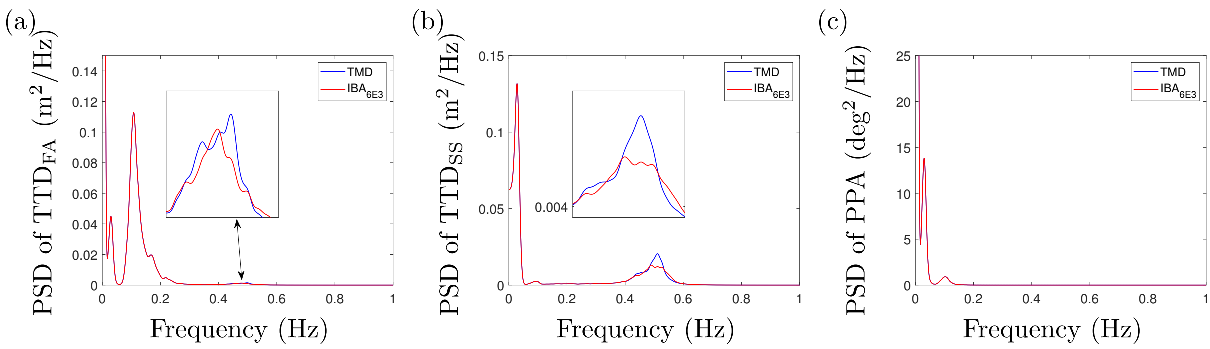

Fig. 3.19 Frequency responses of the spar-buoy turbine under DLC 6.1a with the tower top displacement (TTD) in the (a) fore-aft (FA) direction, (b) side-to-side (SS) direction, and (c) with the platform pitch angle (PPA).

3.5 Summary of the chapter

In this chapter, the generic 1PT1NG (1-physical-terminal-1-nominal-ground) network is derived to characterise a full set of independent passive vibration absorbers consisting of one reaction mass connected via the combination of springs, dampers and inerters to the primary structure through a single attachment point. Graph theory is employed to define the series-parallel connection and construct the generic 1PT1NG network. A systematic procedure is employed to identify beneficial 1PT1NG inerter-based absorbers (IBAs). Structural vibrations of a fix-bottom and a floating offshore wind turbine are reduced using the identified absorbers as an application example.

Simplified linear wind turbine models are first established based on their corresponding OpenFAST models to identify the beneficial IBAs which are used to reduce the tower top displacements. In order to assess their performance in realistic conditions, the source code of the OpenFAST is modified to include the transfer functions of any 1PT1NG IBAs. This enables the full investigation of generalised absorber configurations applied to various turbine systems using OpenFAST. Then, by employing the identified optimal IBAs, the monopile and spar-buoy turbines are simulated under different wind and wave conditions, including normal operational condition (corresponding to the fatigue limit states (FLS) and extreme load condition (corresponding to the ultimate limit states (ULS)) with the conventional vibration absorber, the TMD, as a benchmark. Results for this case study are obtained and concluded as follows:

(1) Based on the established linear monopile and spar-buoy turbine models, it is shown that no 3-element IBA could provide better performance than the TMD, and all 5-element candidates containing 2 springs, 2 dampers and 1 inerter cannot provide extra benefits over 4 elements IBAs. For the 4-element and 6-element IBA candidates, 4 IBAs for each case are identified which can provide equivalent performance improvements. This expands the design options for the practical implementation of IBAs. Optimisation results show that up to 7.3% and 6.4% performance improvements can be obtained by employing the linear monopile and spar-buoy turbine models, respectively.

(2) Under realistic metocean conditions, the identified IBAs show performance improvements compared to the TMD for the FLS analysis, where the tower damage equivalent load (DEL) can be reduced by 5.8% and 3.3% for the monopile and the spar-buoy turbines, respectively. Reduction of the DEL is larger in the side-to-side direction as there is less aerodynamic damping in this direction. The reason that the reduction for the spar-buoy turbine is smaller than that for the monopile one is that the identified IBAs only tune the tower fore-aft mode of the spar-buoy turbine, while the platform pitch mode is not targeted.

(3) The identified IBAs also show performance improvements compared to the TMD under the ULS analysis. In the time domain, the maximum tower base bending moment is reduced by 2.4% and 1.4% for the monopile and the spar-buoy turbines,

respectively. In the frequency domain, the amplitude of the tower bending mode can be reduced by 37.0% and 39.7% correspondingly.

(4) Compared with the relatively modest performance improvements using IBAs, mass value of the optimum IBAs for the monopile and spar-buoy turbines can be reduced by 25.1% (7486 kg) and 23.2% (7680 kg), respectively, to achieve the same performance as the optimum TMD. This is crucial for the utilisation of IBAs in offshore wind turbine tower vibration mitigations where the total mass added to the nacelle can be substantially reduced.

This case study demonstrates the benefits of the systematic method, where the derived generic 1PT1NG network has the ability of obtaining optimum configurations across a whole range of IBA candidates. Therefore, optimum configurations with pre-determined network topology and complexity can be obtained. Moreover, the fixed-layout absorbers, which has been previously proposed in different references [26, 140, 25] and proved to be effective for the offshore wind turbine systems, can be regarded as a subset of the IBAs identified by employing the geneic 1PT1NG network. In the meantime, more than one configurations with same performance improvements are identified, which might provide more possibilities for the next step physical design of such vibration suppression devices to fit into specific manufacturing requirements. Given these benefits, the method proposed here is extended in the next chapter to a certain type of 2PT1NG networks.

Chapter 4

Immittance-Function-Layout with the application to building structures

In Chapter 3, we have shown advantages of using the generic 1PT1NG (1-physical-terminal-1-nominal-ground) network for identification of beneficial one-attachment-point absorbers with one reaction mass and an arbitrary number of springs, dampers and inerters. However, this captures only a subset of independent absorbers that include a reaction mass. There are still a lot of independent vibration absorbers, which contain two attachment points to the primary system with a reaction mass included, that cannot be covered by the 1PT1NG network. An example from the literature is a device making use of both inerter and mass elements, namely the tuned mass damper inerter (TMDI) proposed by Marian and Giaralis [23]. The TMDI has shown significant performance benefits for mitigating seismic vibrations [76, 24, 149] compared to the traditional TMD.

For 1PT1NG networks such as the TMD, generic networks constructed in Chapter 3 can be employed for the systematic identification of beneficial network configurations. Yet there is no approach being developed which consider 2PT1NG networks with one reaction mass and an arbitrary number of springs, dampers and inerters. In this chapter, we will partially address this problem by introducing the Immittance-Function-Layout (IFL), which includes two Immittance-Function-Blocks (IF-Blocks) and one reaction mass in between. A more general representation will be given in Chapter 5. The IFL is inspired by the topology of the TMDI. Due to the presence of this mass element, forces generated at the two terminals are not equivalent anymore – an Immittance-Function-Matrix (IF-Matrix) is hence derived to describe the force-velocity relationships at the terminals. With this IF-Matrix, a full class of IFL-type series-parallel networks can be efficiently characterised, and the optimum configurations covered by this IFL can be identified.

This chapter begins with the introduction of an example three-storey building model, together with its performance criteria compared by using different typical vibration suppression devices. Then the single-IFL and dual-IFL devices are proposed. In Section 4.2, a systematic approach incorporating the single-IFL type device is used to identify the optimum configuration with pre-determined non-mass elements. Dual-IFL type device is investigated in Section 4.3, where several beneficial configurations are also identified. The obtained optimum configurations are tested under the real-life earthquake excitations. A 10-storey building model is also employed to further verify the effectiveness of the proposed systematic approach. Finally, conclusions are drawn in Section 4.4.

The approach introduced here formed the basis for the following publication:

- Y.-Y. Li, SY. Zhang, J. Z. Jiang, S. Neild (2019). Identification of beneficial mass-included inerter-based vibration suppression configurations. Journal of the Franklin Institute, 356(14), 7836-7854.

The IFL network together with this systematic approach is developed by Yi-Yuan Li and Dr. Sara Ying Zhang. The simulation is finished by Yi-Yuan Li. Dr Jason Zheng Jiang and Prof. Simon Neild have provided valuable suggestions on this research.

4.1 Building model, performance criteria and the Immittance-Function-Layout

4.1.1 Three-storey building model and the performance criteria

Firstly, a 3-storey structure (as shown in Fig. 4.1(a)) is modelled as a lumped mass system, incorporating each of the three vibration suppression devices once, namely, the TMD, the TID and the TMDI, as shown in Fig. 4.1(b)-(d). The study is extended in Section 4.2 and 4.3 to incorporate a generic suppression device that incorporates the mass element. Floor mass and inter-storey stiffness of the 1st, 2nd and 3rd floor are denoted as M_1, M_2, M_3, and k_{s1}, k_{s2}, k_{s3}, respectively. In this chapter, the floor mass is taken to be $M_1 = M_2 = M_3 = M = 1000\,\mathrm{kg}$ and the inter-storey stiffness is $k_{s1} = k_{s2} = k_{s3} = k_s = 1500\,\mathrm{kN/m}$. The structural damping is taken to be zero, in line with [21, 30], since it is typically small compared with that of the control device. The vibration suppression device is located between the 2nd and 3rd floor, where F_u and F_l represents the force exerted by the vibration suppression device to the upper and lower floors, respectively.

The equations of motion for this 3-storey building model integrating the vibration absorber can be represented by Eq. (4.1) in the Laplace domain:

$$\begin{bmatrix} M & 0 & 0 \\ 0 & M & 0 \\ 0 & 0 & M \end{bmatrix} \begin{bmatrix} s^2X_1(s) \\ s^2X_2(s) \\ s^2X_3(s) \end{bmatrix} + \begin{bmatrix} 2k_s & -k_s & 0 \\ -k_s & 2k_s & -k_s \\ 0 & -k_s & k_s \end{bmatrix} \begin{bmatrix} X_1(s) \\ X_2(s) \\ X_3(s) \end{bmatrix} = \begin{bmatrix} k_sR(s) \\ -F_l(s) \\ F_u(s) \end{bmatrix} \tag{4.1}$$

where $X_1(s)$, $X_2(s)$, $X_3(s)$ and $R(s)$ are displacements of different floors and the ground, respectively, in the Laplace domain (note $x_i(t) \xrightarrow{\mathcal{L}} X_i(s)$, $x_0(t) \xrightarrow{\mathcal{L}} X_0(s)$,and $f_u(t) \xrightarrow{\mathcal{L}} F_u(s)$, $f_l(t) \xrightarrow{\mathcal{L}} F_l(s)$).

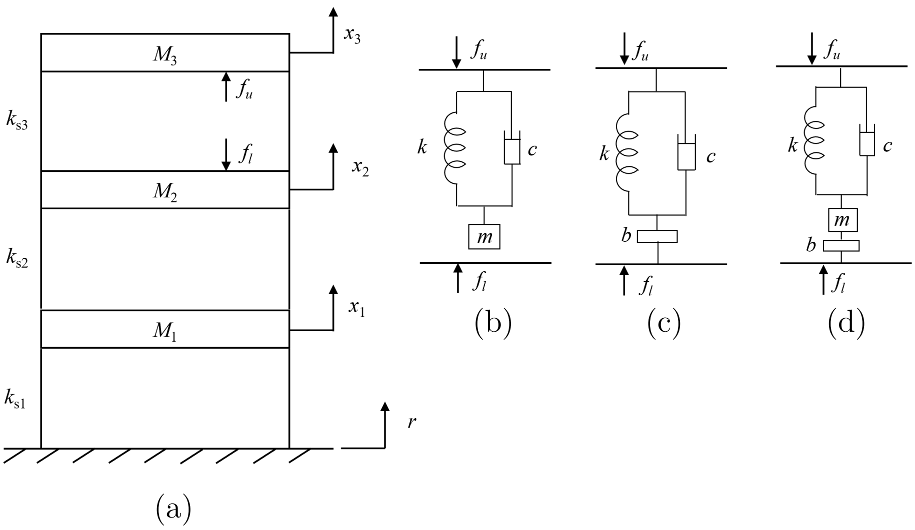

Fig. 4.1 (a) An example 3-storey building model with typical vibration suppression devices, including (b) the TMD, (c) the TID, and (d) the TMDI.

In this work, we consider the inter-storey drift displacements, accounting for the seismic damage of the building model, as the performance index. The inter-storey drift is denoted as X_{di} with $i = 1, 2, 3$ in Laplace domain, $X_{di}(s) = X_i(s) - X_{i-1}(s)$ with $X_0(s)$ representing the ground displacement $R(s)$. In this way, the inter-storey drift $X_{di}(s)$ can be obtained from Eq. (4.1). With the obtained X_{di}, the objective function is defined:

$$\begin{gathered} J_\infty = \max_{i=1,2,3}\left(\left\|T_{s^2R\to X_{di}}(s)\right\|_\infty\right) \\ \text{subject to: } m = 150\,\text{kg},\ b \in [0, 1000]\,\text{kg} \end{gathered} \tag{4.2}$$

where $T_{s^2R\rightarrow X_{di}}$ denotes the transfer function from ground acceleration $s^2R(s)$ to inter-storey drifts $X_{di}(s)$ and $\|T_{s^2R\rightarrow X_{di}}(s)\|_\infty$ is the standard H_∞ norm, which represents the maximum magnitude of $T_{s^2R\rightarrow X_{di}}$ across all frequencies. Based on the previous studies [9], the larger the mass value, the better the performance of the TMD. However, in practice, a very large mass is not achievable because of the weight and space constraints. Therefore, in this paper, we fix the mass value to be $m = 150$ kg, which is 5% of the whole building mass. On the other hand, the inerter can achieve higher inertance value using gearings in mechanical inerters [12] or adjusting the piston-cylinder cross-sectional area ratio in fluid inerters [3, 64]. Hence, in this study, an upper bound of 1000 kg is used to constrain the inertance value b, which is equal to the mass of one floor.

We note that there are many performance criteria adopted for building vibration suppression, such as relative displacement, inter-storey drift, and weighted frequency distributions [50]. The building model used can indeed be more complicated as well. The specific formulation of this mathematical problem serves the purpose of demonstrating the proposed systematic approach. Same procedure specified in this work can be applied to different mechanical systems and performance criteria.

4.1.2 Performance of three typical layouts

In this sub-section, three typical absorbers are investigated, which are the TMD, TID and TMDI, as shown in Fig. 4.1(b)-(d). The objective function J_∞ in Eq. (4.2) is optimised to identify the absorber parameter values using a combination of *patternsearch* and *fminsearch* in Matlab, with *fminsearch* refining the results obtained via *patternsearch*. Results for these three devices are summarised in Table 4.1. It can be seen that with the same added mass where $m = 150$ kg, the TMDI can provide a 36.6% performance improvement compared with the TMD, and it also outperforms the TID with 38.8% smaller value of J_∞ using much lower level of inertance. Since the TMDI provides the best performance in this example, it is used as a benchmark for the studies in Sections 4.2 and 4.3. Response of the optimum TMD will also be included because this is a very widely studied device. It should be noted that based on the previous study [21], the TID can achieve better performance by mounting it at the bottom of the host building structures along with larger inertance, while the TMD is more effective at the top. Moreover, as demonstrated in [149], the TMDI generally performances better when located between the higher floors than at the bottom. Since the focus of this work is to demonstrate the advantages of the proposed systematic approach under same optimisation scenario, rather than comprehensively explore the optimum design for a specific engineering problem, we only consider the absorbers mounted at the same location, i.e, the top floor in this study. We choose this floor because the candidate absorbers are all mass-included configurations, where most of the previous studies locate the mass-included absorbers (such as the TMD [51] and the TMDI [24]) at the top floor. Other floors can also be chosen to demonstrate the advantages of the proposed approach. With the identified network layouts, their optimum location can also be further explored for practical applications. But this is beyond the scope of this study, and it can be considered as future works. Fig. 4.2 shows the frequency responses of the three inter-storey drifts $T_{s^2R \to X_{di}}$ integrating one of the three optimised configurations. It can be observed that the peaks in the first mode natural frequency are split into two peaks where TID and TMDI are used. However, the TMD splitting peaks are difficult to observe. This is because these peaks are very close together, at 2.54 Hz and 2.63 Hz.

Table 4.1 Optimisation results using the TMD, TID and TMDI layouts

Optimum configurations	J_∞	k (kN/m)	c (kNs/m)	$b \in [0, 1000]$ (kg)
TMD	0.0172	38.76	1.71	/
TID	0.0178	354.14	4.47	1000
TMDI	0.0109	59.38	1.27	80.16

4.1.3 Immittance-Function-Layout

The significant performance benefit of the TMDI over the studied TMD and the inerter-based TID demonstrates the potential advantages of the mass-included inerter-based absorbers with two attachment points. The possible topological connections with a mass, inerters, dampers and springs are numerous. Hence, it is extremely challenging to systematically identify the most beneficial configurations amongst them. In order to achieve so, an Immittance-Function-Layout (IFL) is proposed. This is a generic network layout with Immittance-Function-Blocks (IF-Block) included, where the IF-Blocks represents sub-networks consisting of springs, dampers and inerters. The proposed IFL is shown in Fig. 4.3, where

$$Y_i(s) = \frac{F_i(s)}{V_i(s)} \text{ with } i = u, l \tag{4.3}$$

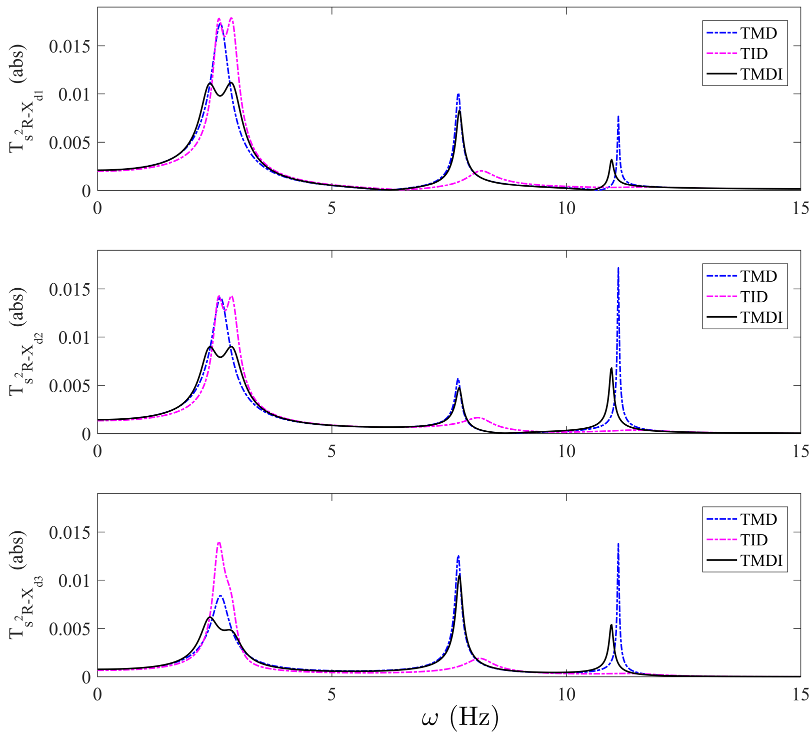

Fig. 4.2 Frequency domain responses comparison of the building structure inter-storey drifts with the optimum TMD, TID and TMDI.

$Y_u(s)$ and $Y_l(s)$ are the force-velocity passive mechanical admittance representing IF-Blocks, which consist of non-mass elements only, and connect to the upper and lower floor, respectively. $F_u(s)$, $F_l(s)$ are the forces exerted by the corresponding IF-Blocks, and $V_u(s)$, $V_l(s)$ are the relative velocities across their two terminals. Note that although the topological connection of the added mass is given and fixed in prior, different numbers of degrees-of-freedom (DOFs) will be introduced regarding different layouts. When elements or sub-networks are connected in series, extra DOFs are introduced.

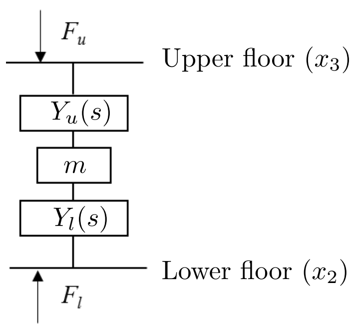

Fig. 4.3 The proposed single-IFL type mass-included inerter-based device.

Since mass is included in the IFL device, the forces F_u and F_l exerted on the two corresponding floors are not equal in magnitude. They are related to the displacements $X_2(s)$ and $X_3(s)$ and the Immittance-Function-Matrix (IF-Matrix) is give as:

$$\begin{bmatrix} F_l(s) \\ F_u(s) \end{bmatrix} = \begin{bmatrix} -\dfrac{Y_l(s)(ms^2 + sY_u(s))}{ms + Y_l(s) + Y_u(s)} & \dfrac{sY_u(s)Y_l(s)}{ms + Y_u(s) + Y_l(s)} \\ -\dfrac{sY_l(s)Y_u(s)}{ms + Y_u(s) + Y_l(s)} & \dfrac{Y_u(s)(ms^2 + sY_l(s))}{ms + Y_u(s) + Y_l(s)} \end{bmatrix} \begin{bmatrix} X_2(s) \\ X_3(s) \end{bmatrix} \tag{4.4}$$

Using the IF-Matrix as in Eq. (4.4), forces $F_l(s)$ and $F_u(s)$ exerted by a full set of IFL-type vibration suppression devices can be obtained. Taking the TMDI as an example, we have $Y_u(s) = k/s + c$ and $Y_l(s) = bs$. It should be noted that the proposed IFL also covers special cases like the TMD, where $Y_l(s)$ or $Y_u(s)$ equals 0, and the TID, where $m = 0$ and $Y_l(s) = \infty$. With $Y_u(s) = k/s + c$ and $Y_l(s) = 0$, the forces exerted by the TMD are $F_u(s) = ms^2Y_u(s)X_3(s)/(ms + Y_u(s))$, $F_l(s) = 0$; for TID, $Y_u(s) = 1/(1/(bs) + 1/(k/s + c))$, $Y_l(s) = \infty$ and $m = 0\,\mathrm{kg}$, therefore, $F_l(s) = F_u(s) = sY_u(X_3 - X_2)$.

It has been shown by previous researchers (e.g. in [53]) that multiple TMDs are more effective than a single TMD for vibration suppression. To this end, two parallel-connected IFL layout, which is termed as a dual-IFL device, is proposed, as shown in Fig. 4.8 of Section 4.3. Identification of beneficial single-IFL and dual-IFL type devices will be discussed in Sections 4.2 and 4.3, respectively.

4.2 Identification of optimum configurations with a single mass-included inerter-based device

In this section, a systematic approach for optimum configuration identification is introduced for a single-IFL type device. Performances of the obtained single-IFL configurations are analysed in detail.

4.2.1 Non-mass elements distribution possibilities in the upper and lower sub-networks

Without loss of generality, assuming there are n number of non-mass elements in a single-IFL device, it can be denoted as $\mathrm{IFL}_{im(n-i)}$, shown at the top layout of Fig. 4.4. The subscripts i and $(n-i)$ represent the number of non-mass elements contained in the upper and lower sub-networks, respectively. $Y_{u,i}(s)$ is the structural admittance of the upper sub-network with i non-mass elements, and $Y_{l,(n-i)}(s)$ represents the structural admittance of the lower sub-network with $(n-i)$ non-mass elements. It should be noted that both $Y_{u,i}(s)$ and $Y_{l,(n-i)}(s)$ can be an open connection where the admittance function equals 0, or a rigid connection where the admittance function equals ∞. For both cases, the sub-network contains no element, and we denote as $i = 0$ (for open connection) and $i = \infty$ (for rigid connection). Hence, there are $n + 3$ element distribution possibilities in total, which are denoted as $\mathrm{IFL}_{\infty mn}$, IFL_{0mn}, $\mathrm{IFL}_{1m(n-1)}$,..., $\mathrm{IFL}_{im(n-i)}$,..., $\mathrm{IFL}_{(n-1)m1}$, IFL_{nm0}, and $\mathrm{IFL}_{nm\infty}$, as shown in Fig. 4.4. After the number of non-mass elements in each sub-network is determined, the structure-immittance approach is adopted to cover the full set of series-parallel topological connection possibilities.

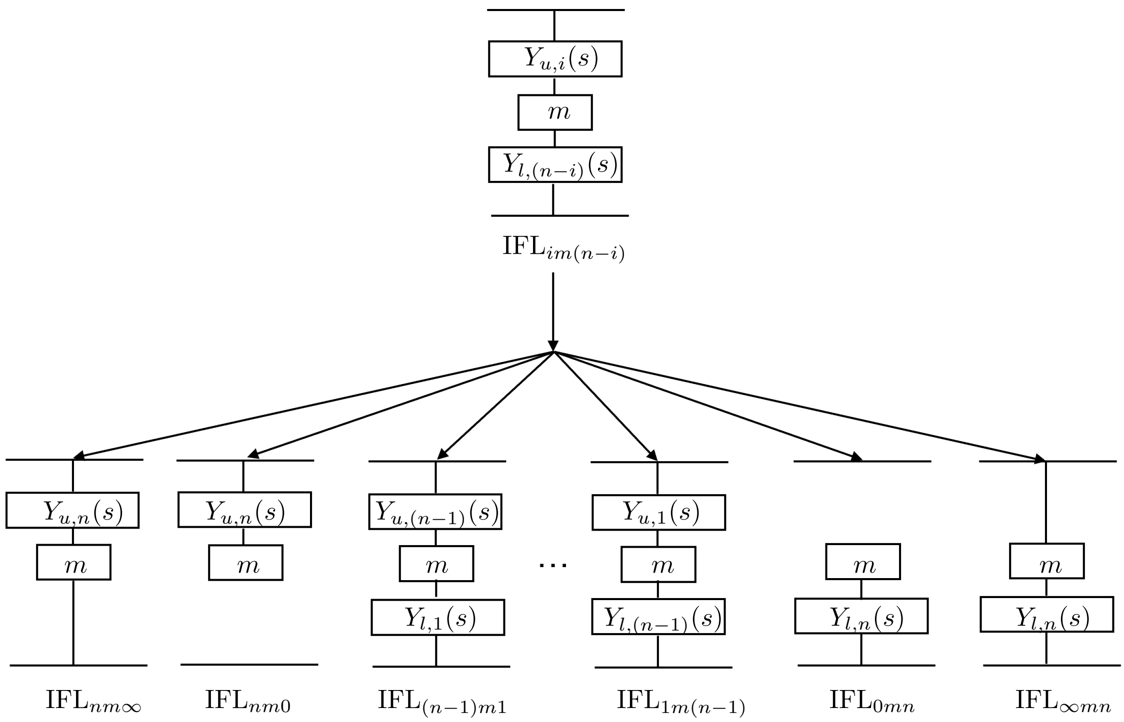

Fig. 4.4 The complete element distribution possibilities for single-IFL with n non-mass elements.

Regarding the number of each non-mass element type, three cases are considered for single-IFL device. These are Case I: 1 spring, 1 damper and 1 inerter combination, denoted as 1k1c1b case; Case II: 2 springs, 1 damper and 1 inerter combination, denoted as 2k1c1b case; and Case III: 1 spring, 2 dampers and 1 inerter combination, denoted as 1k2c1b case. We will use Case II to explain in detail how the systematic approach is conducted.

For Case II, there are 7 non-mass distribution possibilities, which are $\text{IFL}_{4m\infty}$, IFL_{4m0}, IFL_{3m1}, IFL_{2m2}, IFL_{1m3}, IFL_{0m4} and $\text{IFL}_{\infty m4}$. Now we use IFL_{3m1} as an example to demonstrate how the structure-immittance approach is employed. Three possible combinations of elements in $Y_u(s)$ can be obtained and the remaining one element will be in $Y_{l,1}(s)$. These three combinations are 2 springs and 1 damper (termed as 2k1c); 2 springs and 1 inerter (termed as 2k1b); 1 spring, 1 damper and 1 inerter (termed 1k1c1b). For the 1k1c1b combination, two generic networks, shown as Q_{11} and Q_{12} of Fig. 2.6 can be obtained based on the structure-immittance approach, for which the admittance functions can be derived as Eq. (2.8), which cover all the possible combinations of one spring, one damper and one inerter. It should be noted that since at most one spring of the networks shown in Fig. 2.6 is present, for $Y_{11}(s)$ in Eq. (2.8), at least three of the parameters k_2, $1/k_3$, k_4, k_6 must be equal to zero, and for $Y_{12}(s)$, at least three of the parameters $1/k_1$, $1/k_2$, k_3, $1/k_5$ must be equal to zero. For the combinations of 2k1c and 2k1b, two generic network will suffice. Therefore, the optimisation process will be conducted 4 times for the IFL_{3m1} layout. For $\text{IFL}_{4m\infty}$, IFL_{4m0}, IFL_{2m2}, IFL_{1m3}, IFL_{0m4} and $\text{IFL}_{\infty m4}$, the structural admittances can be obtained by following the similar procedure. It can be calculated that 8 generic networks (and the corresponding structural admittances) will be needed for Case II, which can cover 104 layouts in total. Indeed, as the total number of elements becomes larger, there will be more candidate network layouts, which will lead the proposed approach more complicated. But the significance of this approach is that it is systematic, which makes it easier to analyse all the possible absorbers; and by making use of the structure-immittance approach, significantly less implementations are needed for the optimisation. Without this proposed systematic approach, it is firstly difficult to enumerate all the possible candidate layouts and secondly hard to take all these layouts into consideration for the optimisation. Furthermore, this approach can be implemented as a computer algorithm, for which the distribution of element types and numbers can be directly obtained. We anticipate that there will be some redundancy in the resulted network, but this will not affect the optimisation results, although there might be more than one minima of the cost function that result in identical configurations once the redundancy is noted.

4.2.2 Optimisation results

Following the above systematic approach, the optimisation procedure is conducted using the structural admittances such as $Y_{11}(s)$ and $Y_{12}(s)$ in Eq. (2.8) and $Y_{21}(s)$ and $Y_{22}(s)$ in Eq. (2.9). The results are summarised in Table 4.2. For Case I and Case III, the most beneficial configuration is the TMDI with the parameter values shown in Table 4.1. For Case II, the most beneficial configuration is shown in Fig. 4.5, termed C1, with the objective function value $J_\infty = 0.0101$ using the parameter values shown in Table 4.2. The C1 configuration improves the performance by 7.3% and 41.3% compared with the TMDI and TMD, respectively. Note that two more DOFs (x_1 and x_2) are added when attaching the C1 absorber to the main system, as shown in Fig. 4.5. Besides, C1 only has one attachment point to the hosting structure, so it will also be less affected by the effects such as brace stiffness and backlash compared to the TMDI.

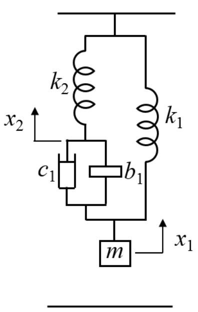

Fig. 4.5 The optimum single-IFL type device configuration C1, obtained from Case II, with two more DOFs adding to the building system.

Table 4.2 Optimisation results using the single-IFL type device for Cases I, II and III

Case	optimum configuration	J_∞	improvement compared with the TMDI	k_1 (kN/m)	k_2 (kN/m)	c_1 (kNs/m)	$b_1 \in [0, 1000]$ (kg)
I (1k1c1b)	TMDI	0.0109	/	59.38	/	1.27	80.16
II (2k1c1b)	C1	0.0101	7.3%	89.14	41.86	0.81	23.91
III (1k2c1b)	TMDI	0.0109	/	59.38	/	1.27	80.16

Fig. 4.6 shows the frequency responses of the three inter-storey drifts $T_{s^2R\rightarrow X_{di}}$ integrating the optimum configuration C1, together with the optimum TMD and TMDI. Considering the internal resonance of the device alone, the resonant frequencies for C1 are 3.72 Hz and 6.53 Hz, which target the vicinity of the first and second modes of the main structure, respectively. It can be seen from Fig. 4.6 that, the peaks at the vicinity of the first model natural frequency are further reduced by using the C1 configuration, compared with both optimum TMD and TMDI configurations. Peaks for the second and third modes are also effectively suppressed.

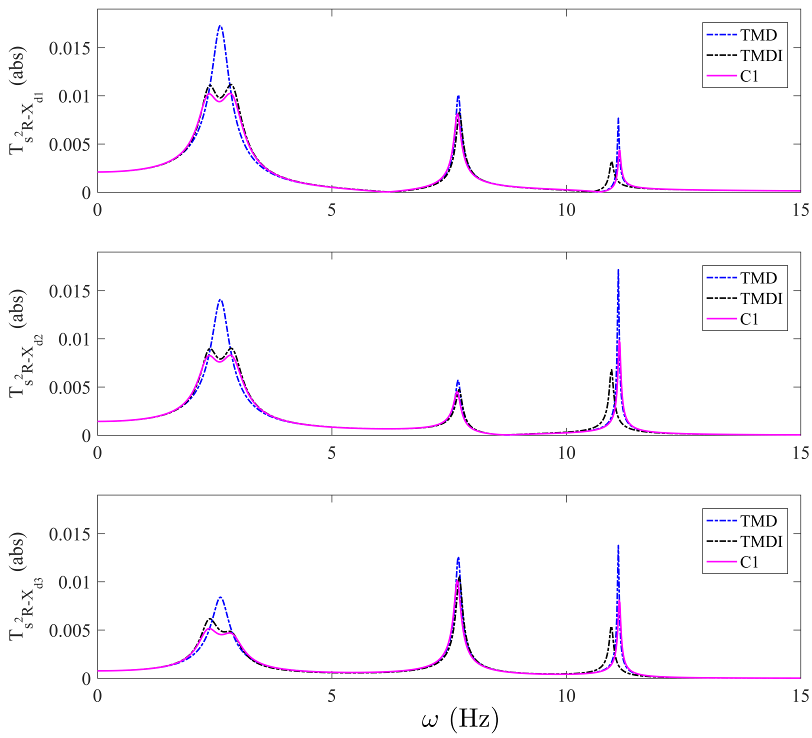

Fig. 4.6 Frequency domain responses comparison of the building structure inter-storey drifts with the optimum TMD, TMDI and C1 configurations.

The effect of the inerter's size on the performance, J_∞, of the main structure with configuration C1, is shown in Fig. 4.7. It can be observed that the optimum performance occurs when $b = 23.91$ kg and as the value of b increases from this, J_∞ becomes larger. This is because the movement between the two terminals across the damper c_1 is diminished as the inerter's size becomes larger. In the extreme case that b is infinite, the damper is locked. Furthermore, it can be calculated that, in order to achieve the same level of performance as C1, $J_\infty = 0.0101$, the mass of the TMD and TMDI needs to be increased by 1.83 and 1.74 times of the original value where $m = 150\,$kg, respectively.

Also for the TID, it can be calculated that the inertance value needs to be 133 times larger compared with that of C1 as shown in Table 4.2 to match its performance.

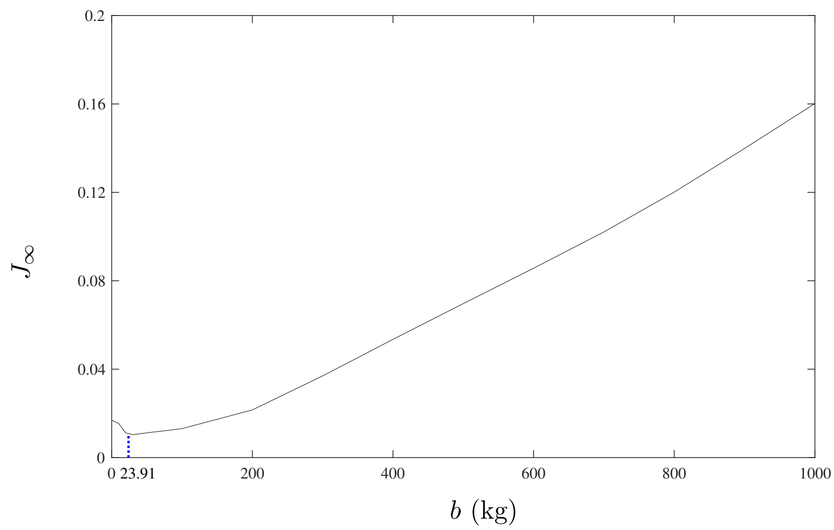

Fig. 4.7 Relationship of the performance index J_∞ with respect to different inertance value in C1.

4.3 Identification of optimum configurations with two mass-included inerter-based devices

This section demonstrates how the systematic approach can be applied when a dual-IFL device is used. Performances of obtained dual-IFL configurations are also analysed in detail.

4.3.1 Non-mass element distribution possibilities in a dual-IFL device

A dual-IFL containing n non-mass elements is proposed in Fig. 4.8, where n_1 and n_2 are the number of non-mass elements contained in the left IFL and right IFL of the dual-IFL device, respectively, with $n_1 + n_2 = n$. It should be noted that when $n_1 = 0$ or $n_2 = 0$, the dual-IFL device is reduced to a single-IFL device, which has been discussed in Section 4.2. This dual-IFL is denoted as $\mathrm{IFL}_{im_1(n_1-i),jm_2(n_2-j)}$. Here, $YL_{u,i}(s)$ and $YL_{l,(n_1-i)}(s)$ are the structural admittances of the upper and lower sub-networks in the left IFL, which contains i and (n_1-i) non-mass elements, respectively. Similarly, $YR_{u,j}(s)$ and $YR_{l,(n_2-j)}(s)$ are the structural admittances of the upper and lower sub-networks in the right IFL, which contains j and $(n_2 - j)$ non-mass elements, respectively. Following a similar procedure to that presented in Section 4.2, all non-mass elements distribution possibilities for the dual-IFL device can be enumerated. For simplicity, this procedure is not presented in detail. With the determined element number for each sub-network, the structure-immittance approach will be adopted to include all possible configurations for optimisation. In this section, the total mass value is chosen as $m_1 + m_2 = 150$kg. The inertance value is constrained that $b \leq 1000$kg, in consistency with the rest of the paper.

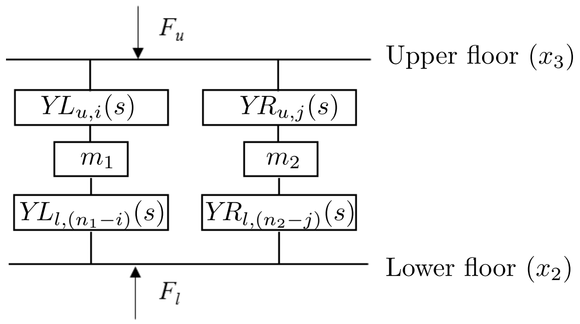

Fig. 4.8 Dual-IFL type devices containing n non-mass elements, where $n_1 + n_2 = n$.

4.3.2 Optimisation results

Three cases are considered in this section, which are Case IV: 2 springs, 1 damper and 1 inerter combination, denoted as 2k1c1b case; Case V: 1 spring, 2 dampers and 1 inerter combination, denoted as 1k2c1b case; Case VI: 2 springs, 2 dampers and 1 inerter combination, denoted as 2k2c1b case. To constrain the computational complexity, here we limit the element number in each sub-network in Fig. 4.8 to be no more than 4. By conducting the proposed systematic method, the optimum configurations are obtained, with the newly identified ones shown in Fig. 4.9. The corresponding parameter values are summarised in Table 4.3. For Case IV, the optimum configuration is C1, same as the optimum configuration identified in Section 4.2. The reason we cannot get a better performance configuration is that there is only 1 damper, which means one of the IFL device is un-damped. The most beneficial configurations for Case V and Case VI are C2 and C3, respectively. Note that C2 introduces one additional DOF and C3 introduces two extra DOFs to the main system, which are shown in Fig. 4.9(a) and (b). C2L and C2R represent the network configurations at the left and right hand side of C2, and same notation is used for C3. It can be seen that the layout of both C2L and C3L are TMD, and C2R and C3R are both 2-physical-terminal (2PT) networks (as introduced in Fig. 3.2 of Section 3.1). Therefore, both C2 and C3 are still networks with two physical terminals and one notional ground terminal (2PT1NG). For C2, the objective function is

$J_\infty = 0.0079$, and for C3 is $J_\infty = 0.0071$, with the corresponding parameter values for both listed in Table 4.3. Again, as stated in Section 3.3, with more elements included in the identified absorbers, although the system dynamic performance is improved, the combined nonlinear effects of these elements could have great impacts on the overall performance. Nonlinearity of these identified absobers should be fully investigated before they are used for real engineering applications.

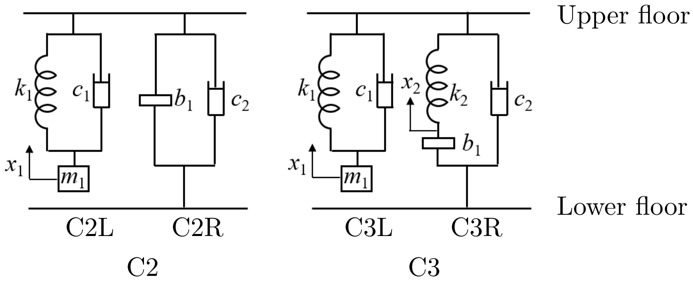

Fig. 4.9 Identified optimum dual-TFLs configurations C2 and C3 from Case V and Case VI, respectively, along with the extra DOFs they introduce to the building system.

Table 4.3 Optimisation results using the dual-IFL device for Cases IV, V and VI

Case	Optimum configu-ration	J_∞	Improvement compared with the TMDI	k_1 (kN/m)	k_2 (kN/m)	c_1 (kNs/m)	c_2 (kNs/m)	$b_1 \in [0, 1000]$ (kg)
IV (2k1c1b)	C1	0.0101	7.3%	89.14	41.86	0.81	/	23.91
V (1k2c1b)	C2	0.0079	27.5%	37.80	/	0.89	45.26	1000
VI (2k2c1b)	C3	0.0071	34.9%	35.27	589.46	0.86	37.37	1000

Fig. 4.10 shows the frequency responses of C2 and C3, together with those of the optimum TMD and TMDI. It can be seen that significant performance advantages have been obtained. Considering the internal resonance of the device alone, for C2, there is only one frequency located at 2.40 Hz. Similar to a TMD, this is close to the building's first natural frequency. Therefore the peaks of the building's first natural frequency is split into 2 when the full system is considered, which are located at $f_1 = 2.32$ Hz and $f_2 = 2.97$ Hz, respectively. Two frequencies of C3 are 2.44 Hz and 3.86 Hz, both of which

target the building's first mode. As a result, the peaks in the first mode natural frequency are split into 3 frequencies, which are $f_1 = 2.25$ Hz, $f_2 = 2.89$ Hz and $f_3 = 3.38$ Hz, all around the first natural frequency of the building model. Fig. 4.11(a) and (b) present the frequency responses of the first inter-storey drift $T_{s^2R \to X_{d1}}$ for the configuration C2, C2L, C2R and C3, C3L, C3R, by using the optimum parameter values obtained for C2 and C3, respectively. The reason we only choose the first inter-storey drift is because it

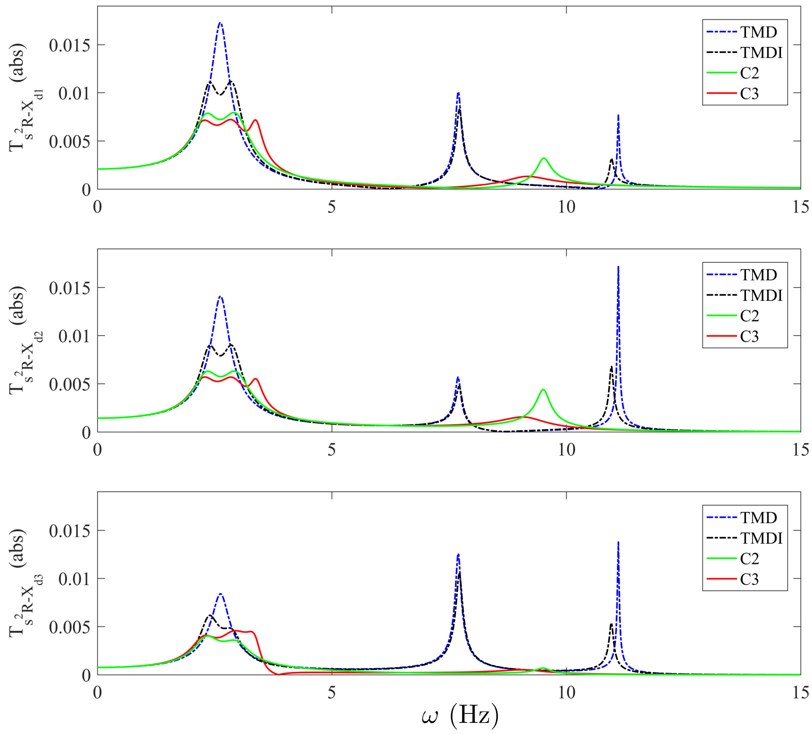

Fig. 4.10 Frequency domain responses comparison of the building structure inter-storey drifts with the optimum TMD, TMDI, C2 and C3 configurations.

has the largest response amongst all the three inter-storey drifts. Besides, the trends for $T_{s^2R \to X_{d2}}$ and $T_{s^2R \to X_{d3}}$ are the same as $T_{s^2R \to X_{d1}}$, so they are not included for brevity. It is interesting to observe that C2L (resp. C3L) mainly target the first natural frequency, splitting the first mode into two peaks (resp. three peaks), whereas, the second and third modes have not been affected by C2L (resp. C3L). On the other hand, C2R (resp. C3R) alone mainly target the higher modes of the main structure.

Now consider the mass value for a TMD, TID or TMDI to achieve the same performance as C3, namely $J_\infty = 0.0071$. The mass of the TMD and TMDI needs to be increased by 2.83 and 4.72 times the original $m = 150$ kg, respectively. As for the TID, it is unable to

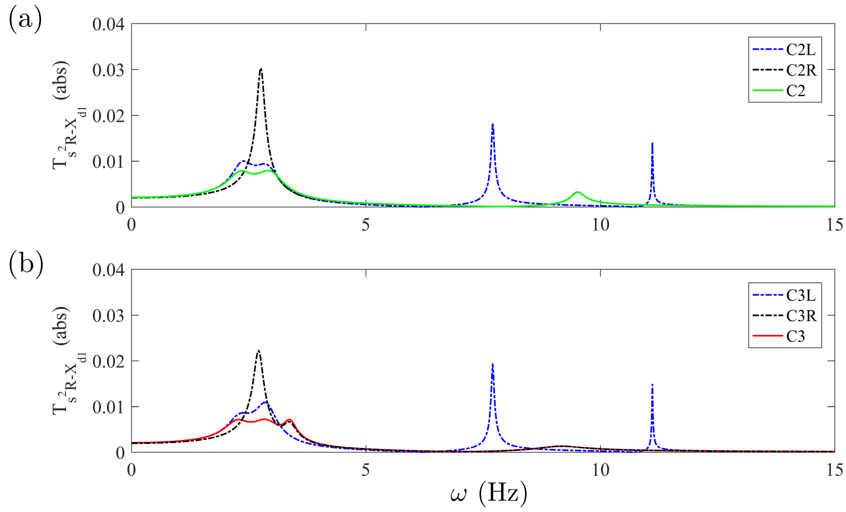

Fig. 4.11 Frequency domain responses comparison of the building structure inter-storey drift $T_{s^2R\rightarrow X_{d1}}$ with (a) C2 and C2L, C2R alone; (b) C3 and C3L, C3R alone.

achieve the same performance as C3 even when the inertance value is unconstrained and the minimum $J_\infty = 0.0092$.

4.3.3 Verification of the obtained beneficial absorbers

Using the identified configurations, the building's response subjected to two real-life earthquake excitations are examined. One is a 50 second ground acceleration record from the 1995 Kobe earthquake in Japan, with the time history ground acceleration and single-sided Fourier spectrum shown in Fig. 4.12(a) and Fig. 4.13(a), respectively. The other is a recording from the 2011 Tohoku earthquake with a longer duration, see Fig. 4.14(a) and Fig. 4.15(a).

Fig. 4.12(b) shows a time history of the inter-storey drift of the first floor relative to the ground under the Kobe earthquake, with the black, blue, green and red lines represent the responses incorporating the optimum configurations TMDI, C1, C2 and C3, respectively. It can be observed that the results of the inter-storey drift time histories responses are consistent with the performance index J_∞, where the performance from best to worst is C3, C2, C1, then the TMDI. Fig. 4.13(b) shows the single-sided Fourier spectrum of the inter-storey drift X_{d1} incorporating the TMDI, C1, C2 and C3, respectively. The highest amplitudes are attained at low frequencies, hence only the 0-7 Hz frequency ranges is shown. The first natural frequency of the structure is $f_1 = 2.74$ Hz, tuned to match the high amplitude frequency region of the chosen ground motion. The relative displacement time history and the single-sided Fourier spectrum of the inter-storey drift X_{d1} under

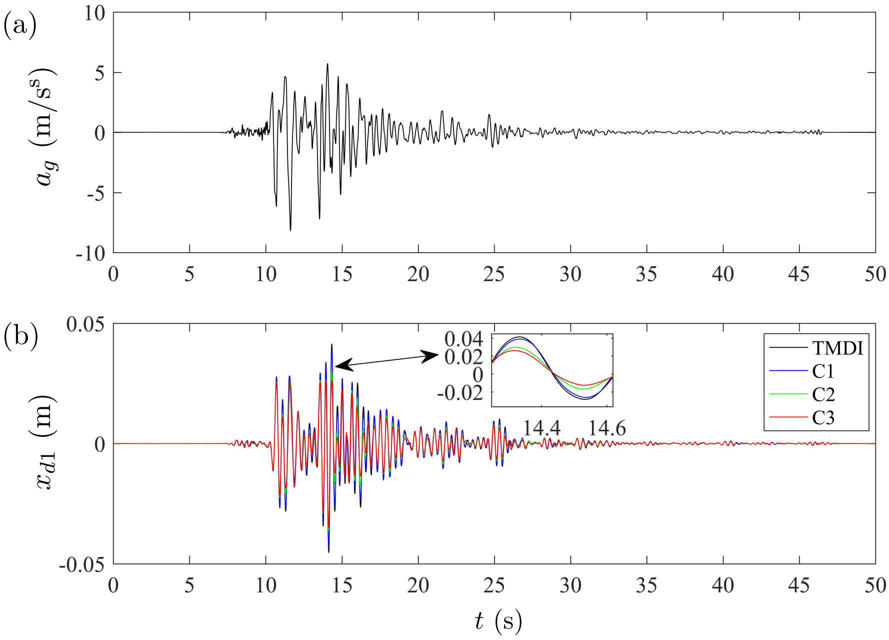

Fig. 4.12 Time-history of the (a) ground acceleration, and the (b) inter-storey drift of the first floor relative to the ground with C1, C2, C3 and the optimum TMDI, where the Kobe earthquake input is used.

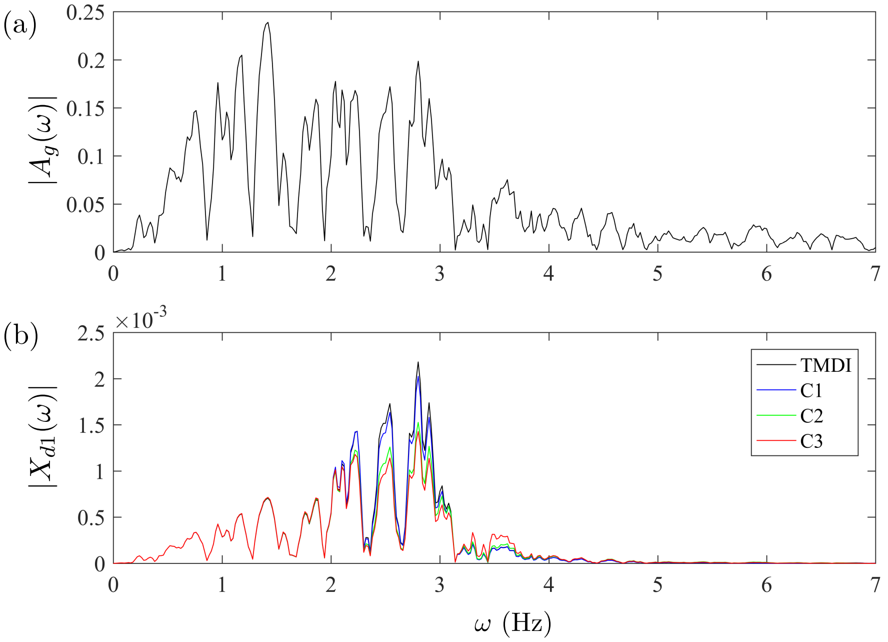

Fig. 4.13 Single-sided Fourier spectra of the (a) ground acceleration, and the (b) inter-storey drift of the first floor relative to the ground with C1, C2, C3 and the optimum TMDI, where the Kobe earthquake input is used.

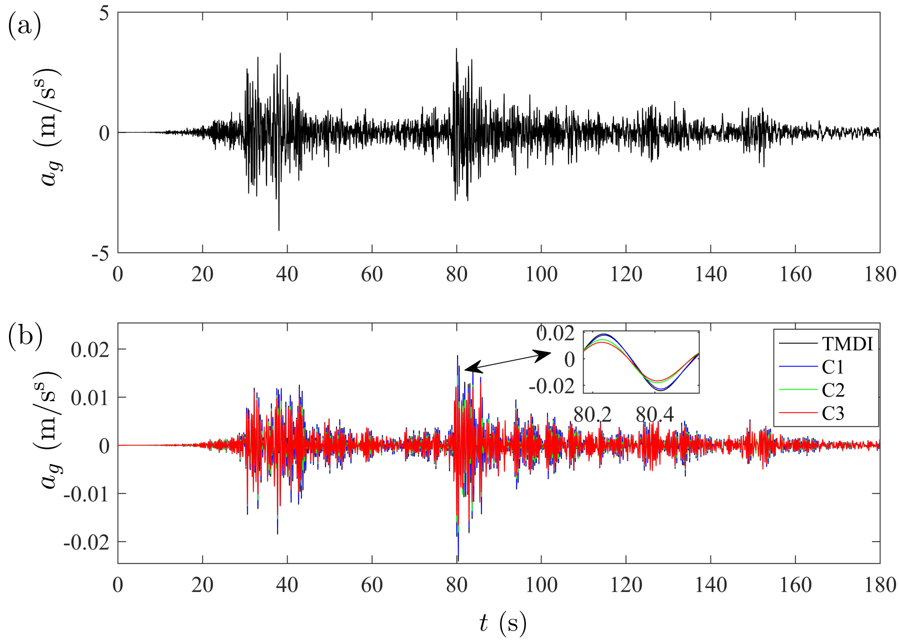

Fig. 4.14 Time-history of the (a) ground acceleration, and the (b) inter-storey drift of the first floor relative to the ground with C1, C2, C3 and the optimum TMDI, where the Tohoku earthquake input is used.

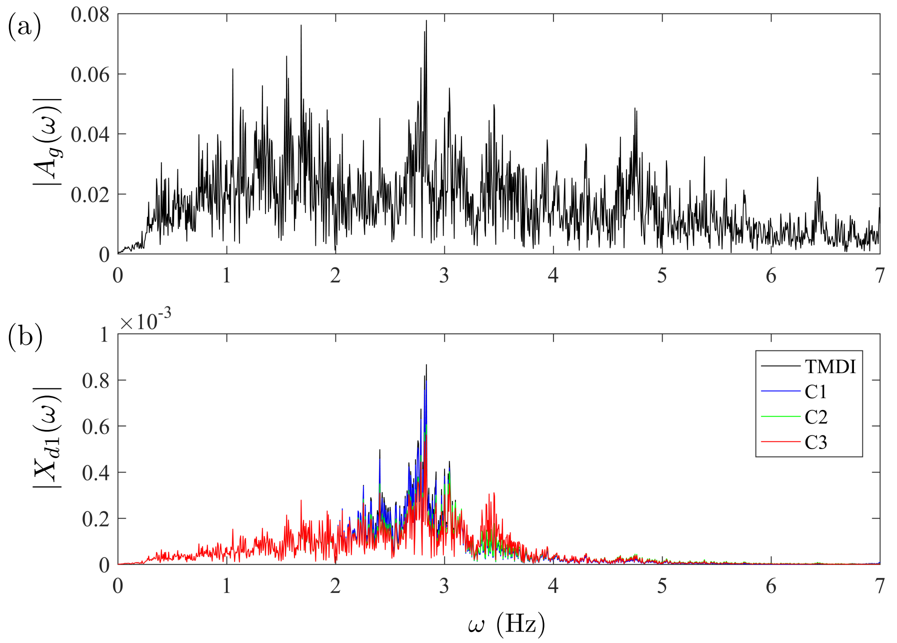

Fig. 4.15 Single-sided Fourier spectra of the (a) ground acceleration; and the (b) inter-storey drift of the first floor relative to the ground with C1, C2, C3 and the optimum TMDI, where the Tohoku earthquake input is used.

the Tohoku earthquake are shown in Fig. 4.14(b) and Fig. 4.15(b), respectively. Again, it can be seen that the configuration C3 achieves the best seismic performance, followed by C2 and C1, and finally the optimum TMDI.

In order to further verify the effectiveness of this approach, a 10-storey building model subjected to base excitation is also considered, where the floor mass and inter-storey stiffness remain consistent with the 3-storey building, i.e. 1000 kg and 1500 kN/m, respectively. The identified configurations C1, C2 and C3 are re-optimised with the TMD and the TMDI as comparison. Results are shown in Table 4.4 and Fig. 4.16, from which superior performance can still be obtained by using C1, C2 and C3 on the 10-storey building.

Table 4.4 Optimisation results of the TMD, TMDI, C1, C2 and C3 on a 10-storey building model

Optimum configurations	J_∞	Improvements compared with the TMDI	k_1 (kN/m)	k_2 (kN/m)	c_1 (kNs/m)	c_2 (kNs/m)	$b \in [0, 1000]$ (kg)
TMD	0.144	/	4.78	/	0.600	/	/
TMDI	0.117	/	54.6	/	0.491	/	18.5
C1	0.106	9.4%	42.9	4.97	0.436	/	7.34
C2	0.048	59.0%	4.74	/	0.175	146.5	1000
C3	0.047	59.8%	4.73	36.7	0.176	86.5	1000

Frequency responses of the first floor inter-storey drift relative to the ground for the TMD, TMDI and C3 are shown in Fig. 4.16. Similar to 3-storey building case, frequencies of C3 target the building's first mode, splitting the first mode where $f_1 = 0.85$ Hz, $f_2 = 0.97$ Hz, $f_3 = 0.98$ Hz. Only two peaks can be observed in the figure, this is because f_2 and f_3 are very close to each other. Note that if the systematic approach is fully adopted where all possible configurations are considered, even more enhanced performance might be achieved.

It should be noted that only the network layouts C1, C2 and C3, which are identified in the 3-storey case study, are re-optimised for the 10-storey building. If the full set of single- and double-IFL networks with predetermined number of elements are considered,

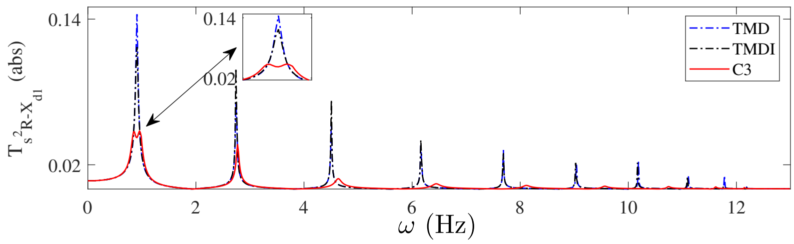

Fig. 4.16 Frequency domain responses of the first floor inter-storey drift relative to the ground for the TMD, TMDI and C3 on a 10-storey building model.

different optimal network configurations could possibly be obtained. It is similar for the case when more storeys are considered or for heterogeneous buildings where not all floor weight and stiffness are equal. This is because with different building models, mode frequencies and mode shapes of these building systems are different. When interacting with the dynamics of different absorbers, new network configurations could possibly be obtained.

4.4 Summary of the chapter

In this chapter, an Immittance-Function-Layout (IFL) is proposed, which can cover a complete set of networks with a layout that two IF-Blocks and one mass element are connected in series with the mass in between. By using the proposed IFL, a systematic procedure is provided to identify the most beneficial configurations with pre-determined numbers of non-mass elements. In order to cover two-mass-included inerter-based devices as well as identifying more beneficial configurations, dual-IFL type devices with two parallel-connected IFL layouts are also considered. The main conclusions and results are obtained and summarised as follows:

(1) The proposed IFL is effective in identifying optimal network configurations, where an example is given to mitigate the maximum inter-storey drift of a three-storey building model subjected to base excitation. Totally three optimal configurations, C1, C2 and C3, which incorporate inerter(s), spring(s), damper(s), and mass(es) have been obtained. C1 is a single-IFL type device, with 7.3% improvements obtained compared with the optimum TMDI. C2 and C3, which are still 2PT1NG networks, are obtained through the dual-IFL devices with up to 34.9% improvements. These two networks cannot be obtained by using the previously proposed structure-immittance approach as the structure-immittance approach can only be used to identify 2PT networks. This demonstrates the advantages of the proposed IFL that

the IFL can be used to identify more beneficial networks which cannot be covered by the structure-immittance approach.

(2) It has been shown that the dual-IFL type devices outperform the single-IFL devices with same mass constraints. This is because, for the identified dual-IFL device, one IFL mainly targets the building's first natural frequency, and the other IFL is able to target higher frequencies.

(3) Finally, real-life earthquake inputs are used on the 3-storey building model incorporating the identified absorbers, which show advantages of those absorbers on mitigating seismic vibrations compared to the optimum TMDI. A 10-storey building model subjected to base excitation is also adopted to further verify the effectiveness of the identified absorbers.

The proposed IFL captures a certain range of mass-included devices with two attachment points to the primary structure in a comprehensive way. Significant benefits have been obtained with the identified networks. Considering that all these networks are essentially two 2PT1NG networks, this show the potential performance improvements of 2PT1NG networks. Therefore, in the next chapter, a complete set of 2PT1NG networks will be explored to fully demonstrate the network performance through a systematic approach.

Chapter 5

Generic 2PT1NG networks with the application to building structure

In this chapter, the generic 2PT1NG network is formulated to cover all possible series-parallel networks with 2 physical terminals (PTs) and one notionally grounded (NG) terminal (this terminal allows the connection of a reaction mass).

The significant performance benefit of the C2 and C3 obtained in Chapter 4 over the traditional TMD, the TID, and the TMDI demonstrates the potential advantages of vibration absorbers where all four mechanical elements, inerter(s), damper(s), spring(s) and mass(es) are used. The possible topological connections with these elements included are numerous, and it is extremely challenging to systematically identify the most beneficial configurations amongst them. In Chapter 3, the generic 1PT1NG network, which is a complete set of networks containing one PT and one NG, has been investigated. In Chapter 4, the IFL network, which covers a certain set of networks with two PTs and one NG (termed as the 2PT1NG network), are also discussed. However, there are still various 2PT1NG networks, which cannot be covered by the IFL-type network. They could potentially provide more preferred dynamic properties. An example network which is 2PT1NG, but cannot be covered by the IFL type network is shown in Fig. 5.1. To fully explore a complete set of mass-included vibration absorbers with two PTs, generic 2PT1NG networks are derived in this chapter based on the work done in Chapters 3 and 4. Graph theory [128, 150] is again employed to construct the topological connections. Together with the generic 1PT1NG network derived in Chapter 3, all possible networks with series–parallel connections of one reaction mass and a pre-determined number of springs, dampers and inerters can be covered.

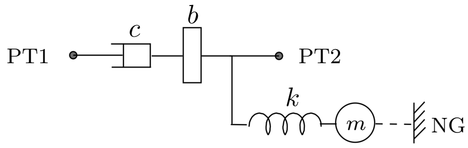

Fig. 5.1 An example 2PT1NG network which cannot be covered by the IFL.

This chapter is structured as follows. In Section 5.1, the problem of identifying the optimum reaction-mass-included vibration absorbers with two attachment points is formulated. Section 5.2 enumerates all possible absorber layouts through the constructed generic 2PT1NG Networks — this captures a complete set of absorber possibilities including one reaction mass and a pre-determined number of springs, dampers and inerters connected in series-parallel. In Section 5.3, the proposed generic 2PT1NG networks are applied to an example 3-storey structure, demonstrating the performance advantages that can be achieved. Conclusions are drawn in Section 5.4.

The approach introduced here formed the basis for the following publication:

- SY. Zhang, Y.-Y. Li, J. Z. Jiang, S. Neild, J. H. MacDonald (2019). A methodology for identifying optimum vibration absorbers with a reaction mass. Proceedings of the Royal Society A, 475(2228), 20190232.

The geneic 2PT1NG network together with this systematic approach is developed by Yi-Yuan Li and Dr. Sara Ying Zhang. Dr Jason Zheng Jiang, Prof. Simon Neild and Prof. John MacDonald have provided valuable suggestions on this research.

5.1 Problem formulation

When a reaction mass is included in the network, a systematic approach becomes challenging, as the reaction mass is a one-terminal element (as illustrated in Fig. 3.1). In order to include the reaction mass in a systematic network identification approach, it is treated as a special two-terminal element, with one terminal notionally connected to the ground, denoted as a notional-ground (NG). Accordingly, terminals connected to physical attachments are denoted as physical-terminals (PTs) when considering their network representations. Therefore, similar to the 1PT1NG network demonstrated in Section 3.1, by denoting the absorber attachment points 1 (resp. 2) as PT1 (resp. PT2) in the network representation, the TMDI (Fig. 5.2 (a)) can be depicted as a network shown in Fig. 5.2(b). It is no longer two-terminal, but a three-terminal network with two PTs and one NG, denoted as a '2PT1NG network'.

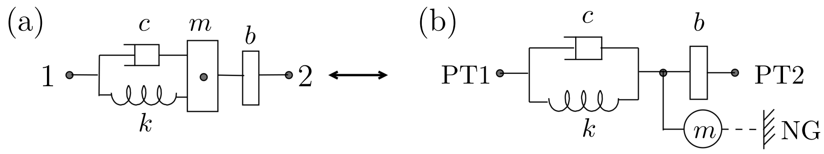

Fig. 5.2 (a) The TMDI absorber schematic plot, and (b) its network representation.

Fig. 5.3 shows a general representation of a 2PT1NG network, with forces f_1, f_2 and velocities v_1, v_2 at two PTs. Note that because of the reaction mass, in contrast to the 2PT network (whose admittance function is $Y(s) = F(s)/(V_1(s) - V_2(s))$, see Fig. 3.2(b)), the forces f_1, f_2 of the 2PT1NG network are not equal and opposite. To describe the relations between the velocities and the forces in the Laplace domain, an Immittance-Function-Matrix (IF-Matrix), denoted as $\mathbf{L}(s)$, is required. The derivation of IF-Matrix for a given 2PT1NG network is detailed in Appendix B.

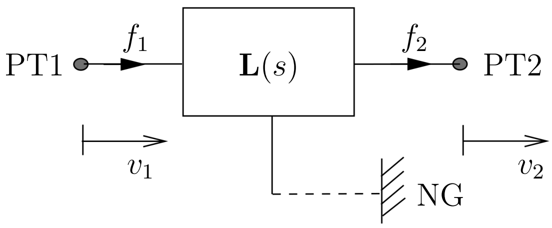

Fig. 5.3 2PT1NG network.

The rest of the paper addresses the following two questions:

(1) Given one reaction mass and any pre-determined number of inerters, dampers and springs, how to enumerate all possible series-parallel '2PT1NG' network layouts?
(2) Based on (1), how to systematically identify the optimum absorber configuration for a given vibration suppression problem?

In order to address Question (1), procedures to construct 2PT1NG Immittance-Function-Networks (IF-Networks) need to be introduced. Similar to Chapter 3, an IF-Network refers to a network layout with its 2PT sub-networks represented by Immittance-Function-Blocks (IF-Blocks, e.g. Fig. 3.2(b)). Generic IF-Networks which capture all 2PT1NG IF-Network possibilities for given conditions will be identified. Different distribution cases of the pre-determined numbers of inerters, dampers and springs in the IF-Blocks of the generic IF-Networks will then be discussed to obtain all possible series-parallel 2PT1NG network layouts.

5.2 2PT1NG network layout enumeration

In this section, 2PT1NG network layouts with a reaction mass are considered. The series and parallel connections between a 2PT and a 2PT1NG network are firstly described, after which a procedure to formulate 2PT1NG IF-Networks is introduced. The generic 2PT1NG IF-Networks, covering all the IF-Network possibilities with a given number of IF-Blocks, are formulated. Using these generic IF-Networks, the enumeration of all possible network layouts is then discussed, together with the IF-Matrix derived for systematic optimisation.

5.2.1 Connection between 2PT and 2PT1NG networks

Using the same correspondence between mechanical networks and graphs as the one used in Section 3.2, where each element of the network is depicted as a branch, and terminals and internal connection points are as vertices, any 2PT1NG network can be represented by a three-terminal graph with one of the terminal-vertices corresponding to the NG. Taking the TMDI (Fig. 5.4(a1)) as an example, its graph representation can be depicted as Fig. 5.4(a2), which consists of three terminal-vertices and one intersection-vertex.

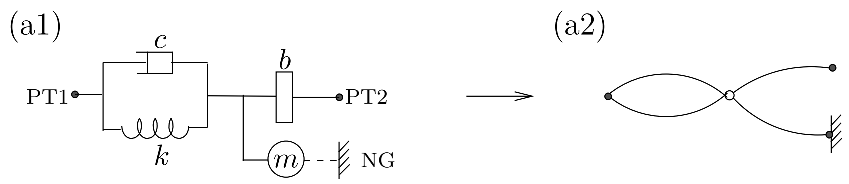

Fig. 5.4 (a) An example 2PT1NG network, the TMDI; and (b) its graph representation.

To formulate series-parallel 2PT1NG networks, the series and parallel connections between a 2PT and a 2PT1NG network need to be introduced based on the definitions for three-terminal graphs [150]. In [150], the series connection concept is similar to that for the connection between two two-terminal graphs, as described in Section 3.2. For a parallel connection, both terminal-vertices of a two-terminal graph and two of the three terminal-vertices of a three-terminal graph are connected together. The resulting graph has three terminal-vertices, same as the original three-terminal graph, but now two of them are shared with the original two-terminal graph. Based on these connection rules, considering the connection of an example two-terminal graph representing any 2PT network (Fig. 5.5(a1)) and a three-terminal graph representing a 2PT1NG network (shown in Fig. 5.5(a2)), the series connection results in two possibilities, shown in Fig. 5.5(a3) and (a4), respectively. By coalescing one terminal-vertex of Fig. 5.5(a1) with the left

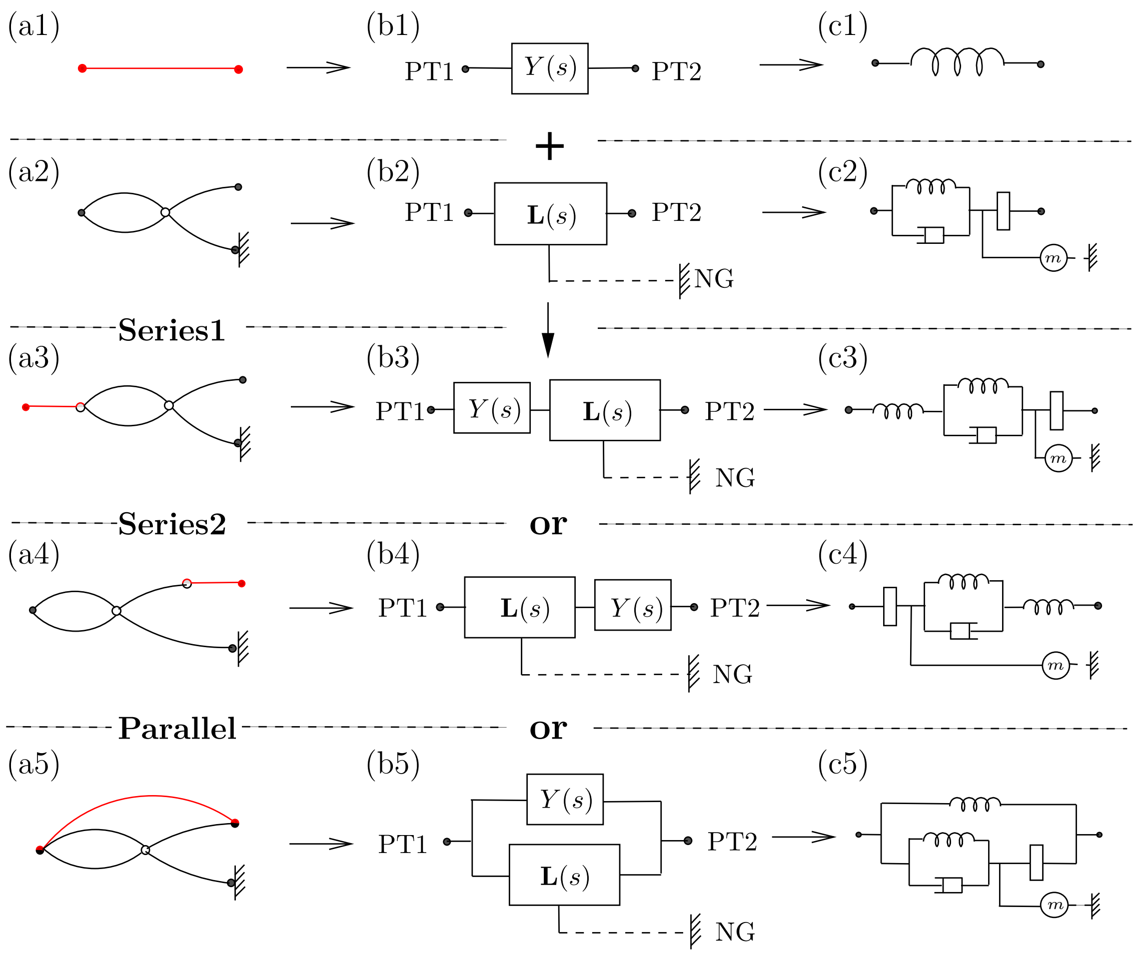

Fig. 5.5 Series and parallel connections between a 2PT network and a 2PT1NG network, represented as connections between (a) graphs, (b) IF-Networks and (c) example network layouts.

terminal-vertex of Fig. 5.5(a2), Fig. 5.5(a3) is obtained, while Fig. 5.5(a4) is formulated by connecting Fig. 5.5(a1) with the right terminal of Fig. 5.5(a2). Fig. 5.5(a5) shows the graph obtained by the parallel connection; because of the existence of NG, the parallel connection can only result in this possibility. The IF-Network examples obtained from the graphs are shown in Fig. 5.5(b1-b5). By depicting the IF-Network representations $Y(s)$ and $\mathbf{L}(s)$ as specific layout examples, the series and parallel connections between a 2PT network (spring) and a 2PT1NG network (TMDI) are shown in Fig. 5.5(c1-c5).

5.2.2 Formulation of the generic 2PT1NG Immittance-Function-Network

In order to formulate 2PT1NG IF-Networks, similar to 1PT1NG case, a collection of a reaction mass and a finite number of IF-Blocks is now considered. A sequence of steps is introduced based on the work of Nishizeki & Saito [150], shown in Fig. 5.6. At each step, a sub-network (either a 1PT1NG network or an IF-Block) is connected in series or in parallel with the network formed in the previous step. While such procedure is note unique, using this procedure, any series-parallel 2PT1NG IF-Network can be obtained. In the procedure, after each formulation step, we will carry out any obvious network simplification, same as the simplifications we carried out for the 1PT1NG case in Chapter 3, for example if two IF-Blocks are connected in series or in parallel, they will be *reduced* again to a single IF-Block. Similar to [150], in which the construction

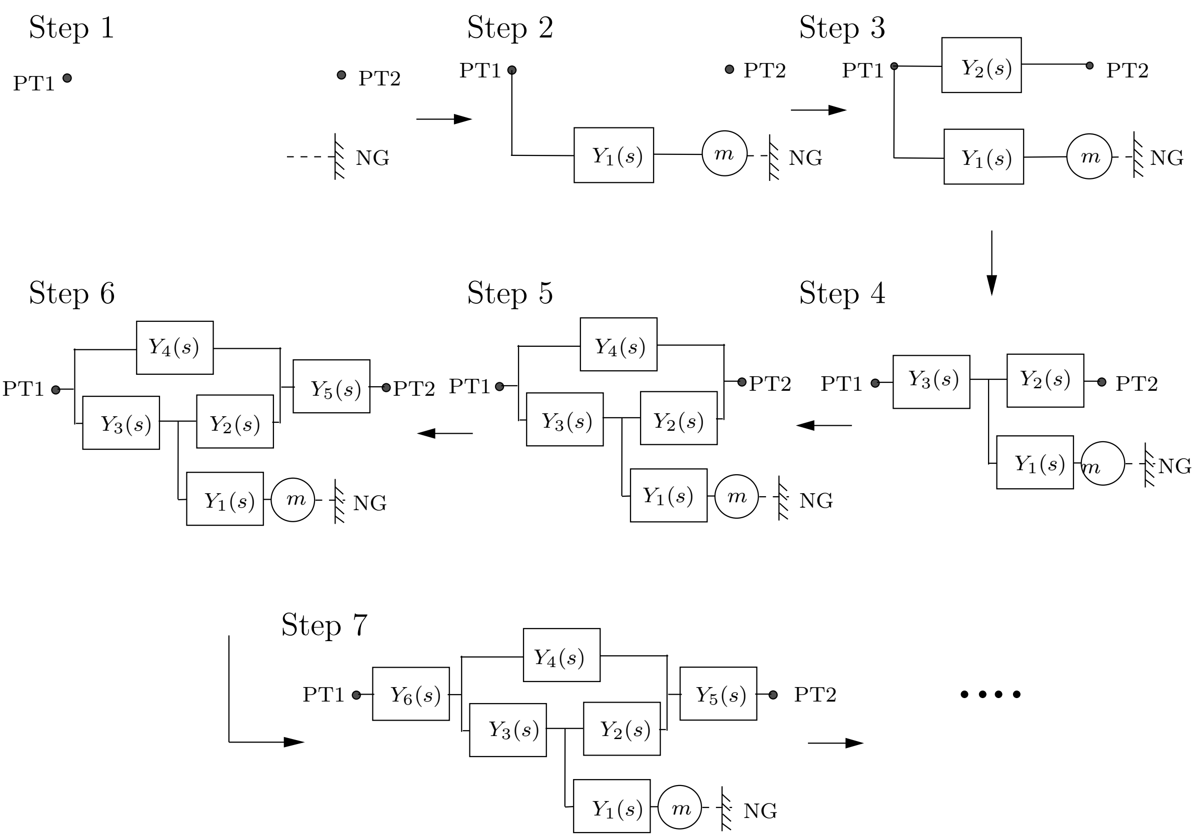

Fig. 5.6 A procedure to form all possible series-parallel 2PT1NG IF-Networks with a reaction mass and a pre-determined number of IF-Blocks.

of a three-terminal series-parallel graph begins with an empty graph, Fig. 5.6–Step 1 is taken as the start. We first consider joining the two terminals, PT1 and NG. Using the generic 1PT1NG IF-Network obtained in Section 3.2 (Fig. 3.5), a new network shown in Fig. 5.6–Step 2 is obtained. The next step is to add a single IF-Block $Y_2(s)$ to the network, resulting in Fig. 5.6–Step 3 (via a parallel connection between the terminals PT1 and PT2). Consider adding the next IF-Block, $Y_3(s)$, resulting in the new IF-Network shown in Fig. 5.6–Step 4 using the Series1 connection in Fig. 5.5. Note that all the other connection possibilities between Fig. 5.6–Step 3 and the IF-Block $Y_3(s)$ can all be simplified to Fig. 5.6–Step 3. From Step 4, only a parallel IF-Block can be added, with the resulting IF-Network shown in Fig. 5.6–Step 5, as any series IF-Blocks to the network of Step 4 can be *reduced* to the network of Step 4. Following from Step 5, only series additions modify the network. Both Series1 and Series2 connections in Fig. 5.5 need to be considered, and we define connecting to PT2 as Step 6, resulting in the network of Fig. 5.6–Step 6. An additional IF-Block is then added in series at PT1 – the resultant network is shown in Fig. 5.6–Step 7. Consequent steps will be adding IF-Blocks in parallel then in series by repeating Steps 5-7, until all IF-Blocks in the original collection are used. Following this procedure, all possible IF-Networks can be obtained.

In order to formulate generic IF-Networks, it needs to be discussed whether a specific IF-Block exists. To this end, the terminology *eliminated* and *present* are introduced here. An IF-Block is defined to be *eliminated* as its immittance function takes the value of 0 or ∞ – the value is chosen to ensure that the included components (i.e. the IF-Blocks and the reaction mass) or any two of the terminals, PT1, PT2 and NG, are not locked rigid and that none of the terminals is disconnected. An IF-Block is regarded as *present* if it is not eliminated. Consider the IF-Block $Y_1(s)$ shown in Fig. 5.6; if it is eliminated, its admittance function must take the value of ∞; otherwise the NG will be disconnected. For $Y_2(s)$, its removal must correspond to $Y_2(s) = \infty$; otherwise the PT2 will be disconnected. Also for $Y_3(s)$, we must set $Y_3(s) = \infty$; otherwise the PT1 in Fig. 5.6–Step 4 will be disconnected. Consider the parallel added IF-Block $Y_4(s)$: if it is eliminated, it must take the value of 0 (otherwise PT1 and PT2 in Fig. 5.6–Step 5 will be locked rigid). For the series added IF-Blocks $Y_5(s)$ and $Y_6(s)$: we must set them as ∞ to ensure that the terminals of the resulting networks (see Fig. 5.6–Step 6 and Step 7) are not disconnected. Following the same argument, the additional IF-Blocks added in parallel (resp. series) connection must take the value of 0 (resp. ∞) when they are eliminated.

The rest part of this subsection focuses on generating generic IF-Networks. Different from 1PT1NG networks, where one generic IF-Network is sufficient (Fig. 3.5), for 2PT1NG networks, different generic IF-Networks are needed depending on the number of IF-Blocks which are present. Now consider the possible 2PT1NG IF-Networks with a pre-determined number, R, of IF-Blocks. Suppose that the generic IF-Network, representing $R - 1$ IF-Blocks, has been formulated, denoted as $\mathbf{L}_{R-1}(s)$, all the IF-Networks with R IF-Blocks can be subsequently obtained by adding an extra IF-Block to it. The generic IF-Network, $\mathbf{L}_R(s)$, covering all the obtained IF-Network possibilities, can then be formulated, satisfying the condition that R IF-Blocks are present. Following this argument, the generic IF-Network for any R value can be formulated. Note that the generic IF-Network has more IF-Blocks than is allowed, hence requires the condition that R IF-Blocks are present. We will now discuss the $R = 1$ case, then move on to $R = 2$ and beyond.

- For $R = 1$: We first consider the case where in Step 1 of Fig. 5.6, $Y_1(s)$ is present. The resulting network is Fig. 5.6–Step 2, which is a 1PT1NG network (with PT2 disconnected). Hence this case is not valid and $Y_1(s)$ must be eliminated. When $Y_2(s)$ is present, a 2PT1NG IF-Network is obtained, shown in Appendix B, Fig. B.1(a). If $Y_2(s)$ is not present, the connection of $Y_3(s)$ results in a new 2PT1NG IF-Network, see Fig. B.1(b), Appendix B. If $Y_3(s)$ is eliminated, PT1 and PT2 are rigidly connected and any follow-on steps in Fig. 5.6 only result in a 1PT1NG network. Hence, two network possibilities (Fig. B.1, Appendix B) are obtained for the $R = 1$ case, with which the generic IF-Network can be obtained as $\mathbf{L}_1(s)$ in Table 5.1, satisfying the condition that only one IF-Block is present.
- For $R = 2$: The IF-Networks can be formulated by adding one additional IF-Block to the generic IF-Network $\mathbf{L}_1(s)$ in Table 5.1. Firstly, we set both $Y_2(s)$ and $Y_3(s)$ in $\mathbf{L}_1(s)$ as present, this results in an IF-Network shown in Fig. B.2(a), Appendix B. We then consider the case where $Y_1(s)$ is present. This means either $Y_2(s)$ or $Y_3(s)$ can be present, resulting in two new IF-Networks shown in Appendix B, Fig. B.2(b, c). At last, an extra IF-Block $Y_4(s)$ is added to $\mathbf{L}_1(s)$ in parallel connection, and its presence will result in the removal of $Y_2(s)$ or $Y_3(s)$, however, the resulting networks can be simplified to the network with one IF-Block. Hence, the network $\mathbf{L}_2(s)$ shown in Table 5.1 is the generic IF-Network for $R = 2$ case, satisfying the condition that two IF-Blocks are present.
- For $R = 3$: An extra IF-Block is added to the generic IF-Network $\mathbf{L}_2(s)$ in series or in parallel, to formulate all the IF-Networks with three IF-Blocks. We first set three IF-Blocks in $\mathbf{L}_2(s)$ as present, an IF-Network shown in Appendix B, Fig. B.3(a) is hence obtained. By adding an additional IF-Block $Y_4(s)$ in parallel to $\mathbf{L}_2(s)$, its presence will result in the removal of $Y_1(s)$; otherwise the resulting network will be *reduced* to a network with two IF-Blocks. This results in an IF-Network of Fig. B.3(b). Hence, the generic IF-Network for $R = 3$ can be formulated as $\mathbf{L}_3(s)$ in Table 5.1, subject to the condition that three IF-Blocks are present.
- For $R = 4$: An IF-Network shown in Fig. B.4(a), Appendix B can be firstly obtained by setting all four IF-Blocks in $\mathbf{L}_3(s)$ as present. An extra IF-Block, $Y_5(s)$ is then added in series to the right of $\mathbf{L}_3(s)$ and if it is present, only the removal of $Y_1(s)$ can result

in a new IF-Block, see Appendix B, Fig. B.4(b). Consider the case that $Y_6(s)$ is added in series to the left of $\mathbf{L}_3(s)$. An IF-Network of Fig. B.4(c) can be obtained. Hence, the generic IF-Network for $R = 4$ can be formulated as $\mathbf{L}_4(s)$ in Table 5.1, with the condition that four IF-Blocks are present.

- Generalisation: Using the similar argument, the generic IF-Network representing more numbers of IF-Blocks can be obtained, as shown in Table 5.1. For the odd R (with $R \geq 5$), the generic IF-Network is formulated by adding an IF-Block $Y_{\frac{3R-1}{2}}(s)$ in parallel to $\mathbf{L}_{R-1}(s)$. The subscript $\frac{3R-1}{2}$ of the IF-Block represents the total number of IF-Blocks required in the generic IF-Network, $\mathbf{L}_R(s)$. Also for the even R (with $R \geq 6$), the generic IF-Network can be formulated by series connecting two IF-Blocks $Y_{\frac{3R}{2}-1}(s)$ and $Y_{\frac{3R}{2}}(s)$ with $\mathbf{L}_{R-1}(s)$, where in total $\frac{3R}{2}$ numbers of IF-Blocks are required.

The generic IF-Network results of the above are summarised in Table 5.1, which can then be used for enumerating all possible network layouts.

Table 5.1 Generic 2PT1NG IF-Networks, $\mathbf{L}_R(s)$, with the condition of R IF-Blocks present

	Odd R		Even R
$R = 1$ ($\mathbf{L}_1(s)$)	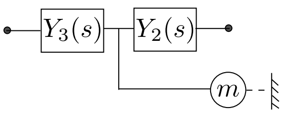	$R = 2$ ($\mathbf{L}_2(s)$)	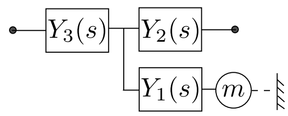
$R = 3$ ($\mathbf{L}_3(s)$)	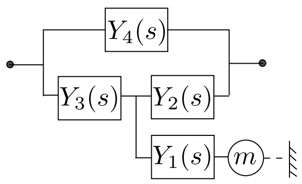	$R = 4$ ($\mathbf{L}_4(s)$)	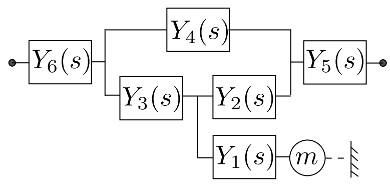
⋮		⋮	
$R \geq 3$ ($\mathbf{L}_R(s)$)	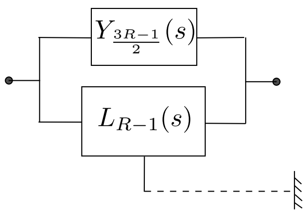	$R \geq 4$ ($\mathbf{L}_R(s)$)	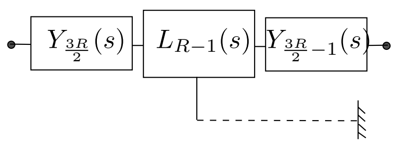

5.2.3 Network layout enumeration and Immittance-Function-Matrix derivation

For the enumeration of 2PT1NG network layouts with a reaction mass element and N 2PT elements (springs, dampers and inerters), the obtained generic IF-Networks with $R = 1,\ 2,\ \ldots,\ N$ in Table 5.1 can be used. We first distribute the N 2PT elements into R present IF-Blocks (other IF-Blocks are eliminated), and secondly allocating element types into each present IF-Block. After this, the element types and numbers will be determined for each IF-Block in the generic IF-Networks. The structure-immittance approach [30] is then adopted to derive the corresponding immittance functions of the blocks, which is able to cover the full set of possible 2PT network connections.

With the obtained immittance functions of the included IF-Blocks, the IF-Matrix for each generic IF-Network is derived based on the procedure shown in Appendix B, which can then be used for optimisation studies. We denote that the IF-Matrix for a 2PT1NG network can be derived by deriving its equations of motion. However, there are a great number of possible network layouts, a more straightforward and simpler approach for deriving the IF-Matrix is needed – this is provided and explained in detail in Appendix B.

5.3 2PT1NG network case demonstration

In this section, the 2PT1NG network case with one damper, one spring and one inerter is analysed. All possible 2PT1NG network layouts are enumerated using the generic IF-Networks in Table 5.1. The IF-Matrix for each generic IF-Network is derived and applied to the example structure. Significant performance advantages with 2PT1NG network layouts will be demonstrated at the end of this section.

5.3.1 Network layouts enumeration

For the 2PT1NG networks with one damper, one spring and one inerter, we have $N = 3$. Hence, three generic IF-Networks with $R = 1$, $R = 2$ and $R = 3$, shown as $\mathbf{L}_1(s)$, $\mathbf{L}_2(s)$ and $\mathbf{L}_3(s)$ in Table 5.1, will be used.

Consider the generic IF-Network for $R = 1$, $\mathbf{L}_1(s)$ of Table 5.1, all the three 2PT elements should be distributed in one IF-Block and the other IF-Block is eliminated. As a result, in total 16 2PT1NG network layouts are enumerated for systematic analysis, and the structure-immittance approach [30] is adopted to express the admittance function of the present IF-Block. The admittance function is the structural admittances for one inerter, one damper and one spring case, shown in Eq. (2.8). By expressing the force-velocity transfer function matrix of the generic IF-Network shown in Table 5.1 and making use of the condition that one IF-Block is eliminated, we can obtain the IF-Matrix $\mathbf{L}_1(s)$ as (B.3) in Appendix B, with the condition that one of the admittance functions, $Y_1(s)$, $Y_2(s)$, takes the expression as structural admittances of (2.8), and the other one must equal ∞.

For the generic IF-Network with $R = 2$, shown as $\mathbf{L}_2(s)$ of Table 5.1, two of the three IF-Blocks are present, between which the three 2PT elements are distributed in. For these two present IF-Blocks, one should include one 2PT element and the other one consists of the remaining two elements. For example, when $Y_1(s)$ and $Y_2(s)$ in $\mathbf{L}_2(s)$ (Table 5.1) are present and $Y_1(s)$ includes one element, such as a spring, the other two elements (the damper and inerter) are contained in $Y_2(s)$, resulting in two network possibilities by connecting damper in series or in parallel with the inerter. Consider that there are three different element types and switching $Y_1(s)$ with $Y_2(s)$ will result in different network possibilities, the generic IF-Network with one IF-Block eliminated covers 36 network layouts. Finally, the IF-Matrix for this generic IF-Network, $\mathbf{L}_2(s)$, can be derived as (B.4) in Appendix B, where one of admittance functions $Y_1(s)$, $Y_2(s)$, $Y_3(s)$ equals ∞, one is the force-velocity transfer function of a single 2PT element, and the third requests structural admittance for the remaining two 2PT elements. Consider the case that $Y_1(s)$ represents a spring k and $Y_2(s)$ includes one damper c and one inerter b, we should make $Y_3(s) = \infty$, $Y_1(s) = k/s$ and $Y_2(s)$ takes the expression of a structural admittance obtained for one damper and one inerter case, given as:

$$Y_2(s) = \frac{c_2(bs + c_1)}{(bs + c_1 + c_2)} \tag{5.1}$$

with the condition that one of the parameters c_1 or $1/c_2$ is positive and the other one equals zero.

Considering the generic IF-Network obtained for $R = 3$ case, shown as $\mathbf{L}_3(s)$ of Table 5.1, three of the four IF-Blocks must be present and each of them contains one 2PT element. By removing one IF-Block and distributing three different element types into the present IF-Blocks, all the 2PT1NG network layouts for this case can be enumerated. Note that when $Y_2(s)$ or $Y_3(s)$ is eliminated with its admittance function as ∞, the resulting IF-Network will be *reduced* to that with two IF-Blocks, hence are omitted for the network layouts enumeration. From the generic IF-Network, in total of 12 network layouts are finally enumerated. These network layouts can be represented by the IF-Matrix $\mathbf{L}_3(s)$, derived based on (B.4) and (B.6) in Appendix B, given as

$$\mathbf{L}_3(s) = \left(\mathbf{L}_2(s) + Y_4(s)\begin{bmatrix} 1 & -1 \\ -1 & 1 \end{bmatrix}\right) \tag{5.2}$$

where either $Y_1(s) = \infty$ or $Y_4(s) = 0$ and the remaining three admittance functions are the force-velocity transfer functions of three different 2PT element types.

These obtained IF-Matrices can then be used for given vibration suppression problems. Importantly, using the method proposed here, all possible series-parallel 2PT1NG network layouts, with one reaction mass, one spring, one damper and one inerter are covered. In addition, by making use of the structure-immittance approach, all the possible layouts can be analysed in a systematic way and by optimising these using the objective functions considered, the optimal configuration can be obtained across all the network possibilities. In the following subsection, the results obtained in this part will be applied to a 3-DOF building structure example, to illustrate the benefits of the proposed design approach. For the one reaction mass, one inerter, one damper and one spring case, in total 64 2PT1NG network layouts can be enumerated and covered by three generic IF-Networks, amongst which the optimum configuration can be obtained by three optimisations.

5.3.2 Numerical application on the example structure

To demonstrate the advantages of the proposed generic 2PT1NG network, a 3-DOF building model similar to the one used in Section 4.1 is adopted here with some modifications. The model is redrawn in Fig. 5.7 to highlight these differences. The suppression system is taken to be the 2PT1NG network including one reaction mass, one inerter, one damper and one spring. The value of the reaction mass is taken as 1000 kg. Vibration absorbers attached to two floors are usually installed via a brace that spans between storey levels. Inevitably this brace has some compliance, so a brace stiffness k_b in series with the absorber and connecting to the lower floor is included. In this study, the structure parameters are adopted as $m_s = 10000$ kg, $k_s = 15000$ kN/m, and the brace stiffness is taken as $k_b = 0.2k_s$, in line with [151]. Forces $-f_u$ and $-f_l$ are exerted on the upper and lower floors, respectively. The forces are defined as positive to the right on the absorber. As stated in Section 4.1.2, the focus of this study is to demonstrate the advantages of the proposed systematic approach under same optimisation scenario, rather than comprehensively explore the optimum design for a specific engineering problem. Therefore, we only consider the absorbers mounted at the top floor. Other floors can also be chosen for demonstration purpose. With the identified network layouts, their exact optimum location can also be further explored for practical applications.

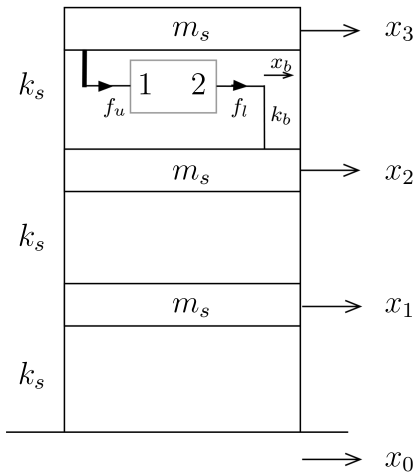

Fig. 5.7 Schematic plot of a 3-DOF building model.

Due to the brace stiffness k_b, an additional DOF with displacement x_b is introduced, where $F_l = k_b(X_2 - X_b)$ in the Laplace domain. In this example, the inter-storey drift displacement, which is a measure of the potential seismic damage of a structure, is taken as the performance measure. The frequency response function of the ith floor inter-storey drift displacement, denoted as X_{d_i}, can be obtained similarly from Eq. (4.1) with $X_{d_i} = X_i - X_{i-1}$, where $i = 1, 2, 3$. The objective function, related to the inter-storey drift displacements, is then defined as:

$$J_d = \max_{i=1,2,3} \left(\left\| T_{s^2 X_0 \to X_{d_i}}(s) \right\|_\infty \right) \tag{5.3}$$

where $T_{s^2 X_0 \to X_{d_i}}$ denotes the transfer function from the earthquake acceleration to the inter-storey drift displacements and $\left\| T_{s^2 X_0 \to X_{d_i}}(s) \right\|_\infty$ is the maximum value of $T_{s^2 X_0 \to X_{d_i}}$ where i=1, 2, 3.

For the 2PT1NG network with each of the four element types, three generic IF-Networks, $\mathbf{L}_1(s)$, $\mathbf{L}_2(s)$ and $\mathbf{L}_3(s)$, are formulated in Section 5.2, covering all the 2PT1NG network possibilities. These obtained generic IF-Networks, together with their corresponding IF-Matrix as shown in Eq. (B.3, B.4, 5.2), are then used to minimise the objective function J_d. For example, for 2PT1NG networks covered by the generic IF-Network, $\mathbf{L}_1(s)$, the IF-Matrix – Eq. (B.3) is adopted as the transfer function matrix of the vibration suppression device, with which the objective function J_d can be obtained based on Eq. (5.3). In Eq. (B.3), the present admittance function $Y_2(s)$ or $Y_3(s)$ formulated using the structure-immittance approach is then optimised to identify the optimal 2PT network configuration out of all the eight possible layouts made up of one inerter, one damper and one spring. Together with this obtained 2PT network, the optimal 2PT1NG

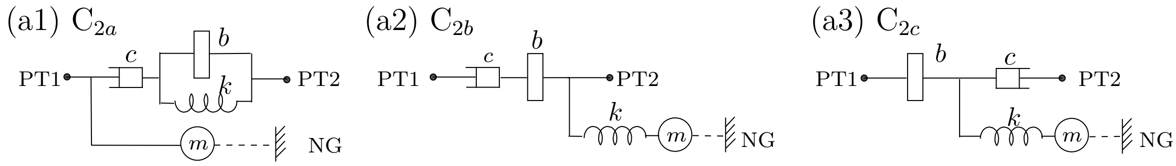

Fig. 5.8 Optimal 2PT1NG configurations for the one inerter, one damper and one spring case for (a1) $R = 1$, (a2) $R = 2$ and (a3) $R = 3$ case.

network configuration can then be obtained from the corresponding generic IF-Network, $\mathbf{L}_1(s)$, of Table 5.1. The optimal configurations for three generic IF-Network cases with $R = 1,\ 2,\ 3$ have been obtained as Fig. 5.8 (a1), (a2) and (a3), respectively, denoted as C_{2a}, C_{2b}, C_{2c}. The previously derived generic 1PT1NG network is also employed here to obtain the optimum 1PT1NG network for comparison following the same performance criteria and objective function J_d, where configuration C_1 is obtained in Fig. 5.9. The corresponding optimal results in terms of J_d are summarised in Table 5.2, together with the optimum parameter values. The previously proposed layouts, such as the TMD, the TID, the TMDI and C_1 are also considered here for comparison.

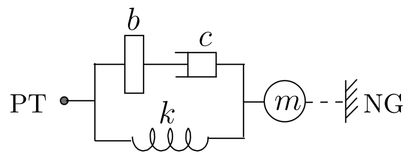

Fig. 5.9 The obtained optimum 1PT1NG configuration C_1.

For the generic IF-Network, $\mathbf{L}_1(s)$ of Table 5.1, out of the 16 possible layouts, the optimisation indicates that the configuration C_{2a} is optimal. The corresponding optimal value of the objective function J_d is 0.0195 shown in Table 5.2, slightly smaller than that of the TID. Considering generic IF-Network representing two IF-Blocks, we notice that the TMDI is covered by this network ($\mathbf{L}_2(s)$ of Table 5.1), with $Y_1(s) = \infty$, $Y_2(s) = bs$ and $Y_3(s) = k/s + c$. However, the TMDI is not the optimum configuration for this case, and the resulting optimum configuration is shown in Fig. 5.8(a2), with which the value of J_d is obtained as 0.0102. It can be seen that comparing with the TMDI, C_{2b} can provide almost 30% performance improvement when $b = 9.91 \times 10^3$ kg, $c = 4.28 \times 10^2$ kNs/m and $k = 2.26 \times 10^2$ kN/m. Fig. 5.8(a3) shows the optimum absorber configuration C_{2c} for

Table 5.2 Optimisation results for the one reaction mass, one inerter, one damper and one spring case.

Configurations	**Performance** J_d ($\times 10^{-3}$ s^2)	**Optimal parameter values** (kg, kNs/m, kN/m)
TMD (no b)	25.0 (–)	$c = 11.7,\ k = 2.75 \times 10^2$
TID (no m)	19.6 (21.6%)	$b = 7.94 \times 10^3,\ c = 7.50 \times 10^2,\ k = 4.35 \times 10^3$
C_1 (a 1PT1NG device)	16.3 (34.8%)	$b = 1.05 \times 10^3,\ c = 30.5,\ k = 4.92 \times 10^2$
TMDI (a $R = 2$ case device)	14.5 (42.0%)	$b = 1.12 \times 10^3,\ c = 9.50,\ k = 6.22 \times 10^2$
C_{2a}	19.5 (22.0%)	$b = 8.95 \times 10^3,\ c = 7.65 \times 10^2,\ k = 16.8$
C_{2b}	10.2 (59.2%)	$b = 9.91 \times 10^3,\ c = 4.28 \times 10^2,\ k = 2.26 \times 10^2$
C_{2c}	8.60 (65.6%)	$b = 8.10 \times 10^3,\ c = 3.26 \times 10^2,\ k = 2.13 \times 10^2$

the $R = 3$ case, which gives the value of J_d as 0.0086, approximately 41% smaller than that of the TMDI and almost 66% better than the TMD. It can also be seen that the C_{2c} is the most effective vibration suppression device, amongst all the 64 series-parallel 2PT1NG networks consisting of one reaction mass and each of the three 2PT element types. From Table 5.2, we note that the configuration C_{2c} outperforms the C_1 with 47.2% performance improvement in J_d. This suggests that the 2PT1NG network, i.e. one which has connection points on the second and third storey, can provide better seismic performance than the 1PT1NG one (which is connected to the third storey only) with the same numbers of each element type. Considering that the generic network of the 1PT1NG network is a 2PT network connected to a mass element (as illustrated in Fig. 3.5, Chapter 3), the 2PT part can hence be obtained using the structure-immittance approach. This demonstrates that the proposed generic 2PT1NG network can be used to identify more beneficial configurations with better performance improvements compared to the structure-immittance approach when using the same number of elements.

Fig. 5.10 shows the frequency responses of three inter-storey drifts transfer functions with the identified beneficial absorber configurations. It can be seen that rather than splitting the first fundamental frequency into two seperate frequencies, both the C_{2b} and the C_{2c} split it into three frequencies, hence resulting in smaller values of the drift displacements comparing with the other configurations, such as the TMDI. This is because both C_{2b} and C_{2c} contain additional DOF compared to other devices. Also note that the configuration C_{2c} results in the smallest inter-storey drift values of all the three floors in the vicinity

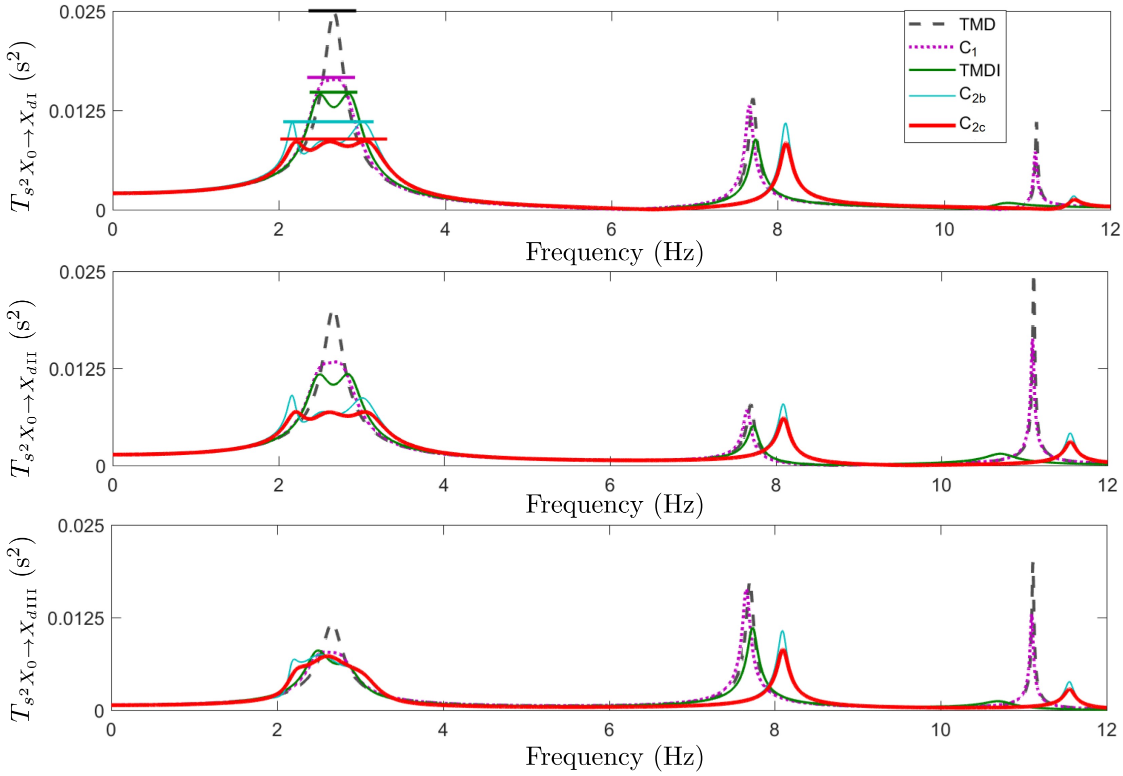

Fig. 5.10 Frequency domain responses of the inter-storey drifts with the TMD (black dashed), TMDI (green solid), C_1 (purple dotted), C_{2b} (thin cyan solid) and C_{2c} (thick red solid).

of not only the first fundamental frequency, but also the second and third fundamental frequencies.

5.4 Summary of the chapter

This chapter presents a systematic characterisation and analysis of passive 2PT1NG Networks. Independent vibration absorbers with two attachment points and one reaction mass can be covered by such networks. Generic 2PT1NG networks, representing the topological connections of one mass and an arbitrary number of IF-Blocks are developed. Therefore, a full set of network layouts with pre-determined numbers of inerters, dampers and springs can be captured and enumerated. Main conclusions and results are summarised as follows:

1) A sequence of steps is introduced based on the graph theory. With this procedure, any 2PT1NG networks connected in series-parallel can be formulated. Based on it, each generic IF-Network with a specific number of IF-Blocks can be obtained. Combined

with the structural immittances, 2PT1NG network with a predetermined number of inerters, dampers, springs and one reaction mass can be obtained systematically. By using the force-velocity Immittance-Function-Matrices, dynamics of vibration suppression devices with two attachment points can be described and used for vibration suppression problems.

2) A 3-DOF building model is considered to mitigate the maximum inter-storey drift, and the number of inerter, damper and spring included in the vibration suppression device is restricted to be one for each. Optimal configurations are obtained out of 64 candidate network layouts. Considering the devices with two attachment points and one reaction mass (2PT1NG networks), the most beneficial configuration can provide almost 66% better performance than the TMD and also outperforms the TMDI with 41% performance improvement.

This case study has demonstrated the significant advantages of the proposed generic 2PT1NG networks and the corresponding systematic identification procedure. It is a powerful tool to identify independent vibration absorbers for uni-directional vibration suppression. However, in terms of interlinked vibration absorbers which are widely used to suppress multi-dimensional vibrations of the primary system, the above developed generic networks are of little use. Therefore, in the next chapter, we will focus on a certain type of interlinked vibration systems which can be represented as three-terminal networks. A generic network along with a systematic identification procedure will also be provided.

Chapter 6

Generic three-terminal networks with the application to vehicle interlinked suspension design

The generic networks developed in the previous chapters can only be adopted to identify independent vibration absorbers, which contains one reaction mass and arbitrary two-terminal element with no more than two attachment-points to the primary system, for the uni-dimensional vibration suppression problems.

However, in terms of interlinked vibration absorbers which are widely used to suppress multi-dimensional vibrations of the primary system, the above developed generic networks are of little use. Two interlinked vibration absorber examples are given here: the vehicle interlinked suspension [6] shown in Fig. 6.1(a) is used to suppress the vehicle vibrations in both the roll and heave directions; same as the wind turbine gearbox interlinked mounting system [7]) as shown in Fig. 6.1(b). With proper design, such interlinked absorbers can be represented as three-terminal networks. However, a systematic procedure is less well developed for the three-terminal network, although many studies have been done by employing the classical network synthesis theory as introduced in Chapter 2. The drawbacks for these studies are that, minimal realisation in terms of the total number of elements used is not considered, nor could all three transformerless elements be included in the network at the same time.

To better serve the purpose of identifying beneficial interlinked absorbers from a full set of candidates with the least possible number of elements, similar to the previous chapters, a generic-network-based approach is proposed to realise the series-parallel three-terminal networks with predetermined numbers of transformerless elements (for ex-

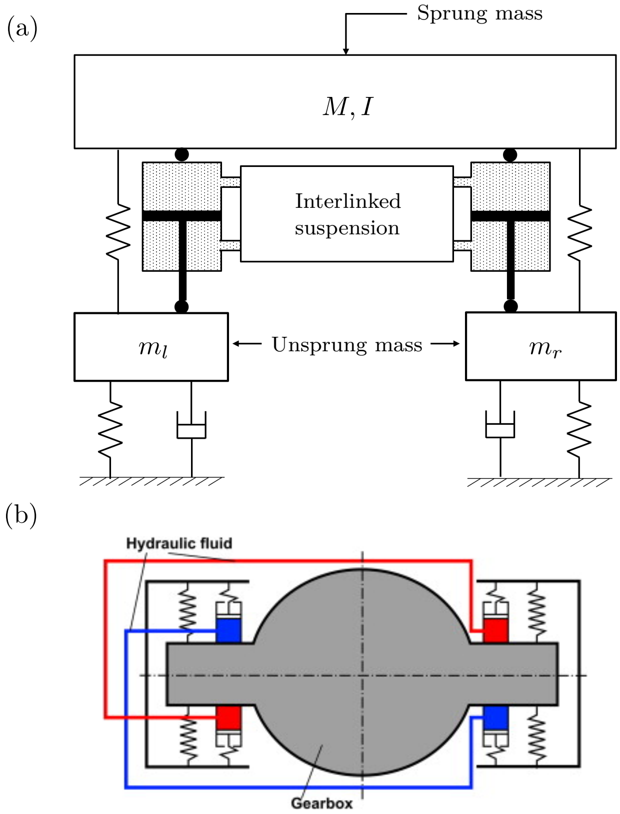

Fig. 6.1 Example dynamic systems where the HIS can be applied to: (a) suspension design for a front half-car model, following [6]; (b) mount design for the wind turbine gearbox, reproduced from [7].

ample, resistors, inductors and capacitors in the electric domain). This is again achieved by first defining the series-parallel connections using the graph theory [150]. Then, following the definition, Immittance-Function-Blocks (IF-Blocks), i.e., a series-parallel two-terminal network containing a predetermined number of passive transformerless elements, can be used to form three-terminal Immittance-Function-Networks (IF-Networks). Then, the Generic-Immittance-Function-Network (GIFN) is developed to represent all topological possibilities of these IF-Networks. Through this approach, both the ability to investigate a full class of series-parallel three-terminal networks, and the means to control the complexity, topology and element types in resulting networks can be provided simultaneously.

This chapter is structured as follows. In Section 6.1, an example series-parallel three-terminal network representing a hydraulically interlinked system (HIS) is first given, together with their mathematical expressions. The problem of identifying the optimum series-parallel three-terminal networks is also formulated. The systematic approach is developed in Section 6.2 by constructing the Generic-Immittance-Function-Network — this captures the full set of three-terminal network possibilities with series-parallel connections. In Section 6.3, the proposed HIS is used for a half-car model suspension design, in which the optimum network is identified using the systematic approach proposed in Section 6.2 to achieve the best vehicle performance. Conclusions are drawn in Section 6.4.

6.1 Interlinked vibration absorber to three-terminal network

In this study, the hydraulically interlinked system (HIS) for half-car suspension design will be used as an example to demonstrate the development of the interlinked vibration absorber identification approach. With the discussion in Section 6.2 focusing on the suspension device and its network representation, details of the half-car model and its corresponding parameters will be included in Section 6.3.

6.1.1 Hydraulically interlinked system for vehicle suspension design

We adopted the HIS introduced in [6] as an example, which considers an anti-oppositional arrangement (stiffen out-of-phase motion relative to in-phase motion) as shown in Fig. 6.2. It possesses left-right symmetry, consisting of two hydraulic circuits, each comprising three damper valves, a nitrogen filled accumulator, and a hydraulic pipeline. It is assumed that the relationship between the fluid pressure and the piston flow is linear, and the cross-line leakage occurring between chambers and pistons is not considered in this study [6]. The HIS introduced here is the same as the one used in [6], except that the cross-section areas are equal here for simplicity. (Note that the methodology we developed is also applicable to pistons with unequal cross-section areas.)

P_{ij}, q_{ij}, A_{ij} and v_{ij} with $i = l$ or r and $j = 1$ or 2 are fluid pressure, fluid flow rate, cross-section area of each piston chamber, and the velocity of each piston end. l and r represent left and right sides, and 1 and 2 represent upper and lower chambers, respectively. F_{ld} and F_{rd} are dynamic forces exerted to the interlinked suspension at left and right pistons. Δv_l and Δv_r are the relative velocities exhibit at each end of the suspension struts. All positive directions are illustrated in the figure, where positive velocities are when the piston end velocity v_{ij} moves up, Δv_l moves up, and Δv_r moves down (to maintain

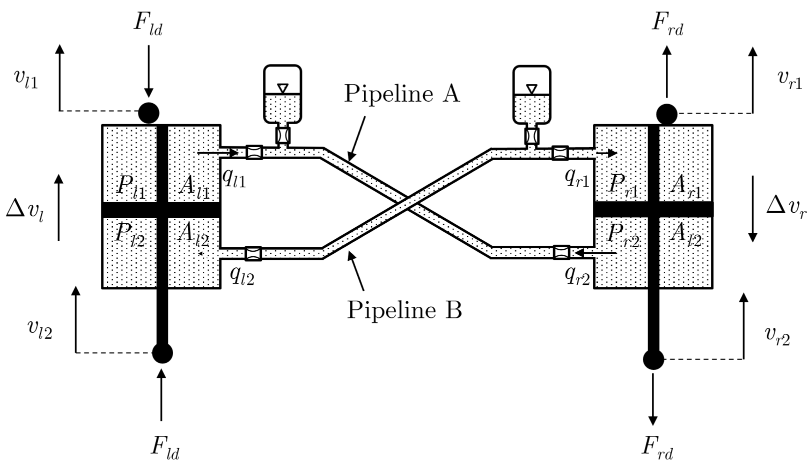

Fig. 6.2 Example hydraulically interlinked suspension configuration, following [6].

the roll movement performance). Hence the suspension dynamic forces F_{ld} and F_{rd} are defined as positive with compression on the left side and extension on the right side. Taking $\mathbf{Z}_h$ as the hydraulic impedance matrix from the fluid flow $\tilde{\mathbf{q}} = [\tilde{q}_{l1}, \tilde{q}_{r2}, \tilde{q}_{l2}, \tilde{q}_{r1}]^T$ to the pressure difference $\Delta\tilde{\mathbf{P}} = [\tilde{P}_{l1} - \tilde{P}_{l10}, \tilde{P}_{r2} - \tilde{P}_{r20}, \tilde{P}_{l20} - \tilde{P}_{l2}, \tilde{P}_{r10} - \tilde{P}_{r1}]^T$ in the Laplace domain, this gives

$$\Delta\tilde{\mathbf{P}} = \mathbf{Z}_h\tilde{\mathbf{q}} \tag{6.1}$$

where $\tilde{}$ indicates the Laplace representation of these variables.

Fig. 6.3 (a) and (b) illustrate the fluid flow in pipelines A and B, respectively, where P_{A1} and P_{B1}, q_{Aa} and q_{Ba} are the fluid pressure and flow rate at the bottle neck of each accumulator. P_{A0} and P_{B0} are the initial hydraulic pressure inside the accumulators, which should equal the initial pressure in each pipeline (i.e., $P_{A0} = P_{l10} = P_{r20}$ and $P_{B0} = P_{r10} = P_{l20}$). P_{Aa} and P_{Ba} are the instant hydraulic pressures inside the accumulators. Assuming a linear relationship between the fluid flow and pressure [6], the differential relationships for hydraulic elements, the resistance, compliance and inertance, can be expressed as R, C and I, respectively [6, 64]. Hence, corresponding network representations for each pipeline can be found in Fig. 6.3(c) and (d), respectively. They are both three-terminal networks, with relationships that $q_{l1} + q_{r2} = q_{Aa}$ and $q_{l2} + q_{r1} = q_{Ba}$. These two networks can be redrawn as networks shown in Fig. 6.3(e) and (f), where

$$
\begin{aligned}
&Z_{hA1} = R_{A1} + I_{A1}s, \quad Z_{hB1} = R_{B1} + I_{B1}s \\
&Z_{hA2} = R_{A2} + I_{A2}s, \quad Z_{hB2} = R_{B2} + I_{B2}s \\
&Z_{hAa} = R_{Aa} + \frac{1}{C_{Aa}s}, \quad Z_{hBa} = R_{Ba} + \frac{1}{C_{Aa}s}
\end{aligned}
\tag{6.2}
$$

Thus, the impedance matrix of the default hydraulic interlinked suspension system can be expressed as:

$$
\mathbf{Z}_h = \begin{bmatrix} \mathbf{Z}_{hA} & \mathbf{0} \\ \mathbf{0} & \mathbf{Z}_{hB} \end{bmatrix} = \begin{bmatrix} Z_{hA1} + Z_{hAa} & Z_{hAa} & 0 & 0 \\ Z_{hAa} & Z_{hA2} + Z_{hAa} & 0 & 0 \\ 0 & 0 & Z_{hB1} + Z_{hBa} & Z_{hBa} \\ 0 & 0 & Z_{hBa} & Z_{hB2} + Z_{hBa} \end{bmatrix}
\tag{6.3}
$$

with $\mathbf{Z}_{hA}$ and $\mathbf{Z}_{hB}$ as the impedance matrices of pipelines A and B, respectively.

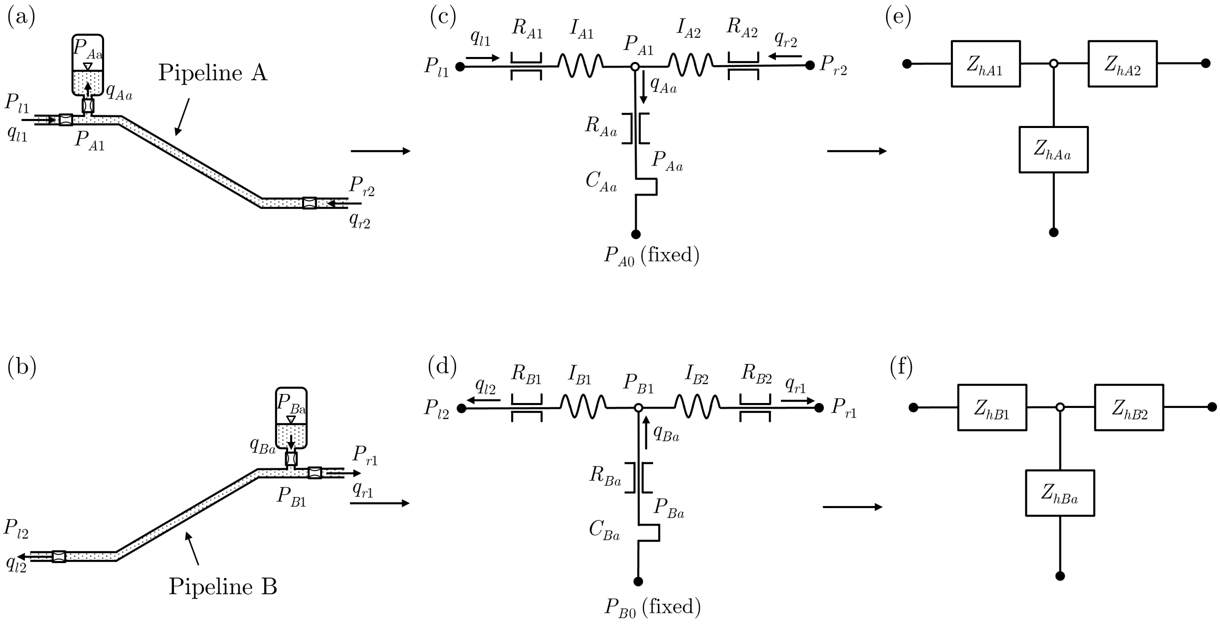

Fig. 6.3 HIS pipeline configurations and the corresponding networks

The relationship of the HIS dynamic force $\tilde{\mathbf{F}}_d$ and the relative velocity of the HIS $\mathbf{\Delta\tilde{v}}$ in the Laplace domain can be represented as $\tilde{\mathbf{F}}_d = \mathbf{Y}_m \mathbf{\Delta\tilde{v}}$ where $\mathbf{Y}_m$ is the mechanical admittance matrix, $\tilde{\mathbf{F}}_d = [\tilde{F}_{ld}, \tilde{F}_{rd}]^T$, and $\mathbf{\Delta\tilde{v}} = [\Delta\tilde{v}_l, \Delta\tilde{v}_r]^T$. Thus we can obtain the relationship between the hydraulic impedance matrix and its equivalent mechanical admittance matrix:

$$\mathbf{Y}_m = \mathbf{D}\mathbf{A}\mathbf{Z}_h\mathbf{A}\mathbf{D}^T \tag{6.4}$$

where

$$\mathbf{D} = \begin{bmatrix} 1 & 0 & 1 & 0 \\ 0 & 1 & 0 & 1 \end{bmatrix}$$

is the position matrix; $\mathbf{A} = diag[A_{l1}, A_{r2}, A_{l2}, A_{r1}]$ is the area matrix. Detailed derivation of the hydraulic suspension impedance and its mechanical admittance can be found in Appendix C.

To this end, the mathematical properties of the HIS is obtained, which is represented as two hydraulic three-terminal networks, as illustrated in Fig. 6.3 (c) and (d).

6.1.2 Problem formulation

The pipeline shown in Fig. 6.3 is only one possible HIS configuration, while there are plenty of other design possibilities. Two typical three-terminal network examples are the T and π networks, as illustrated in Fig. 6.4 (a) and (b), respectively, with only the hydraulic resistance elements included in them for illustration. These two networks can be represented as Immittance-Function-Networks (IF-Networks) as shown in Fig. 6.4(c) and (d) (termed T-IF-Network and π-IF-Network, respectively). Similar to the previous chapters, here Z_1, Z_2 and Z_3 are defined as the Immittance-Function-Blocks (IF-Blocks), which are 2PT networks containing an arbitrary number of passive transformerless elements that satisfy series-parallel connections, and an IF-Network refers to a block topology of a network with its sub-networks represented by IF-Blocks. Similarly, networks shown in Fig. 6.3 (e) and (f) are also IF-Networks. It can be seen that they are both T-IF-Network, with Z_{hA1}, Z_{hA2}, Z_{hAa}, Z_{hB1}, Z_{hB2}, Z_{hBa} shown in Eq. (6.2).

A general representation of the three-terminal network in the hydraulic domain can be found in Fig. 6.5, where the fluid flow rate q_1 and q_2 flowing through terminal 1 and 2 must equal the flow flowing out of terminal 3. This definition is analogous to the three-terminal network defined in the electrical domain [102] through the electrical-mechanical-hydraulic-pneumatic analogy [28]. For example, the fluid flow rate (resp. pressure) is analogous to the electrical current (resp. potential) following the electrical-hydraulic analogy.

In order to obtain the optimum HIS to improve the vehicle system performance, all possible HIS network configurations should be investigated. Therefore, a systematic approach is desired to cover a full set of series-parallel three-terminal networks with a

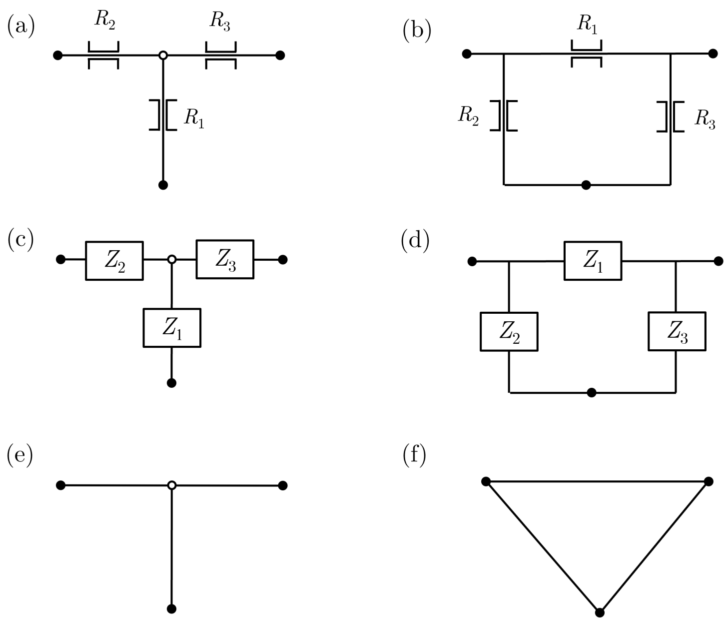

Fig. 6.4 (a) T network example; (b) π network example; (c) T-IF-Network; (d) π-IF-Network; (e) graph representation of the T-IF-Network; (f) graph representation of the pi-IF-Network.

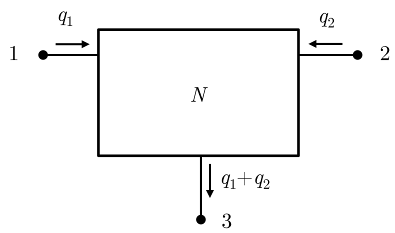

Fig. 6.5 General representation of the hydraulic three-terminal network.

predetermined number of transformerless elements. To this end, two questions need to be addressed:

(a) What are all the possible IF-Network topologies with a predetermined number of elements?

(b) With these IF-Networks, how should the elements be distributed across the IF-Blocks?

These two questions are answered in the following section by deriving the Generic-Immittance-Function-Network (GIFN) to capture all IF-Network topological possibilities. Then element distributions are discussed with IF-Block immittance functions represented by structural immittances [30].

6.2 Three-terminal network enumeration and case demonstration

In this section, series and parallel connections between an IF-Block and a three-terminal network are firstly described by adopting concepts presented by Nishizeki, *et al.* [150] in the graph domain. Generic-Immittance-Function-Network (GIFN) is then constructed, which gives the complete topological information of all possible series-parallel three-terminal networks with a pre-determined number of transformerless elements. Later, explicit networks are enumerated by representing the IF-Blocks with the structural immittances. This approach is then demonstrated by an example system in which the elements are limited to one inertance, one compliance and one resistance.

6.2.1 Series-parallel connection of an IF-Block to a three-terminal network

For readers' convenience, the definition of a graph stated in Chapter 3 is repeated here: A graph $G = (V, E)$ is a pair consisting a finite set V whose elements are vertices, and a finite set E, which are paired vertices with elements called branches (or edges) [127]. As stated in Chapter 3, in the electrical domain, the graph of a network represents the topological connections of different elements [130, 152]. A graph representation is useful in certain circumstances where only the network topology matters, for example, T-, star- and Y-networks are identical with respect to their topological representation, and same as the π-, delta- and Δ-networks. Similar to Chapters 3 and 5, the correspondence between graphs and hydraulic networks is introduced here.

We choose to represent the IF-Blocks with branches, and terminals and internal connection points with vertices in this chapter. Thus, any IF-Network with specific connection topology can be depicted as a graph, with a set of branches interconnected at their vertices. For example, the T-IF-Network (shown in Fig. 6.4 (c)) can be represented as a graph (shown in Fig. 6.4(e)), with three branches representing the IF-Blocks, three terminal-vertices (shown as solid circles) representing the terminals, and one intersection-vertex (a hollow circle) representing the inter-connected point of the network. Similarly, the π-IF-Network (Fig. 6.4(d)) can also be represented as a graph shown in Fig. 6.4(f).

With the graph representation, again series-parallel graph connection defined in [150] can be directly applied to construct series-parallel three-terminal networks. The definition is modified here to fit the subject of this work:

Definition: Given two graphs $G_1(V_1, E_1)$ and $G_2(V_2, E_2)$, where G_1 has two terminal vertices v_{1a}, v_{1b}, and G_2 has three terminal vertices v_{2a}, v_{2b}, v_{2c}. They have no vertex in common, i.e., $V_1 \cap V_2 = \emptyset$.

- *Series connection* is an operation of coalescing one of the terminal-vertices of G_1 with one of the terminal-vertices of G_2 into an intersection-vertex of the resulting three-terminal graph, of which the remaining terminal-vertices becomes the new terminal-vertices.

- *Parallel connection* is an operation of coalescing both terminal-vertices of G_1 with two of the three terminal-vertices of G_2 to form a new three-terminal graph, where the coalesced terminal-vertices remain terminal-vertices of the resulting three-terminal graph.

Note that both these connection types can only be applied to terminal-vertexes. Therefore, no further connections can be added to the formed intersection-vertices.

As an example, for series connections, take G_1 as the graph of a simplest two-terminal network consisting only one hydraulic resistance as seen in Fig. 6.6 (a1), and G_2 as the graph of the π-IF-Network as shown in Fig. 6.6(a2). Three series connections are possible, giving three new graphs shown in Fig. 6.6(a3)-(a5). One terminal-vertex of G_1, i.e., v_{1b}, and one terminal-vertex of G_2, i.e., v_{2a} (resp. v_{2b} and v_{2c}) are connected to form an intersection-vertex, and the remaining terminal-vertex set $[v_{1a}, v_{2b}, v_{2c}]$ (resp. $[v_{1a}, v_{2a}, v_{2c}]$ and $[v_{1a}, v_{2a}, v_{2b}]$) will be the terminal-vertices of the resulting graphs. These three series connections are termed S1, S2 and S3, respectively. Graphs shown in Fig. 6.6 (a1)-(a5) correspond to the IF-Networks shown in Fig. 6.6(b1)-(b5), where Z_1, Z_2, Z_3, Z_4 are IF-Blocks representing any possible series-parallel two-terminal networks. As an example by depicting the two-terminal network Z_4 as a hydraulic resistance (Fig. 6.6 (c1)) and the three-terminal network consisting Z_1, Z_2, Z_3 as an example π-network which contains one hydraulic resistance in each IF-Block as shown in Fig. 6.6 (c2), the series connections between them formulate the resulting three-terminal networks shown in Fig. 6.6(c3)-(c5). Note that in this example, we restrict ourselves to just hydraulic resistances, but each IF-Block shown in Fig. 6.6(b1)-(b5) could contain any types of transformerless elements.

For parallel connections, again taking G_1 as the graph of a hydraulic resistance as shown in Fig. 6.7(a1), while G_2 as the graph of the T-IF-Network as shown in Fig. 6.7(a2), three parallel connections are possible, giving three new graphs shown in Fig. 6.7(a3)-(a5). Both terminal-vertices v_{1a} and v_{1b} of G_1 are coalesced with two of the three terminal-

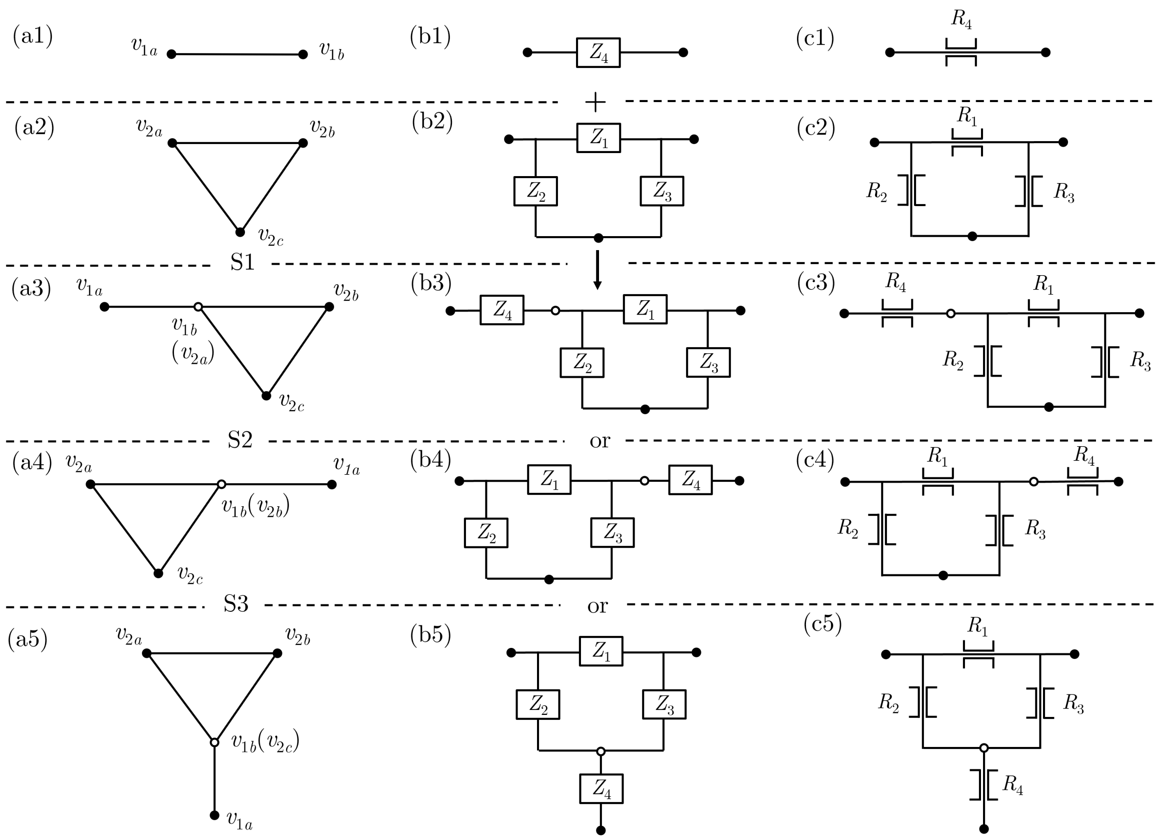

Fig. 6.6 An IF-Block connected to the IF-Network in series, where (a1) Graph G_1 with two terminal vertices v_{1a} and v_{1b}; (a2) Graph G_2 with three terminal vertices v_{2a}, v_{2b} and v_{2c}; (a3-a5) three different series graph connections; (b1-b5) corresponding IF-Networks; (c1-c5) example network layouts.

vertices v_{2a} and v_{2b} (resp. v_{2a} and v_{2c}, v_{2b} and v_{2c}) of G_2 as the new terminal-vertices of the resulting three-terminal graphs, hence $v_{1a} = v_{2a}$ (resp. $v_{1a} = v_{2a}$, and $v_{1a} = v_{2b}$) and $v_{1b} = v_{2b}$ (resp. $v_{1b} = v_{2c}$, and $v_{1b} = v_{2c}$). These three parallel connections are termed P1, P2 and P3, respectively. Graphs shown in Fig. 6.7(a1)-(a5) correspond to the IF-Networks shown in Fig. 6.7(b1)-(b5), where Z_1, Z_2, Z_3, Z_4 are IF-Blocks representing any possible series-parallel two-terminal networks. By depicting the network Z_4 as a hydraulic resistance (Fig. 6.7 (c1)) and the three-terminal network consisting Z_1, Z_2, Z_3 as an example T-network which contains one hydraulic resistance in each IF-Block as shown in Fig. 6.7(c2), the parallel connections between them formulate the resulting three-terminal networks shown in Fig. 6.7(c3)-(c5). Again, although we restrict ourselves to just hydraulic resistances in this example, each IF-Block shown in Fig. 6.7(b1)-(b5) could contain any types of transformerless elements.

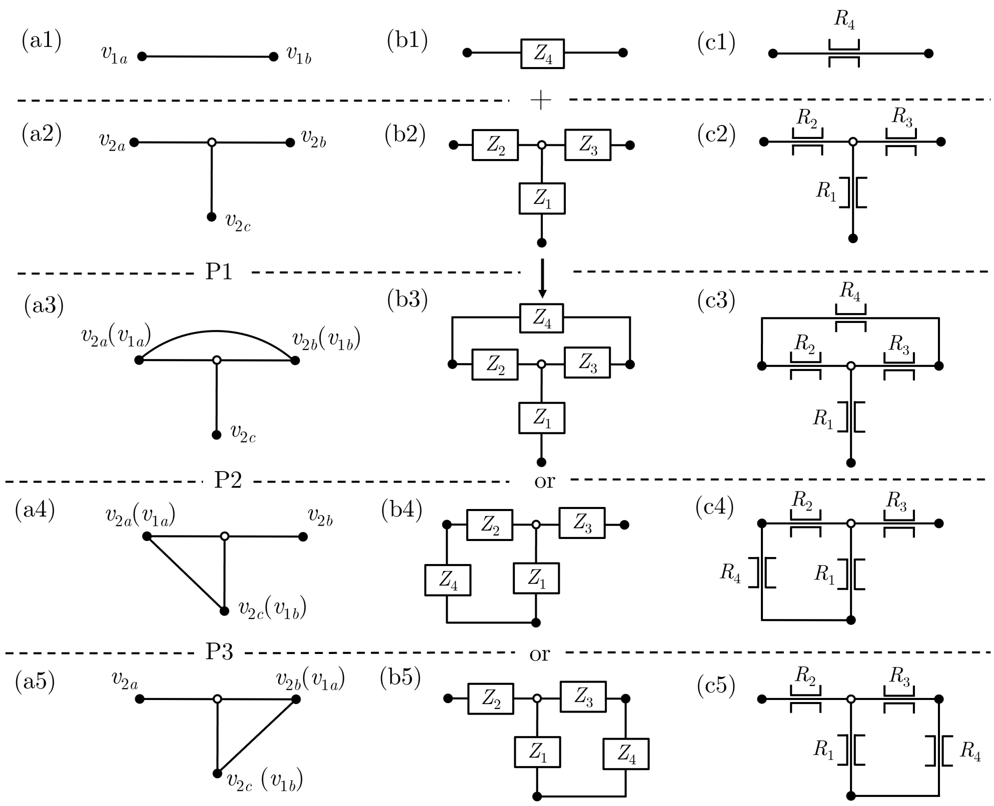

Fig. 6.7 An IF-Block connected to the IF-Network in parallel, where (a1) Graph G_1 with two terminal vertices v_{1a} and v_{1b}; (a2) Graph G_2 with three terminal vertices v_{2a}, v_{2b} and v_{2c}; (a3-a5) three different parallel graph connections; (b1-b5)corresponding IF-Networks; (c1-c5) example network layouts.

The Immittance-Function-Matrix (IF-Matrix) of the obtained IF-Networks under series-parallel connections can be found in Appendix C.

6.2.2 Construction of the Generic-Immittance-Function-Network

With the series-parallel connections defined above, we move on to formulate all possible IF-Networks with a finite number of IF-Blocks. To achieve this, one way is to directly list all possible IF-Networks with the specific IF-Block number. However, it becomes extremely difficult and even prohibited with the number increasing. It is also impossible to verify whether the listed sets are complete or not. To address these problems, the Generic-Immittance-Function-Network (GIFN) is introduced, which is an IF-Network covering the complete topology information of a full set of series-parallel three-terminal IF-Networks with a predetermined IF-Block number. Considering there are i IF-Blocks in an IF-Network, the corresponding GIFN is termed as GIFN$_i$. In the following part of this section, the approach of constructing GIFN_i will be provided. Here the graph theory is again employed to facilitate the procedure. Same as the Chapter 5, we will start with an empty three-terminal graph, where a series of branches (i.e., IF-Blocks) will be added one-by-one. Note that there will always be three terminal-vertices existing after each branch is connected. For these branches, they can be either shorting branches which has zero impedance or ∞ admittance, or non-shorting branches, where the impedance (or admittance) of the corresponding IF-Block exists. For a non-trivial three-terminal graph, there shouldn't be any isolated vertices. Therefore, at least two branches are needed to link the vertex pair. Although it is allowable to use a shorting branch to link them, a parallel connection of a shorting branch to a three-terminal graph will only coalesce two vertices to one vertex. Thus the three-terminal graph becomes a two-terminal graph. Alternatively, a series connection of a shorting branch to a three-terminal graph won't make any difference to the original graph. Therefore, at least two non-shorting branches are needed to form a non-trivial three-terminal graph. This means the IF-Block number $i \geq 2$ for any non-trivial IF-Network. In the following part, different GIFNs will be constructed with any given IF-Block number i.

Taking the case where $i = 2$, to form all possible IF-Networks, an empty three-terminal graph and two non-shorting branches are needed. The construction of a three-terminal series–parallel graph begins with an empty graph, as shown in Fig. 6.8(a1) of Step 1. Step 1 is to add one branch to the empty graph, in which only the parallel connection is possible. There are totally three different parallel connection possibilities, leading to three graphs formed as shown in Fig. 6.8(b1)-(b3) of Step 2. Then the second branch is added to the obtained graphs in Step 2. Again, only parallel connections are possible, resulting in three distinct graphs as shown in Fig. 6.8(c1)-(c3) of Step 3. The reason that only parallel connections are possible in these two steps is that series connections will lead to isolated terminal vertex (vertices), which will form trivial graphs. For example, if we choose a series connection in step 1, then in step 2, there will always be at least one isolated terminal vertex. Therefore, graphs shown in Step 3 represent all possible IF-Networks containing two IF-Blocks. It can be observed that a π-IF-Network can cover all possible topology of these IF-Networks, which means the GIFN_2 is a π-IF-Network, as listed in Table 6.1. Note that a T-IF-Network is also one possible GIFN_2, if the terminal vertices v_{2a}, v_{2c} and v_{2b}, respectively, from each graph shown in Fig. 6.8 (c1)-(c3) are regarded as the intersection-vertex of the graph representing T-IF-Network. In this study, we choose to use the π-IF-Network as the GIFN_2. Although the GIFN_i obtained from the following procedure is not the only GIFN for three-terminal IF-Networks with i IF-Blocks, it is sufficient to cover all desired IF-Networks.

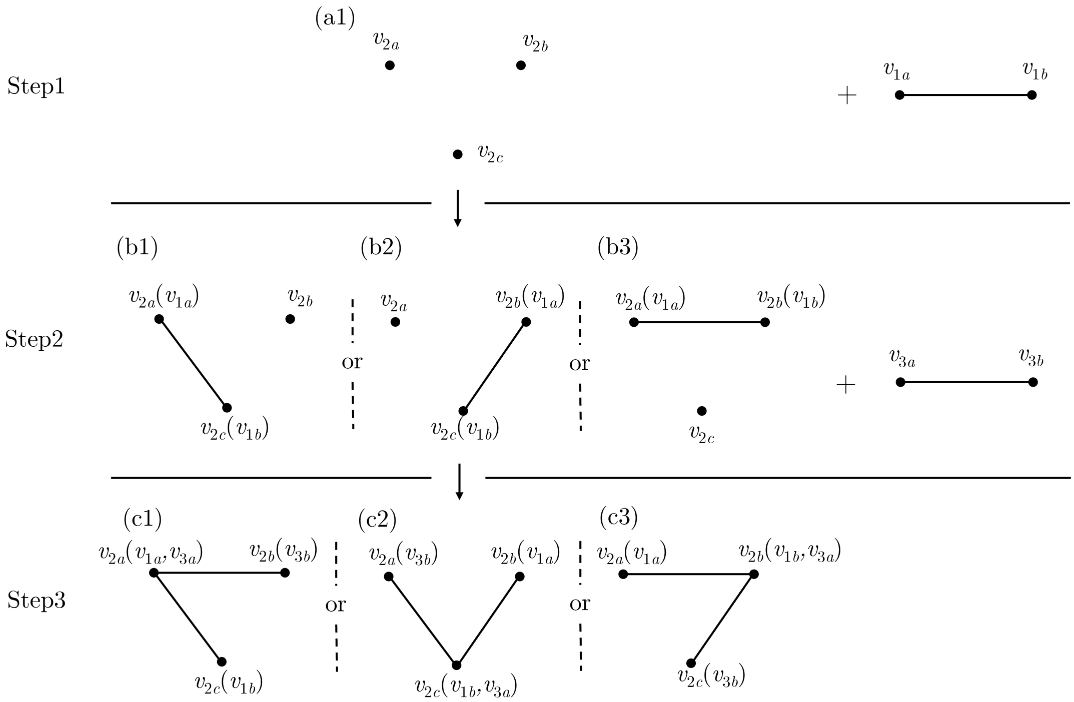

Fig. 6.8 The procedures to form all possible three-terminal graphs containing two branches.

When $i = 3$, similar to Step 1 and Step 2 in Fig. 6.8, an additional branch will be added to the graphs obtained in Step 3 to construct new three-terminal graphs. Hence, IF-Networks consisting of three IF-Blocks can be obtained by adding an additional IF-Block to the IF-Networks with two IF-Blocks. The GIFN_3 will then be obtained by considering all connection possibilities of adding an additional IF-Block to the GIFN_2. In this case, only series connections are possible. This is because any parallel connections to GIFN_2 won't change the resulting network as the added IF-Blocks will be *reduced*. For example, if the added IF-Block Z_4 (shown in Fig. 6.6(b1)) and the π-IF-Network (shown in Fig. 6.6(b2)) are connected in parallel as P1 connection, Z_1 and Z_4 will be *reduced* to a single IF-Block. Hence, only series connections are possible, and the resulting GIFN_3 is obtained as shown in Table 6.1.

When $i = 4$, GIFN_4 can be derived similarly by considering all possible connections of adding one additional IF-Block to the obtained GIFN_3. In this case, only parallel connections are possible, as any series connection to GIFN_3 will make the obtained IF-Network *reduced* to the original one. Hence the obtained GIFN_4 is shown in Table 6.1.

In general, GIFN$_i$ can be derived by considering all possibilities of adding one IF-Block to the GIFN$_{i-1}$. If i is an odd number, only series connections are possible, hence the GIFN$_i$ is obtained by adding all series connections (S1, S2, S3) to GIFN$_{i-1}$. While if i is an even number, only parallel connections are possible, and the GIFN$_i$ is obtained by adding all parallel connections (P1, P2, P3) to GIFN$_{i-1}$. General representations of the GIFN$_i$ are summarised in Table 6.1, with their corresponding IF-Matrix shown in Appendix C.

Table 6.1 GIFN$_i$, with the condition that i IF-Blocks are present.

	i is even number		i is odd number
$i = 2$	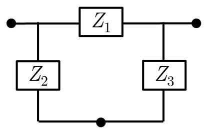	$i = 3$	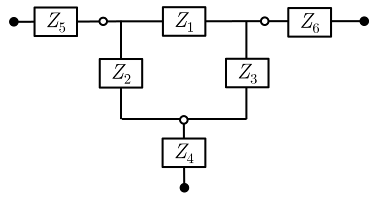
$i = 4$	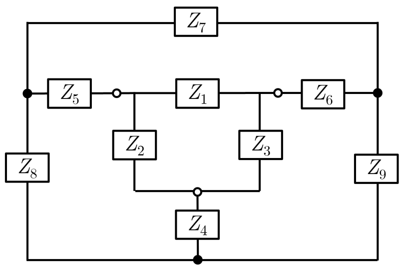	$i = 5$	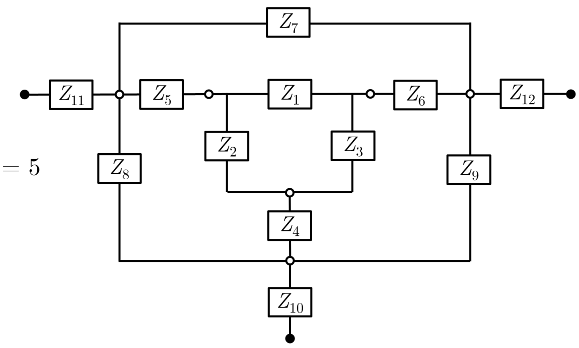
$i = 6, 8, ...$	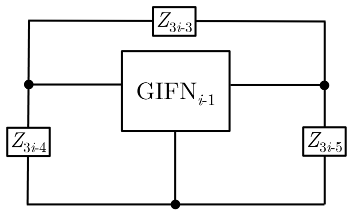	$i = 7, 9, ...$	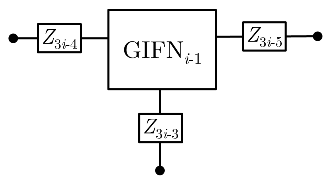

6.2.3 Enumeration of three-terminal networks

With the obtained GIFN$_i$, we can now recover all possible three-terminal networks from it. This can be divided to two parts. The first part is to consider how to recover the desired IF-Networks with allowable number of IF-Block, and the second one is to enumerate all possible networks by distributing the pre-determined elements to these

IF-Blocks. Note that the GIFN_i is a generalised network containing all the possible IF-Network layouts. Therefore, the GIFN_i needs more IF-Blocks than the limit set for the desired IF-Networks. To recover a valid IF-Network from the GIFN_i, we take the GIFN_i and eliminate unnecessary IF-Blocks until only i IF-Blocks are present in the network. Again, same as the term used in Chapter 5, an IF-Block will be *eliminated* by setting its immittance function to be 0 or ∞ depending on its connection type, if it is redundant for a certain IF-Network topology. An IF-Block is regarded as *present* if it is not eliminated. A range of IF-Networks will be recovered by varying the choice of which IF-Blocks are eliminated. For example, the GIFN_3 shown in Fig. 6.10 contains 6 IF-Blocks. In order to obtain a π-IF-Network using the GIFN_3, Z_1, Z_2 and Z_3 should be present, and all the others would be eliminated. While, to obtain a T-IF-Network, one possible solution is to let Z_1, Z_3 and Z_6 be present, and eliminate all the other IF-Blocks. In the following part, an Elimination Rule is introduced, which will be used to recover all possible IF-Networks from the obtained GIFN_i.

<u>Elimination Rule</u>: The IF-Blocks can be eliminated by letting impedance (resp. admittance) functions of redundant parallel IF-Blocks equal to ∞ (resp. 0), and of redundant series impedance (resp. admittance) functions equal to 0 (resp. ∞). In graph representations, it is interpolated as opening the parallel branches and shorting the series branches.

The elimination rule is chosen to ensure that any eliminated IF-Block won't lead to rigidly connected terminals or isolated terminals when forming the resulting IF-Network by adding IF-Blocks one-by-one to an empty three-terminal network. Take GIFN_3 in Table 6.1 as an example. GIFN_3 is constructed by adding the IF-Block Z_1, Z_2 and Z_3 in parallel to an empty three-terminal network to form GIFN_2, then adding the IF-Block Z_4, Z_5 and Z_6 in series to GIFN_2 to form GIFN_3, see Table 6.1. If the parallel branch representing IF-Block Z_1 (same as Z_2 and Z_3) is shorted, two terminal-vertices will be coalesced to one terminal-vertex when forming the GIFN_2, which means two of the three terminals are locked rigidly at this step. When the series branch representing IF-Block Z_4 (same as Z_5 and Z_6) is opened, one terminal-vertex will be isolated when forming the GIFN_3. Similarly, shorting the parallel IF-Blocks Z_7, Z_8 and Z_9 in GIFN_4 will always lead to two terminals connected rigidly, and opening series IF-Blocks Z_{10}, Z_{11} and Z_{12} in GIFN_5 will also lead to isolated terminals when forming the resulting IF-Networks. Therefore, only opening parallel IF-Blocks and shorting series IF-Blocks are possible.

With the obtained GIFN_i and the Elimination Rule, all possible IF-Networks with a certain number of IF-Blocks can be obtained. With these, the structure-immittance approach [30] can be employed to assign the pre-determined elements into each IF-Block. Thus, any series-parallel three-terminal networks containing a predetermined number and type of passive transformerless elements (e.g., the compliance, resistance, and inertance in the hydraulic domain) can be obtained systemically. In the following, an example will be given to demonstrate the enumeration process.

Consider an example where we wish to obtain all possible series-parallel three-terminal networks including 3 hydraulic elements (1 compliance C, 1 inertance I and 1 resistance R in this case). The desired networks will include 2 or 3 IF-Blocks. For GIFN$_2$ listed in Table 6.1, one out of three IF-Blocks will be eliminated. If block Z_1 (resp. Z_2 and Z_3) is eliminated, the resulting IF-Network is shown in Fig. 6.9(a) (resp. (b) and (c)). The three predetermined passive elements are then distributed in these two IF-Blocks, which

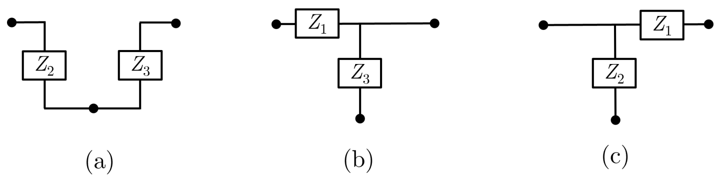

Fig. 6.9 All possible IF-Networks containing 2 IF-Blocks.

means one of the present IF-Blocks includes one element and the other one includes the remaining two elements. For example, when Z_1 and Z_2 are present, representing the IF-Network shown in Fig. 6.9 (c), if Z_1 includes C, and the other two elements, R and I, are contained in Z_2, this results in two network possibilities by connecting R in series or in parallel with I. Z_2 takes the expression of a structural impedance [30] obtained for one resistance and one inertance case, given as

$$Z_2 = \frac{C_1 R_1 s + 1}{s(C_1 C_2 R_1 s + C_1 + C_2)} \tag{6.5}$$

with the condition that only one of the compliance $1/C_1$ or C_2 exists, and the other one equals zero. Since there are three different element types and switching Z_1 with Z_2 will result in different network possibilities, the GIFN$_2$ that covers totally three IF-Network will include 36 network layouts.

Now starting with GIFN$_3$ and eliminating IF-Blocks until only 3 are present gives 10 non-trivial IF-networks. However, some of these derived IF-Networks are identical, removing these results in 8 distinct IF-Networks. Amongst them, some IF-Networks can be simplified, with them reduced to IF-Networks containing 2 IF-Blocks, which were captured by the IF-Networks derived from the GIFN$_2$. For example, if IF-Blocks Z_2, Z_4

and Z_6 in GIFN$_3$ are eliminated, the resulting IF-Network is equivalent to the IF-Network shown in Fig. 6.9(b) with Z_1 and Z_5 reduced to one IF-Block. Although they are valid IF-Networks recovered from GIFN$_3$, we will take them as repeated networks, and they will be excluded to remain a concise network set recovered from GIFN$_3$. A redundancy check is conducted to exclude the repeated ones by distributing passive elements amongst these IF-Blocks, and then comparing impedance matrices of the obtained networks. This can be achieved easily through a MATLAB© program by comparing the symbolic expressions of these impedance matrices. If the symbolic expressions are identical, the later impedance matrix which represents a redundant IF-network will be excluded from the complete set. The results give 2 new IF-networks, as shown in Fig. 6.10. Three passive elements are distributed amongst these IF-Blocks with each IF-Block include one element, resulting in 6 networks from each IF-Network. Hence, there are 12 additional networks recovered from the GIFN$_3$. Combined with the networks recovered from GIFN$_2$, in total 48 networks, which are the complete set of network layouts containing 1 inertance, 1 compliance and 1 resistance, will be obtained.

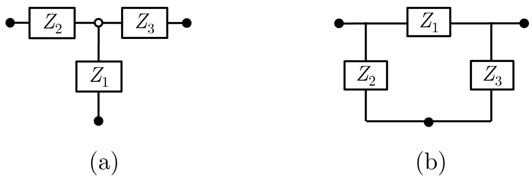

Fig. 6.10 IF-Networks with 3 IF-Blocks after redundancy check.

6.3 Application Example

The HIS derived in Section 6.1 is now included within a half car model as an example to demonstrate how the proposed approach can be used to identify the most beneficial HIS suspension with restricted topological complexity for vehicle suspension design. Other types of the interlinked suspension system, such as the pneumatic [59] or mechatronic [15] ones, or other engineering applications involving multi-dimensional vibrations, such as the wind turbine gearbox mounting systems [7], could also be considered.

6.3.1 Half-car model

To retain simplicity, whilst still accounting for details of the HIS system, a lumped-mass, roll-plane, four-degree-of-freedom (4-DOF) half-car model is adopted here. This model is the same as the one used in [6], as shown in Fig. 6.11. The system consists of linear tyre damping (c_{tl}, c_{tr}) and stiffness (k_{tl}, k_{tr}), and linear conventional suspension stiffness (k_{sl}, k_{sr}). It also possesses left-right symmetry. M, m_l and m_r are the mass value of the sprung mass, left and right unsprung masses, respectively. I is the sprung mass moment of inertia. b_l and b_r are the distances from the sprung mass centre to the left and right suspension struts, respectively. Parameters of the half-car model are given in Table 6.2. The HIS configuration illustrated in Fig. 6.3 with one accumulator on each pipeline is considered as the default HIS system. All parameters keep the same values as the one used in [6], except that the crossing sectional area of the piston is taken as 4.124×10^{-4} m^2 in this study.

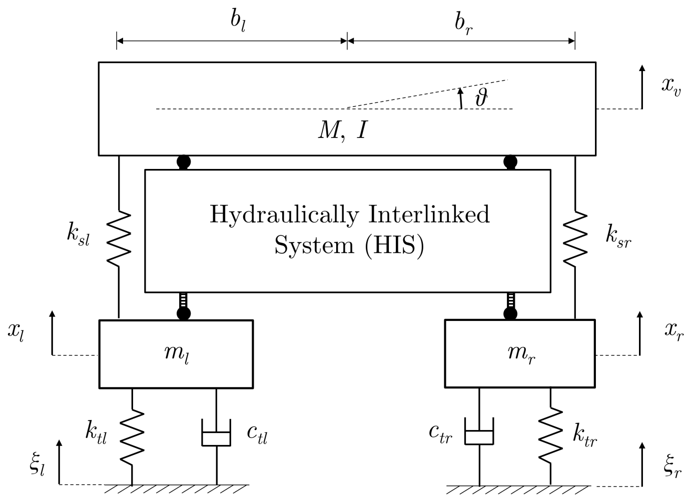

Fig. 6.11 Half-car model combined with the HIS suspension

Table 6.2 Parameter values of the Vehicle system (subscript $j = l$ or r, indicating the left or right, respectively)

Symbol	**Value**	**Units**	**Description**
M, m_j	750, 35	kg	Sprung and unsprung mass
I	320	kg·m^2	Sprung mass moment of inertia about roll axis
b_j	0.8	m	Distance from sprung mass centre to suspension strut
k_{sj}, k_{tj}	20, 200	kN/m	Mechanical suspensionkg·m^2 spring and tyre spring stiffness
c_{tj}	300	Ns/m	Tyre damping

The equations of motion of the HIS-integrated half-car model in the Laplace domain is shown in Eq. 6.6:

$$[s^2\mathbf{M} + s\mathbf{C} + \mathbf{K} + s\mathbf{D}_y^T\mathbf{Y}_m\mathbf{D}_y]\tilde{\mathbf{x}} = \tilde{\mathbf{F}} \tag{6.6}$$

with the mass, damping and stiffness matrices $\mathbf{M}$, $\mathbf{C}$ and $\mathbf{K}$ expressed as:

$$\mathbf{M} = \begin{bmatrix} m_l & 0 & 0 & 0 \\ 0 & m_r & 0 & 0 \\ 0 & 0 & M & 0 \\ 0 & 0 & 0 & I \end{bmatrix} \quad \mathbf{C} = \begin{bmatrix} c_{tl} & 0 & 0 & 0 \\ 0 & c_{tr} & 0 & 0 \\ 0 & 0 & 0 & 0 \\ 0 & 0 & 0 & 0 \end{bmatrix}$$
$$\mathbf{K} = \begin{bmatrix} k_{sl} + k_{tl} & 0 & -k_{sl} & k_{sl} b_l \\ 0 & k_{sr} + k_{tr} & -k_{sr} & -k_{sr} b_r \\ -k_{sl} & -k_{sr} & k_{sl} + k_{sr} & k_{sr} b_r - k_{sl} b_l \\ k_{sl} b_l & -k_{sr} b_r & k_{sr} b_r - k_{sl} b_l & k_{sl} b_l^2 + k_{sr} b_r^2 \end{bmatrix} \tag{6.7}$$

and the hydraulic force $\tilde{\mathbf{F}}_h$ as:

$$\tilde{\mathbf{F}}_h = \mathbf{Y}_m \Delta \tilde{\mathbf{v}}_h = \mathbf{Y}_m \tilde{\mathbf{D}}_y \tilde{\mathbf{x}} s$$
$$\text{where } \mathbf{D}_y = \begin{bmatrix} 1 & 0 & -1 & b_l \\ 0 & -1 & 1 & b_r \end{bmatrix} \tag{6.8}$$

$\tilde{\mathbf{x}} = [\tilde{x}_l, \tilde{x}_r, \tilde{x}_v, \tilde{\theta}]^T$ is the displacement vector representing the half car left wheel, right wheel, car body translational and rotational movements in the Laplace domain, with positive directions shown in Fig. 6.11. It is defined under the rotational scenario so the left piston is pressed and the right piston is extended. $\mathbf{Y}_m$ is the admittance matrix from the force $\tilde{\mathbf{F}}_h$ to the relative velocity $\Delta \tilde{\mathbf{v}}_h$. $\mathbf{D}_y$ is the position matrix.

Now consider a road displacement input to the half car system $\tilde{\boldsymbol{\xi}} = [\tilde{\xi}_l, \tilde{\xi}_r, 0, 0]^T$, $\tilde{\mathbf{F}} = \mathbf{B}\tilde{\boldsymbol{\xi}}$ is the vector of applied road forces. $\mathbf{B}$ is a 4×4 matrix comprising all zero elements except the upper two diagonal terms, where $B_{11} = sc_{tl} + k_{tl}$ and $B_{22} = sc_{tr} + k_{tr}$. Use $\mathbf{H}_d$ to represent the transfer function from the road input $\tilde{\boldsymbol{\xi}}$ to the vehicle displacement $\tilde{\mathbf{x}}$. By setting $\mathbf{H} = s^2\mathbf{M} + s\mathbf{C} + \mathbf{K} + s\mathbf{D}_y^T \mathbf{Y}_m \mathbf{D}_y$, the vehicle displacement $\tilde{\mathbf{x}}$ can thus be solved as:

$$\tilde{\boldsymbol{x}} = \mathbf{H}_d \tilde{\boldsymbol{\xi}} = \mathbf{H}^{-1} \mathbf{B} \tilde{\boldsymbol{\xi}} \tag{6.9}$$

To this end, the performance of the half-car system will be evaluated to identify the optimum hydraulic interlinked suspension. In this study, the objective function J is chosen as the maximum right suspension force under the single wheel bump input with left suspension force constrained to be no larger than the default system. Three more constraints are added to guarantee the vehicle ride comfort and roll performance. One is the H_2 norm of the sprung mass displacement under a random rough road input. The other two are roll angle and roll velocity of the half-car model under fishhook manoeuvre. The objective function and the constraints can be expressed as:

$$\begin{aligned} & J = max|F_{Lsusp}| \text{ under single wheel bump} \\ & \\ & \text{with constraints:} \\ & ||\tilde{x}_v||_{2_{opt}} \leq ||\tilde{x}_v||_{2_{def}} \text{ under rough road input} \\ & max|\theta|_{opt} \leq max|\theta|_{def} \text{ under fishhook manoeuvre} \\ & max|\dot{\theta}|_{opt} \leq max|\dot{\theta}|_{def} \text{ under fishhook manoeuvre} \end{aligned} \tag{6.10}$$

Note that, for a fair comparison, parameters of the default HIS system are also optimised following Eq.(6.10) with constraints obtained by using the hydraulic parameters given in [6]. Thus, the optimised default HIS parameter values are listed in Table 6.3. With these parameter values, a new set of more strict constraints can be obtained, which will be used for the further identification of beneficial network configurations.

The single wheel bump input with a sine wave shape is applied to the left wheel of the half car model to excite both bounce and roll modes of the vehicle [6]. The bump has a length of 0.5 m, and the vehicle goes through it with a velocity of 13.4 m/s. The profile of this single wheel bump can be found in Fig. 6.12. For the random rough road input, it

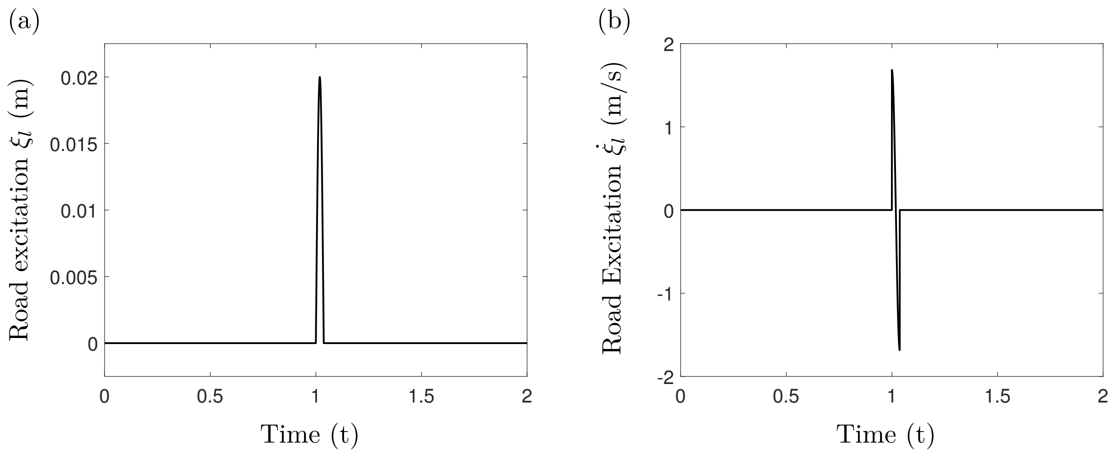

Fig. 6.12 Single Wheel Bump Road Input with (a) the road displacement excitation ξ_l; (b) the road velocity excitation $\dot{\xi}_l$.

is the same as the one used in [153]. So the introduction of this input won't be repeated in this study. Details of its mathematical expression can be found in Appendix D. Since no tyre-model is considered for the half car model, fishhook manoeuvre is not directly applicable to it. Hence, a fishhook steering angle (as shown in Fig. 6.13(a)) is firstly applied to a 9-DOF full-car model to generate a roll moment (as shown in Fig. 6.13(b)), which will then be adopted in this half-car model. The 9-DOF full car model is the same as the one used in [154], while the model parameters are in line with the half-car model used in this study, which means the sprung mass is 2×750 kg, the sprung mass inertia is 2×320 kg·m^2, and other parameters are same as the ones shown in Table 6.2. Although the HIS can be directly applied to the 9-DOF full car model, this case study is to demonstrate the proposed identification approach, and a 4-DOF half car model with one pair of interlinked suspension system is sufficient for the demonstration purpose.

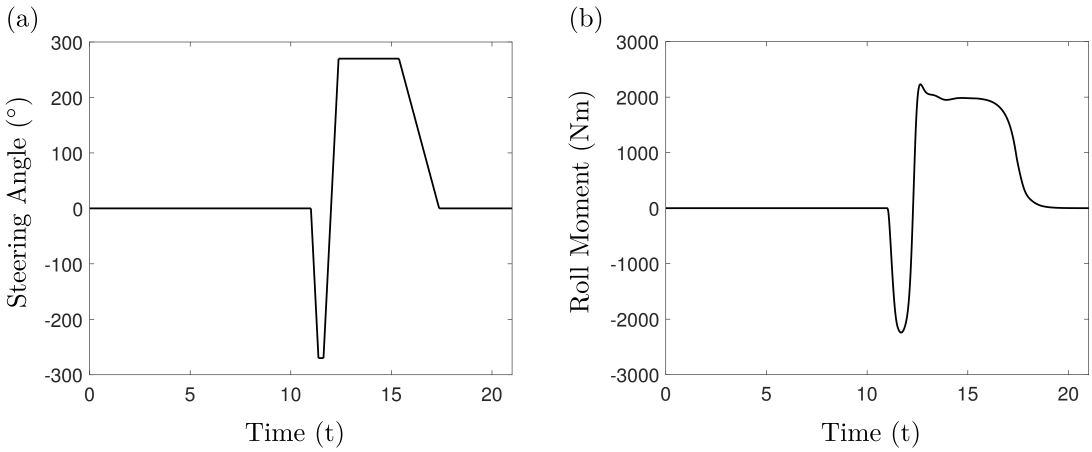

Fig. 6.13 Fishhook manoeuvre: (a) the steering angle that applied to the full-car model; (b) the roll moment generated by the full-car model.

6.3.2 Numerical application on the example model

To identify beneficial HIS networks for the half-car model, four passive hydraulic elements, one resistance, one compliance and two inertance, are considered for each pipeline. The $GIFN_2$, $GIFN_3$ and $GIFN_4$ are used to derive all possible IF-Network layouts with 2, 3 and 4 IF-Blocks, respectively. The structure-immittance approach is then employed to distribute four passive elements into these IF-Blocks to enumerate all possible networks. Based on the procedure demonstrated in Section 6.2, there are totally 96, 162 and 204 layouts available for $GIFN_2$, $GIFN_3$ and $GIFN_4$, respectively, after performing the redundancy check. Recall the three-element case in Section 6.2, where the networks recovered from $GIFN_3$ are excluded if they are identical to the networks recovered from $GIFN_2$. Similarly, certain networks, which are identical to networks recovered from $GIFN_3$ and $GIFN_2$, are also excluded from the network set recovered from $GIFN_4$. These obtained networks, together with their corresponding impedance matrices, are used to minimize the objective function. In this specific roll-plane half-car case study, non-zero roll static stiffness must exist as the roll static stiffness is critical to the vehicle roll mode. Any layouts resulting in a zero roll static stiffness will be exempted from this case study, leaving a total of 50 layouts, specifically of 12, 16 and 22 layouts with respect to the GIFN_2, GIFN_3 and GIFN_4.

Amongst all possible network candidates, optimal network layouts for IF-Networks generated from the GIFN_2, GIFN_3 and GIFN_4 identified as L1, L2 and L3, respectively, are shown in Fig. 6.14. Optimal results in values of the objective function are summarized in Table 6.3, together with the corresponding parameter values. For L1, the optimal

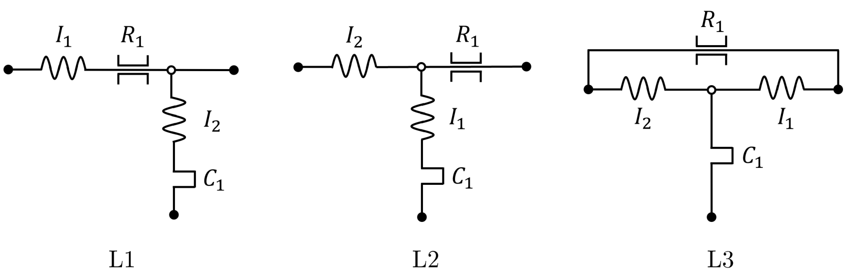

Fig. 6.14 The obtained optimal HIS networks L1, L2 and L3, recovered from GIFN_2, GIFN_3 and GIFN_4, respectively.

configuration results in a maximum right suspension force of 113.73 N, which represents a 24.9% improvement compared to the default HIS system. The corresponding parameter values are $I_1 = 5.83\times10^7$ kg/m^4, $I_2 = 1.51\times10^7$ kg/m^4, $R_1 = 1.29\times10^10$ kg/(s·m^4) and $C_1 = 1/(7.31\times10^{10})$ m^{4}s^2/kg. Note that the performance of L2 is identical to L1 for this specific anti-oppositional HIS arrangement, as pipelines A and B are symmetrical to each other in the left-right direction, which means the derived admittance matrices of the equivalent mechanical network $\mathbf{Y}_m$ for L1 and L2 are the same. L3 can provide an optimal right suspension force of 122.72 N, with 19.0% performance improvement. The parameter values of L3 are: $I_1 = 7.00\times10^9$ kg/m^4, $I_2 = 1.05\times10^7$ kg/m^4, $R_1 = 1.28\times10^{10}$ kg/(s·m^4) and $C_1 = 1/(7.40\times10^{10})$ m^{4}s^2/kg. Fig. 6.15 shows the right suspension force of the 4-DOF half car model with different HIS configurations. The performance of L1 is not shown in Fig. 6.15 as it is equivalent to L2 for this case study. It can be seen that the maximum right suspension force happens around 1.15 s under single-wheel bump input. The identified beneficial networks L2 and L3 can substantially reduce the maximum right suspension force without any compromise of the vehicle roll performance.

Table 6.3 Optimisation results for two inertances, one resistance, one compliance case

Configurations	Performance (N)	Imp.	Optimal parameter values
Default	151.53	/	I_{A1} = 3.91×10^7 kg/m^4 R_{A1} = 1.92×10^9 kg/(s·m^4) I_{A2} = 1.68×10^7 kg/m^4 R_{A2} = 1.00×10^9 kg/(s·m^4) R_{Aa} = 2.42×10^8 kg/(s·m^4) C_{Aa} = 1/(6.68×10^{10}) m^{4}s^2/kg
L1	113.73	24.9%	I_1 = 5.83×10^7 kg/m^4 I_2 = 1.51×10^7 kg/m^4 R_1 = 1.29×10^{1}0 kg/(s·m^4) C_1 = 1/(7.31×10^{10}) m^{4}s^2/kg
L2	113.73	24.9%	I_1 = 1.51×10^7 kg/m^4 I_2 = 5.83×10^7 kg/m^4 R_1 = 1.29×10^{10} kg/(s·m^4) C_1 = 1/(7.31×10^{10}) m^{4}s^2/kg
L3	122.72	19.0%	I_1 = 7.00×10^9 kg/m^4 I_2 = 1.05×10^7 kg/m^4 R_1 = 1.28×10^{10} kg/(s·m^4) C_1 = 1/(7.40×10^{10}) m^{4}s^2/kg

6.4 Summary of the chapter

In this chapter, a systematic procedure is proposed to identify beneficial passive three-terminal series-parallel networks which can be used for interlink vibration suppression system identification. A full set of such network layouts with pre-determined numbers of passive transformerless elements (such as the compliance, resistance and inertance elements in the hydraulic domain) are captured and enumerated. This is achieved by using the Generic-Immittance-Function-Network (GIFN) to represent the topological connection possibilities of Immittance-Function-Blocks (IF-Blocks), and using the structural immittances to describe the 2PT networks in each IF-Block.

The benefits of this approach are shown using a 4-DOF half car model integrating a hydraulically-interlinked system (HIS). Three beneficial suspension networks were identified using the proposed approach. 24.9% improvement is obtained for the vehicle ride comfort, compared to the optimum default suspension design with no compromise of the vehicle roll performance. From the obtained optimisation results, the proposed approach has the following advantages:

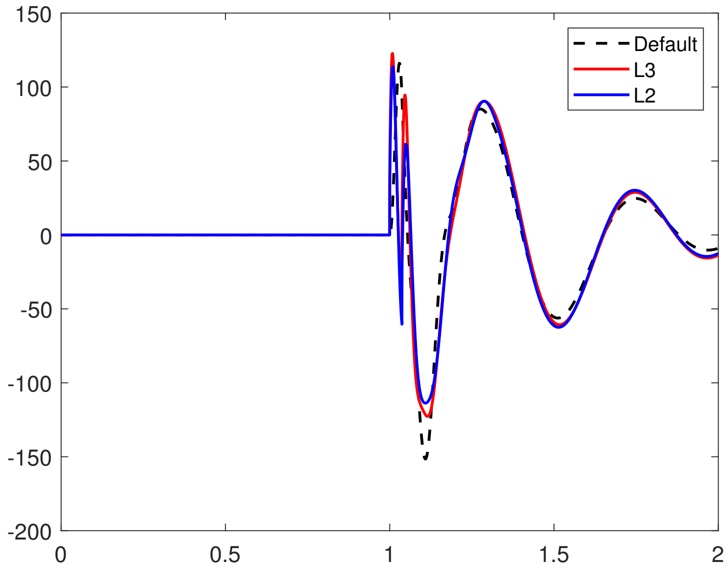

Fig. 6.15 The half-car model right suspension force employing different HIS networks

1. It provides a systematic procedure to capturing all possible passive series-parallel three-terminal network configurations with a constrained network complexity. The desired networks are recovered from a series of GIFN derived in this chapter. Significant performance benefits could be obtained through this systematic procedure.

2. While only 4 elements are needed in the identified beneficial configurations, there are totally 6 elements in the default system. With the elements number of the identified passive HIS system less than the default one, this could potentially reduce the complexity of the desired suspension in practical applications.

3. More than one configuration with same performance are identified, which will provide more design possibilities for the next-step physical realisation of such HIS system to fit into specific manufacturing requirements.

Chapter 7

Conclusions and outlook

In this thesis, the network-synthesis-based identification methodology is developed to design optimal passive vibration absorbers with pre-determined network complexity and topology. This methodology is applied to three engineering systems, including the offshore wind turbine, building structure and vehicle systems, to suppress their vibrations. In this chapter, a summary of the main advantages of this methodology is presented. Findings and conclusions of applying it to different engineering problems are also drawn. Following this, a number of avenues for future research are outlined.

7.1 Conclusions

7.1.1 Network-synthesis-based identification methodology

The main focus of this thesis is to develop a methodology to systematically identify optimum passive networks with predetermined network complexity and topology. The identified networks can be realised as multi-physical domain devices for various engineering vibration suppression problems.

With the introduction of the inerter, the force-current analogy is completed with the mechanical elements fully analogous to the electrical ones. This analogy can also be extended to other domains, such as the acoustic, thermal and hydraulic domain. Hence, the network synthesis theory originally developed for electrical networks is directly applicable to realising networks in other domains. However, the classical network synthesis approaches didn't consider the minimal realisation of a network, which will potentially introduce a large number of elements in the network. For example, a positive-real biquadratic immittance realised using Bott-Duffin synthesis [29] requires nine elements connected in series-parallel in the network. Unlike the electrical systems, mechanical networks have strict weight and space constraints for real-life applications. Hence, minimal realisation of mechanical networks is much more critical due to practical considerations around alignment, linkages and size. Recently, an attractive approach, named the structure-immittance approach, has been proposed by Zhang *et al.* [30]. It tackles the problem of how to systematically realise a network with a pre-determined number of passive non-mass elements (i.e., springs, dampers and inerters).

Mathematically, an ideal lumped mass is equivalent to an ideal inerter with one of the two terminals notionally connected to the ground. However, the mass element has its unique merit since attaching absorbers' terminals physically to the ground might be unrealistic for many application. Therefore, it is beneficial to integrate the reaction mass into the systematic network identification procedure. Considering the fact that most independent vibration suppression devices have no more than two attachment points to the primary system, in this study, a complete set of independent passive vibration absorbers is first explored, which consist of one reaction mass and a pre-determined number of springs, dampers, inerters connected in series-parallel. The mass element is treated as a special two-terminal element, with one terminal notionally connected to the ground, denoted as a notional-ground (NG), and the attachment point is treated as a physical terminal (PT) in the corresponding network representation. In Chapter 3, we start with networks containing one PT and one NG (1PT1NG). Graph theory is employed in Chapter 3 to facilitate the derivation of topological connection possibilities of generic 1PT1NG network. Combined with their immittance expressions, all possible networks with one reaction mass and a predetermined number of passive two-terminal elements connected to the primary structure through one attachment point are enumerated systematically.

In addition to the optimum networks obtained using the generic 1PT1NG network, there are still plenty of mass-included devices which has two physical terminals (2PTs) yet cannot be covered by the generic 1PT1NG network. One example is the tuned-mass-damper-inerter (TMDI). It has shown significant performance benefits to mitigate unwanted vibrations. To further investigate networks with two physical terminals and one nominal terminal (termed 2PT1NG network), inspired by the layout of the TMDI, an Immittance-Function-Layout (IFL) is introduced in Chapter 4. The IFL includes two Immittance-Function-Blocks (IF-Blocks) and one reaction mass in between. Due to the presence of this mass element, forces generated at the network's two terminals are not equivalent any more, therefore an immittance function matrix is derived to describe the forces-velocities relationship across two terminals. With this immittance function matrix, a complete set of the IFL-type networks (which is a subset of all possible 2PT1NG networks) with pre-determined number of inerters, dampers and springs connected in series-parallel can be systematically characterised, and the optimum configurations covered by this IFL can be identified.

In addition to the IFL-type networks covered in Chapter 4, there are still a wide range of 2PT1NG networks who haven't been considered and could potentially provide better dynamic properties. To fully explore the one-reaction-mass-included vibration absorbers with two physical terminals, the generic 2PT1NG network is investigated in Chapter 5, based on the work done in Chapters 3 and 4. Graph theory is again employed to construct the topological connections. Together with the generic 1PG1NG network derived in Chapter 3, all possible networks with series-parallel connections of one reaction mass and a pre-determined number of springs, dampers and inerters with no more than two attachment points can be covered.

The above proposed generic networks are only applicable to independent vibration absorbers which are normally used for uni-dimensional vibration suppression problems. While, the interlinked vibration absorbers also have a wide range of applications on various dynamic systems for their multi-dimensional vibration suppression. With proper design, a set of interlinked absorbers can be regarded as three-terminal networks. Therefore, in Chapter 6, a systematic network identification procedure with constrained network complexity is developed for three-terminal networks. The Generic-Immittance-Function-Network (GIFN) is proosed in this chapter, which is the general representation of all possible three-terminal Immittance-Function-Networks (IF-Networks). The Graph theory is also employed in this chapter to demonstrate the topological connection of three-terminal networks. The obtained GIFN could cover a full set of series-parallel three-terminal networks with predetermined number of transformerless elements (for example, resistors, inductors and capacitors in the electric domain). Thus, the optimum three-terminal networks which can be used to design interlinked vibration absorbers are obtained.

7.1.2 Applications to various engineering systems

Through the introduced generic networks and the systematic identification procedure, beneficial absorbers are obtained for various engineering vibration problems.

In Chapter 3, the generic 1PT1NG network is employed to identify beneficial inerter-based absorbers (IBAs) to reduce the structural vibrations of an example fix-bottom offshore wind turbine, the monopile, and an example floating offshore wind turbine, the spar-buoy. First, simplified linear models are established to identify beneficial absorbers which will reduce the turbine tower top displacements. Optimisation results show that up to 7.3% and 6.4% performance improvements can be obtained for the linear monopile and spar-buoy turbine models, respectively, with the optimum TMD as a benchmark. A nonlinear aero-hydro-servo-elastic coupled simulation tool, the OpenFAST, developed by the National Renewable Energy Laboratory (NREL), is employed to further assess the IBAs' performance under realistic loading conditions. The source code of the OpenFAST is modified to include transfer functions of all 1PT1NG networks. By employing the identified optimal IBAs, the monopile and spar-buoy turbines are simulated under different wind and wave conditions. These include the normal operational condition (corresponding to the fatigue load states (FLS) and the extreme load condition (corresponding to the ultimate load states (ULS)). Under the FLS analysis, the tower damage equivalent load (DEL) can be reduced by 5.8% and 3.3% for the monopile and spar-buoy turbines, respectively. The reduction of the DEL is larger in the side-to-side direction as there is less aerodynamic damping in this direction. The reason that the reduction for the spar-buoy turbine is smaller than the monopile is that the identified IBAs only tune the tower fore-aft mode, while the platform pitch mode is not targeted for the spar-buoy turbine. Under the ULS analysis, the maximum tower base bending moment is reduced by 2.4% and 1.4% for the monopile and the spar-buoy turbines, respectively, in the time domain. While in the frequency domain, the amplitude of the tower bending mode can be reduced by 37.0% and 39.7% correspondingly. The potential mass value reduction of the optimum IBAs is also investigated for the monopile and spar-buoy turbines. Results show that the mass value can be reduced by 25.1% (i.e., 7486 kg) and 23.2% (i.e., 7680 kg), respectively, to achieve the same performance as the optimum TMD. This is of importance for the utilisation of IBAs on offshore wind turbine tower vibration mitigations, as the total mass added to the nacelle can be substantially reduced.

In Chapter 4, the derived IFL-type networks are applied to an example three-storey building model, with the single IFL-type and the dual-IFL type devices (with two parallel-connected IFL layout) both considered in the case study. The proposed IFL is effective in identifying optimal network configurations to mitigate the maximum inter-storey drift of a three-storey building model when subjected to th base excitation. Totally three optimal configurations, i.e., C1, C2 and C3, are obtained. C1 is a single-IFL type device, with 7.3% improvements obtained compared with the optimum TMDI. C2 and C3 are identified through the dual-IFL devices, with up to 34.9% imprveoments obtained. It has been shown that the dual-IFL type devices outperforms the single-IFL devices with same mass constraints. This is because, for the identified dual-IFL device, one IFL mainly targets the building's first natural frequency, and the other IFL is able to target higher frequencies. Then, real-life earthquake inputs are used on the 3-storey building model incorporating the identified absorbers. Simulation results show advantages of those absorbers on mitigating seismic vibrations compared to the optimum TMDI. A 10-storey building model subjected to base excitation is also adopted to further verify the effectiveness of the identified absorbers.

In Chapter 5, the derived generic 2PT1NG network is again applied to the three-storey building model to reduce its maximum inter-storey drift. The number of the inerters, dampers, springs and masses in a vibration suppression device is restricted to be one for each, hence there are totally 64 candidate network layouts. Optimal 2PT1NG network configurations are obtained amongst these candidates, where the most beneficial configuration can provide 66% better performance than the optimum TMD and also outperforms the optimum TMDI with 41% improvements.

In Chapter 6, a hydraulically-interlinked system (HIS) is considered as an example for the vehicle interlinked suspension design. Other types of interlinked suspension system, such as the pneumatic or mechatronic ones, or other engineering applications involving multi-dimensional vibrations, such as the wind turbine gearbox mounting systems, can also be considered as case studies to demonstrate the advantages of the derived generic network. In this case study, the vehicle right suspension force is taken as the objective function under a left-wheel bump-input. In the same time, the vehicle sprung mass acceleration under a random road input and the vehicle roll angle and velocity under a fishhook manoeuvre are also considered as constraints. Optimisation results show that, signifiant vehicle ride comfort improvements (up to 24.9%) are obtained with less components needed (only four elements are needed compared to six components used in the default system) and no compromise for the vehicle roll performance. Moreover, more than one network configurations with same performance improvements are also obtained.

7.1.3 Advantages of this methodology

From the obtained results of applying generic networks to various engineering problems, it is straightforward to conclude the advantages of the developed network-synthesis-based identification methodology.

First, a systematic procedure is introduced to identify a complete set of networks with predetermined network complexity (number of elements) and topology (how the elements are connected with each other). This is especially important for mechanical (and hydraulic) vibration absorbers due to practical considerations around alignment, linkages and size. The minimal realisation of such networks is considered in this methodology. In Chapter 6, while only 4 elements are required in the identified beneficial configurations, there are totally 6 elements in the default system. With the identified elements number less than the default one, this could potentially reduce the complexity of the desired suspension in practical applications.

Moreover, the identified absorbers could provide significant performance improvements compared to the traditional one provided that same elements number is included in these absorbers. For example, in Chapter 5, with 1 spring, 1 damper, 1 inerter and 1 reaction mass, the identified network C_{2c} could provide 41% improvements compared to the optimum TMDI. It also outperforms the 1PT1NG configuration C_1 with 47.2% improvements, which can be considered as being obtained by employing the structure-immittance approach.

For certain applications, more than one optimum networks are identified with same performance improvements. This will provide more possibilities for the next-step physical design of such absorbers to fit into specific manufacturing requirements. For example, in Chapter 3, four different absorbers $\mathrm{IBA}_{4\mathrm{E}1}$, $\mathrm{IBA}_{4\mathrm{E}2}$, $\mathrm{IBA}_{4\mathrm{E}3}$ and $\mathrm{IBA}_{4\mathrm{E}4}$ are identified with identical performance improvements when employing 4 elements for both the monopile and the spar-buoy type turbines. $\mathrm{IBA}_{6\mathrm{E}1}$ and $\mathrm{IBA}_{6\mathrm{E}2}$ are identified for the monopile, $\mathrm{IBA}_{6\mathrm{E}3}$ and $\mathrm{IBA}_{6\mathrm{E}4}$ are identified for the spar-buoy with identical performance improvements when employing 6 elements. Moreover, in chapter 6, networks L1 and L2 provide same performance for the half-car model.

Finally, it can be widely used for various network identification related problems. The engineering applications demonstrated in Chapters 3-6 are only several examples. The proposed approach is also applicable to any other dynamic systems, such as the railway vehicle, aircraft, bridge, etc, for their vibration suppression. Moreover, the identified absorbers can be realised using multi-physical domain properties (i.e., mechanical, electrical, hydraulic, pneumatic) subjected to different application scenario.

7.2 Future work

Whilst the network-synthesis-based identification methodology presented in this thesis provides new and practical insight to the design of beneficial vibration absorbers, it also reveals a number of avenues of research that may be of further value, which are outlined here.

- **Multi-port (mass-included) network realisation** In this thesis, only two-terminal (Chapter 3) and three-terminal (Chapter 4-6) networks are investigated. While the multi-port network identification with predetermined network topology and complexity is also practically useful in many engineering applications, such as the full-vehicle interlinked suspension design with four-wheel suspensions connected together [155]. Moreover, as mentioned in Chpater 3, the mass element has its unique merit as attaching absorbers' terminals physically to the ground might be unrealistic for many applications. It is also worth to investigate the mass-included three-terminal and multi-port network identification approach.

- **Model and feasibility study extension** For vibration suppression examples shown in this thesis, most case studies employ simplified models to demonstrate the effectiveness of the proposed network identification methodology. It is worth to consider a sophisticated model with detailed information and to examine the sensitivity of the obtained devices when subjected to a more realistic model. For example, the three-storey building model used in Chapters 4 and 5 didn't include the damping of the primary system. It could provide an insight of how the damping will affect the identified absorbers' performance if it is included in the building model. Moreover, the half car model employed in Chapter 6 is a four-DOF system. It is worth to investigate what the vehicle performance would be if the vehicle is modelled in a professional vehicle simulation software, such as the CarMaker [156]. The feasibility study could also be refined to be more representative for real application. For example, the absorbers are only placed at the top floor of the building models considered in Chapters 4 and 5. While placing them at other floor could potentially achieve better performance. This could be further explored for practical applications.

- **Uncertainty and nonlinearity investigation** The systems and absorbers' parameters considered in this work are all taken as deterministic. However, it is extremely difficult or even prohibited to obtain the exact values of these parameters in reality. For example, the system's damping effect is difficult to be accurately obtained. Moreover, the nonlinearity of the identified absorbers are not considered yet. It has been stated [1, 62, 141] that the inerter and damper nonlinearity has great impact on the system overall dynamics and could potentially degrade system performance. Therefore, the uncertainty and nonlinearity of the primary system and the absorber should be both considered before the identified absorbers are applied for practical engineering system vibration suppression problems.

- **Multi-physical domain prototype realisation** The absorbers identified in this thesis are represented by their passive element properties (i.e., stiffness, damping, inertance in the mechanical domain, and compliance, resistance, inertance in the hydraulic domain). There is still a gap between the element properties and their physical realisations. It is also possible that one component in the prototype might include more than one element properties. For example, to realise the hydraulic inertance, a helical tube [3] can be used, where the length and area value of the helical tube need to be determined. In the meantime, there is also damping effect existing, which represents the resistance of the fluid flow in a pipeline. How to find a one-to-one correspondence between the network and the prototype realisation needs to be further explored. Moreover, different element properties can be combined together to form an integrated device, such as a hall-bush device with the fluid passageway as shown in [157]. A general prototype design methodology under multi-physical domain principle is also needed.

- **Experimental testing** The networks identified in this thesis and the performance improvements are simulation results. To facilitate the industrial applications of the proposed beneficial absorbers, it is essential to experimentally verify their performance advantages. Prototypes of such absorbers should be established, tested and adjusted considering uncertainties, inherent nonlinearity and hysteresis effects in the devices. For example, additional nonlinearity exists in the hydraulically interlinked systems identified in Chapter 6. They should be verified experimentally.

Appendix A

Implementation of 1PT1NG networks to Open-FAST

Considering the equation of motion of an IBA in the X direction based on the previous study done by La Cava and Lackner [158]:

$$\begin{aligned} & m_X \ddot{x}_{IBA_X/P} - m_X(\dot{\phi}_P^2 + \dot{\psi}_P^2) x_{IBA_X/P} + \mathcal{L}^{-1}(Y'(s)) \ddot{x}_{IBA_X/P} \\ & = m_X a_{G_X/O} + (F_{ext_X} + F_{StopFrc_X}) - m_X \ddot{x}_{P/O} \end{aligned} \tag{A.1}$$

where m_X is the mass value of an absorber in X direction. Subscripts O, P and IBA represent the origin point of the global inertial reference frame, the origin point of the non-inertial reference frame fixed to the tower top where IBAs are at rest, and the origin point of an IBA, respectively. $x_{IBA_X/P}$ is the displacement of an IBA relative to the tower top non-inertial reference frame origin point IBA. a_G is the gravity acceleration. Now setting:

$$\mathbf{B}_X u_X = m_X a_{G_X/O} + (F_{ext_X} + F_{StopFrc_X}) - m_X \ddot{x}_{P/O} \tag{A.2}$$

where u_X is the input vector with input matrix denoted by $\mathbf{B}_X$. Note that $\mathcal{L}^{-1}(Y'(s))\ddot{x}_{IBA_X/P}$ is the output force F_f generated between the two terminals of the network, where the x in Eq.(3.10) is the $x_{IBA_X/P}$ in Eq.(A.1. Therefore, Eq.(A.1) can be rewritten as:

$$m_X \ddot{x}_{IBA_X/P} - m_X(\dot{\phi}_P^2 + \dot{\psi}_P^2) x_{IBA_X/P} + F_f = \mathbf{B}_X u_X \tag{A.3}$$

Integrate Eq.(3.10) on both sides considering all variables with zero initial condition, and substitute it into Eq.(A.3).

$$\begin{aligned}&m_X\ddot{x}_{IBA_X/P} - m_X(\dot{\phi}_P^2 + \dot{\psi}_P^2)x_{IBA_X/P} + \mathbf{c}_1(\mathbf{A}_1 \textstyle\int \boldsymbol{\omega}_f + \mathbf{b}_1\dot{x}_{IBA_X/P}) + \\ &d_1\ddot{x}_{IBA_X/P} = \mathbf{B}_X u_X\end{aligned} \tag{A.4}$$

Then the equation of motion can be reformulated by grouping orders of $x_{IBA_X/P}$:

$$M_X\ddot{x}_{IBA_X/P} + C_X\dot{x}_{IBA_X/P} + K_X x_{IBA_X/P} + \mathbf{c}_1\mathbf{A}_1 \textstyle\int \boldsymbol{\omega}_f \quad = \quad \mathbf{B}_X u_X \tag{A.5}$$

where

$$\begin{aligned}M_X &= m_X + d_1\\ C_X &= \mathbf{c}_1\mathbf{b}_1\\ K_X &= -m_X(\dot{\phi}_P^2 + \dot{\psi}_P^2)\end{aligned}$$

Combining the absorber's mass states x with its ficitious states $\int \boldsymbol{\omega}_f$, the entire system can now be written in the state-space form in the time domain as follows:

$$\dot{x}_{w_X} \quad = \quad \mathbf{A}_{ss_X} x_{w_X} + \mathbf{B}_{ss_X} u_X \tag{A.6}$$

with

$$x_{w_X} = \begin{bmatrix} \dot{x}_{IBA_X/P} \\ x_{IBA_X/P} \\ \int \boldsymbol{\omega}_f \end{bmatrix}, \mathbf{A}_{ss_X} \quad = \begin{bmatrix} -M_X^{-1}C_X & -M_X^{-1}K_X & -M_X^{-1}\mathbf{c}_1\mathbf{A}_1 \\ 1 & 0 & \mathbf{0} \\ \mathbf{b}_1 & \mathbf{0} & \mathbf{A}_1 \end{bmatrix}, \mathbf{B}_{ss_X} = \begin{bmatrix} M_X^{-1}\mathbf{B}_X \\ \mathbf{0}_{(N+1)\times 1} \end{bmatrix}$$

N is the dimension of the fictitious states. Therefore, with the zero initial condition, the force exerted by the IBA in X direction (i.e. Eq(3.9)) can be reformed as:

$$F_{f_X} \quad = \quad \mathbf{c}_1(\mathbf{A}_1 \textstyle\int \boldsymbol{\omega}_f + \mathbf{b}_1\dot{x}_{IBA_X/P}) + d_1\ddot{x}_{IBA_X/P} \tag{A.7}$$

similarly, for an IBA in the Y direction, the state space equation and the force expression are obtained as:

$$\dot{x}_{w_Y} = \mathbf{A}_{ss_Y} x_{w_Y} + \mathbf{B}_{ss_Y} u_Y \tag{A.8}$$

and

$$F_{f_Y} = \mathbf{c}_1(\mathbf{A}_1 \int \boldsymbol{\omega}_f + \mathbf{b}_1 \dot{x}_{IBA_Y/P}) + d_1 \ddot{x}_{IBA_Y/P} \tag{A.9}$$

where

$$x_{w_Y} = \begin{bmatrix} \dot{x}_{TMD_Y/P} \\ x_{TMD_Y/P} \\ \int \boldsymbol{\omega}_f \end{bmatrix}, \mathbf{A}_{ss_Y} = \begin{bmatrix} -M_Y^{-1} C_Y & -M_Y^{-1} K_Y & -M_Y^{-1} \mathbf{c}_1 \mathbf{A}_1 \\ 1 & 0 & \mathbf{0} \\ \mathbf{b}_1 & \mathbf{0} & \mathbf{A}_1 \end{bmatrix}, \mathbf{B}_{ss_Y} = \begin{bmatrix} M_Y^{-1} \mathbf{B}_Y \\ \mathbf{0}_{(N+1)\times 1} \end{bmatrix}$$

and

$$M_Y = m_Y + d_1, \quad C_Y = \mathbf{c}_1 \mathbf{b}_1, \quad K_Y = -m_Y(\dot{\theta}_P^2 + \dot{\psi}_P^2)$$

Hence, by implementing Eq.(A.6-A.9) into the IBA module, transfer functions of different 1PT1NG IBAs can be included in OpenFAST.

Appendix B

IF-Matrix and 2PT1NG IF-network

B.1 Derivation of the IF-Matrix

Consider a 2PT1NG network shown in Fig. 5.3 with velocities $v_1,\ v_2$ and forces $f_1,\ f_2$ at the two physical-terminals PT1 and PT2. Its Immittance-Function-Matrix $\mathbf{L}(s)$, relating the velocities with the forces in Laplace domain, is defined as:

$$\begin{bmatrix} F_1 \\ F_2 \end{bmatrix} = \mathbf{L}(s) \begin{bmatrix} V_1 \\ V_2 \end{bmatrix}, \tag{B.1}$$

where $\mathbf{L}(s)$ is a 2×2 matrix, made up of four admittance functions, denoted as $\mathbf{L}(1,1),\ \mathbf{L}(1,2),\ \mathbf{L}(2,1)$ and $\mathbf{L}(2,2)$.

For the generic IF-Network, $\mathbf{L}_1(s)$ shown in Table 5.1, the equation of motion, in Laplace domain, can be derived as:

$$F_1 = sY_3(s)(V_1 - V_m), \quad F_2 = sY_2(s)(V_2 - V_m), \quad \text{and} \quad msV_m = F_1 + F_2, \tag{B.2}$$

where V_m is the velocity of the reaction mass with its value defined as positive to the right. By expressing V_m as a function of $V_1,\ V_2$, the IF-Matrix of the generic IF-Network, $\mathbf{L}_1(s)$, can be written as:

$$\mathbf{L}_1(s) = \frac{Y_2(s)Y_3(s)}{Y_2(s) + Y_3(s) + ms} \begin{bmatrix} \dfrac{(Y_2(s) + ms)}{Y_2(s)} & -1 \\ -1 & \dfrac{(Y_3(s) + ms)}{Y_3(s)} \end{bmatrix}. \tag{B.3}$$

The IF-Matrix of the generic IF-Network for the $R = 2$ case, shown in Table 5.1, can then be obtained by replacing ms in (B.3) with $Y_m(s)$, to give

$$\mathbf{L}_2(s) = \frac{Y_2(s)Y_3(s)}{Y_2(s)+Y_3(s)+Y_m(s)} \begin{bmatrix} \dfrac{(Y_2(s)+Y_m(s))}{Y_2(s)} & -1 \\ -1 & \dfrac{(Y_3(s)+Y_m(s))}{Y_3(s)} \end{bmatrix}. \tag{B.4}$$

where

$$Y_m(s) = Y_1(s)ms/(Y_1(s)+ms) \tag{B.5}$$

represents a mass connected in series with the IF-Block $Y_1(s)$. Built on (B.4), the IF-Matrix of the generic IF-Networks, $\mathbf{L}_R(s)$, for the even R case ($R \geq 3$, see the left-hand side of Table 5.1), can be obtained by a parallel connection between $\mathbf{L}_{R-1}(s)$ and $Y_{\frac{3R-1}{2}}(s)$, given by

$$\mathbf{L}_R(s) = \left(\mathbf{L}_{R-1}(s) + Y_{\frac{3R-1}{2}}(s) \begin{bmatrix} 1 & -1 \\ -1 & 1 \end{bmatrix}\right) \tag{B.6}$$

For the series connection between $\mathbf{L}_{R-1}(s)$ and two IF-Blocks $Y_{\frac{3R}{2}-1}(s)$, $Y_{\frac{3R}{2}}(s)$ (see the right-hand side of Table 5.1), the IF-Matrix can be formulated by first deriving $\mathbf{L}'_R(s)$, using

$$\mathbf{L}'_R(s) = \frac{1}{Y_{\frac{3R}{2}-1}(s) + \mathbf{L}_{R-1}(2,2)} \left(Y_{\frac{3R}{2}-1}(s)\mathbf{L}_{R-1}(s) + \begin{bmatrix} |\mathbf{L}_{R-1}(s)| & 0 \\ 0 & 0 \end{bmatrix}\right) \tag{B.7}$$

and then substituting this into

$$\mathbf{L}_R(s) = \frac{1}{Y_{\frac{3R}{2}}(s) + \mathbf{L}'_R(1,1)} \left(Y_{\frac{3R}{2}}(s)\mathbf{L}'_R(s) + \begin{bmatrix} 0 & 0 \\ 0 & |\mathbf{L}'_R(s)| \end{bmatrix}\right) \tag{B.8}$$

B.2 2PT1NG IF-Network possibilities with $R = 1,\ 2,\ 3,\ 4$

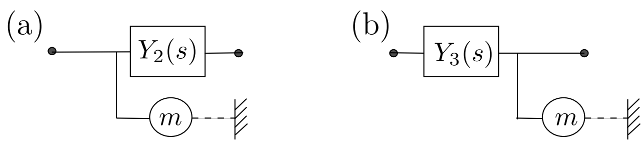

Fig. B.1 IF-Network cases for $R = 1$.

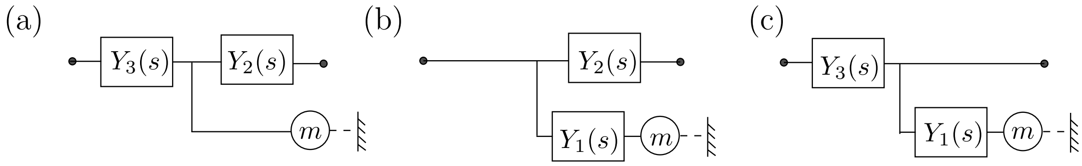

Fig. B.2 IF-Network cases for $R = 2$.

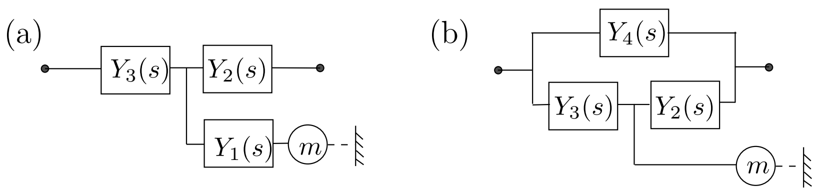

Fig. B.3 IF-Network cases for $R = 3$.

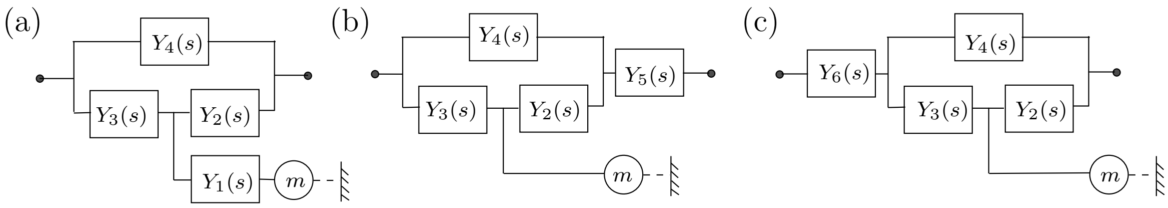

Fig. B.4 IF-Network cases for $R = 4$.

Appendix C

Hydraulically interlinked system and the three-terminal network IF-Matrix

C.1 Derivation of the hydraulically interlinked system

Fluid properties of the pipeline A in the Laplace domain can be expressed as:

$$
\begin{aligned}
(\tilde{P}_{l1} - \tilde{P}_{A1}) &= (R_{A1} + I_{A1}s)\tilde{q}_{l1} \\
(\tilde{P}_{r2} - \tilde{P}_{A1}) &= (R_{A2} + I_{A2}s)\tilde{q}_{r2} \\
(\tilde{P}_{A1} - \tilde{P}_{A0}) &= (R_{Aa} + \frac{1}{C_{Aa}s})\tilde{q}_{Aa}
\end{aligned}
\tag{C.1}
$$

Since $\tilde{q}_{l1} + \tilde{q}_{r2} = \tilde{q}_{Aa}$, Eq. (C.1) can be re-organised as follows by eliminating $\tilde{P}_{A1}$:

$$
\begin{bmatrix} \tilde{P}_{l1} - \tilde{P}_{l10} \\ \tilde{P}_{r2} - \tilde{P}_{r20} \end{bmatrix} = \begin{bmatrix} R_{A1} + I_{A1}s + R_{Aa} + \frac{1}{C_{Aa}s} & R_{Aa} + \frac{1}{C_{Aa}s} \\ R_{Aa} + \frac{1}{C_{Aa}s} & R_{A2} + I_{A2}s + R_{Aa} + \frac{1}{C_{Aa}s} \end{bmatrix} \begin{bmatrix} \tilde{q}_{l1} \\ \tilde{q}_{r2} \end{bmatrix} \tag{C.2}
$$

Fluid properties of the pipeline B can be expressed in a similar way in the Laplace domain, where the equations to describe the fluid properties are:

$$\begin{aligned}(\tilde{P}_{B1} - \tilde{P}_{l2}) &= (R_{B1} + I_{B1}s)\tilde{q}_{l2} \\ (\tilde{P}_{B1} - \tilde{P}_{r1}) &= (R_{B2} + I_{B2}s)\tilde{q}_{r1} \\ (\tilde{P}_{B0} - \tilde{P}_{B1}) &= (R_{Ba} + \frac{1}{C_{Ba}s})\tilde{q}_{Ba}\end{aligned} \tag{C.3}$$

since $\tilde{q}_{r1} + \tilde{q}_{l2} = \tilde{q}_{Ba}$, Eq. C.3 can be reorganised as follows by eliminating $\tilde{P}_{B1}$:

$$\begin{bmatrix}\tilde{P}_{l20} - \tilde{P}_{l2} \\ \tilde{P}_{r10} - \tilde{P}_{r1}\end{bmatrix} = \begin{bmatrix} R_{B1} + I_{B1}s + R_{Ba} + \dfrac{1}{C_{Ba}s} & R_{Ba} + \dfrac{1}{C_{Ba}s} \\ R_{Ba} + \dfrac{1}{C_{Ba}s} & R_{B2} + I_{B2}s + R_{Ba} + \dfrac{1}{C_{Ba}s}\end{bmatrix} \begin{bmatrix}\tilde{q}_{l2} \\ \tilde{q}_{r1}\end{bmatrix} \tag{C.4}$$

Therefore, the hydraulic impedance $\mathbf{Z}_h$ can be obtained as Eq. (6.3) through Eqs. (C.2) and (C.4).

To obtain dynamic forces F_{ld} and F_{rd} exerted by the left and right pistons, they can be expressed as:

$$\begin{aligned}F_{ld} &= F_l - F_{l0} \\ F_{rd} &= F_r - F_{r0}\end{aligned} \tag{C.5}$$

with

$$\begin{cases} F_l = P_{l1}A_{l1} - P_{l2}A_{l2} \\ F_r = P_{r2}A_{r2} - P_{r1}A_{r1}\end{cases} \text{and} \begin{cases} F_{l0} = P_{l10}A_{l1} - P_{l20}A_{l2} \\ F_{r0} = P_{r20}A_{r2} - P_{r10}A_{r1}\end{cases}$$

F_{l0}, F_{r0} and F_l, F_r are the initial forces and total forces on the left and right pistons, respectively. Here P_{ij0} represent the initial fluid pressure inside each chamber. $F_{l0} = 0$ and $F_{r0} = 0$ considering initial pressures $P_{l10} = P_{l20} = P_{r10} = P_{r20}$. Hence the dynamic forces F_{ld} and F_{rd} equal the total suspension forces F_l and F_r, respectively. The relationship between total suspension forces and pressure differences can now be written as:

$$\mathbf{F} = \begin{bmatrix}F_l \\ F_r\end{bmatrix} = \begin{bmatrix}F_{ld} \\ F_{rd}\end{bmatrix} = \begin{bmatrix}1 & 0 & 1 & 0 \\ 0 & 1 & 0 & 1\end{bmatrix} \begin{bmatrix}A_{l1} & 0 & 0 & 0 \\ 0 & A_{r2} & 0 & 0 \\ 0 & 0 & A_{l2} & 0 \\ 0 & 0 & 0 & A_{r1}\end{bmatrix} \begin{bmatrix}P_{l1} - P_{l10} \\ P_{r2} - P_{r20} \\ P_{l20} - P_{l2} \\ P_{r10} - P_{r1}\end{bmatrix} = \mathbf{D}\,\mathbf{A}\,\Delta\mathbf{P} \tag{C.6}$$

where $\mathbf{D}$ is the position matrix; $\mathbf{A}$ is the area matrix; and $\Delta\mathbf{P}$ is the pressure difference vector.

The relationship between the hydraulic flow $\mathbf{q}$ and the piston relative velocity $\Delta\mathbf{v}$ can be easily obtained as

$$\mathbf{q} = \begin{bmatrix} q_{l1} \\ q_{r2} \\ q_{l2} \\ q_{r1} \end{bmatrix} = \begin{bmatrix} A_{l1} & 0 & 0 & 0 \\ 0 & A_{r2} & 0 & 0 \\ 0 & 0 & A_{l2} & 0 \\ 0 & 0 & 0 & A_{r1} \end{bmatrix} \begin{bmatrix} 1 & 0 \\ 0 & 1 \\ 1 & 0 \\ 0 & 1 \end{bmatrix} \begin{bmatrix} \Delta v_l \\ \Delta v_r \end{bmatrix} = \mathbf{A}\mathbf{D}^T \Delta\mathbf{v} \tag{C.7}$$

Taking the Laplace transformation of Eqs. (C.6) and (C.7), and combining them with Eq. (6.1), it can be obtained that

$$\tilde{\mathbf{F}}_h = \tilde{\mathbf{F}}_{h_d} = \mathbf{D}\mathbf{A}\mathbf{Z}_h\mathbf{A}\mathbf{D}^T \Delta\tilde{\mathbf{v}}_h \tag{C.8}$$

Therefore, the mechanical admittance matrix $\mathbf{Y}_m$ is obtained in Eq. (6.4).

C.2 IF-Matrix of the Three-terminal IF-Network

The IF-Matrix of the π-IF-Network as shown in Fig. 6.6 (b2) can be expressed as:

$$\mathbf{Z}_\pi = \begin{bmatrix} \frac{1}{Z_1} + \frac{1}{Z_2} & -\frac{1}{Z_1} \\ -\frac{1}{Z_1} & \frac{1}{Z_1} + \frac{1}{Z_3} \end{bmatrix}^{-1} \tag{C.9}$$

Thus, for series connections S1, S2 and S3, the IF-Matrices of the IF-Networks shown in Fig. 6.6 (b3)-(b5) can be expressed as:

$$\mathbf{Z}_{S1} = \mathbf{Z}_\pi + \begin{bmatrix} Z_4 & 0 \\ 0 & 0 \end{bmatrix} \tag{C.10}$$

$$\mathbf{Z}_{S2} = \mathbf{Z}_\pi + \begin{bmatrix} 0 & 0 \\ 0 & Z_4 \end{bmatrix} \tag{C.11}$$

$$\mathbf{Z}_{S3} = \mathbf{Z}_\pi + \begin{bmatrix} Z_4 & Z_4 \\ Z_4 & Z_4 \end{bmatrix} \tag{C.12}$$

The IF-Matrix of the T-IF-Network as shown in Fig. 6.7 (b2) can be expressed as:

$$\mathbf{Z}_T = \begin{bmatrix} Z_1 + Z_2 & Z_1 \\ Z_1 & Z_1 + Z_3 \end{bmatrix} \tag{C.13}$$

For parallel connections P1, P2 and P3, IF-Matrices of the resulting IF-Networks as shown in Fig. 6.7 (b3)-(b5) can be expressed as:

$$\mathbf{Z}_{P1} = \left\{ \mathbf{Z}_T^{-1} + \begin{bmatrix} \frac{1}{Z_4} & 0 \\ 0 & 0 \end{bmatrix} \right\}^{-1} \tag{C.14}$$

$$\mathbf{Z}_{P2} = \left\{ \mathbf{Z}_T^{-1} + \begin{bmatrix} 0 & 0 \\ 0 & \frac{1}{Z_4} \end{bmatrix} \right\}^{-1} \tag{C.15}$$

$$\mathbf{Z}_{P3} = \left\{ \mathbf{Z}_T^{-1} + \begin{bmatrix} \frac{1}{Z_4} & -\frac{1}{Z_4} \\ -\frac{1}{Z_4} & \frac{1}{Z_4} \end{bmatrix} \right\}^{-1} \tag{C.16}$$

When i is an even number, the general representation of the GIFN$_i$ is:

$$\mathbf{Z}_{GIFN_i} = \left\{ \mathbf{Z}_{GIFN_{i-1}}{}^{-1} + \begin{bmatrix} \frac{1}{Z_{3i-3}} + \frac{1}{Z_{3i-4}} & -\frac{1}{Z_{3i-3}} \\ -\frac{1}{Z_{3i-3}} & \frac{1}{Z_{3i-3}} + \frac{1}{Z_{3i-5}} \end{bmatrix} \right\}^{-1} \tag{C.17}$$

When i is an odd number, the general representation of the GIFN$_i$ is:

$$\mathbf{Z}_{GIFN_i} = \mathbf{Z}_{GIFN_{i-1}} + \begin{bmatrix} Z_{3i-3} + Z_{3i-4} & Z_{3i-3} \\ Z_{3i-3} & Z_{3i-3} + Z_{3i-5} \end{bmatrix} \tag{C.18}$$

Appendix D

Random road input profile

This random rough road input is the same as the one used in [153]. Following the isotropy property, the road displacement spectral density matrix $\mathbf{S}^{\xi}$ is represented as:

$$\mathbf{S}^{\xi} = \begin{bmatrix} S_D^{\xi} & S_X^{\xi} \\ S_x^{\xi} & S_D^{\xi} \end{bmatrix} \tag{D.1}$$

where S_D^{ξ} is the direct (single-side) spectral density and S_x^{ξ} is the cross spectral density. S_D^{ξ} adopted in this study is the 'single slope' representation, expressed in terms of the wave number n as:

$$S_D^{\xi}(n) = c|n|^{-2w} \tag{D.2}$$

The closed form solution for the cross spectral density for this road model is:

$$S_X^{\xi}(n) = \frac{2c(\pi b/n)^w}{\Gamma(w)} K_w(2\pi bn) \tag{D.3}$$

In the foregoing equations, c is the road roughness coefficient; v is the vehicle traverse velocity. For a vehicle traversing the ground with constant velocity v, these spatial PSD functions can be expressed as a function of the angular frequency, by making the substitution $n = \omega/2\pi v$. $\Gamma(\cdot)$ denotes the gamma function; and $K_w(\cdot)$ is the modified Bessel function of the second kind with order w. Command *besselk* is used in MATLAB© to represent this function. A value of 1 for w represents a white noise velocity input of constant (single-sided) spectral density. A c value of 1.6×10^{-6} is used.

The vehicle acceleration transfer function $\mathbf{H}_a = s^2\mathbf{H}_d$, therefore, the obtained $\mathbf{H}_a$ and $\mathbf{S}^\xi$ can be used to calculate the response spectral density matrix:

$$\mathbf{S}_{resp}(\omega) = \mathbf{H}_a^* \mathbf{S}^\xi(\omega) \mathbf{H}_a^T \tag{D.4}$$

where the symbol * and ^{T} denote the complex conjugate and matrix transpose, respectively.

References

[1] C. Papageorgiou, N. E. Houghton, M. C. Smith, Experimental testing and analysis of inerter devices, Journal of Dynamic Systems, Measurement, and Control 131 (1), 011001. doi:10.1115/1.3023120.

[2] F.-C. Wang, M.-F. Hong, T.-C. Lin, Designing and testing a hydraulic inerter, Proceedings of the Institution of Mechanical Engineers, Part C: Journal of Mechanical Engineering Science 225 (1) (2011) 66–72. doi:10.1243/09544062JMES2199.

[3] S. J. Swift, M. C. Smith, A. R. Glover, C. Papageorgiou, B. Gartner, N. E. Houghton, Design and modelling of a fluid inerter, International Journal of Control 86 (11) (2013) 2035–2051. doi:10.1080/00207179.2013.842263.

[4] A. Morelli, Synthesis of electrical and mechanical networks of restricted complexity, Ph.D. thesis, University of Cambridge (2019).

[5] G. M. Stewart, M. A. Lackner, Offshore wind turbine load reduction employing optimal passive tuned mass damping systems, IEEE Transactions on Control Systems Technology 21 (4) (2013) 1090–1104. doi:10.1109/TCST.2013.2260825.

[6] N. Zhang, W. A. Smith, J. Jeyakumaran, Hydraulically interconnected vehicle suspension: Background and modelling, Vehicle System Dynamics 48 (1) (2010) 17–40. doi:10.1080/00423110903243182.

[7] J. Helsen, P. Peeters, K. Vanslambrouck, F. Vanhollebeke, W. Desmet, The dynamic behavior induced by different wind turbine gearbox suspension methods assessed by means of the flexible multibody technique, Renewable Energy 69 (2014) 336–346. doi:https://doi.org/10.1016/j.renene.2014.03.036.

[8] Y. Li, Optimal design methodologies for passive vibration suppression, Ph.D. thesis, University of Bristol (2018).

[9] J. D. Hartog, Mechanical vibration, McGraw-Hill Book Company, 1956.

[10] T. T. Soong, M. C. Costantinou, Passive and active structural vibration control in civil engineering, Springer-Verlag Wien, 1994.

[11] M. Smith, Synthesis of mechanical nnetwork: the inerter, IEEE Transactions on Automatic Control 47 (10) (2002) 1648–1662. doi:10.1109/TAC.2002.803532.

[12] M. C. Smith, F.-C. Wang, Performance benefits in passive vehicle suspensions employing inerters, Vehicle System Dynamics 42 (4) (2004) 235–257. doi:10.1080/00423110412331289871.

[13] C. Papageorgiou, M. C. Smith, Positive real synthesis using matrix inequalities for mechanical networks: application to vehicle suspension, IEEE Transactions on Control Systems Technology 14 (3) (2006) 423–435. doi:10.1109/TCST.2005.863663.

[14] F. Scheibe, M. C. Smith, Analytical solutions for optimal ride comfort and tyre grip for passive vehicle suspensions, Vehicle System Dynamics 47 (10) (2009) 1229–1252. doi:10.1080/00423110802588323.

[15] F.-C. Wang, H.-A. Chan, Vehicle suspensions with a mechatronic network strut, Vehicle System Dynamics 49 (5) (2011) 811–830. doi:10.1080/00423111003797143.

[16] Y. Shen, Y. Liu, L. Chen, X. Yang, Optimal design and experimental research of vehicle suspension based on a hydraulic electric inerter, Mechatronics 61 (2019) 12–19. doi:https://doi.org/10.1016/j.mechatronics.2019.05.002.

[17] F.-C. Wang, M.-K. Liao, B.-H. Liao, W.-J. Su, H.-A. Chan, The performance improvements of train suspension systems with mechanical networks employing inerters, Vehicle System Dynamics 47 (7) (2009) 805–830. doi:10.1080/00423110802385951.

[18] F.-C. Wang, M.-K. Liao, The lateral stability of train suspension systems employing inerters, Vehicle System Dynamics 48 (5) (2010) 619–643. doi:10.1080/00423110902993654.

[19] J. Z. Jiang, A. Z. Matamoros-Sanchez, R. M. Goodall, M. C. Smith, Passive suspensions incorporating inerters for railway vehicles, Vehicle System Dynamics 50 (2012) 263–276. doi:10.1080/00423114.2012.665166.

[20] J. Z. Jiang, A. Z. Matamoros-Sanchez, A. Zolotas, R. M. Goodall, M. C. Smith, Passive suspensions for ride quality improvement of two-axle railway vehicles, Proceedings of the Institution of Mechanical Engineers, Part F: Journal of Rail and Rapid Transit 229 (3) (2015) 315–329. doi:10.1177/0954409713511592.

[21] I. F. Lazar, S. A. Neild, D. J. Wagg, Using an inerter-based device for structural vibration suppression, Earthquake Engineering and Structure Dynamics 43 (2014) 1129–1147. doi:https://doi.org/10.1002/eqe.2390.

[22] K. Ikago, K. Saito, N. Inoue, Seismic control of single-degree-of-freedom structure using tuned viscous mass damper, Earthquake Engineering & Structural Dynamics 41 (3) (2012) 453–474. doi:https://doi.org/10.1002/eqe.1138.

[23] L. Marian, A. Giaralis, Optimal design of a novel tuned mass-damper–inerter (TMDI) passive vibration control configuration for stochastically support-excited structural systems, Probabilistic Engineering Mechanics 38 (2014) 156–164. doi:https://doi.org/10.1016/j.probengmech.2014.03.007.

[24] A. Giaralis, F. Petrini, Wind-induced vibration mitigation in tall buildings using the tuned mass-damper-inerter, Journal of Structural Engineering 143 (9) (2017) 04017127. doi:https://doi.org/10.1061/(ASCE)ST.1943-541X.0001863.

[25] Y. Hu, J. Wang, M. Chen, Z. Li, Y. Sun, Load mitigation for a barge-type floating offshore wind turbine via inerter-based passive structural control, Engineering

Structures 177 (2018) 198–209. doi:https://doi.org/10.1016/j.engstruct.2018.09.063.

[26] R. Zhang, Z. Zhao, K. Dai, Seismic response mitigation of a wind turbine tower using a tuned parallel inerter mass system, Engineering Structures 180 (2019) 29–39. doi:https://doi.org/10.1016/j.engstruct.2018.11.020.

[27] S. Sarkar, B. Fitzgerald, Vibration control of spar-type floating offshore wind turbine towers using a tuned mass-damper-inerter, Structural Control and Health Monitoring 27 (1) (2020) e2471. doi:https://doi.org/10.1002/stc.2471.

[28] J. C. Schönfeld, Analogy of hydraulic, mechanical, acoustic and electric systems, Applied Scientific Research Section A 3 (1) (1954) 417–450. doi:https://doi.org/10.1007/BF02123920.

[29] R. Bott, R. J. Duffin, Impedance synthesis without use of transformers, Journal of Applied Physics 20 (8) (1949) 816. doi:10.1063/1.1698532.

[30] S. Y. Zhang, J. Z. Jiang, S. A. Neild, Passive vibration control: a structure-immittance approach, Proceedings of the Royal Society A: Mathematical, Physical and Engineering Sciences 473 (2201) (2017) 20170011. doi:10.1098/rspa.2017.0011.

[31] P. Kundur, J. Paserba, V. Ajjarapu, G. Andersson, A. Bose, C. Canizares, N. Hatziargyriou, D. Hill, A. Stankovic, C. Taylor, T. Van Cutsem, V. Vittal, Definition and classification of power system stability IEEE/CIGRE joint task force on stability terms and definitions, IEEE Transactions on Power Systems 19 (3) (2004) 1387–1401. doi:10.1109/TPWRS.2004.825981.

[32] H. Frahm, Device for damping vibrations of bodies, US patent, 989958 (1911).

[33] M. D. Symans, M. C. Constantinou, Semi-active control systems for seismic protection of structures: a state-of-the-art review, Engineering Structures 21 (6) (1999) 469–487. doi:https://doi.org/10.1016/S0141-0296(97)00225-3.

[34] B. F. Spencer, S. Nagarajaiah, State of the art of structural control, Journal of Structural Engineering 129 (7) (2003) 845–856. doi:10.1061/(ASCE)0733-9445(2003)129:7(845).

[35] B. Spencer, M. Sain, Controlling buildings: a new frontier in feedback, IEEE Control Systems Magazine 17 (6) (1997) 19–35. doi:10.1109/37.642972.

[36] M. Q. Feng, M. Shinozuka, S. Fujii, Friction & controllable sliding isolation system, Journal of Engineering Mechanics 119 (9) (1993) 1845–1864. doi:10.1061/(ASCE)0733-9399(1993)119:9(1845).

[37] Q. Feng, Use of a variable damper for hybrid control of bridge response under earthquake, Proc. U.S. National Workshop on Struct. Control Research.
URL https://ci.nii.ac.jp/naid/10006922731/en/

[38] J.-C. Chen, Response of large space structures with stiffness control, Journal of Spacecraft and Rockets 21 (5) (1984) 463–467. doi:10.2514/3.25681.

[39] R. C. Ehrgott, S. F. Masri, Modeling the oscillatory dynamic behaviour of electrorheological materials in shear, Smart Materials and Structures 1 (4) (1992) 275–285. doi:10.1088/0964-1726/1/4/002.

[40] B. F. Spencer, S. J. Dyke, M. K. Sain, J. D. Carlson, Phenomenological model for magnetorheological dampers, Journal of Engineering Mechanics 123 (3) (1997) 230–238. doi:10.1061/(ASCE)0733-9399(1997)123:3(230).

[41] S. J. Dyke, B. F. Spencer, M. K. Sain, J. D. Carlson, Modeling and control of magnetorheological dampers for seismic response reduction, Smart Materials and Structures 5 (5) (1996) 565–575. doi:10.1088/0964-1726/5/5/006.

[42] D. H. Wang, W. H. Liao, Semi-active suspension systems for railway vehicles using magnetorheological dampers. part I: system integration and modelling, Vehicle System Dynamics 47 (11) (2009) 1305–1325. doi:10.1080/00423110802538328.

[43] D. Karnopp, M. J. Crosby, R. A. Harwood, Vibration control using semi-active force generators, Journal of Engineering for Industry 96 (2) (1974) 619–626. doi:10.1115/1.3438373.

[44] T. T. Soong, G. F. Dargush, Passive energy dissipation systems in structural engineering, Chichester, UK: Wiley.

[45] S. Krenk, Frequency analysis of the tuned mass damper, Journal of Applied Mechanics 72 (6) (2005) 936–942. doi:10.1115/1.2062867.

[46] J. Snowdown, Steady-state behavior of the dynamic absorber, The Journal of the Acoustical Society of America 31 (8) (1959) 1096–1103. doi:10.1121/1.1907832.

[47] K. C. Falcon, B. J. Stone, W. D. Simcock, C. Andrew, Optimization of vibration aabsorber: a graphical method for use on idealized systems with restricted damping, Jouranl Mechanical Engineering Science 9 (5) (1967) 374–381. doi:10.1243/JMES_JOUR_1967_009_058_02.

[48] T. Ioi, K. Ikeda, On the dynamic vibration damped absorber of the vibration system, Bulletin of JSME 21 (151) (1978) 64–71. doi:10.1299/jsme1958.21.64.

[49] G. Warburton, Optimum absorber parameters for minimizing vibration response, Earthquake Engineering & Structural Dynamics 9 (3) (1981) 251–262. doi:https://doi.org/10.1002/eqe.4290090306.

[50] G. Warburton, Optimum absorber parameters for various combinations of response and excitation parameters, Earthquake Engineering & Structural Dynamics 10 (3) 381–401. doi:https://doi.org/10.1002/eqe.4290100304.

[51] R. Villaverde, Reduction seismic response with heavily-damped vibration absorbers, Earthquake Engineering & Structural Dynamics 13 (1) (1985) 33–42. doi:https://doi.org/10.1002/eqe.4290130105.

[52] F. Sadek, B. Mohraz, A. W. Taylor, R. M. Chung, A method of estimating the parameters of tuned mass dampers for seismic applications, Earthquake Engineering & Structural Dynamics 26 (6) 617–635. doi:https://doi.org/10.1002/(SICI)1096-9845(199706)26:6<617::AID-EQE664>3.0.CO;2-Z.

[53] K. Iwanami, K. Seto, Optimum design of dual tuned mass dampers and their effectiveness, Proceedings of the JSME(C) 50 (1984) 44–52.

[54] M. Z. Ren, A variant design of the dynamic vibration absorber, Journal of Sound and Vibration 245 (4) (2001) 762–770. doi:10.1006/jsvi.2001.3564.

[55] P. Xiang, A. Nishitani, Optimum design for more effective tuned mass damper system and its application to base-isolated buildings, Structural Control and Health Monitoring 21 (1) (2014) 98–114. doi:https://doi.org/10.1002/stc.1556.

[56] I. J. Busch-Vishniac, Electromechanical sensors and ctuators, Springer, New York, NY, 1999. doi:DOIhttps://doi.org/10.1007/978-1-4612-1434-2.

[57] F. A. Firestone, A new analogy between mechanical and electrical systems, The Journal of the Acoustical Society of America 4 (3) (1933) 249–267. doi:10.1121/1.1915605.

[58] S. Rakheja, H. Su, T. S. Sankar, Analysis of a passive sequential hydraulic damper for vehicle suspension, Vehicle System Dynamics 19 (5) (1990) 289–312. doi:10.1080/00423119008968949.

[59] H. Zhu, J. Yang, Y. Zhang, Dual-chamber pneumatically interconnected suspension: Modeling and theoretical analysis, Mechanical Systems and Signal Processing 147 (2021) 107125. doi:https://doi.org/10.1016/j.ymssp.2020.107125.

[60] H. Ren, S. Chen, Y. Zhao, G. Liu, L. Yang, State observer-based sliding mode control for semi-active hydro-pneumatic suspension, Vehicle System Dynamics 54 (2) (2016) 168–190. doi:10.1080/00423114.2015.1122818.

[61] F.-C. Wang, M.-K. Liao, B.-H. Liao, W.-J. Su, H.-A. Chan, The performance improvements of train suspension systems with mechanical networks employing inerters, Vehicle System Dynamics 47 (7) (2009) 805–830. doi:10.1080/00423110802385951.

[62] F.-C. Wang, W.-J. Su, Impact of inerter nonlinearities on vehicle suspension control, Vehicle System Dynamics 46 (7) (2008) 575–595. doi:10.1080/00423110701519031.

[63] M. C. Smith, Force controlling mechanical device, US patent, US7316303B2 (2008).

[64] X. Liu, B. Titurus, J. Z. Jiang, A. Harrison, Model identification methodology for fluid-based inerters, Mechanical Systems and Signal Processing 106 (2018) 479–494. doi:https://doi.org/10.1016/j.ymssp.2018.01.018.

[65] Secrets of the inerter revealed kernel description, https://www.cam.ac.uk/research/news/secrets-of-the-inerter-revealed, Last accessed: 30-Jun-2021.

[66] M. Z. Chen, Y. Hu, C. Li, G. Chen, Performance benefits of using inerter in semiactive suspensions, IEEE Transactions on Control Systems Technology 23 (4) (2014) 1571–1577. doi:10.1109/TCST.2014.2364954.

[67] Y. Hu, M. Z. Chen, Y. Sun, Comfort-oriented vehicle suspension design with skyhook inerter configuration, Journal of Sound and Vibration 405 (2017) 34–47. doi:https://doi.org/10.1016/j.jsv.2017.05.036.

[68] F.-C. Wang, M.-R. Hsieh, H.-J. Chen, Stability and performance analysis of a full-train system with inerters, Vehicle System Dynamics 50 (4) (2012) 545–571. doi:10.1080/00423114.2011.606368.

[69] A. Z. Matamoros-Sanchez, R. M. Goodall, Novel mechatronic solutions incorporating inerters for railway vehicle vertical secondary suspensions, Vehicle System Dynamics 53 (2) (2015) 113–136. doi:10.1080/00423114.2014.983529.

[70] F.-C. Wang, C.-W. Chen, M.-K. Liao, M.-F. Hong, Performance analyses of building suspension control with inerters, 2007, pp. 3786–3791. doi:10.1109/CDC.2007.4434186.

[71] F.-C. Wang, M.-F. Hong, C.-W. Chen, Building suspensions with inerters, Proceedings of the Institution of Mechanical Engineers, Part C: Journal of Mechanical Engineering Science 224 (8) (2010) 1605–1616. doi:10.1243/09544062JMES1909.

[72] I. Takewaki, S. Murakami, S. Yoshitomi, M. Tsuji, Fundamental mechanism of earthquake response reduction in building structures with inertial dampers, Structural Control and Health Monitoring 19 (6) (2012) 590–608. doi:https://doi.org/10.1002/stc.457.

[73] T. Furuhashi, S. Ishimaru, Mode control seismic design with dynamic mass, Proceedings of the 14th World Conference on Earthquake Engineering, Beijing, China, 2008.

[74] H. Garrido, O. Curadelli, D. Ambrosini, Improvement of tuned mass damper by using rotational inertia through tuned viscous mass damper, Engineering Structures 56 (2013) 2149 – 2153. doi:https://doi.org/10.1016/j.engstruct.2013.08.044.

[75] A. Giaralis, A. A. Taflanidis, Reliability-based design of tuned mass-damper inerter (TMDI) equipped multi-storey frame buildings under seismic excitation, 12th International Conference on Applications of Statistics and Probability in Civil Engineering, 2015.

[76] L. Marian, A. Giaralis, The tuned mass-damper-inerter for harmonic vibrations suppression, attached mass reduction, and energy harvesting, Smart Structures and Systems 19 (2017) 665–678. doi:10.12989/sss.2017.19.6.665.

[77] K. Yamamoto, M. C. Smith, Bounded disturbance amplification for mass chains with passive interconnection, IEEE Transactions on Automatic Control 61 (6) (2016) 1565–1574. doi:10.1109/TAC.2015.2478126.

[78] Y. Hu, M. Z. Chen, Inerter-based passive structural control for load mitigation of wind turbines, Chinese Control And Decision Conference (CCDC) (2017) 3056–3061.

[79] Y. Hu, M. Z. Chen, Passive structural control with inerters for a floating offshore wind turbine, 36th Chinese Control Conference (CCC) (2017) 9266–9271.

[80] R. Ma, K. Bi, H. Hao, Mitigation of heave response of semi-submersible platform (SSP) using tuned heave plate inerter (THPI), Engineering Structures 177 (2018) 357–373. doi:https://doi.org/10.1016/j.engstruct.2018.09.085.

[81] R. Ma, K. Bi, H. Hao, A novel rotational inertia damper for heave motion suppression of semisubmersible platform in the shallow sea, Structural Control and Health Monitoring 26 (7) (2019) e2368. doi:https://doi.org/10.1002/stc.2368.

[82] I. Lazar, S. Neild, D. Wagg, Vibration suppression of cables using tuned inerter dampers, Engineering Structures 122 (2016) 62–71. doi:https://doi.org/10.1016/j.engstruct.2016.04.017.

[83] S. Krenk, Resonant inerter based vibration absorbers on flexible structures, Journal of the Franklin Institute 356 (14) (2019) 7704–7730, special Issue on Inerter-based Systems. doi:https://doi.org/10.1016/j.jfranklin.2018.11.038.

[84] J. Luo, J. Z. Jiang, J. H. G. Macdonald, Cable vibration suppression with inerter-based absorbers, Journal of Engineering Mechanics 145 (2) (2019) 04018134. doi:10.1061/(ASCE)EM.1943-7889.0001554.

[85] K. Xu, K. Bi, Q. Han, X. Li, X. Du, Using tuned mass damper inerter to mitigate vortex-induced vibration of long-span bridges: Analytical study, Engineering Structures 182 (2019) 101–111. doi:https://doi.org/10.1016/j.engstruct.2018.12.067.

[86] J. Dai, Z.-D. Xu, P.-P. Gai, Z.-W. Hu, Optimal design of tuned mass damper inerter with a maxwell element for mitigating the vortex-induced vibration in bridges, Mechanical Systems and Signal Processing 148 (2021) 107180. doi:https://doi.org/10.1016/j.ymssp.2020.107180.

[87] B. D. O. Anderson, S. Vongpanitlerd, Network Analysis and Synthesis: A Modern Systems Theory Approach, Prentice-Hall, Englewood Cliffs, NJ, USA, 1973.

[88] V. Belevitch, Classical network theory, Holden-day, 1968.

[89] N. Balabanian, T. A. Bickart, Electrical Network Theory, New York: Wiley, 1969.

[90] R. M. Foster, A reactance theorem, Bell System Technical Journal 3 (2) (1924) 259–267. doi:https://doi.org/10.1002/j.1538-7305.1924.tb01358.x.

[91] W. Cauer, Die verwirklichung von wechselstromwiderständen vorgeschriebener frequenzabhängigkeit, Archiv für Elektrotechnik 17 (4) (1926) 355–388. doi:https://doi.org/10.1007/BF01662000.

[92] O. Brune, Synthesis of a finite two-terminal network whose driving-point impedance is a prescribed function of frequency, Ph.D. thesis, Massachusetts Institute of Technology (1931).

[93] T. T. Hughes, On the synthesis of passive networks without transformers, Ph.D. thesis, University of Cambridge (2014).

[94] F. Reza, Synthesis without ideal transformers, Journal of Applied Physics 25 (1954) 807–808.

[95] A. Fialkow, I. Gerst, Impedance synthesis without mutual coupling, Quarterly of Applied Mathematics 12 (4) (1955) 420–422.
URL http://www.jstor.org/stable/43634158

[96] S. Darlington, Synthesis of reactance 4-poles which produce prescribed insertion loss characteristics: including special applications to filter design, Journal of Mathematics and Physics 18 (1-4) (1939) 257–353. doi:https://doi.org/10.1002/sapm1939181257.

[97] P. Tissi, Synthesis of lumped n-ports via reactance extraction, Ph.D. thesis, Polytechnic Institute of Brooklyn.

[98] C. M. Gewertz, Synthesis of a finite, four-terminal net-work from its prescribed driving-point functions and transfer function, Journal of Mathematics and Physics 12 (1-4) (1933) 1–257. doi:https://doi.org/10.1002/sapm19331211.

[99] E. A. Guillemin, Synthesis of RC-networks, Journal of Mathematics and Physics 28 (1-4) (1949) 22–42. doi:https://doi.org/10.1002/sapm194928122.

[100] A. Fialkow, I. Gerst, The transfer function of general two terminal-pair RC networks, Quarterly of Applied Mathematics 10 (2) (1952) 113–127.
URL http://www.jstor.org/stable/43633938

[101] A. Fialkow, I. Gerst, The maximum gain of an RC network, Proceedings of the IRE 41 (3) (1953) 392–395. doi:10.1109/JRPROC.1953.274389.

[102] H. Lucal, Synthesis of three-terminal RC networks, IRE Transactions on Circuit Theory 2 (3) (1955) 308–316. doi:10.1109/TCT.1955.1085259.

[103] E. Kuh, Synthesis of RC grounded two-ports, IRE Transactions on Circuit Theory 5 (1) (1958) 55–61. doi:10.1109/TCT.1958.1086423.

[104] I. Cederbaum, Some properties of the transfer function of unbalanced RC networks, Proceedings of the IEE-Part C: Monographs 103 (4) (1956) 400–406.
URL https://digital-library.theiet.org/content/journals/10.1049/pi-c.1956.0053

[105] P. Lin, R. Siskind, A simplified cascade synthesis of RC transfer functions, IEEE Transactions on Circuit Theory 12 (1) (1965) 98–106. doi:10.1109/TCT.1965.1082380.

[106] R. Kalman, Old and new directions of research in system theory, In Perspectives in Mathematical System Theory, Control, and Signal Processing (2010) 3–13doi:10.1007/978-3-540-93918-4_1.

[107] E. L. Ladenheim, A synthesis of biquadratic impedances, Master's thesis, Polytechnic Institute of Brooklyn (1948).

[108] L. V. Auth, Synthesis of a subclass of biquadratic immittance functions, Ph.D. thesis, University of Illinois, Urbana, Illinois (1962).

[109] L. V. Auth, RLC biquadratic driving-point synthesis using the resistive three-port, IEEE Transactions on Circuit Theory 11 (1) (1964) 82–88. doi:10.1109/TCT.1964.1082265.

[110] G. Elias, B. Tellegen, Theorie der wisselstromen, Noordhoff, 1951.
URL https://books.google.co.uk/books?id=Ef8hnwEACAAJ

[111] M. Z. Q. Chen, M. C. Smith, Recent Advances in Learning and Control, Springer London, London, 2008.

[112] M. Z. Q. Chen, M. C. Smith, Restricted complexity network realizations for passive mechanical control, IEEE Transactions on Automatic Control 54 (10) (2009) 2290–2301. doi:10.1109/TAC.2009.2028953.

[113] M. Z. Q. Chen, K. Wang, Y. Zou, G. Chen, Realization of three-port spring networks with inerter for effective mechanical control, IEEE Transactions on Automatic Control 60 (10) (2015) 2722–2727. doi:10.1109/TAC.2015.2394875.

[114] K. Wang, M. Z. Q. Chen, Minimal realizations of three-port resistive networks, IEEE Transactions on Circuits and Systems I: Regular Papers 62 (4) (2015) 986–994. doi:10.1109/TCSI.2015.2390560.

[115] I. Cederbaum, Conditions for the impedance and admittance matrices of n-ports without ideal transformers, Proceedings of the IEE - Part C: Monographs 105 (1958) 245–251(6).
URL https://digital-library.theiet.org/content/journals/10.1049/pi-c.1958.0033

[116] P. Slepian, On paramount matrices, Quarterly of Applied Mathematics 18 (3) (1960) 263–269.
URL http://www.jstor.org/stable/43636344

[117] M. Reichert, Die kanonisch und übertragerfrei realisierbaren zweipolfunktionen zweiten grades (Transformerless and canonic realisation of biquadratic immittance functions), Arch. Elek. Ubertragung 23 (1969) 201–208.

[118] J. Z. Jiang, M. C. Smith, On the theorem of reichert, Systems & Control Letters 61 (12) (2012) 1124–1131. doi:https://doi.org/10.1016/j.sysconle.2012.09.009.

[119] S. Y. Zhang, J. Z. Jiang, M. C. Smith, A new proof of reichert's theorem, In 2016 IEEE 55th Conference on Decision and Control (CDC) (2016) 2615–2619doi:10.1109/CDC.2016.7798656.

[120] J. Z. Jiang, M. C. Smith, Regular positive-real functions and five-element network synthesis for electrical and mechanical networks, IEEE Transactions on Automatic Control 56 (6) (2010) 1275–1290. doi:10.1109/TAC.2010.2077810.

[121] J. Z. Jiang, M. C. Smith, Series-parallel six-element synthesis of biquadratic impedances, IEEE Transactions on Circuits and Systems I: Regular Papers 59 (11) (2012) 2543–2554. doi:10.1109/TCSI.2012.2206492.

[122] A. Morelli, M. C. Smith, Passive Network Synthesis: an approach to classification, Society for Industrial and Applied Mathematics, Philadelphia, PA, 2019.

[123] S. Tirtoprodjo, Bicubic functions with real multiple poles and zeros, IEEE Transactions on Circuit Theory 18 (4) (1971) 470–471. doi:10.1109/TCT.1971.1083307.

[124] S. Tirtoprodjo., Series-parallel RLC synthesis of bicubic impedance, Electronics letters 9 (1973) 370–372.

[125] T. H. Hughes, Minimal series–parallel network realizations of bicubic impedances, IEEE Transactions on Automatic Control 65 (12) (2020) 4997–5011. doi:10.1109/TAC.2020.2968859.

[126] K. Wang, M. Z. Q. Chen, Passive mechanical realizations of bicubic impedances with no more than five elements for inerter-based control design, Journal of the Franklin Institute 358 (10) (2021) 5353–5385. doi:https://doi.org/10.1016/j.jfranklin.2021.05.005.

[127] B. Bollobas, Modern graph theory, Springer Science & Business Media, 2013.

[128] D. Eppstein, Parallel recognition of series-parallel graphs, Information and Computation 98 (1) (1991) 41–55. doi:https://doi.org/10.1016/0890-5401(92)90041-D.

[129] OpenFAST NREL, https://openfast.readthedocs.io/en/main, Last accessed: 06-Nov-2021.

[130] F. Harary, Graph theory and electric networks, IRE Transactions on Circuit Theory 6 (5) (1959) 95–109. doi:10.1109/TCT.1959.1086594.

[131] J. Jonkman, S. Butterfield, W. Musial, G. Scott, Definition of a 5-MW reference wind turbine for offshore system development, Tech. Rep. NREL/TP-500-38060, National Renewable Energy Laboratory, Golden, Colorado (2009).

[132] Y. Si, H. R. Karimi, H. Gao, Modelling and optimization of a passive structural control design for a spar-type floating wind turbine, Engineering Structures 69 (2014) 168–182. doi:https://doi.org/10.1016/j.engstruct.2014.03.011.

[133] H. Zuo, K. Bi, H. Hao, Using multiple tuned mass dampers to control offshore wind turbine vibrations under multiple hazards, Engineering Structures 141 (2017) 303–315. doi:https://doi.org/10.1016/j.engstruct.2017.03.006.

[134] C. Sun, Semi-active control of monopile offshore wind turbines under multi-hazards, Mechanical Systems and Signal Processing 99 (2018) 285–305. doi:https://doi.org/10.1016/j.ymssp.2017.06.016.

[135] J. Jonkman, W. Musial, Offshore code comparison collaboration (OC3) for IEA task 23 offshore wind technology and deployment, Tech. Rep. NREL/TP-5000-48191, National Renewable Energy Laboratory, Golden, Colorado (2010).

[136] J. Jonkman, S. Butterfield, P. Passon, T. Camp, J. Nichols, J. Azcona, A. Martinez, Offshore code comparison collaboration within IEA wind annex XXIII: Phase II results regarding monopile foundation modeling, Tech. Rep. NREL/TP-500-42471, National Renewable Energy Laboratory, Golden, Colorado (2008).

[137] J. Jonkman, Definition of the floating system for phase IV of OC3, Tech. Rep. NREL/TP-500-47535, National Renewable Energy Laboratory, Golden, Colorado (2010).

[138] S. Y. Zhang, J. Z. Jiang, S. Neild, Optimal configurations for a linear vibration suppression device in a multi-storey building, Structural Control and Health Monitoring 24 (3) (2017) e1887. doi:https://doi.org/10.1002/stc.1887.

[139] M. R. Bonyadi, Z. Michalewicz, Particle swarm optimization for single objective continuous space problems: A review, Evolutionary Computation 25 (1) (2017) 1–54. doi:10.1162/EVCO_r_00180.

[140] J. Høgsberg, Vibration control by piezoelectric proof-mass absorber with resistive-inductive shunt, Mechanics of Advanced Materials and Structures 28 (2) (2021) 141–153. doi:10.1080/15376494.2018.1551587.

[141] A. Dall'Asta, E. Tubaldi, L. Ragni, Influence of the nonlinear behavior of viscous dampers on the seismic demand hazard of building frames, Earthquake Engineering & Structural Dynamics 45 (1) (2016) 149–169. doi:https://doi.org/10.1002/eqe.2623.

[142] M. A. Lackner, M. A. Rotea, Passive structural control of offshore wind turbines, Wind Energy 14 (3) (2011) 373–388. doi:https://doi.org/10.1002/we.426.

[143] S. Park, M. A. Lackner, P. Pourazarm, A. Rodriguez Tsouroukdissian, J. Cross-Whiter, An investigation on the impacts of passive and semiactive structural control on a fixed bottom and a floating offshore wind turbine, Wind Energy 22 (11) (2019) 1451–1471. doi:https://doi.org/10.1002/we.2381.

[144] F. F. Kuo, Network analysis and synthesis, John Wiley and Sons, 1962, 2nd Ed.

[145] T. Fischer, W. De Vries, B. Schmidt, Upwind design basis (WP4: offshore foundation and support structures), Tech. rep., University of Stuttgart, Allmandring 5B, 70550 Stuttgart, Germany (2010).

[146] IEC TC88, Design requirements for offshore wind turbines, Tech. Rep. IEC 61400-3, International Electrotechnial Commission, Allmandring 5B, 70550 Stuttgart, Germany (2009).

[147] L. Haid, G. Stewart, J. Jonkman, A. Robertson, M. Lackner, D. Matha, Simulation-length requirements in the loads analysis of offshore floating wind turbines, Tech. Rep. NREL/CP-5000-58153, National Renewable Energy Laboratory, Golden, Colorado (2013).

[148] G. Hayman, Mlife theory manual for version 1.00, Tech. rep., National Renewable Energy Laboratory, Golden, Colorado (2012).

[149] A. Giaralis, A. Taflanidis, Optimal tuned mass-damper-inerter (TMDI) design for seismically excited mdof structures with model uncertainties based on reliability criteria, Structural Control and Health Monitoring 25 (2018) e2082. doi:https://doi.org/10.1002/stc.2082.

[150] T. Nishizeki, N. Saito, Necessary and sufficient condition for a graph to be three-terminal series-parallel, IEEE Transactions on Circuits and Systems 22 (8) (1975) 648–653. doi:10.1109/TCS.1975.1084108.

[151] Y.-T. Chen, Y. H. Chai, Effects of brace stiffness on performance of structures with supplemental maxwell model-based brace–damper systems, Earthquake Engineering & Structural Dynamics 40 (1) (2011) 75–92. doi:https://doi.org/10.1002/eqe.1023.

[152] E. A. Guillemin, Introductory Circuit Theory, New York: John Wiley & Sons, 1953.

[153] W. A. Smith, N. Zhang, J. Jeyakumaran, Hydraulically interconnected vehicle suspension: theoretical and experimental ride analysis, Vehicle System Dynamics 48 (1) (2010) 41–64. doi:10.1080/00423110903243190.

[154] N. Zhang, G.-M. Dong, H.-P. Du, Investigation into untripped rollover of light vehicles in the modified fishhook and the sine maneuvers. part i: Vehicle modelling, roll and yaw instability, Vehicle System Dynamics 46 (4) (2008) 271–293. doi:10.1080/00423110701344752.

[155] D. Cao, S. Rakheja, C.-Y. Su, Roll- and pitch-plane coupled hydro-pneumatic suspension, Vehicle System Dynamics 48 (3) (2010) 361–386. doi:10.1080/00423110902883251.

[156] CarMaker IPG Automotive, https://ipg-automotive.com/products-services/simulation-software/carmaker/, Last accessed: 07-Sep-2021.

[157] T. D. Lewis, J. Z. Jiang, S. A. Neild, C. Gong, S. D. Iwnicki, Using an inerter-based suspension to improve both passenger comfort and track wear in railway vehicles, Vehicle System Dynamics 58 (3) (2020) 472–493. doi:10.1080/00423114.2019.1589535.

[158] W. La Cava, M. Lackner, Theory manual for the tuned mass damper module in fast v8, University of Massachusetts Amherst: Amherst, MA, USA.
URL https://nwtc.nrel.gov/system/files/TMD_theory_manual.pdf